

Dissertation zur Erlangung des Doktorgrades der Fakultät für Chemie  
und Pharmazie der Ludwig-Maximilians-Universität München

Activity of the SPCA1 calcium ATPase couples  
sphingomyelin synthesis to sorting of secretory proteins  
in the *trans*-Golgi network

Mehrshad Pakdel

aus

Rasht, Iran

2019

---

Erklärung

Diese Dissertation wurde im Sinne von § 7 der Promotionsordnung vom 28. November 2011 von Herrn Prof. Dr. Reinhard Fässler betreut.

Eidesstattliche Versicherung

Diese Dissertation wurde eigenständig und ohne unerlaubte Hilfe erarbeitet.

München, ..... 05.09.2019 .....

Mehrshad Pakdel  
.....

Dissertation eingereicht am

15.03.2019  
.....

1. Gutachter:

Prof. Dr. Reinhard Fässler

2. Gutachter:

Prof. Dr. Ralf Jungmann

Mündliche Prüfung am

15.07.2019  
.....

Table of contents

<b>Table of contents</b> .....	<b>III</b>
<b>1 List of abbreviations</b> .....	<b>V</b>
<b>2 List of figures</b> .....	<b>IX</b>
<b>3 Summary</b> .....	<b>1</b>
<b>4 Introduction</b> .....	<b>2</b>
4.1 <i>Intracellular compartmentalization requires protein transport</i> .....	2
4.2 <i>The endoplasmic reticulum</i> .....	3
4.2.1 The dynamic organization of the endoplasmic reticulum.....	3
4.2.2 Protein synthesis and recognition by signal recognition particle .....	5
4.2.3 Co-translational translocation across the ER .....	9
4.2.4 Mechanisms of post-translational translocation.....	10
4.2.5 Protein folding and quality control in the ER .....	13
4.2.6 ER-associated degradation of misfolded proteins .....	16
4.2.7 Exit from the ER .....	18
4.2.8 ER-Golgi intermediate compartment and retrograde transport.....	20
4.3 <i>Organization of membrane traffic and fusion</i> .....	21
4.3.1 Rab GTPases coordinate vesicle traffic.....	21
4.3.2 SNAREs are key elements for membrane fusion .....	23
4.4 <i>The Golgi complex</i> .....	25
4.4.1 Discovery of the Golgi apparatus – a historical perspective.....	25
4.4.2 The structure of the Golgi complex.....	26
4.4.3 Intra-Golgi transport – a heated debate .....	28
4.4.4 Post-translational modifications in the Golgi .....	30
4.5 <i>Lipid metabolism in membrane traffic pathways</i> .....	31
4.5.1 Phosphoinositides provide membrane organelle identity.....	33
4.5.2 Sphingolipid metabolism and traffic.....	35
4.6 <i>Cargo sorting in the trans-Golgi network</i> .....	41
4.6.1 Sorting of GPI-anchored proteins .....	42
4.6.2 Sorting of integral transmembrane proteins.....	43
4.6.3 Transport of soluble lysosomal hydrolases.....	45
4.6.4 Secretory storage granule formation.....	46
4.6.5 Calcium based sorting of soluble cargo at the TGN.....	47

<b>5 Aims of this thesis .....</b>	<b>53</b>
<b>6 Results .....</b>	<b>54</b>
6.1 <i>Secretory cargo sorting by Ca<sup>2+</sup>-dependent Cab45 oligomerization at the trans-Golgi network .....</i>	<i>54</i>
6.2 <i>Activity of the SPCA1 Calcium Pump Couples Sphingomyelin Synthesis to Sorting of Secretory Proteins in the trans-Golgi Network.....</i>	<i>55</i>
<b>7 Discussion.....</b>	<b>57</b>
7.1 <i>SPCA1 regulation by Cofilin and F-actin dynamics .....</i>	<i>57</i>
7.2 <i>How does sphingomyelin promote SPCA1 activity? .....</i>	<i>59</i>
7.3 <i>Coupling Cab45-cargo complexes to secretory vesicle formation.....</i>	<i>64</i>
<b>8 Outlook and concluding remarks.....</b>	<b>68</b>
<b>9 References .....</b>	<b>69</b>
<b>Widmung.....</b>	<b>XI</b>
<b>Danksagungen.....</b>	<b>XII</b>

## 1 List of abbreviations

1,2-Dioleoyl-sn-glycero-3-phosphocholine	DOPC
actin depolymerizing factor	ADF
activating transcription factor 6	ATF6
adenosine triphosphate	ATP
amino acids in cell culture	SILAC
An engineered non-toxic Equinatoxin II sphingomyelin reporter	EQ-SM
binding immunoglobulin protein	BiP
C1P transfer protein	CPTP
calcium release-activated calcium channel protein 1	ORAI1
cartilage oligomeric matrix protein	COMP
cell division control protein 42	Cdc42
ceramide transfer protein	CERT
ceramide-1-phosphate	C1P
ceramide-synthase	CerS
chromogranin A	CgA
chromogranin B	CgB
clathrin-coated vesicles	CCVs
coat protein complex	COP
cryo-electron microscopy	cryo-EM
cytoskeleton-associated protein 4	CKAP4
deoxyribonucleic acid	DNA
diacylglycerol	DAG
Direct stochastic optical reconstruction microscopy	dSTORM
early endosome antigen 1	EEA1
endoplasmic reticulum	ER
endosomal sorting complexes required for transport	ESCRT
ER exit sites	ERES
ER-associated degradation	ERAD
ER-Golgi intermediate compartments	ERGIC
G protein coupled receptors	GPCRs
giant unilamellar vesicles	GUVs
glucose-stimulated insulin secretion	GSIS
glucosylceramide	GlcCer

## 1 List of abbreviations

---

glycerophospholipids	GPLs
glycophosphatidylinositol	GPI
glycosyltransferase	GT
Golgi-localized, $\gamma$ -ear-containing Arf-binding proteins	GGAs
GRIP-related Arf binding	GRAP
GTPase activating protein	GAP
guanine exchange factor	GEF
guanosine-triphosphate	GTP
guided entry of tail-anchored proteins	GET
Heat shock protein	Hsp
heterotetrameric adaptor protein complexes	APs
including epidermal growth factor receptor	EGFR
inositol 1,4,5-trisphosphate	IP3
inositol bisphosphate	IP <sub>3</sub>
inositol-requiring protein 1	IRE1
Jasplakinolide	Jasp
Latrunculin A	LatA
LIM kinase	LIMK
lysosomal integral membrane protein type 2	LIMP-2
Lysozyme C	LyzC
M6P receptor	MPR
major histocompatibility complex	MHC
mannose-6-phosphate	M6P
mass spectrometry	MS
N-ethylmaleimide-sensitive factor	NSF
NSF attachment protein	SNAP
nuclear envelope	NE
nucleotide	nt
oligosaccharyltransferase	OST
p21-activated kinase	Pak1
pac-sphingosine	pac-sph
phosphatidylcholine	PC
phosphatidylethanolamine	PE
phosphatidylinositol	PtdIns
Phosphatidylinositol 3-phosphate	PI3P

## 1 List of abbreviations

---

phosphatidylinositol-four-phosphate adaptor protein 2	FAPP2
phosphatidylserine	PS
phosphoinositides	PIs
Phospholipase C	PLC
phosphorylation-type	P-Type ATPase
plasma membrane	PM
plasma membrane Ca <sup>2+</sup> -ATPases	PMCA4
post-translational modification	PTM
prolyl peptidyl <i>cis-trans</i> isomerases	PPIases
protein kinase C	PKC
protein kinase D	PKD
protein kinase RNA-like ER kinase	PERK
Protein spinster homologue 2	SPNS2
quality control	QC
RAS-related 1	Sar1
retention using selective hooks	RUSH
ribonucleic acid	RNA
ribosome-nascent chain	SRP-RNC
sarcoplasmic-endoplasmic reticulum Ca <sup>2+</sup> ATPase	SERCA
secretogranin II	SGCII
secretory granules	SGs
Secretory Pathway Ca <sup>2+</sup> -ATPase 1	SPCA1
signal peptide peptidase	SPP
signal peptide	SP
signal recognition particle	SRP
signal-sequence tagged horseradish peroxidase	ss-HRP
soluble NSF attachment protein receptor	SNARE
sphingomyelin	SM
Sphingomyelin synthase	SMS
sphingomyelinase	SMase
sphingomyelinases	SMases
sphingosine-1 -phosphate	S1P
SRP receptor	SR
store-operated Ca <sup>2+</sup> -entry	SOCE
Stromal interaction molecule 1	STIM1

## 1 List of abbreviations

---

Structured illumination microscopy	SIM
super-resolution	SR
T-cell antigen receptor	TCR
tail-anchored	TA
thioredoxin-related transmembrane protein 1	TMX1
total internal reflection	TIRF
trans-Golgi network	TGN
transmembrane recognition complex of 40 kDa	TRC40
UDP-glucose:glycoprotein glucosyltransferase	UGGT
unfolded protein response	UPR
voltage-activated potassium channel	Kv channel
Wiskott–Aldrich syndrome protein	WASP
$\beta$ -glucocerebrosidase	$\beta$ GC

## 2 List of figures

Figure 1. General mechanism of protein translocation, sorting and vesicular transport in compartmentalized cells. ....	2
Figure 2. The endoplasmic reticulum builds a large network of interconnecting membrane compartments.....	4
Figure 3. Secondary structure and molecular model of the SRP.....	5
Figure 4. Structural insights of the SRP-RNC complex and schematic model of SRP-mediated co-translatonal protein targeting to the ER.....	7
Figure 5. Models of co-translational and post-translational protein insertion of secretory proteins and the GET-mediated insertion of tail-anchored proteins.....	11
Figure 6. N-glycan linked directed protein folding and quality control .....	14
Figure 7. The unfolded protein response (UPR) and ER-associated degradation (ERAD) are quality control mechanisms that control and clear ER stress.....	17
Figure 8. Sequential steps of COPII-coated vesicle formation that promote ER exit of transmembrane- as well as secretory cargo. ....	19
Figure 9. Schematic cartoon of the SNARE mediated membrane fusion cycle and subsequent SNARE complex disassembly by NSF.....	23
Figure 10. Camillo Golgi - from structure and organization of the nervous system to the discovery of the Golgi apparatus .....	25
Figure 11. The structural organization of the mammalian Golgi complex.....	27
Figure 12. Two possible modes of intra-Golgi transport of cargo proteins.....	29
Figure 13. Cellular distribution of lipid types that are incorporated into membranes .....	32

Figure 14. Structure and dynamic organization of phosphoinositides..... 34

Figure 15. Structural diversity and metabolism pathway of bioactive sphingolipids..... 37

Figure 16. Vesicular and non-vesicular transport pathways of bioactive sphingolipids ..... 39

Figure 17. Diverse cargo sorting pathways at the TGN ensure transport of proteins to their  
destined locations..... 42

Figure 18. The P-Type  $\text{Ca}^{2+}$ -ATPase SPCA1 regulates  $\text{Ca}^{2+}$  import at the TGN..... 49

Figure 19. Cofilin binds to a portion of the cytosolic P-domain of SPCA1 ..... 50

Figure 20. Cab45 binds to  $\text{Ca}^{2+}$  ions with 6 EF-hand domains ..... 51

Figure 21. Known ion pumps that require sphingomyelin for their proper activity ..... 62

Figure 22. Analogous mechanisms that might contribute to secretory vesicle formation to couple  
sphingomyelin synthesis, SPCA1  $\text{Ca}^{2+}$ -import and Cab45-dependent cargo sorting ..... 65

## 3 Summary

Newly synthesized lipids and secretory proteins are sorted in the *trans*-Golgi Network (TGN) into secretory vesicles for their transport to the plasma membrane or secretion. Sorting of transmembrane proteins as well as soluble lysosomal hydrolases at the TGN has been studied extensively in the past. However, the molecular mechanisms underlying how lipid metabolism and sorting of secretory proteins are coupled to establish distinct trafficking routes for cargo and lipid transport, are still unknown. A previously described sorting machinery at the TGN is required for packaging of secretory cargos in a  $\text{Ca}^{2+}$ -dependent manner. The  $\text{Ca}^{2+}$ -ATPase SPCA1 promotes  $\text{Ca}^{2+}$ -import in an ADF/Cofilin- and F-actin-dependent manner. The TGN-luminal protein Cab45 together with active  $\text{Ca}^{2+}$ -import are then required for efficient sorting of secretory cargos. Biochemical oligomerization assays showed that Cab45 selectively binds to its cargo Lysozyme C (LyzC) and reversibly oligomerizes upon  $\text{Ca}^{2+}$ -addition thereby promoting the sorting of secretory cargo in an oligomerization-driven sorting mechanism. In my thesis I used a comparative proximity biotinylation proteomics approach of isolated sphingomyelin (SM)-rich secretory vesicles to identify Cab45 in these types of carriers. By using live-cell microscopy, Cab45 and its cargo LyzC was shown to exit the Golgi and to be secreted in SM-rich vesicles. Development of a retention using selective hooks (RUSH)-based cargo sorting assay allowed to monitor cargo sorting kinetics of LyzC and the lysosomal hydrolase cathepsin D. Depletion of Cab45 and SM synthesis at the Golgi lead to a significant kinetic sorting delay of LyzC vesicle formation while cathepsin D sorting was unaffected. To assess the effects of local SM synthesis at the TGN on  $\text{Ca}^{2+}$ -import activity by SPCA1, a FRET-based  $\text{Ca}^{2+}$ -import assay revealed that disruption of SM synthesis in the TGN significantly decreased  $\text{Ca}^{2+}$ -flux activity by SPCA1. Furthermore, by combining a UV-crosslink competent metabolic precursor of SM and immunoprecipitation experiments SPCA1 was shown to closely associate with SM in TGN membranes. These results demonstrate that local SM synthesis promotes SPCA1  $\text{Ca}^{2+}$ -import activity and thus is required for sorting of secretory proteins into SM-rich vesicles in a Cab45-dependent oligomerization-driven sorting mechanism. These new insights propel our understanding of the Golgi apparatus as the major trafficking hub and cargo sorting station within cells.

## 4 Introduction

### 4.1 Intracellular compartmentalization requires protein transport

Evolution has led to continuous development throughout all living organisms of all domains of life. Evolutionary mechanisms such as natural selection, gene mutations, gene transfers and endosymbiosis resulted in evolutionary adaptations through millions of years leading to the emerge of complex eukaryotic cells possessing increased cellular complexity compared to their ancestors (Archibald, 2015; Williams et al., 2013). With increasing cellular complexity and size, eukaryotic cells evolved intracellular compartmentalization to better control biochemical reactions spatiotemporally. Compartments emerged as cell membrane-limited cell organelles with defined pH, ion concentrations and protein compositions (Diekmann and Pereira-Leal, 2013; Gabaldón and Pittis, 2015). While evolving intracellular compartments, the raising challenge became to ensure proteins and lipids are transported to their destined location (Diekmann and Pereira-Leal, 2013).

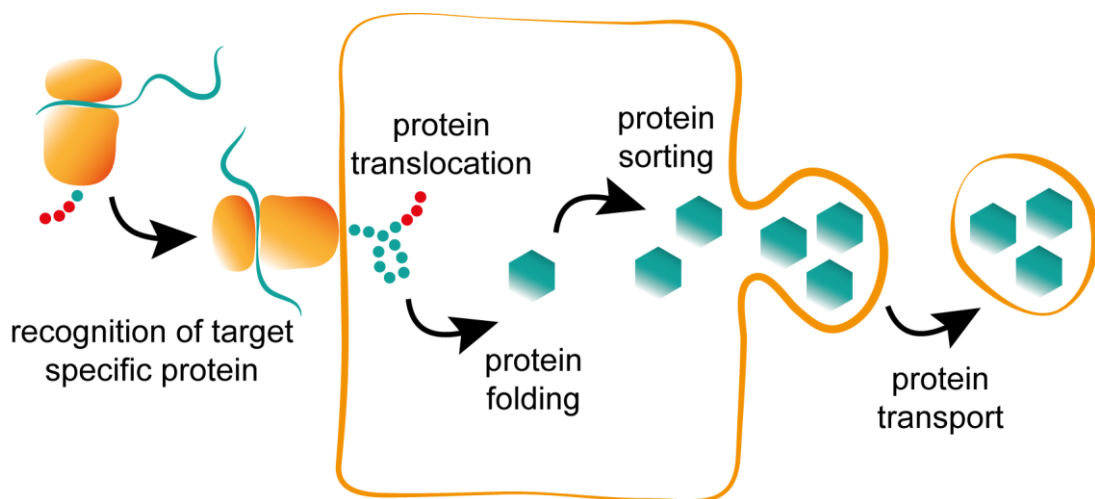


**Figure 1. General mechanism of protein translocation, sorting and vesicular transport in compartmentalized cells.** Newly synthesized proteins are specifically captured in solution and targeted to the membrane of the next compartment. These proteins are then translocated into a membrane-limited cellular compartment. After correct folding, proteins are recognized and sorted into transport vesicles for subsequent transport to their next cellular destination.

To overcome the challenge of protein transport, eukaryotic cells evolved the endomembrane system that is highly specific in protein recognition, translocation and sorting machineries directing the traffic of proteins and lipids to their functionally relevant compartments (Figure 1) (Bohnsack and Schleiff, 2010; Diekmann and Pereira-Leal, 2013; Gabaldón and Pittis, 2015; Lippincott-Schwartz et al., 2000). Undoubtedly, eukaryotic cells possess many specialized cellular compartments such as the nucleus, mitochondria or peroxisomes that fulfill key cellular functions including compartmentalization of chromosomal deoxyribonucleic acid (DNA) as well as ribonucleic acid (RNA) transcription and splicing reactions, cellular respiration, lipid metabolism and radical clearing (Diekmann and Pereira-Leal, 2013). However, this doctoral thesis focuses on molecular mechanisms of protein sorting during the secretory pathway. But how do newly synthesized proteins initially enter the secretory pathway?

## 4.2 The endoplasmic reticulum

### 4.2.1 The dynamic organization of the endoplasmic reticulum

The endoplasmic reticulum (ER) is the “starting point of the secretory pathway” and is the largest membrane-bound organelle in eukaryotic cells that has been studied extensively over the past decades (Lippincott-Schwartz et al., 2000; Phillips and Voeltz, 2015; Rapoport, 1992, 2007). The ER has a variety of essential cellular functions such as protein synthesis of all transmembrane and secretory proteins that establish approx. 30% of the cellular proteome (Fagerberg et al., 2010; Wallin and Heijne, 2008). Furthermore, the ER functions in *de novo* lipid synthesis and serves as a dynamic  $\text{Ca}^{2+}$  storage (Phillips and Voeltz, 2015). The ER builds a large network of linked membrane compartments including tubules and cisternae that expand throughout the cell (Figure 2A, B) (Lippincott-Schwartz et al., 2000). The largest domain of the ER wraps around the cell nucleus forming the nuclear envelope (NE). Protrusions from the second membrane layer of the NE form the peripheral ER that includes flat membrane cisternae as well as tubules that can form membrane contact sites with different organelles including endosomes and mitochondria for organelle positioning, dynamic  $\text{Ca}^{2+}$  crosstalk, lipid exchange and protein transport (Phillips and Voeltz, 2015). Studies have shown that flat membrane

cisternae also known as ER sheets are widely associated with ribosomes for secretory protein synthesis. By contrast, ER tubules that build an interconnected network to the cell periphery contain fewer ribosomes and are therefore called “smooth ER” (Shibata et al., 2006; Phillips and Voeltz, 2015).

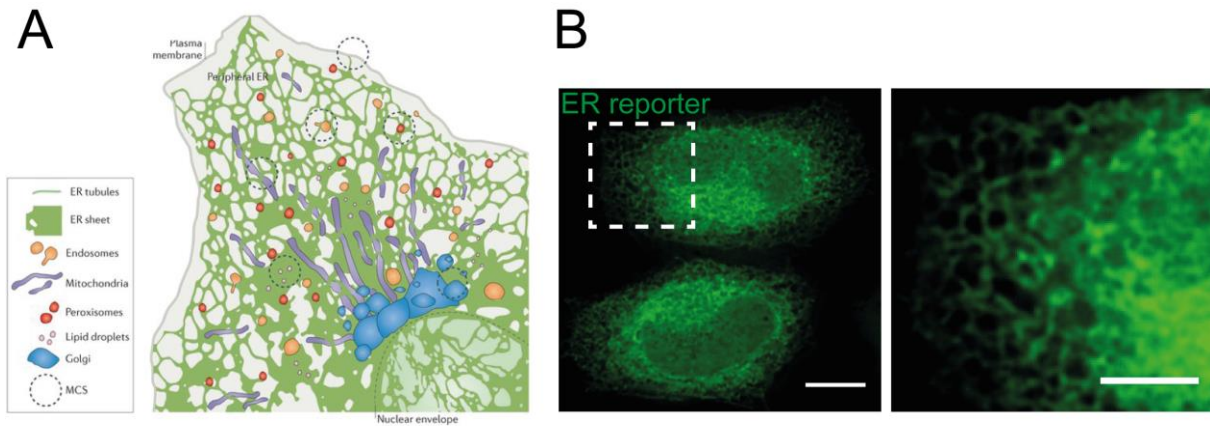


**Figure 2. The endoplasmic reticulum builds a large network of interconnecting membrane compartments.** (A) ER networks consist of ER sheets and tubules (green). The ER associates with cell organelles such as endosomes (orange), mitochondria (purple), peroxisomes (red), lipid droplets (pink) and the Golgi apparatus (blue). The ER forms membrane contact sites (MCS) with these organelles (dashed circles) for dynamic  $\text{Ca}^{2+}$  crosstalk and protein transport. Figure adapted from Phillips and Voeltz, 2015. (B) Visualization of ER networks in living cells by expression of a GFP-labeled ER reporter in HeLa cells. Micrographs were acquired by live-cell widefield microscopy. Bars, 10  $\mu\text{m}$ . Inset, 5  $\mu\text{m}$ .

Recent studies compared the structural differences of ER sheets and tubules (Westrat et al., 2015). While ER sheets form flat sheets with a luminal spacing between the membranes of  $\sim 50$  nm in mammalian cells, tubules are highly dynamic with high membrane curvature (Westrat et al., 2015). This feature of increased membrane curvature in mammalian cells, leads to a higher surface-to-volume ratio increasing the efficiency of surface-dependent functions of ER tubules (Westrat et al., 2015). By contrast, ER sheets fulfill better functions in luminal processes (Westrat et al., 2015). However, a recent study of the Lippincott-Schwartz laboratory changed the view on ER sheets (Nixon-Abell et al., 2016). By using super-resolution (SR) microscopy with high spatiotemporal resolution combined with novel analytical approaches, the authors

suggested that flat membrane sheets are instead densely packed tubular networks newly termed “ER matrix”, thus claiming ER sheets have been misinterpreted as a result of missing spatiotemporal resolution of previously used low resolution techniques (Nixon-Abell et al., 2016). ER matrices instead show dynamic oscillations of ER tubules and junctions therefore displaying a variety of different morphologies (Nixon-Abell et al., 2016). These novel and controversial findings advanced our view on the dynamic organization and structure of the ER, however further studies will be required to confirm the identification of ER matrices.

#### 4.2.2 Protein synthesis and recognition by signal recognition particle

The discovery of the signal recognition particle (SRP) revealed how secretory proteins translocate into the ER and was a huge step forward of understanding the key mechanisms and the starting point of the secretory pathway (Matlin, 2002). The Blobel laboratory in the late 1970s and early 1980s found in a series of studies a protein complex consisting of 6 polypeptides that was bound to polysomes (Meyer and Dobberstein, 1980a, 1980b; Walter and Blobel, 1980).

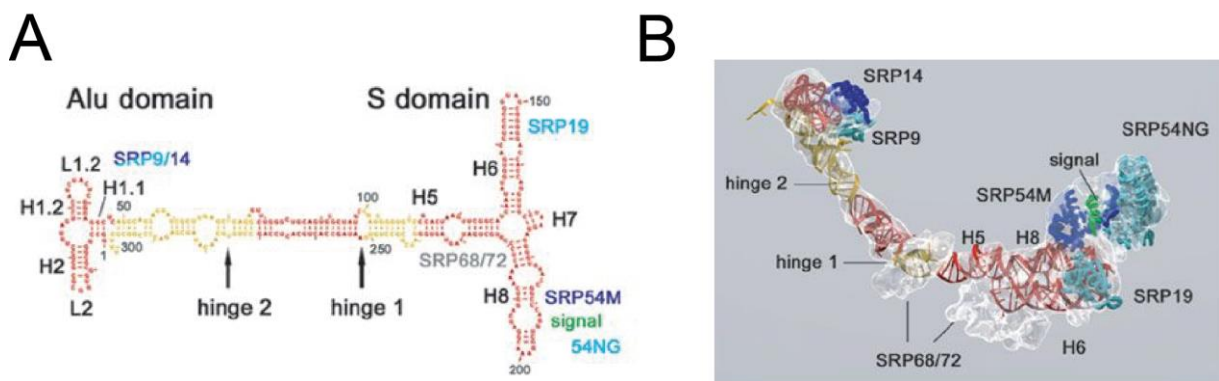


**Figure 3. Secondary structure and molecular model of the SRP.** (A) Secondary structure of SRP 7SL RNA and indicated SRP protein subunit binding sites. SRP RNA helices (H) and hinges are indicated. (B) Molecular model of the SRP RNA associated with SRP protein subunits indicated as protein densities. Figures adapted from Halic et al., 2004.

The complex actively synthesized secretory proteins followed by initial arrest of protein synthesis. After addition of microsomal membranes, the complex – now called signal

recognition particle (SRP) - associated with microsomes thereby mediating protein translocation into the ER (Figure 3A, B) (Walter et al., 1981; Walter and Blobel, 1981a, 1981b). After the discovery of the SRP, the understanding of the underlying molecular mechanisms behind translocation of newly synthesized proteins into the ER greatly progressed in the past decades (Nyathi et al., 2013; Voorhees and Hegde, 2016). The SRP exhibits three main functions during the process of co-translational targeting of secretory and transmembrane proteins: initially SRP recognizes and binds to signal peptides (SP) exiting the ribosome, next it transiently arrests peptide elongation and finally, it supports protein translocation to the ER by binding to the SRP receptor (SR) (Halic et al., 2004). The importance of the SRP during protein targeting is also highlighted by its appearance during evolution being a universal molecular feature in all kingdoms of life (Koch et al., 2003). While SRP-dependent protein targeting in bacteria and chloroplasts show slight differences in their molecular mechanisms, the main function of the SRP by recognizing protein and small RNA is conserved in all species (Koch et al., 2003). There are mainly two different modes of actions how proteins can translocate across the ER or into the ER membrane. Secretory and transmembrane proteins are co-translationally inserted into the ER while tail-anchored proteins are post-translationally inserted into the ER membrane and this will be discussed later in this introduction (Johnson et al., 2013; Nyathi et al., 2013). During co-translational translocation, the SRP binds to hydrophobic elements of the nascent polypeptide by recognizing either an N-terminal SP or the first transmembrane domain (Voorhees and Hegde, 2016). SPs possess characteristic features of a central hydrophobic patch of 6 – 15 amino acids that is flanked by polar residues on both N- and C-terminal sides of the SP (Martoglio and Dobberstein, 1998; von Heijne, 1985). However, previous work suggested that the hydrophobicity of the SP alone is not sufficient for SRP engagement (Huber et al., 2005). By screening SPs with a variety of hydrophobic amino acid residues, the authors found a threshold hydrophobicity for SRP engagement. Interestingly, all SPs required at least the threshold hydrophobicity while few SPs above the threshold failed in SRP recognition (Huber et al., 2005). These results indicate that the simple property of hydrophobicity alone is important but not sufficient and that additional molecular features of the SP such as the conformation of the SP to the ribosome, its helical tendency, the polypeptide chain length and the availability of N-terminal basic residues may play important roles during SP to SRP

recognition (Huber et al., 2005; Nyathi et al., 2013). Interestingly, the C-terminal polar side of SPs often contains uncharged residues, which often consist of helix-breaking proline and glycine at the -3 and -1 positions and thereby mark the site of SP cleavage (Martoglio and Dobberstein, 1998; von Heijne, 1990). Surprisingly, recognition of the SP by SRP does not require defined primary protein sequences and additionally shows high variability of the SP length, often ranging from 15 to 50 amino acid residues (Martoglio and Dobberstein, 1998; von Heijne, 1986). SRP is a ribonucleoprotein complex and comprises six protein subunits SRP9, SRP14, SRP19, SRP54, SPR68, SRP72 and one 7SL RNA that is approx. 300 nucleotide (nt) in length (Figure 3A, B) (Nyathi et al., 2013). By folding into a double stranded secondary structure, the 7SL RNA forms an elongated y-shaped fork that can be structurally separated into two domains consisting of the Alu and S domains (Figure 3A, B) (Nyathi et al., 2013).

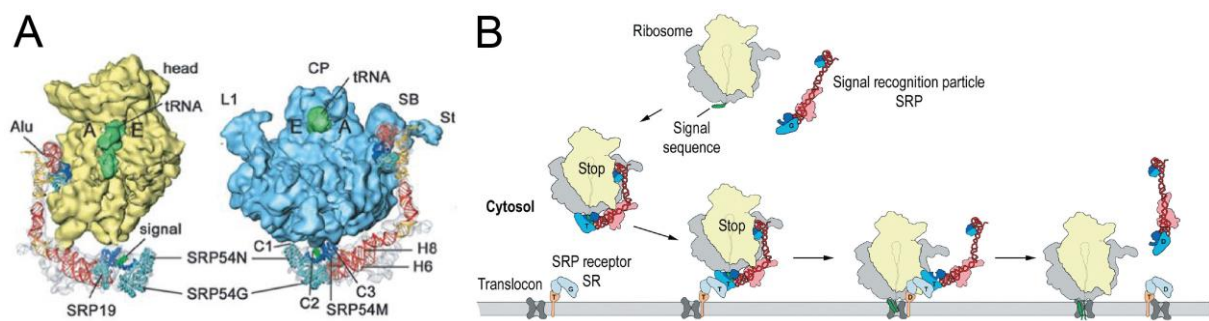


**Figure 4. Structural insights of the SRP-RNC complex and schematic model of SRP-mediated co-translational protein targeting to the ER.** (A) Cryo-EM structure of SRP-RNC complex showing the ribosomal P-site rRNA highlighted in green. The left image shows the SRP structure from the 60S side, the right image from the 40S side. SPR Alu domain, SRP19, SRP54 subunits and SP are indicated. Adapted from Halic et al., 2004. (B) Schematic model SRP cycle illustrates SRP to ribosome recruitment through the emerging SP. Peptide elongation is subsequently stalled and the SRP-RNC complex is targeted to the SR. After transfer of the RNC to the translocon channel, GTP hydrolysis triggers the dissociation of the SRP and SR. Adapted from Halic and Beckmann, 2005.

The Alu domain forms a complex of helices 3-5 of the 7SL RNA and the SRP9-SRP14 heterodimer. The S-domain consists of the forked region of 7SL RNA and the SRP19, SRP54,

SRP68 and SRP72 subunits, and is required for SP binding and translocation (Figure 3A, B) (Halic et al., 2004; Nyathi et al., 2013). Within this complex SRP19 is involved in SRP assembly while SRP54 has a key role in recognizing the SP and interacting with the SR in a guanosine-triphosphate (GTP)-dependent manner (Connolly and Gilmore, 1989; Halic et al., 2004; Siegel and Walter, 1988). Binding to the nascent chain that is still associated with the ribosome, the SRP then interacts with high affinity with ribosomes thereby forming the SRP and the ribosome-nascent chain (SRP-RNC) complex (Figure 4B) (Bornemann et al., 2008). The SRP-RNC complex transiently arrests peptide elongation prior to membrane translocation (Figure 4B) (Keenan et al., 2001; Walter and Blobel, 1981b). Given the remarkable size of a ribosome of 25 – 30 nm and based on structural insights estimated distance of 250 Å between the ribosomal exit tunnel and the elongation factor binding site (Halic et al., 2004; Wilson and Doudna Cate, 2012), the question arises how the SRP can bind the RNC at the ribosomal exit tunnel and simultaneously halt peptide elongation (Halic et al., 2004)? Advances in cryo-electron microscopy (cryo-EM) revealed mammalian structures of SRP bound to 80S RNC (Figure 4A) (Halic et al., 2004). SRP possesses an elongated bent conformation parting the Alu and S domains with a length of 260-280 Å, that is consistent with the size of a ribosome (Halic et al., 2004). Interestingly, the three connections of the S domain with the ribosome are mediated exclusively by the SRP54 subunit by binding the large ribosome subunit with its N domain, with the N-terminal of the SRP54 M domain, and interacting by the C-terminal region of the M domain, with helix 24 of the 25S ribosomal RNA (Figure 4A) (Halic et al., 2006, 2004). By contrast to the S domain, the Alu domain consisting of the Alu RNA bound to SRP9/14 heterodimer is essential for stalling peptide elongation (Bousset et al., 2014; Halic et al., 2004). The Alu domain interactions to the ribosome are established by the 5' RNP with its first 48 nt and the SRP9/14 heterodimer (Halic et al., 2004). The Alu domain contact sites directly compete with the binding site of the eukaryotic elongation factor 2 (eEF2) therefore leading to peptide elongation arrest (Figure 4A) (Gomez-Lorenzo et al., 2000; Halic et al., 2004; Spahn et al., 2004). These unique structural features allow the SRP to bind to the RNC but also to stall peptide elongation at the same time (Figure 4B).

### 4.2.3 Co-translational translocation across the ER

The step of translocation to the ER membrane is mediated by the SR that consists of two distinct subunits (Dilks et al., 2004; Keenan et al., 2001). The soluble SR  $\alpha$ -subunit functions as a GTPase and is anchored to the SR  $\beta$ -subunit that is an integral membrane protein of the ER (Aviram and Schuldiner, 2017; Keenan et al., 2001). GTP binding of the SRP54 subunit and SR  $\alpha$ -subunit mediates the translocation of the SRP-RNC complex to the ER membrane by forming a complex on the ER membrane (Aviram and Schuldiner, 2017; Keenan et al., 2001). After translocation to the ER and interaction with SR, SRP transfers the RNC to the SR translocon complex (Keenan et al., 2001; Nyathi et al., 2013). After releasing the SP to the translocon, GTP is hydrolysed by SRP-SR complex thereby causing the release of SRP from SR (Keenan et al., 2001). Dissociation of SRP then leads to its recycling thereby allowing a new round of targeting (Aviram and Schuldiner, 2017). The delivery of the RNC to the heterotrimeric Sec61 translocon complex leads to the formation of a “gated translocation channel that is selectively opened by SP or transmembrane domains” (Voorhees and Hegde, 2016). The Sec61 channel consists of three subunits  $\alpha$ ,  $\beta$ , and  $\gamma$  (Park and Rapoport, 2012). Crystal structures of an archaeal SecY complex, the homologue of Sec61, revealed the ability of the  $\alpha$ -subunit to open at the front forming a “lateral gate” (Berg et al., 2003; Park and Rapoport, 2012). At its rear side, the two parts of the  $\alpha$ -subunit are connected to the  $\gamma$ -subunit. At its rear side, the two parts of the  $\alpha$ -subunit are connected to the  $\gamma$ -subunit (Berg et al., 2003; Park and Rapoport, 2012). Surprisingly, the  $\beta$ -subunit shows only few interactions with the  $\alpha$ -subunit explaining why the  $\beta$ -subunit is less conserved (Park and Rapoport, 2012). These structural features of the Sec61 complex allow first to open the translocation channel by interactions either to the ribosome, the Sec62/Sec63 complex, or prokaryotic SecA. The Sec62/Sec63 complex as well as SecA are required by post-translational translocation (Rapoport, 2007) and will be described in the next section. After ribosome binding to Sec61, the SP intercalates into the walls of the channel thereby promoting the formation of a lateral opened gate (Park and Rapoport, 2012). Protein translation then resumes and the SP remains bound to the opened channel during translocation while the subsequent polypeptide moves through the channel (Park and Rapoport, 2012). Interestingly, ribosomal GTP hydrolysis is required for peptide elongation while polypeptide transfer through the channel is GTP-independent (Connolly and Gilmore, 1986; Park and

Rapoport, 2012). After these crucial steps during the onset of the secretory pathway, newly synthesized polypeptides arrive into the lumen of the ER where they are further processed.

### 4.2.4 Mechanisms of post-translational translocation

The last section summarized the principles of co-translational targeting and translocation by SRP, SR and Sec61 as the first discovered ER-targeting pathway (Figure 5A) (Walter and Blobel, 1981a, 1981b). The majority of secretory proteins can be targeted to the ER co-translationally highlighting the importance of the co-translational translocation pathway (Aviram and Schuldiner, 2017; Jan et al., 2014). However, cells have developed additional translocation pathway such as the binding immunoglobulin protein (BiP)-dependent pathway (Figure 5B) (Linxweiler et al., 2017). During this post-translational translocation pathway translated polypeptides are fully synthesized in the cytosol since their SPs are shorter in mammals and are therefore not recognized by SRP (Figure 5B) (Linxweiler et al., 2017). To prevent premature protein folding, cytosolic Heat shock protein 40 (Hsp40) and Hsp70 chaperones bind to the newly translated polypeptides and keep their SP free for interactions with the Sec61 translocation channel (Figure 5B) (Barlowe and Miller, 2013; Linxweiler et al., 2017). Structural features of substrates determine the requirement of Sec62 as well as SRP for post-translational targeting to Sec61 (Linxweiler et al., 2017). The  $\alpha$ ,  $\beta$ , and  $\gamma$  subunits of Sec61 can directly interact with Sec62 and Sec63 by forming oligomers of the core element of the translocation machinery (Linxweiler et al., 2017). Mammalian Sec62 has the capability to bind the ribosomal exit tunnel with two conserved domains that are located at its N-terminus (Linxweiler et al., 2017; Müller et al., 2010). The role of ribosomal binding to Sec62 and its mechanistic action remains still elusive. However, many studies indicate Sec62 to be required for efficient post-translational translocation of proteins (Linxweiler et al., 2017). On the contrary, Sec63 facilitates substrate translocation by binding to ER-luminal chaperones (Rapoport, 2007). Compared to co-translational translocation, the driving force of the ribosome is missing during post-translational translocation. Therefore, in order to prevent “back-sliding” of the translating polypeptide BiP binds to the ER-luminal J-domain of Sec63 and interacts with the newly translocating polypeptides to promote their translocation by an adenosine triphosphate (ATP)-

dependent ratcheting mechanism (Figure 5B) (Denks et al., 2014; Linxweiler et al., 2017). In prokaryotes, post-translational protein translocation is mediated by the translocation channel SecY which cooperates with the cytosolic ATPase SecA (Rapoport, 2007).

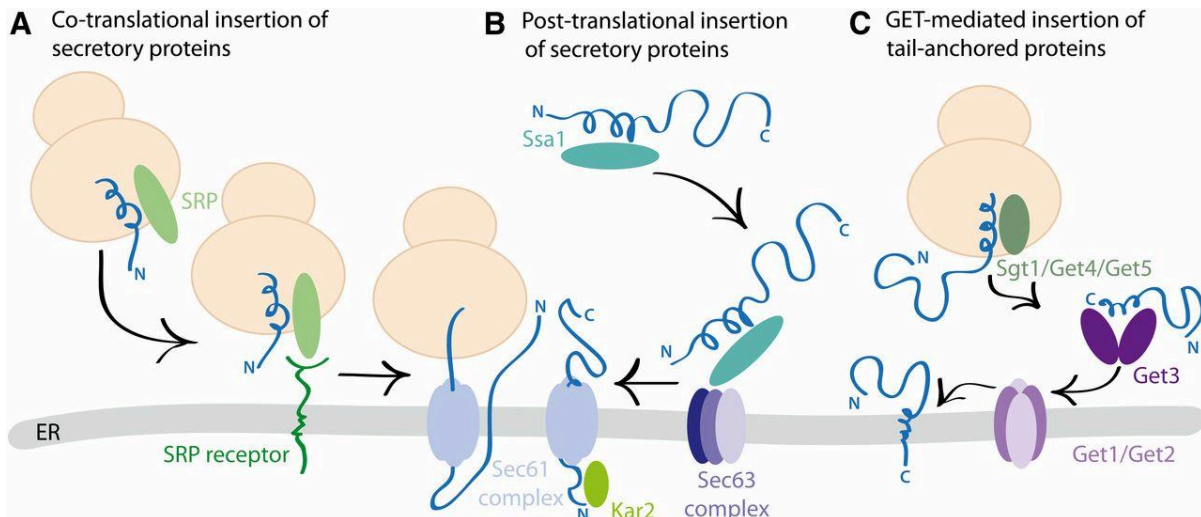


**Figure 5. Models of co-translational and post-translational protein insertion of secretory proteins and the GET-mediated insertion of tail-anchored proteins.** (A) Co-translational protein insertion is mediated by SRP recognition of the substrate, ribosomal elongation arrest, translocation to the SR and hand over to the Sec61 translocon. (B) Post-translocation protein translocation of secretory proteins is mediated by cytosolic chaperones Hsp40 and Hsp70 (Ssa1 in yeast) allowing recruitment to the Sec63 and Sec61 translocation complex at the ER. Translocation of the polypeptides in this pathway is BiP (Kar2 in yeast) dependent. (C) Insertion of tail-anchored proteins that contain a single transmembrane domain at their very c-terminus is mediated by the GET pathway. Figure adapted from Barlowe and Miller, 2013.

Substrate proteins that are bound by the cytosolic chaperone SecB are passed on to SecA that transfers the polypeptide into the SecY channel (Rapoport, 2007). In contrast to BiP, SecY then facilitates polypeptide translocation by an ATP-dependent pushing mechanism (Rapoport, 2007). During this process, SecA binds with its polypeptide-groove to the substrate and moves the polypeptide further into the channel. After ATP hydrolysis, SecY releases the polypeptide

to capture the next section of the substrate and repeats this cycle until translocation is completed (Park and Rapoport, 2012; Rapoport, 2007). In addition to BiP-mediated or SecA-mediated post-translational translocation, the discovery of the post-translational targeting of tail-anchored (TA) proteins has broadened the view of post-translational targeting pathways (Aviram and Schuldiner, 2017). TA proteins possess a single transmembrane domain at their C-terminus. Consequently the transmembrane domain is only exposed after termination of translation leading to the requirement of an SRP-independent targeting mechanism (Aviram and Schuldiner, 2017). Recent studies discovered the machinery required for TA protein insertion in yeast as the guided entry of tail-anchored proteins (GET) (Figure 5C) (Jonikas et al., 2009; Schuldiner et al., 2008) as well as in mammals as the transmembrane recognition complex of 40 kDa (TRC40) (Favaloro et al., 2008; Stefanovic and Hegde, 2007). Since these pathways are homologues, the yeast GET pathway will be described here exemplarily. The GET pathway is initiated by substrate recognition by the ribosome associated chaperone Sgt2 and handing over to the Get4-Get5 complex (Figure 5C) (Aviram and Schuldiner, 2017). TA proteins are then delivered to the Get3 ATPase chaperone, that dimerizes and subsequently forms a hydrophobic binding cleft (Figure 5C) (Aviram and Schuldiner, 2017; Mateja et al., 2015). By binding to TA proteins, Get3 hydrolyses ATP and targets its membrane receptor in the ER, the Get1-Get2 complex (Figure 5C) (Schuldiner et al., 2008). Finally, the TA protein is released from Get3 due to Get1-Get2 binding (Figure 5C) (Aviram and Schuldiner, 2017). Interestingly, a recent report by the Schuldiner laboratory revealed an additional SRP- and GET-independent protein translocation pathway (Aviram et al., 2016). By using a high-content genetic screen the translocation of the model substrate Gas1 was monitored in a yeast mutant library (Aviram et al., 2016). Gas1 was described as an SRP-independent and only partially GET-dependent substrate, and therefore represents a suitable model substrate to identify a potentially novel targeting mechanism. The genes identified in the genetic screen to affect Gas1 translocation were named SRP-independent targeting (SND) Snd1, Snd2 and Snd3. Cytosolic Snd1 can interact with ER-membrane bound Snd2, Snd3 as well as to the substrate Gas1 (Aviram et al., 2016). Interestingly, the SND complex also interacts with the Sec61 translocon (Aviram et al., 2016). Proximity-specific ribosome profiling showed that target substrates of the SND complex contained transmembrane domains further downstream (> 95 amino acids) of

the optimal recognition window of SRP substrates (Aviram et al., 2016). Notably, SND can compensate for the translocation of SRP substrates as well as for GET-dependent substrates if SRP or GET pathways are perturbed indicating that SND acts as a backup targeting mechanism with broad substrate specificity to ensure cell survival (Aviram et al., 2016).

### 4.2.5 Protein folding and quality control in the ER

After discussing how proteins enter the secretory pathway by either co-translational or post-translational mechanisms, this section will now focus on how proteins subsequently are folded, and quality controlled in the ER. The ER provides an environment that is optimized for protein folding and maturation (Ellgaard and Helenius, 2003; Margittai et al., 2015). The ER supports redox conditions that is required for oxidizing protein thiols for disulfide bond formation and oxidative folding (Margittai et al., 2015). These redox conditions are established by oxidoreductases and electron donors and acceptors including glutathione, pyridine and flavin nucleotides in the ER (Margittai et al., 2015). Additionally, the ER allows exclusive co-translational and post-translational modifications including SP cleavage, N-linked glycosylation and glycosylphosphatidylinositol (GPI)-anchor attachment (Ellgaard and Helenius, 2003). ER quality control (QC) ensures the correct folding of translocated proteins to prevent the formation of potential hazardous transport of misfolded proteins (Ellgaard and Helenius, 2003). After translocation of secretory proteins, their SP is cleaved by the intramembrane-cleaving protease signal peptide peptidase (SPP) cleaving peptides at Gly-X-Gly-Asp motifs (Voss et al., 2013; Weihofen et al., 2002). The proteins are then modified with N-linked glycans on Asparagine (Asn) residues within Asn-X-Ser/Thr motifs (Figure 6) (Braakman and Hebert, 2013). The attachment of N-linked glycans is mediated by the oligosaccharyltransferase (OST) once the Asn sequence motif reaches ~13 amino acids deep into the ER lumen (Braakman and Hebert, 2013). In the next step, the hetero-oligomeric transferase complex transfers a preassembled carbohydrate consisting of defined numbers of glucoses, mannoses and N-acetyl glucosamines ( $\text{Glc}_3\text{Man}_9\text{GlcNAc}_2$ ) to the Asn residue (Braakman and Hebert, 2013). The attached glycan residues alter the physical properties of the proteins by increasing their stability and improving their folding capacity (Braakman and Hebert, 2013).

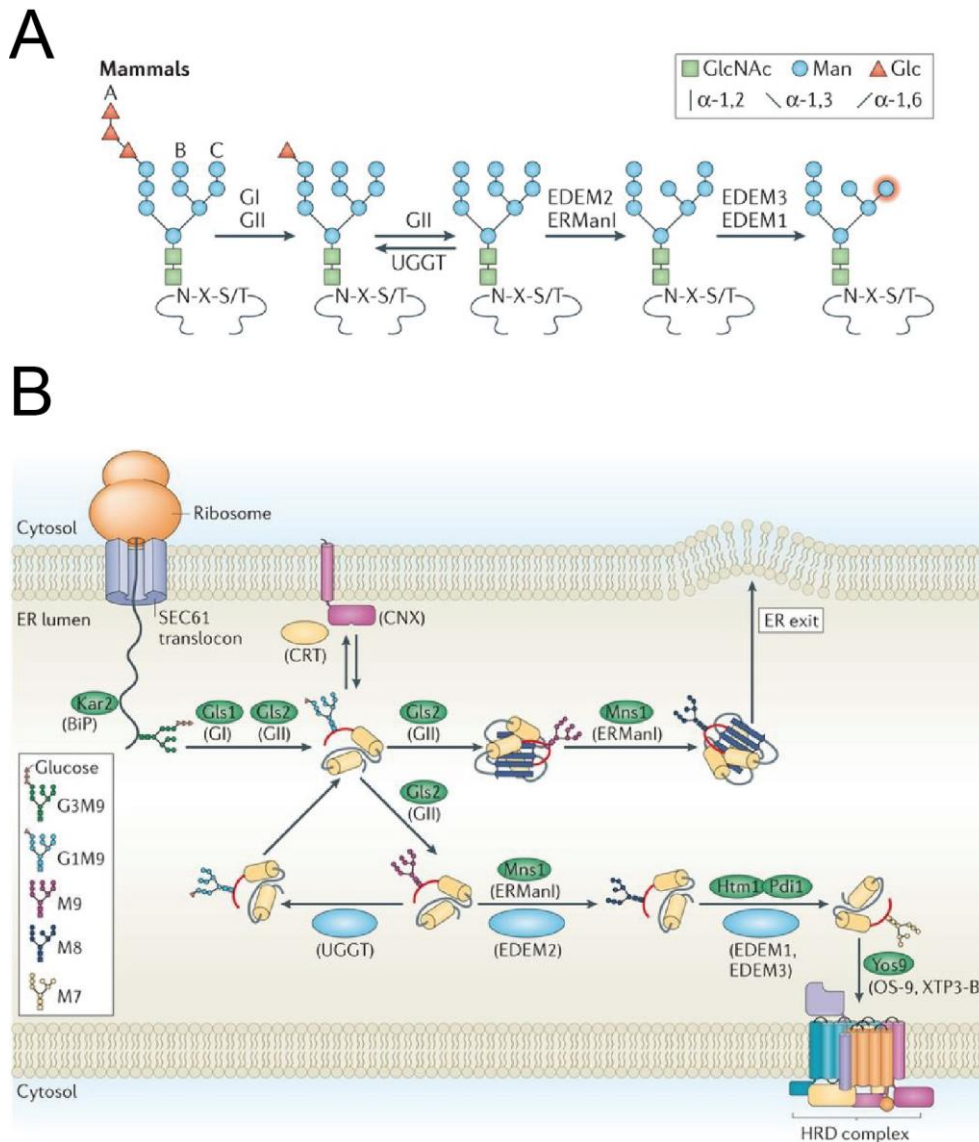


**Figure 6. N-glycan linked directed protein folding and quality control. (A) and (B)** Mammalian N-glycan trimming cascade in the ER is required to recognize native from non-native substrates. The pre-assembled carbohydrate  $\text{Glc}_3\text{Man}_9\text{GlcNAc}_2$  is attached to Asn residues at Asn-X-Ser/Thr motifs. Trimming is initiated, and glucose trimming mediated by glucosidase I and glucosidase II. Mis-folded proteins are re-glucosylated by UDP-glucose:glycoprotein glucosyltransferase (UGGT) for a new cycle of calnexin (CNX) calreticulin (CRT) mediated folding. Removal of mannose residues is mediated by ER degradation-enhancing  $\alpha$ -mannosidase-like protein (ERManI) and, ER mannosidase (EDEM) 1, 2 and 3. Red labeled mannose residue indicates  $\text{Man}_7\text{GlcNAc}_2$  glycan residue that is recognized for subsequent protein re-translocation for its degradation by the Hrd complex. By contrast correctly folded  $\text{Man}_8\text{GlcNAc}_2$  positive substrates will exit the ER to the next compartment. Figures adapted from Xu and Ng, 2015.

While proteins attempt to fold correctly, the glycan-trimming cascade determines its fate of ER export versus protein re-translocation and degradation (Figure 6) (Xu and Ng, 2015). The trimming cascade is initiated by glucosidase I that removes the first glucose residue from the A-branch followed by the removal of the second glucose by glucosidase II resulting in a  $\text{Glc}_1\text{Man}_9\text{GlcNAc}_2$  glycan residue (Xu and Ng, 2015). This glycan structure is then bound to lectin-like ER chaperones calnexin, that is a type I transmembrane protein and calreticulin as a soluble paralogue of calnexin that resides in the ER (Hammond et al., 1994; Peterson et al., 1995). Both calnexin and calreticulin possess a globular carbohydrate-binding domain (Braakman and Hebert, 2013; Schrag et al., 2001). These chaperones possess a variety of functions by slowing down the folding process in a domain specific manner to stabilize the protein, and therefore preventing protein aggregation and turnover (Braakman and Hebert, 2013). Calnexin and calmodulin retain non-native substrates in the ER to support their folding. Furthermore, crucial post-translational modifications that are important for substrate folding are facilitated by calnexin and calreticulin interactions such as disulfide bond formation through their association with the oxidoreductase ERp57 as well as the enzymatic *cis-trans* isomerization of proline residues by the prolyl peptidyl *cis-trans* isomerases (PPIases) (Braakman and Hebert, 2013; Lang et al., 1987; Oliver et al., 1997). Subsequently, glucosidase II is able to cleave the last glucose residue of the  $\text{Glc}_1\text{Man}_9\text{GlcNAc}_2$  glycan modification that prevents re-engagement with calnexin (Xu and Ng, 2015). Loss of the last glucose residue allows UDP-glucose:glycoprotein glucosyltransferase (UGGT) to re-glucosylate inspected proteins bearing still unfolded domains, thereby restoring calnexin-binding ability for another round of QC cycle (Figure 6) (Tessier et al., 2000; Trombetta and Helenius, 2000; Xu and Ng, 2015). This process repeats until the substrates are fully folded and exported out of the ER or until QC mechanisms of the ER break the cycle to clear the ER from misfolded proteins (Figure 6) (Xu and Ng, 2015). What are the molecular mechanisms allowing the ER to remove terminally unfolded substrates from the compartment?

#### 4.2.6 ER-associated degradation of misfolded proteins

The previous section describes how the ER ensures correct folding of newly synthesized proteins by using elaborate QC mechanisms (Figure 6) (Braakman and Hebert, 2013; Xu and Ng, 2015). However, proteins can also mis-fold, hence never reach their native conformation due to spontaneous errors during protein transcription and translation, genetic mutations or exogenous effects such as toxic compounds or cellular stress (Vembar and Brodsky, 2008). To endure this challenge, cells have developed the ER-associated degradation (ERAD) pathway to prevent mis-folding that can lead to cell toxicity and stress (Vembar and Brodsky, 2008). The ability of cells to degrade secretory proteins was first described by Klausner and colleagues postulating either proteases within the ER or a new compartment for protein degradation (Klausner and Sitia, 1990; Lippincott-Schwartz et al., 1988). The requirement for cytosolic factors and the ubiquitin-proteasome system was described later by the Jentsch and others (Hiller et al., 1996; Sommer and Jentsch, 1993). The first step during the ERAD pathway is to recognize non-native substrates that is mediated by ER chaperones such as BiP, which recognize hydrophobic patches on mis-folded proteins (Figure 7) (Ruggiano et al., 2014). In addition, ER membrane-associated ubiquitin ligases (or E3 ligases) that ubiquitinate substrates for subsequent degradation are also involved in substrate recognition (Ruggiano et al., 2014). Interestingly, the different E3 complexes specifically recognize mis-folded domains of the substrates. Proteins with mis-folded domains in the cytoplasmic face are called ERAD-C substrates and are recognized by the Doa10 complex while substrates with luminal (ERAD-L substrates) or intramembrane (ERAD-M substrates) mis-folded domains are recognized by the Hrd1 complex (Figure 7) (Ruggiano et al., 2014). Furthermore, the glycan modifications are also involved in ERAD recognition. Proteins with  $\text{Man}_8\text{GlcNAc}_2$  glycan modification are exported from the ER if properly folded (Ruggiano et al., 2014; Xie et al., 2009). By contrast, proteins harboring  $\text{Man}_7\text{GlcNAc}_2$  glycan modifications in unstructured polypeptide segments that are bound by Hrd3, support ERAD recognition by Hrd1 complex subunit Yos9 (Ruggiano et al., 2014; Xie et al., 2009). However, it has been shown that binding of Yos9 to the  $\alpha 1,6$ -linked mannose residue alone is not sufficient to promote substrate degradation (Xie et al., 2009). Interestingly, some viruses such as the human cytomegalovirus exploit the ERAD machinery

by encoding ER membrane proteins US2 and US11 that associate with newly synthesized major histocompatibility complex (MHC) I molecules and transfer them to the ERAD machinery for their degradation (Lilley and Ploegh, 2004; Ruggiano et al., 2014; E. J. H. . Wiertz et al., 1996; Ye et al., 2004). Consequently, cytomegalovirus infected cells show decreased MHC I complex expression at the PM and therefore are less likely to be detected by the immune system (Ruggiano et al., 2014). After their recognition, misfolded substrates are retrotranslocated back to the cytoplasm by a retrotranslocation channel (Ruggiano et al., 2014).

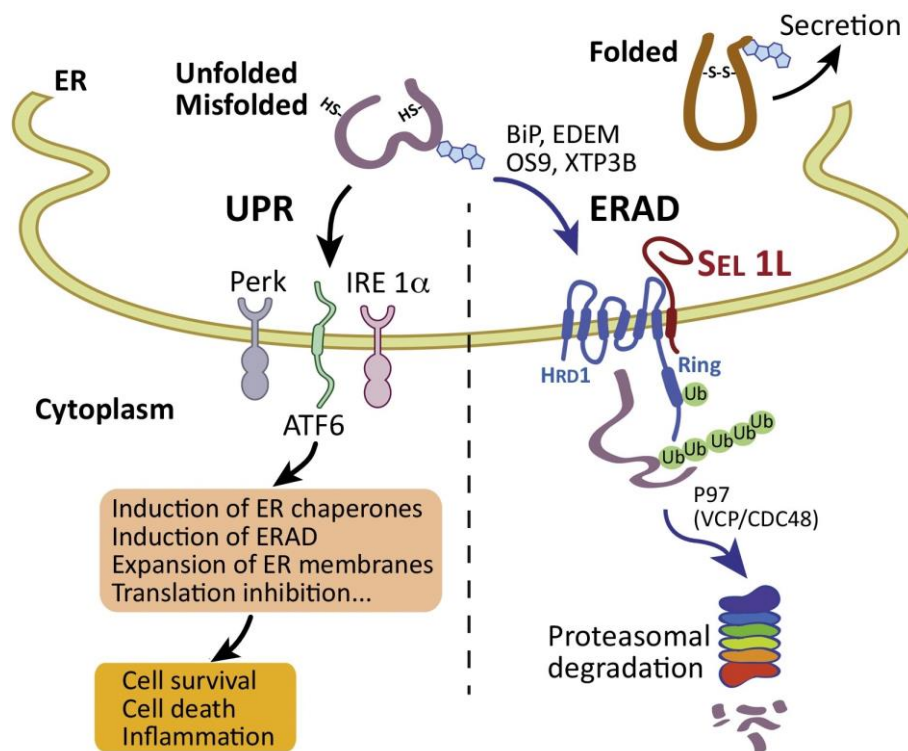


**Figure 7. The unfolded protein response (UPR) and ER-associated degradation (ERAD) are quality control mechanisms that control and clear ER stress.** Properly folded proteins exit the ER for the next compartment. Terminally mis-folded substrates are recognized by ER resident chaperones and delivered to the Hrd1 retrotranslocation complex. Substrates are retrotranslocated by Cdc48/p97 complex in an ATPase-dependent manner and are ubiquitinated for their proteasomal degradation in the cytosol. Prolonged ER stress leads to UPR activation that is mediated by PERK, IRE1 and ATF6 regulating cellular functions such as translational inhibition and ERAD upregulation to prevent cellular damage and promote cell survival. Adapted from Qi et al., 2017.

Surprisingly, the identity of the retrotranslocation channel is still under intense debate within the field. Since Sec61 interacts with ERAD components, some groups described the Sec61 complex to be involved in substrate retrotranslocation (Scott and Schekman, 2008; E. J. H. J. Wiertz et al., 1996). However, recent studies favor the E3 ligase complexes in particular proteins of the Derlin family to be essential for retrotranslocation (Mehnert et al., 2013; Wahlman et al., 2007) while again other groups found strong evidence of Hrd1 to be essential for retrotranslocation of ERAD substrates (Carvalho et al., 2010; Denic et al., 2006). After substrates are retrotranslocated, they are ubiquitinated, which allows recognition by the Cdc48/p97 ATPase complex, that provides the mechanical force to pull substrates from the ER membrane to the cytosol (Figure 7) (Ruggiano et al., 2014). The substrates are then released from the membrane and transferred to the proteasome by cytosolic chaperones where they are finally degraded (Figure 7) (Ruggiano et al., 2014). In case of prolonged cellular stress due to huge amounts of mis-folded proteins in the ER, cells activate the unfolded protein response (UPR) to prevent cellular damage and apoptosis (Figure 7) (Hetz, 2012). UPR is activated by three UPR stress sensors including inositol-requiring protein 1 (IRE1), protein kinase RNA-like ER kinase (PERK) and activating transcription factor 6 (ATF6) (Figure 7) (Domínguez-Martín et al., 2018; Hetz, 2012). By controlling both transcriptional and non-transcriptional processes, the UPR slows down global protein synthesis, while upregulating molecular chaperones and ERAD to reduce mis-folding-induced ER stress (Figure 7) (Hetz, 2012).

### 4.2.7 Exit from the ER

Secretory or Golgi resident proteins that display correct protein folding will be exported to the next compartment, the Golgi complex. These proteins will be sorted into coat protein complex II (COPII) coated transport vesicles from the ER (Brandizzi and Barlowe, 2013). Interestingly, packaging of cargo substrates does not randomly occur throughout the highly interconnected ER network, but rather appears at distinct, long-lived sites of the ER termed ER exit sites (ERES) (Bannykh et al., 1996; Hammond et al., 2000). ERES can form vesicular-tubular membrane structures with a diameter of approx. 0.5  $\mu\text{m}$  and are associated with the COPII machinery (Aridor et al., 2001; Budnik and Stephens, 2009; Hammond et al., 2000). At ERES, cargo

destined for anterograde transport towards the Golgi complex is captured by COPII-coated vesicles (Budnik and Stephens, 2009). The first step of COPII vesicle formation is mediated by the cytosolic small GTPase secretion-associated RAS-related 1 (Sar1) that is activated by its guanine exchange factor (GEF) Sec12 located in the ER membrane (Figure 8) (Budnik and Stephens, 2009). GTP-bound Sar1 exposes an N-terminal amphiphatic helix that inserts into the ER membrane (Bi et al., 2002; Bielli et al., 2005). Membrane bound Sar1 recruits the inner layer of the COPII coat consisting of the Sec23-Sec24 heterodimer by direct interactions of Sar1 with Sec23 (Figure 8) (Yoshihisa et al., 1993). Sec24 in turn, captures cargo that is properly folded for ER export (Figure 8) (Budnik and Stephens, 2009).

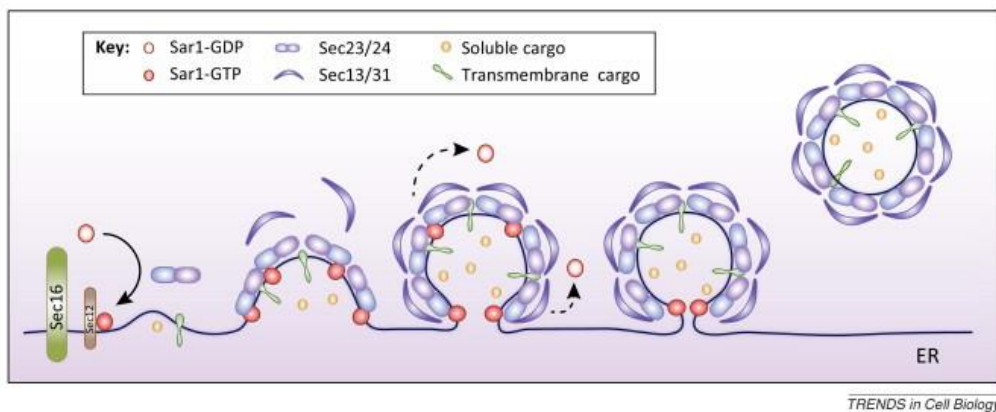


**Figure 8. Sequential steps of COPII-coated vesicle formation that promote ER exit of transmembrane- as well as secretory cargo.** Formation of COPII coats is initiated by the small GTPase Sar1 that is activated by the GEF Sec12. Activated, GTP-bound Sar1 associates with the ER membrane by exposing an amphiphatic helix that becomes inserted into the ER membrane. Sar1-GTP then recruits Sec23-Sec24 that resemble the inner coat layer. Sec24 recruits transmembrane and secretory cargo forming the prebudding complex. Next, the outer layer consisting of Sec13-Sec31 is recruited forming a cage-like coat around the budding vesicle. Finally, Sar1-GTP promotes the scission of the coated vesicle by inducing curvature that results in fission. Sec16 interacts with all COPII components thereby suiting as a scaffold to concentrate COPII vesicles at ERES. Figure adapted from Venditti et al., 2014.

Interestingly, transmembrane cargo is recognized by their cytoplasmic domains exposed to the COPII machinery while COPII requires a transmembrane cargo receptor to capture luminal

and soluble cargo (Gürkan et al., 2006). Evidence suggests that the Sec24 subunit interacts with many cargos through their ER-exit motifs including di-acid residues such as DXE motifs or di-hydrophobic residues (Gürkan et al., 2006; Sato, 2004). At this stage, the inner layer establishes the prebudding complex with captured cargo (Figure 8) (Venditti et al., 2014). During the next step of COPII vesicle formation, the Sec13-Sec31 tetrameric complex is recruited to the prebudding complex shaping the outer layer by forming cage-like structures that induce the formation of a membrane curvature (Figure 8) (Venditti et al., 2014). After nucleation to a vesicle bud, vesicle scission is induced by Sar1-GTP that promotes lipid-packing defects in the inner lipid leaflet resulting in hemifusion and fission (Figure 8) (Bielli et al., 2005; Long et al., 2010; Venditti et al., 2014). Interestingly, ERES provide a platform for COPII assembly since Sec16, a protein that is involved in ERES organization and hence is marking ERES, interacts with Sec23 and Sec13 (Figure 8) (Budnik and Stephens, 2009). Furthermore, depletion of Sec16 delays ER-to-Golgi transport highlighting the importance of Sec16-positive ERES for COPII vesicles formation (Budnik and Stephens, 2009). Recent models therefore suggest that Sec16 may suit as an ERES scaffold recruiting COPII components to distinct zones at the ER (Brandizzi and Barlowe, 2013). After vesicle fission, coat disassembly is triggered by Sar1-GTP hydrolysis, that in absence of its GTPase activating protein (GAP) displays only a slow GTP hydrolysis activity (Antonny et al., 2001). Interestingly, Sec23 subunit suits as the GAP of Sar1 and its GAP activity is further enhanced by Sec13-31 recruitment indicating a feedback mechanism to temporally control and finally trigger coat disassembly after cargo has been selected and the vesicle budded (Sato, 2004).

### 4.2.8 ER-Golgi intermediate compartment and retrograde transport

After cargo has exited the ER at ERES in COPII-coated carriers, the vesicles are transported in mammalian cells along microtubules in a dynein-dependent manner to the ER-Golgi intermediate compartments (ERGIC) before they reach the *cis*-Golgi compartment (Brandizzi and Barlowe, 2013; Presley et al., 1997; Roghi and Allan, 1999). While past models suggested the ERGIC is a specialized ER (Sitia and Meldolesi, 1992) or *cis*-Golgi domain (Mellman and Simons, 1992), recent studies consider the ERGIC rather as an distinct compartment between

ER and *cis*-Golgi (Appenzeller-Herzog and Hauri, 2006; Brandizzi and Barlowe, 2013). The ERGIC that consists of dynamic and pleiomorphic vesicular and tubular structures serves as a hub to concentrate newly synthesized anterograde cargo, and to retrieve ER-resident cargo that is destined for COPI-dependent retrograde transport (Brandizzi and Barlowe, 2013). During retrograde transport, the heptameric COPI complex consisting of subunits ( $\alpha/\beta/\beta'/\epsilon/\gamma/\delta/\zeta$ ), captures and retrieves cargo in a similar manner as described before for COPII-dependent anterograde transport (Jackson, 2014). Similarly as COPII assembly through Sar1-GTP, COPI recruitment to the membrane is initiated by the small GTPase Arf1 that is activated by the membrane-bound ARF GEF Gea1 (Lee et al., 2004). GTP-bound Arf1 exposes an N-terminal amphipathic helix, that is in case of Arf1, capped by a myristoyl group and therefore is recruited to the membrane (Lee et al., 2004). The preassembled COPI coatomer complex is then recruited to Arf1-GTP and interacts with cargo. Cargo recognition by COPI is mediated by the well-known KDEL receptor that captures soluble cargo with an C-terminal KDEL-motif (Lewis and Pelham, 1990; Munro and Pelham, 1987). Furthermore, SNARE proteins are recognized by di-phenylalanine motifs (FFXX) while transmembrane proteins are captured by di-lysine (KKXX) motifs at their C-terminus (Jackson, 2014). After cargo recognition and capture, the COPI coat is polymerized leading to membrane curvature (Lee et al., 2004). Finally, Arf GTPase-activating protein (ARF GAP) stimulates Arf1 GTP-hydrolysis leading to its dissociation of the complex and ultimately to membrane fission (Lee et al., 2004).

### 4.3 Organization of membrane traffic and fusion

#### 4.3.1 Rab GTPases coordinate vesicle traffic

Within cells, membrane enclosed organelles and transport vesicles originate from different sources with unique properties. To maintain organelle and vesicle integrity, the protein family of Rab GTPases that consist of approx. 60 different members specific for distinct intracellular membranes, coordinate vesicle formation, transport, docking and fusion (Pfeffer and Aivazian, 2004; Stenmark, 2009). Rab GTPases possess a C-terminal prenylation modification that leads to their association with cellular membranes (Pfeffer and Aivazian, 2004). Dissociation from

membranes is facilitated by GDP-dissociation inhibitors (GDI) keeping a fraction of Rab proteins in the cytosol (Pfeffer and Aivazian, 2004). In addition, Rab GTPases belong to the group of small GTPases that are in literature often referred to as “molecular switches” since they are active when GTP-bound and inactive when GDP-bound (Stenmark, 2009). GTP binding, hence activation of the Rab GTPases is mediated by specific GEFs that leads to their association with downstream effector proteins (Pfeffer and Aivazian, 2004; Zerial and McBride, 2001). These effectors recruited to membrane-bound Rab GTPases fulfill a variety of functions including membrane tethering e.g. early endosome antigen1 (EEA1) is the effector of Rab5 and an elongated protein with a large coiled-coil domain and Rab5 binding sites at its C- and N-terminus (Simonsen et al., 1998; Zerial and McBride, 2001). In this way, EEA1 tethers early Rab5-positive endosomes together for subsequent fusion and endosomal maturation (Zerial and McBride, 2001). Furthermore, Rab GTPases are involved, albeit not fully essential during budding of COPII-coated vesicles. Rab5 specifically modulates clathrin-coated pits *in vivo* and required for clathrin-coated vesicle formation *in vitro* (Zerial and McBride, 2001). Rab GTPases also fulfill functions during vesicle motility to ensure specificity of the vesicle to their respective motors of the cytoskeleton (Stenmark, 2009). In fact, there has been studies showing actin motors of the Myosin V family to associate with transport vesicles in a Rab-dependent manner (Stenmark, 2009). In addition to actin motors, kinesins can also be effectors of Rab GTPases thereby controlling microtubule-dependent vesicular traffic (Stenmark, 2009). The kinesin motor KIF20A is the effector of the Golgi localizing RAB6, and therefore is required for plus-end-directed kinesin-dependent vesicular transport to the cell periphery (Echard et al., 1998; Stenmark, 2009). Finally, the last members of Rab effectors, soluble N-ethylmaleimide-sensitive factor attachment protein receptors or SNAREs are highly crucial not only for all vesicular fusion events in the secretory pathway but also during synaptic vesicle fusion in neuronal cells (Jahn and Scheller, 2006; Stenmark, 2009). Therefore, SNAREs will be described in greater detail in the next section.

### 4.3.2 SNAREs are key elements for membrane fusion

SNAREs drive all intracellular membrane fusion events from vesicles to organelles as well as homotypic fusion events as e.g. shown during early endosome maturation (Bonifacino and Glick, 2004; Jahn and Scheller, 2006). SNAREs are a large superfamily of proteins that mediate membrane fusion and contain a conserved SNARE motif, a membrane-anchor domain and a variable N-terminal domain (Jahn and Scheller, 2006). Historically, SNAREs were identified as two different sets of SNAREs that work on two opposing membranes. Therefore, they were functionally classified as v-SNAREs (vesicle-membrane) or t-SNAREs (target-membrane) (Figure 9) (Jahn and Scheller, 2006; Söllner et al., 1993).

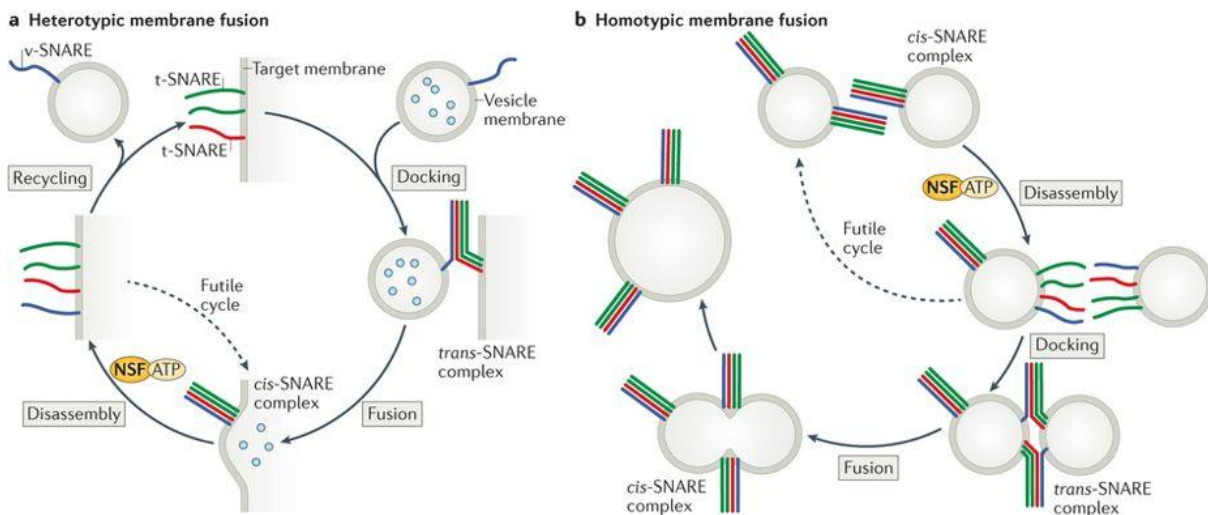


**Figure 9. Schematic cartoon of the SNARE mediated membrane fusion cycle and subsequent SNARE complex disassembly by NSF. (A)** Heterotypic membrane fusion is initiated by one v-SNARE in the vesicle membrane and three t-SNAREs at the target membrane that dock forming the zipper-like four helix bundle of the *trans*-SNARE complex that leads to membrane fusion and cargo release. After membrane fusion, the *cis*-SNARE complex is disassembled by NSF in an ATP-dependent manner and the v-SNARE is recycled back to transport vesicles for another round of membrane fusion. **(B)** In homotypic membrane e.g. during endosomal maturation the membranes of both vesicles contain all v-SNAREs and t-SNAREs leading to docking and fusion of the same vesicle species. Figure adapted from Baker and Hughson, 2016.

The unique structural feature of the SNARE domains allows two appropriate SNAREs to spontaneously form helical core complexes of high stability (Jahn and Scheller, 2006). During this process of heterotypic vesicle fusion, one v-SNARE in a vesicle associates with three t-SNAREs at the target membrane into a membrane-bridging *trans*-SNARE complex assembling to a intermolecular four-helix bundle with complementary SNARE motifs (Figure 9A) (Baker and Hughson, 2016). By contrast, during homotypic vesicle fusion, both vesicles contain all four SNAREs leading to assembly of the *trans*-SNARE complexes (Figure 9B) (Baker and Hughson, 2016). During this process, complex formation is initiated at the N-termini of the SNARE motifs and continues in a “zipper-like manner” to the C-termini thereby passing the energy barrier for membrane fusion (Jahn and Scheller, 2006). After membrane fusion and cargo release, the *trans*-SNARE complex is converted to a *cis*-SNARE complex in which all four SNAREs are associated in a four-helix bundle complex at the target membrane and need to be disassembled for a new cycle of SNARE assembly (Figure 9) (Baker and Hughson, 2016). Since the *trans*-SNARE complexes display low potential energy and are biologically inactive until their dissociation, *trans*-SNARE disassembly requires metabolic energy provided by N-ethylmaleimide-sensitive factor (NSF) (Block et al., 1988; Jahn and Scheller, 2006; Söllner et al., 1993). NSF is a hexameric member of the ATPases associated with various cellular activities (AAA+) protein family that are conserved ATPases often catalyzing reactions associated with conformational remodeling of their substrates such as unfolding or disaggregation (Hanson and Whiteheart, 2005). NSF interacts with the SNARE complexes through its soluble NSF attachment protein (SNAP) cofactors and disassembles the *trans*-SNARE complexes for another round of complex formation (Jahn and Scheller, 2006). While t-SNARE complexes are then ready to engage for another fusion reaction, the v-SNAREs require sorting and transport to the membranes where they originate to maintain vesicle fusion specificity (Figure 9) (Jahn and Scheller, 2006).

## 4.4 The Golgi complex

### 4.4.1 Discovery of the Golgi apparatus – a historical perspective

Camillo Golgi, an Italian biologist and physician, developed in 1873 a method called “the black reaction” that allowed for the first time the visualization of a single nerve cell within a histological sample (Figure 10) (Mazzarello et al., 2009). With this technique, Camillo Golgi could already contribute to the understanding on the structural organization of the nervous system and was awarded together with Ramon y Cajal “in recognition of their work on the structure of the nervous system” the Nobel Prize in Physiology or Medicine in 1906 (Mazzarello et al., 2009; NobelPrize.org, 2018). After continuous improvement of the black reaction, he described in 1898 an intracellular filamentous network and named the structure “apparato reticolare interno” or “internal reticular apparatus” (Figure 10B) (Golgi, 1989a, 1989b; Mazzarello et al., 2009).

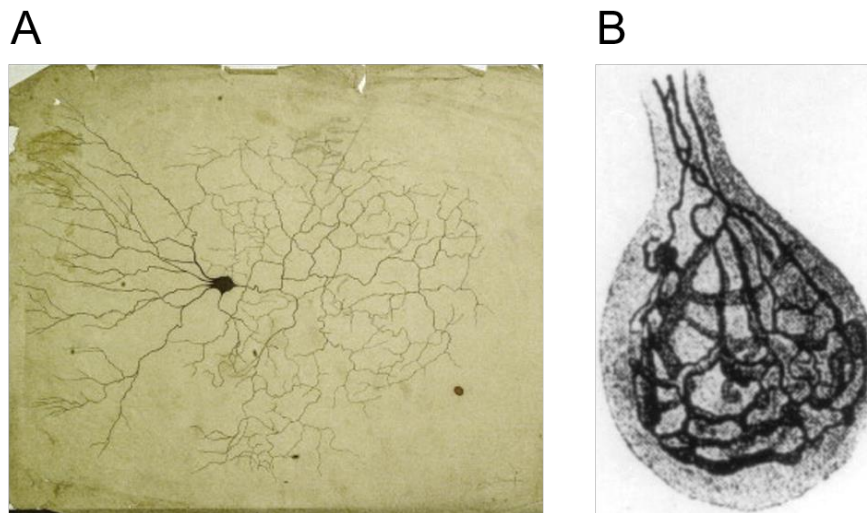


**Figure 10. Camillo Golgi - from structure and organization of the nervous system to the discovery of the Golgi apparatus. (A)** Drawings of Camillo Golgi showing Nerve cells stained with the black reaction. **(B)** First published illustration of the Golgi apparatus in the cell body of a Purkinje cell of the owl *Tyto alba*. Figures adapted from Golgi, 1989a; Mazzarello et al., 2009.

In the course of years, further advances in 3D-EM even allowed the analysis of the Golgi complex in z-sections in a series of tilt angles to reconstitute into 3D tomograms to visualize the structure of the Golgi that will be described in greater detail in the next section (Klumperman, 2011).

### 4.4.2 The structure of the Golgi complex

Over the past decades of research, the general structure and organization of the Golgi consists of several membrane stacks called cisternae (Klumperman, 2011). Depending on the cell type, Golgi complexes can harbor three to 20 membrane stacks, also called cisternae (Day et al., 2013). These cisternae can be divided in three distinct Golgi compartments: the *cis*-, the *medial*- and the *trans*-Golgi compartments (Figure 11) (Klumperman, 2011). Golgi cisternae are often polarized in the way that newly synthesized proteins arrive from the ERGIC to the *cis*-Golgi and exit the Golgi at the *trans*-face (Figure 11) (Day et al., 2013). While in some organisms such as baker's yeast *Saccharomyces cerevisiae* harbor individual Golgi stacks, in most vertebrate cells Golgi cisternae are laterally connected forming "a continuous Golgi ribbon" structure (Figure 11) (Day et al., 2013; Klumperman, 2011). The Golgi ribbon organization is tightly associated with the microtubule network as well as the actin cytoskeleton (Goud and Gleeson, 2010; Thyberg and Moskalewski, 1999). Within the cell, the Golgi is characteristically located in the perinuclear area (Klumperman, 2011). Interestingly, the Golgi complex displays at its cytoplasmic surface large coiled-coiled proteins that are referred to as "golgins" and function as tethers for incoming vesicles thereby contributing to the Golgi ribbon organization (Gillingham and Munro, 2016). Golgins form parallel homodimeric coiled-coil domains leading to a rod-like structure that can reach up to 300 nm in length (Gillingham and Munro, 2016). Importantly, golgins show specificity in their spatial localization within the Golgi complex as well as for incoming vesicles that they tether (Gillingham and Munro, 2016). The golgin GMAP-210 is anchored to the *cis*-Golgi and tethers with its GRIP-related Arf binding (GRAP) domain ER derived carriers (Gillingham and Munro, 2016; Wong and Munro, 2014).

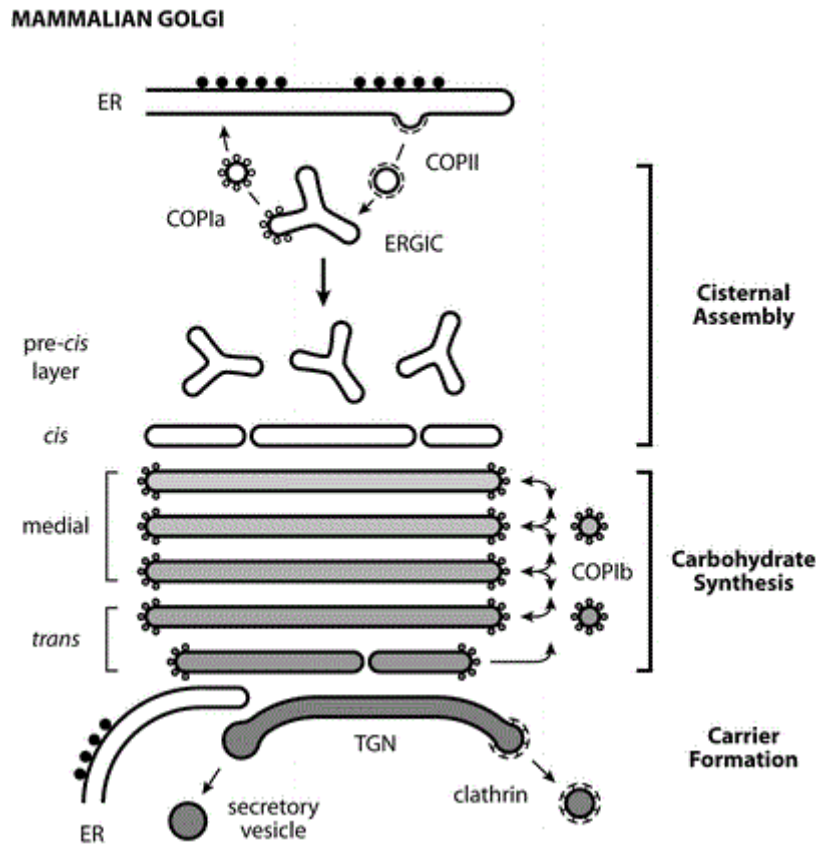


**Figure 11. The structural organization of the mammalian Golgi complex.** During cisternal assembly phase, COPII-coated carriers fuse homotypically to form ERGIC compartments while ER resident proteins are retrieved and transported back to the ER in COPI-coated vesicles. ERGIC intermediates form a *pre-cis* layer. Subsequent fusion of ERGIC intermediates form the *cis*-Golgi cisternae. The *medial*- and *trans*-Golgi cisternae are required for post-translational modifications including glycosylation of proteins and lipids. Finally, the *trans*-Golgi network (TGN) serves as a sorting hub for carrier formation of either secretory vesicles or clathrin-coated transport vesicles. Figure adapted from Day et al., 2013.

By contrast, other golgins such as giantin or GCC88 capture, intra-Golgi vesicles at the Golgi rims or endosomal derived transport vesicles at the *trans*-Golgi, respectively (Gillingham and Munro, 2016). Given the complex and unique structure of the Golgi organelle, in the next section we will focus on the functions that are associated with the Golgi complex.

#### 4.4.3 Intra-Golgi transport – a heated debate

Soon after the confirmation of the existence of the Golgi complex within cells, the process of protein transport associated with the Golgi complex was discovered (Jamieson and Palade, 1967; Mironov et al., 2013). Many important principles of vesicular transport to the Golgi that have also been covered extensively in this introduction, are well established (Emr et al., 2009). Newly synthesized proteins are transported from the ER to the Golgi in COPII coated vesicles, while retrograde transport is mediated in COPI vesicles. However, the involvement of COPI vesicles for forward movement has still not been clarified (Emr et al., 2009; Rabouille and Klumperman, 2005). Along this line, the mode of intra-Golgi transport, especially the vesicular transport and cisternal maturation models, are subject of a long-lasting controversial debate within the field of membrane trafficking (Figure 12) (Elsner et al., 2003; Emr et al., 2009; Glick, 2000; Marsh and Howell, 2002; Pelham and Rothman, 2000; Warren and Malhotra, 1998). Furthermore, the favored hypothesized models are not only restricted to the vesicular transport and cisternal maturation model but rather show a variety of additional models that try to explain intra-Golgi transport and have been described in detail elsewhere (Glick and Luini, 2011). For the scope of this thesis, I will focus on the two main models in the literature: While in the vesicular transport model COPI vesicles carry cargo anterograde from one cisternae to the next, the cisternal maturation model postulates that COPI vesicles move retrograde to transport Golgi enzymes to their specific localization while new cisternae form at the *cis*-face and mature forward through the stacks and shed at the *trans*-Golgi (Figure 12) (Emr et al., 2009; Rabouille and Klumperman, 2005). To cast light into this debate, a group of leading researchers of the membrane trafficking field gathered in 2009 to discuss key questions including the mode of intra-Golgi transport (Emr et al., 2009). Based on published data and critical discussion, the researchers came to the conclusion that it is unclear whether COPI vesicles might carry anterograde cargo making the cisternal maturation model the favored model (Figure 12B) (Emr et al., 2009; Glick and Malhotra, 1998). Past studies of mammalian procollagen I transport support the cisternal maturation model (Emr et al., 2009). Procollagen I folds in the ER into “rod-like” trimers and further assembles in the Golgi into large, stable aggregates of ~300 nm x 150 nm (Beck et al., 1996; Emr et al., 2009).

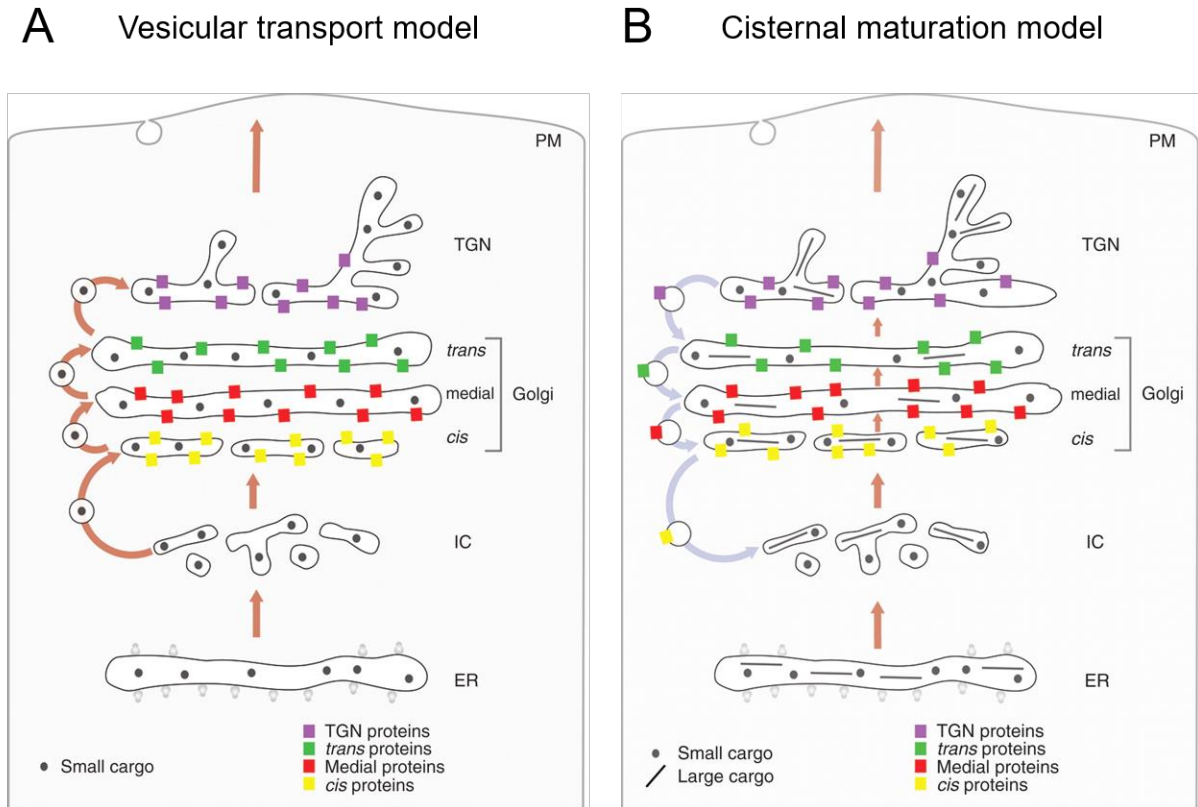


**Figure 12. Two possible modes of intra-Golgi transport of cargo proteins. (A)** The vesicular transport model postulates that COPI vesicles transport cargo and Golgi enzymes anterograde between stable cisternae. **(B)** The cisternal maturation model hypothesizes that COPI vesicles transport cargo and enzymes retrograde while individual cisternae mature forward from the *cis*-face to the *trans*-Golgi. Figure adapted from Glick and Luini, 2011.

Synchronous release experiments combined with 3D-EM demonstrate that procollagen I passes the *cis*-Golgi to the *trans*-Golgi without leaving the lumen of cisternae suggesting anterograde intra-Golgi transport of cargo without the requirement of transport vesicles (Bonfanti et al., 1998; Emr et al., 2009). However, whether or not smaller cargos follow the same route requires further investigation (Emr et al., 2009). Furthermore, cisternal maturation was directly visualized by using green or red labeled early or late Golgi markers in *Saccharomyces cerevisiae* that has no continuous Golgi-ribbon rather shows individual Golgi stacks dispersed throughout the cell (Losev et al., 2006; Matsuura-Tokita et al., 2006). In conclusion, the cisternal maturation model has proven to be to date the most suitable model to describe intra-Golgi transport of

cargo and enzymes. Future advances in live-cell and super-resolution microscopy with high spatial and temporal resolutions will help towards a better understanding of intra-Golgi transport. But what are additional functions of the Golgi complex besides protein transport?

### 4.4.4 Post-translational modifications in the Golgi

As newly synthesized secretory proteins traverse through the Golgi stacks, most of the cargo is modified by post-translational modifications (PTM) (Potelle et al., 2015). Therefore, the Golgi is known to be the main contributor to PTMs of lipids and proteins (Potelle et al., 2015). There are many different PTMs associated with the Golgi including glycosylation, acetylation, sulfation, methylation, palmitoylation, phosphorylation and proteolytic cleavage (Potelle et al., 2015). Importantly, defects in Golgi mediated PTMs have been linked to human diseases (Potelle et al., 2015). For the scope of this introduction, the focus of PTMs in the Golgi will be glycosylation since it is one of the major and to date best described Golgi PTMs. Golgi membranes are abundant in glycosyltransferases (GT), glycosidases, and nucleotide sugar transporters that localize specifically from *cis*- to *trans*-Golgi (Stanley, 2011). After initial glycosylation in the ER, these enzymes function in concert to complete the synthesis of the glycans that can vary in their complexity from the addition of a single sugar to highly complex polymers of more than 200 moieties (Stanley, 2011). Therefore, the completion of glycan structures of glycoproteins, glycosphingolipids, proteoglycans, and GPI-anchors is completed as these proteins and lipids passage through the Golgi complex (Stanley, 2011). The general mechanisms by which a GT transfers a sugar to a glycoprotein requires first a high energy nucleotide sugar that is synthesized in the cytoplasm and is imported by nucleotide sugar transporters (Berninsone and Hirschberg, 2000; Stanley, 2011). The specific sugars are then added to the glycoproteins depending on the GT localization to *cis*-, *medial*-, or *trans*-Golgi while other sugars are removed by glucosidases leading to heterologous glycan structures even at single glycosylation sites (Stanley, 2011). Given the complexity of glycosylation of proteins, undoubtedly the functions associated with glycosylation must be important for cellular homeostasis. Indeed, glycans have structural and modulatory functions by their protective, stabilizing and organization abilities e.g. the glycocalyx covering the surface of all eukaryotic

cells (Varki and Gagneux, 2015). Other proteoglycans that are matrix molecules are important for tissue structure and integrity (Varki and Gagneux, 2015; Varki and Lowe, 2009). Glycan structures can also be indispensable for protein-protein interactions such as the well-known role of mannose-6-phosphate modification during trafficking of lysosomal enzymes to lysosomes that will be discussed in more detail below (Varki and Gagneux, 2015). Furthermore, glycans contribute to cell signaling since O-glycosylation on EGF domain repeats of Notch have been shown to be required for Notch signaling (Acar et al., 2008; Sethi et al., 2010; Stanley, 2011). Conclusively, the Golgi complex is the main hub for PTMs that convey glycoproteins and glycolipids their modifications they require to fulfill a variety of cellular functions including structural and modulatory functions, protein-protein interactions and cell signaling.

### 4.5 Lipid metabolism in membrane traffic pathways

Up to this point, one crucial aspect of membrane trafficking pathways was neglected and will become important for the understanding of the key findings of this thesis. Importantly, not only protein machineries that control key steps of the secretory pathway including co-translational synthesis of secretory proteins, their quality control, sorting into coated transport vesicles but also the lipid environment of each compartment of the secretory pathway plays an important role in membrane traffic. Naturally, lipids are the main components of cellular membranes and display high diversity in their structure and distribution (Figure 13) (Harayama and Riezman, 2018). They function in a variety of cellular processes such as structural membrane components (van Meer et al., 2008), serve as energy sources (Nakamura et al., 2014), function as signaling molecules (Shimizu, 2009), recruit proteins (Saliba et al., 2015), and are substrates for lipid modifications of proteins (Harayama and Riezman, 2018; Resh, 2016). Members of the major membrane lipids consist of glycerophospholipids (GPLs), sphingolipids and sterols that is mainly cholesterol in mammals (Figure 13) (Harayama and Riezman, 2018). The chemical diversity of lipids results from fatty acids that vary in chain length, number and position of double bonds they carry as well as their head groups (Harayama and Riezman, 2018).

## 4 Introduction

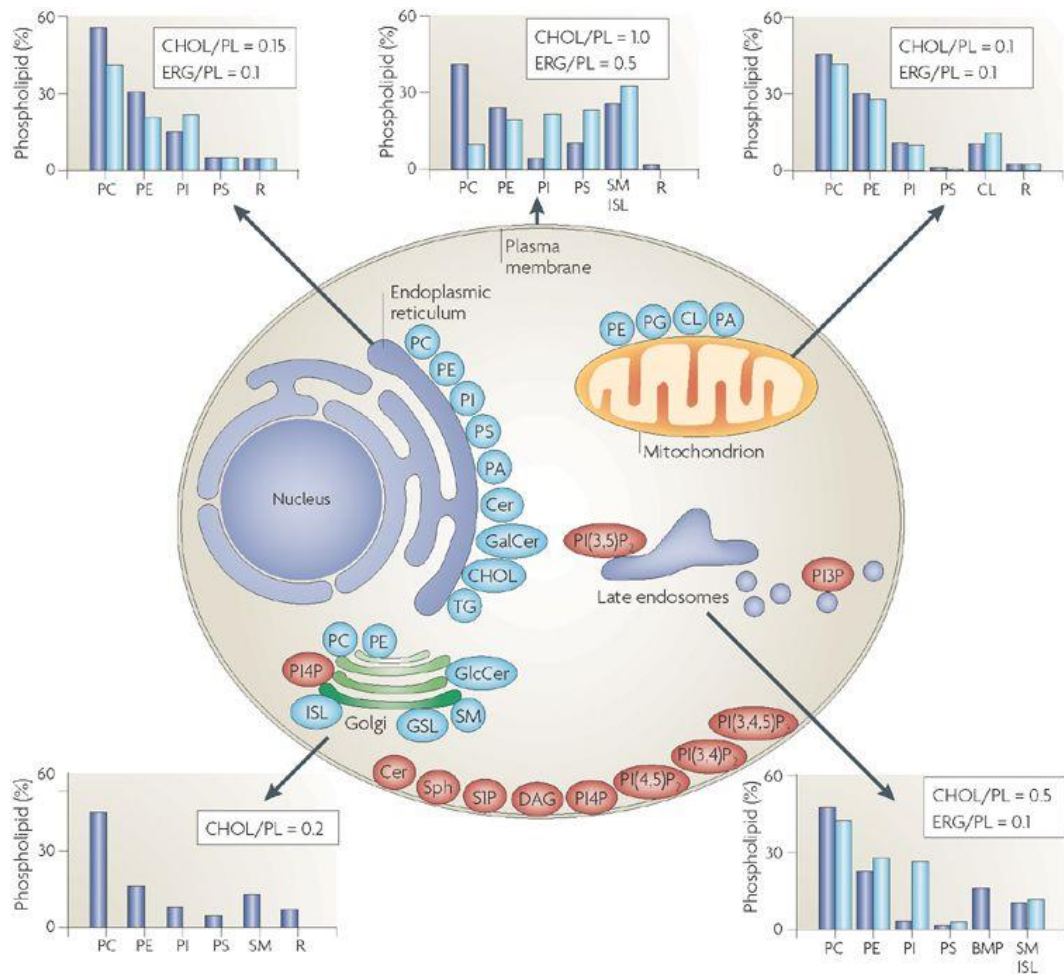


**Figure 13. Cellular distribution of lipid types that are incorporated into membranes.** The graphs for each membrane compartments display the relative lipid composition compared to total phospholipids in mammals (blue) and yeast (light blue). Lipids are highlighted in blue at their major sites of lipid synthesis, while red labeled lipids are involved in organelle recognition and signaling. Glycerophospholipids phosphatidylcholine (PC), phosphatidylethanolamine (PE), phosphatidylinositol (PI), phosphatidylserine (PS) and phosphatidic acid (PA) are assembled in the ER. In addition, the ER synthesizes ceramide (Cer), galactosylceramide (GalCer) and cholesterol and is involved in triacylglycerol (TG) synthesis. The Golgi is involved in the synthesis of sphingomyelin (SM), complex glycosphingolipids (GSLs) and yeast inositol sphingolipid (ISL) synthesis. Mitochondria can synthesize autonomously about 45% of their phospholipids PE, PA and cardiolipin (CL). Further lipid labels: PG, phosphatidylglycerol; PI(3,5)P<sub>2</sub>, phosphatidylinositol-(3,5)-bisphosphate; PI(4,5)P<sub>2</sub>, phosphatidylinositol-(4,5)-bisphosphate; PI(3,4,5)P<sub>3</sub>, phosphatidylinositol-(3,4,5)-trisphosphate; PI4P, phosphatidylinositol-4-phosphate; S1P, sphingosine-1-phosphate; Sph, sphingosine; DAG, diacylglycerol. Figure adapted from van Meer et al., 2008.

For instance, phospholipids are amphiphilic with a hydrophilic head group linked to a hydrophobic tail that favors the assembly of a phospholipid-containing bilayer (De Craene et al., 2017). Membranes are mainly composed of five phospholipids including phosphatidylcholine (PC), phosphatidylethanolamine (PE), phosphatidylserine (PS), phosphatidylinositol (PtdIns) that are synthesized in the ER, which constitutes the main lipid biosynthetic organelle (Figure 13) (van Meer et al., 2008). In fact, the ER produces the most of the structural phospholipids and cholesterol and additionally is involved in triacylglycerol synthesis that is required for fatty acid metabolism (Figure 13) (van Meer et al., 2008). Another important lipid component of cellular membranes is sphingomyelin (SM), which is synthesized in the Golgi and transported to the plasma membrane and contributes to the resistance of the plasma membrane towards mechanical stress (Figure 13) (van Meer et al., 2008). Furthermore, sterols such as cholesterol in mammals known to modulate membrane fluidity are synthesized in the ER (Figure 13) (De Craene et al., 2017). PtdIns generate the phosphoinositides (PIs) by head group phosphorylation at various positions of the inositol moiety and are key players during membrane trafficking (De Craene et al., 2017) as well as signaling pathways (Payraastre et al., 2001) (Figure 13). Therefore, the next section will focus on the role of PIs.

### 4.5.1 Phosphoinositides provide membrane organelle identity

PtdIns are the precursor of PIs and are lipids that are involved in membrane traffic between different cellular compartments (Di Paolo and De Camilli, 2006). Furthermore, they function during cytoskeleton organization (Martin, 1998), and cell signaling (Berridge and Irvine, 1989). Structurally, PtdIns consist of a glycerol that is esterified at its SN1 and SN2 positions by two fatty acid chains and connected via an phosphate group in position SN3 to an inositol ring (Figure 14A) (De Craene et al., 2017). Importantly, the inositol ring in PtdIns can be phosphorylated at positions D3, D4, and D5 leading to seven possible phosphorylated configurations thereby generating the following PIs: Phosphatidylinositol 3-phosphate (PI3P), PI4P, PI5P, PI3,4P<sub>2</sub>, PI3,5P<sub>2</sub>, PI4,5P<sub>2</sub> and PI3,4,5P<sub>3</sub> (Figure 14) (De Craene et al., 2017). PtdIns are synthesized in the ER and can traffic by vesicular transport to different membrane compartments including the Golgi, plasma membrane, early and late endosomes (Figure 14B)

(Di Paolo and De Camilli, 2006). At their different membrane locations, PIs are then specifically phosphorylated and dephosphorylated by PI kinases and phosphatases generating a PI-based code to define organelle identity (Di Paolo and De Camilli, 2006). During this process, the phosphoinositides cooperate with Rab-GTPases by recruiting GAPs and GEFs to membranes by the presence of phosphoinositide-binding modules (Di Paolo and De Camilli, 2006). Furthermore, several PI kinases and IP phosphatases are effectors of Rab-GTPases thus regulating the dynamic PI conversion by positive or negative feedback loops (Honda et al., 1999; Shin et al., 2005). Finally, membrane and GTP-bound active Rab-GTPases act together with PIs as co-receptors to increase recruitment affinity of effectors thereby controlling organelle identity (Behnia and Munro, 2005; Di Paolo and De Camilli, 2006). As an example of this general mode of action of PIs during membrane traffic serves PI3P that has crucial roles during endocytosis and endosomal maturation (Odorizzi et al., 2000).

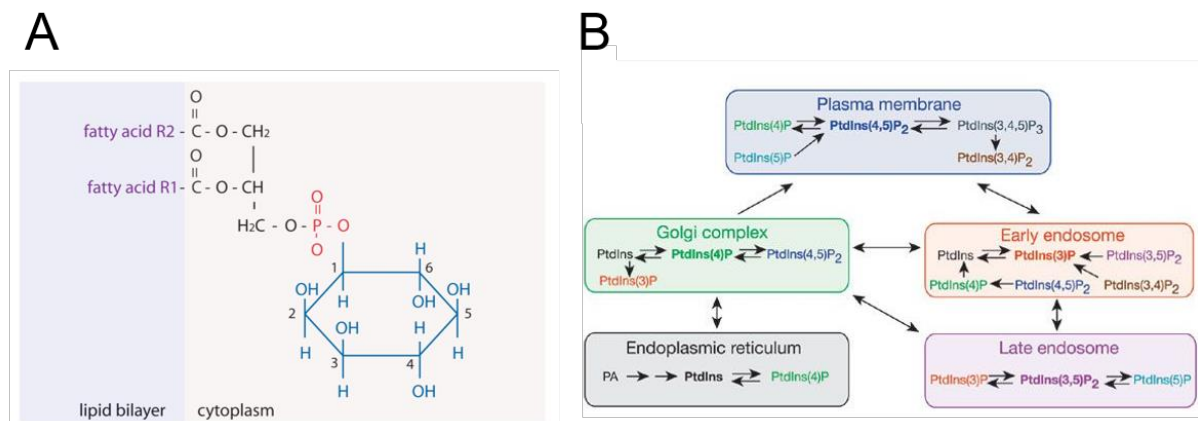


**Figure 14. Structure and dynamic organization of phosphoinositides.** (A) The chemical structure of PIs that consist of a glycerol that is esterified at its SN1 and SN2 positions by two fatty acid chains and is connected via a phosphate group in position SN3 to an inositol ring. The inositol ring can be phosphorylated at positions 3, 4 and 5 leading to seven possible configurations. (B) Synthesis of PtdIns is mediated from phosphatidic acid (PA) or PIs in the ER. PtdIns and PIs can then traffic to other membrane compartments by vesicular transport or cytosolic PtdIns transfer proteins. PtdIns can dynamically be phosphorylated or dephosphorylated highlighted by arrows to different PI species with specificity for different membrane compartments. Figure A adapted from De Craene et al., 2017. Figure B adapted from Di Paolo and De Camilli, 2006.

PI3P binding modules are FYVE and PX domains that are found in EEA1 that is a Rab5 effector and required for homotypic tethering of endosomes (Di Paolo and De Camilli, 2006; Simonsen et al., 1998). Furthermore, members of the endosomal sorting complexes required for transport (ESCRT) 0 and II are recruited to endosomes by interacting with PI3P to sort and sequester ubiquitinated membrane proteins into endosomal intraluminal vesicles for their subsequent degradation (Alonso Y Adell et al., 2016; Mao et al., 2000; Raiborg et al., 2001). PIs also function during cytoskeleton organization promoting cellular motility (Di Paolo and De Camilli, 2006; Pollard and Borisy, 2003). These examples highlight the importance of PtdIns and PI for organelle identity, membrane traffic, signaling and cytoskeleton organization. In the next section, the focus will lie on another important lipid species during membrane traffic pathways, the sphingolipid metabolism.

### 4.5.2 Sphingolipid metabolism and traffic

Sphingolipid metabolism plays an important role for understanding of the key results of this thesis. Therefore, the focus in this section will lie on sphingolipid metabolism and transport to the Golgi and beyond as well as sphingolipid associated functions and diseases. Similar to PtdIns and PIs, sphingolipids form a family of bioactive lipids that include sphingosine, ceramide, sphingosine-1-phosphate (S1P) and ceramide-1-phosphate with distinct subcellular localizations (Hannun and Obeid, 2017). Sphingolipids have effects on protein kinases such as the protein kinase C (PKC) leading to the regulation of diverse cellular functions like actin cytoskeleton dynamics, endocytosis, the cell cycle and apoptosis (Hannun and Obeid, 2008; Smith et al., 2000). In addition, sphingolipids contribute with their physical properties to plasma membrane stress resistance (van Meer et al., 2008). Disorders in the sphingolipid metabolic pathway have been implicated in neurodegenerative processes such as Niemann-Pick disease (Zhou et al., 2016), metabolic disorders and various cancers (Hannun and Obeid, 2017).

#### 4.5.2.1 Structure and metabolic pathway of sphingolipids

Structurally, sphingolipids differ from glycerophospholipids as they possess a hydrophobic sphingoid base backbone, an N-acyl chain and a head group that defines the sphingolipid name (Figure 15A) (Harayama and Riezman, 2018). Furthermore, sphingolipids can reach chemical diversity by their variety in the length and type of the sphingoid base as well as its N-acyl chain type and hydroxylation status (Figure 15A) (Harayama and Riezman, 2018). *De novo* synthesis of sphingolipids starts with the amino acid serine and palmitate which condense to 3-keto-dihydrosphingosine (Linn et al., 2001) and further reduced to dihydrosphingosine that is acylated by a ceramide-synthase (CerS) generating dihydroceramide (Figure 15B) (Hannun and Obeid, 2008; Pewzner-Jung et al., 2006). Importantly, there are six mammalian CerS isoforms showing different specificity for fatty acyl-CoA chain length as their substrates (Wegner et al., 2016). This feature increases the structural variability of subsequent sphingolipid metabolic products dramatically (Wegner et al., 2016). Dihydroceramide is subsequently desaturated to ceramide (Figure 15B) (Causeret et al., 2000). Ceramide serves as a metabolic hub for subsequent sphingolipid biosynthesis. Phosphorylation by ceramide kinase generates ceramide-1-phosphate (Figure 15B) (Wijesinghe et al., 2005). Glycosylation of ceramide is mediated by glucosyl or galactosyl ceramide synthases and subsequently to glycosphingolipids with high complexity (Figure 15B) (Raas-Rothschild et al., 2004). Furthermore, SM synthase (SMS) can transfer a phosphocholine head group from a phosphatidylcholine to ceramide generating sphingomyelin and diacylglycerol (DAG) from PC (Gulbins and Petrache, 2013; Tafesse et al., 2013). By contrast, breakdown of SM to ceramide is catalyzed by sphingomyelinases (SMases) including acid SMase, neutral SMase and alkaline SMase (Hannun and Obeid, 2008). Defects in SMases results in accumulation of SM and leads to severe neurological disorders such as Niemann-Pick disease type A, major depression and Alzheimer's disease (Ong et al., 2015). Ceramide can be broken down to sphingosine by ceramidases. Sphingosine can be recycled back into sphingolipid pathways, or it can be phosphorylated to (S1P) that can be irreversibly cleaved by S1P lyase generating ethanolamine and hexadecanal (Bandhuvula and Saba, 2007; Gulbins and Petrache, 2013; Hannun and Obeid, 2008).

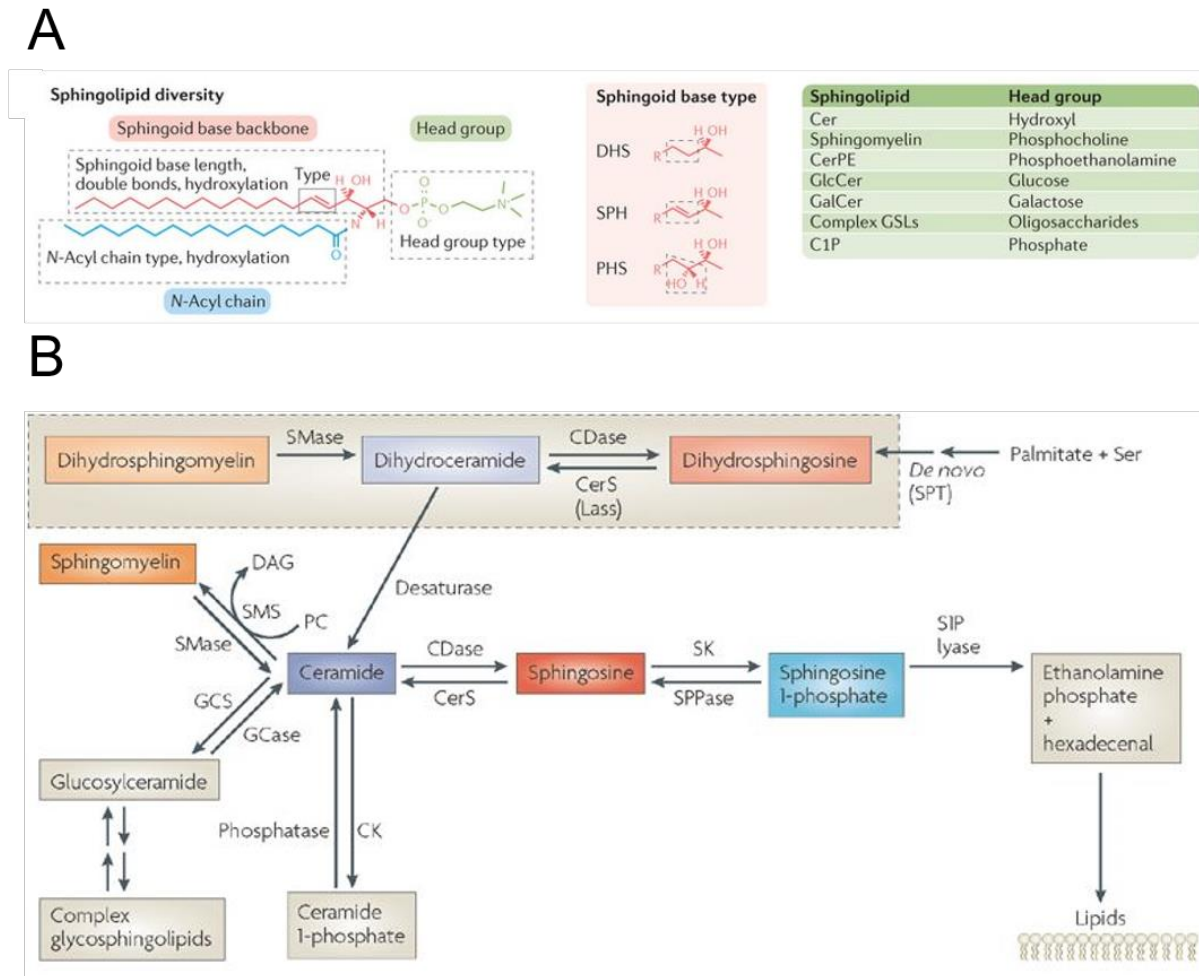


**Figure 15. Structural diversity and metabolism pathway of bioactive sphingolipids.** (A) Structurally, sphingolipids consist of a hydrophobic sphingoid base backbone, a N-acyl chain and a head group that defines the sphingolipid name. Structural diversity is achieved by N-acyl chain hydroxylation as well as sphingoid base type hydroxylation and saturation. (B) *De novo* sphingolipid metabolism starts with palmitate and the amino acid serine that is in two steps metabolized to dihydrosphingosine, dihydroceramide and finally to ceramide. Ceramide builds the center of sphingolipid metabolism and can be metabolized to other bioactive sphingolipids including sphingomyelin, sphingosine derivatives, ceramide 1-phosphate, glucosylceramide and complex glycosphingolipids. The enzymes involved during sphingolipid metabolism are indicated below and above the arrows. Figure A was adapted from Harayama and Riezman, 2018. Figure B adapted from Hannun and Obeid, 2008.

#### 4.5.2.2 Vesicular and non-vesicular transport of sphingolipids

Sphingolipids display distinct subcellular localization. Naturally, due to their hydrophobicity, sphingolipids will reside in compartments of their origin unless active transport mechanisms transfer them to another compartment (Hannun and Obeid, 2017). In fact, specific non-vesicular transporters have been identified in the past for sphingolipids including phosphatidylinositol-four-phosphate adaptor protein 2 (FAPP2) that is required for glucosylceramide (GlcCer) transport between Golgi cisternae (Figure 16C) (Hannun and Obeid, 2017). C1P transfer protein (CPTP) facilitates the transport of ceramide-1-phosphate (C1P) from the Golgi to the plasma membrane in a non-vesicular mechanism (Figure 16D) (Simanshu et al., 2013). Protein spinster homologue 2 (SPNS2) is involved in sphingosine-1-phosphate (S1P) flipping at the plasma membrane thereby stimulating G protein coupled receptors (GPCRs) such as S1P receptors (S1PR1-5) that mediate downstream signaling including proliferation, migration and survival (Figure 16E) (Hannun and Obeid, 2017; Nagahashi et al., 2014). Important for the understanding of the sphingomyelin pathway is to assess how ceramide is transported from the ER to the Golgi where it is further metabolized. Most ceramides are generated in the ER. Importantly, vesicular ceramide transport is coupled to the synthesis of glucosylceramide (Figure 16A) (Funato and Riezman, 2001; Hannun and Obeid, 2017). Alternatively, ceramides are captured by ceramide transfer protein (CERT) and delivered by membrane contact sites in a non-vesicular manner to the Golgi complex (Figure 16B) (Hanada et al., 2003; Hannun and Obeid, 2008; Tagaya and Simmen, 2017). Cytosolic CERT associates to the ER by interacting VAMP-associated Protein (VAP) that is an integral membrane protein localizing to the ER (Figure 16B) (Kawano et al., 2006; Kumagai et al., 2014). CERT then binds to ceramide with its START domain and forms membrane contact sites with the Golgi complex by interacting with PI4P through its PH domain (Hanada, 2017). After established membrane contact sites, CERT facilitates the intermembrane transfer of ceramide to the Golgi complex (Hanada, 2017). This process describes a unique mechanism of non-vesicular lipid transfer and studies suggested similar mechanisms for many other lipid species (Hanada, 2017). However, for the scope of this thesis we will further focus on SM traffic from the Golgi to the PM.

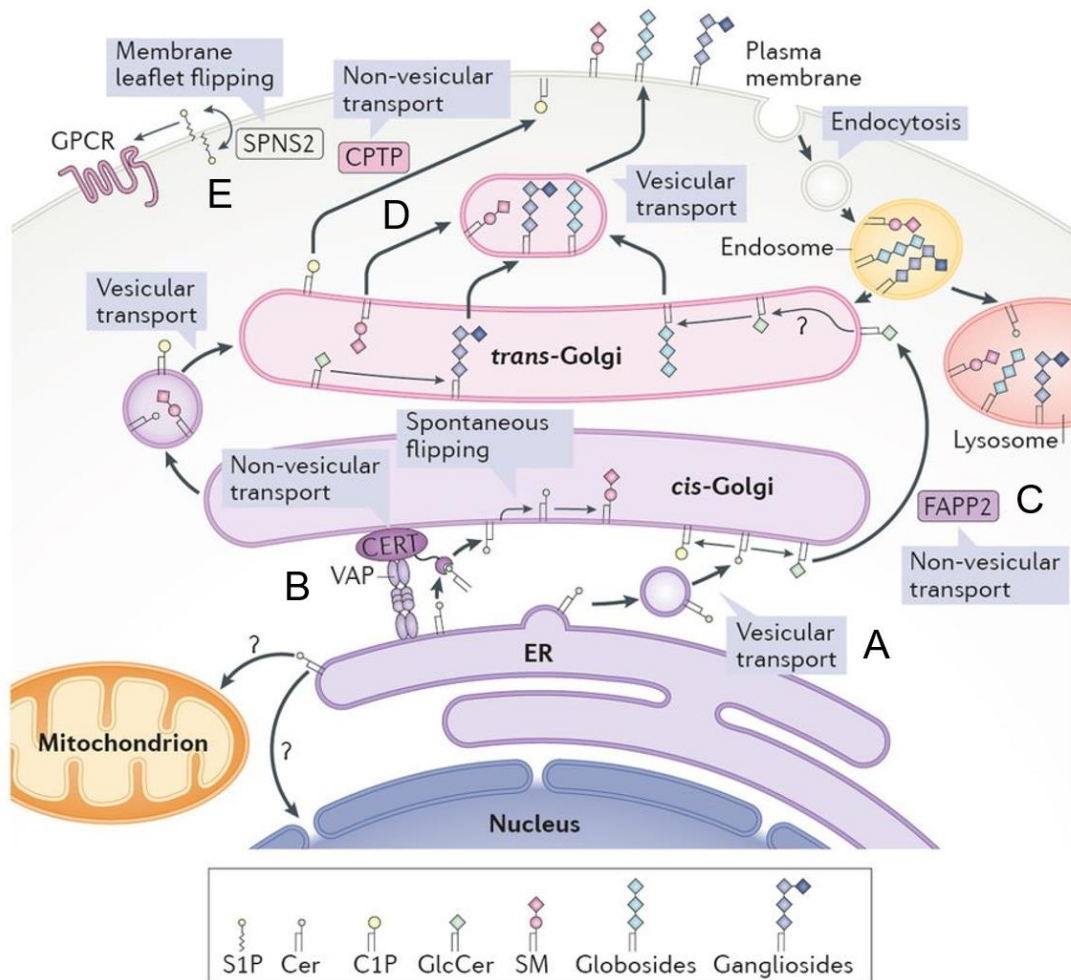


**Figure 16. Vesicular and non-vesicular transport pathways of bioactive sphingolipids.** (A) Vesicular Ceramide transport starts with Ceramide synthesis in the ER. Ceramide is then transported in vesicles to the Golgi where it is exclusively coupled to glucosylceramide synthesis. (B) Non-vesicular Ceramide transport is coupled to sphingomyelin synthesis. Ceramide is transported to the Golgi by ceramide transfer protein (CERT) and VAP by forming membrane contact sites. At the TGN synthesized sphingomyelin is then delivered by vesicular transport in distinct secretory vesicles to the plasma membrane. (C) Transfer protein phosphatidylinositol-four-phosphate adaptor protein 2 (FAPP2) mediates glucosylceramide (GlcCer) transport. (D) Ceramide-1-phosphate (C1P) requires C1P transfer protein (CPTP) for non-vesicular translocation. (E) Protein spinster homologue 2 (SPNS2) is involved in lipid flipping of sphingosine-1-phosphate (S1P) at the plasma membrane. Figure adapted from Hannun and Obeid, 2017.

### 4.5.2.3 Sphingomyelin transport to the plasma membrane

Sphingomyelin is the major sphingolipid in cells and forms in mammals about 2-15% of total tissue phospholipids depending on the tissue analyzed (Koval and Pagano, 1991). Previous studies have shown that depending on cell types 40-90% of cellular sphingomyelin is accessible to exogenous SMases indicating that the majority of sphingomyelin is localized in the PM (Koval and Pagano, 1991). This was further confirmed by subcellular fractionation studies of human fibroblasts estimated 90% of sphingomyelin to be in the PM (Koval and Pagano, 1991). But how is sphingomyelin from the location of its synthesis in the TGN transported to the PM? Analyzing lipid sorting in the TGN is experimentally challenging since visualization of distinct lipid species are technically not feasible (Deng et al., 2016). To analyze and visualize sphingomyelin transport, Christopher Burd's laboratory developed a protein encoding biosensor for sphingomyelin derived from a marine sea anemone *Actinia equina* (Athanasiadis et al., 2001; Deng et al., 2016; Hong et al., 2002; Tanaka et al., 2015). In its wild type version, the biosensor called Equinatoxin II forms cytolytic pores in membranes that contain sphingomyelin (Črnigoj Kristan et al., 2009). Therefore, Equinatoxin II was engineered to a non-toxic sphingomyelin-specific variant "EQ-SM" by introducing a point mutation that stabilizes EQ-SM in a membrane-bound state before the pore formation occurs (Deng et al., 2016; Gutiérrez-Aguirre et al., 2004). By using liposome sedimentation assays and immunofluorescence assays, Deng et al. could show that the EQ-SM probe shows specific binding to sphingomyelin without cytotoxicity (Deng et al., 2016). Furthermore, by using live cell total internal reflection (TIRF) microscopy, they found that fluorescently labeled EQ-SM carriers are sorted and delivered to the plasma membrane in a subset of Golgi derived vesicles that are also enriched in a GPI-anchored model cargo protein consisting of a SP, a fluorescent protein and a GPI acceptor site (Deng et al., 2016). By contrast, EQ-SM was reduced in secretory vesicles that transport the integral membrane protein CD8 $\alpha$  indicating a specific transport pathway for sphingomyelin-rich carriers (Figure 16) (Deng et al., 2016). Along this line, previous studies suggested that disruption of sphingomyelin organization at the TGN leads to impaired vesicle biogenesis as well as defective enzymatic functional domains (Duran et al., 2012; van Galen et al., 2014). Furthermore, sphingomyelin synthesis perturbation leads to

defects in glycosylation, secretory carrier formation and protein secretion (Tafesse et al., 2013; Wakana et al., 2015). However, to date the mechanistic link between sphingolipid metabolism and secretory protein sorting and secretion remains elusive.

### 4.6 Cargo sorting in the *trans*-Golgi network

The TGN consists of tubular membranes emerging from the *trans*-face of the Golgi complex and is well renowned among biologists as the major sorting station of lipids and proteins within cells (Griffiths and Simons, 1986). Newly synthesized lipids and proteins that arrive from previous Golgi compartments are sorted in the TGN into distinct carriers for transport to their destinations (Figure 17) (De Matteis and Luini, 2008). These destinations include the apical PM, the basolateral PM, endosomal and lysosomal compartments as well as secretory storage granules that are specialized compartments in secretory cells (De Matteis and Luini, 2008). Advances over the past years in EM tomography and cryofixation suggested a highly dynamic TGN structure forming post-TGN carriers with pleomorphic tubular-vesicular structures that can originate from the *trans*-Golgi or two adjacent cisternae (Anitei and Hoflack, 2011; Ladinsky et al., 1999; Mogelvang et al., 2004). Given the structure of the TGN, the question about its function arises: How proteins are sorted into distinct transport carriers? There are many different molecular mechanisms how cargo proteins destined for distinct cellular locations can be segregated in the TGN and sorted into specific transport vesicles (Figure 17). In the following sections, the principal mechanisms that were described in the past will be outlined and yet open questions regarding cargo sorting in the TGN will be highlighted.

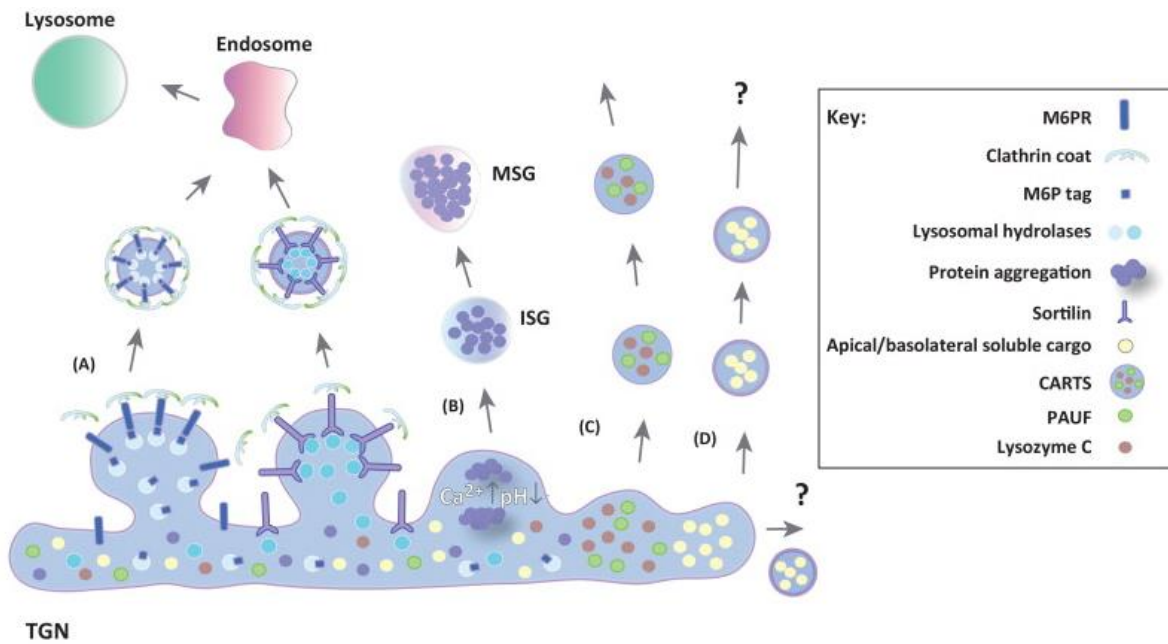


**Figure 17. Diverse cargo sorting pathways at the TGN ensure transport of proteins to their destined locations.** (A) Transmembrane proteins are sorted by adaptor proteins that recruit clathrin lattices that promote clathrin-coated vesicle formation for transport to endolysosomes. Soluble lysosomal hydrolases are captured through their mannose-6-phosphate (M6P) modification by M6P receptor (MPR) or by sortilin in a MPR-independent manner and are sorted to clathrin-coated vesicles for transport to lysosomes. (B) In specialized secretory cells, sorting of granins into secretory storage granules (SGs) is facilitated by their aggregation at high  $\text{Ca}^{2+}$  and low pH environments. (C) The sorting mechanisms of other soluble cargos that are constitutively secreted such as Lysozyme C (LyzC) (D) as well as sorting of apical and basolateral cargo are still poorly understood. Figure adapted from Kienzle and von Blume, 2014.

#### 4.6.1 Sorting of GPI-anchored proteins

GPI-anchored proteins are modified with a glycan backbone that is further acylated in the ER and attached to the C-terminus of newly synthesized proteins that carry a cleavable GPI attachment sites (Muñiz and Zurzolo, 2014). GPI attachment sites are referred to as  $\omega$ -sites, which start with three short chained amino acids followed by a unstructured linker sequence and a hydrophobic c-terminal signal sequence (Mayor and Riezman, 2004). The GPI associates with the attachment site by an amide linkage between the ethanolamine of the GPI and the

accessible carboxyl group after cleavage of the  $\omega$ -site (Mayor and Riezman, 2004). GPI modifications display high variability in side chains and lipid moieties and are crucial for the transport as well as the function of modified proteins (Mayor and Riezman, 2004; Muñiz and Zurzolo, 2014). Since GPI-anchored proteins do not contain cytosolic tails, they cannot directly interact with coat proteins to promote their sorting (Mayor and Riezman, 2004). Therefore, past studies suggested that sorting of GPI-anchored proteins and their transport to the apical surface in epithelial cells depends on their insertion into sphingolipid- and cholesterol-rich microdomains that acts as a sorting platform at the TGN (Muñiz and Zurzolo, 2014; Simons and Ikonen, 1997). These findings are in line with recent studies showing GPI-anchored proteins to be sorted at the TGN and secreted in sphingomyelin-rich secretory vesicles in HeLa cells (Deng et al., 2016). Due to their high lipid content, these lipid microdomains were identified to be detergent-resistant (Brown and Rose, 1992) leading over the years to the lipid-raft hypothesis (Simons and Ikonen, 1997; Simons and Van Meer, 1988), that are controversially debated (Kwik et al., 2003; Munro, 2003; Pike and Miller, 1998). Lipid rafts form ordered and tightly packed lipid platforms (Simons and Ehehalt, 2002). However, association of GPI-anchored proteins to lipid rafts was shown to be a general property of GPI-anchored proteins and a specific mechanism for their sorting at the TGN (Muñiz and Zurzolo, 2014). Therefore, it seems that GPI-anchored protein sorting requires the ability of oligomer formation to increase the affinity to lipid microdomains thereby facilitating their sorting to the apical surface in epithelial cells (Muñiz and Zurzolo, 2014; Paladino et al., 2004). Undoubtedly, the mechanisms of GPI-anchored protein sorting seem to be still not fully understood and will require further studies to clarify sorting mechanisms.

### 4.6.2 Sorting of integral transmembrane proteins

The last section described the challenges of GPI-anchored protein sorting at the TGN. By contrast, the sorting of another class of cargo proteins, the integral transmembrane proteins at the TGN has been well described in many outstanding studies in the past years (Bonifacino and Traub, 2003; De Matteis and Luini, 2008; Guo et al., 2014). Transmembrane proteins are captured during sorting events by signal motifs in their cytoplasmic domains hence recognized

by adaptor proteins that subsequently promote the formation of coated transport vesicles (Figure 17) (Guo et al., 2014). Indeed, the heterotetrameric adaptor protein complexes (APs) and the Golgi-localized,  $\gamma$ -ear-containing Arf-binding proteins (GGAs) (Boman et al., 2000; Dell'Angelica et al., 2000) resemble adaptor proteins that display similar functions during cargo recognition, membrane binding and clathrin coat formation (Owen et al., 2004). APs recognize transmembrane cargo by sorting motifs that contain initial tyrosines (YXX $\Phi$ ), while  $\Phi$  represents amino acids with bulky hydrophobic side chains as well as dileucine sorting motifs ([DE]XXXL[LI]) (Guo et al., 2014; Owen et al., 2004). Studies showed that the tyrosine sorting motif is essential for sorting of transmembrane proteins to lysosomes and the basolateral face of epithelial cells while dileucine sorting motifs are required for transport to late endosomes and specialized endo-lysosomal compartments (Guo et al., 2014). Similarly, GGAs were also shown to regulate cargo sorting from the TGN to endosomes (Bonifacino, 2004). GGAs VHS domains binds to acidic-cluster dileucine motifs (DXXLL) (Misra et al., 2002). Both APs and GGAs bind to Arf1 and PI4P for their membrane recruitment and were shown to even cooperate during cargo packaging into clathrin-coated vesicles (CCVs) (Figure 17) (Guo et al., 2014). Another type of monomeric clathrin adaptors were identified as epsin-related proteins that also regulate cargo traffic between TGN and endosomes. Importantly, mammalian epsinR was shown to be required for retrograde sorting on early or recycling endosomes to the TGN (Guo et al., 2014; Saint-Pol et al., 2004). Moreover, exomer was identified as a cargo adaptor complex that is required for transmembrane protein traffic from TGN to the plasma membrane in yeast (Barfield et al., 2009). After recruitment to the membranes by Arf1 and PI4P interactions, adaptors such as APs and GGAs sort cargo and promote their local enrichment (Guo et al., 2014). Accessory proteins and clathrin triskelion-shaped subunits are then recruited and polymerize to a latticed cage leading to a invaginated bud that is pinched off in a dynamin-independent manner at the TGN (Figure 17) (Traub, 2005). Clathrin adaptors and coats are then rapidly disassembled by Hsc70 and auxillins (Traub, 2005). Finally, late stage membrane remodeling and transport of these carriers is facilitated by actin and the Myosin 1b motor protein (Almeida et al., 2011).

### 4.6.3 Transport of soluble lysosomal hydrolases

During cargo sorting, transmembrane proteins take advantage of their cytoplasmic sorting motifs, but how is the sorting of soluble lysosomal proteins in the TGN facilitated? Acidic lysosomal hydrolases are captured by sorting receptors to promote their sorting into clathrin-coated vesicles destined for transport to lysosomes (Guo et al., 2014). Indeed, Kornfeld and colleagues described the first mechanism that requires the sorting receptor mannose-6-phosphate (M6P) receptor (MPR) for transport of lysosomal hydrolases from the TGN to lysosomes (Figure 17) (Borgne and Hoflack, 1997; Ghosh et al., 2003; Griffiths et al., 1988). The cargos are recognized by their PTM by the addition of M6P that is attached in a sequential enzymatic reaction by recognition of conformational determinants of lysosomal hydrolases to their N-linked oligosaccharides (Braulke and Bonifacino, 2009). The M6P modification was shown to be completed in late Golgi compartments (Rohrer et al., 2001). The MPRs can then capture M6P-modified lysosomal hydrolases and interact with their acidic-cluster dileucine motif in their cytosolic domains as described in the previous section with clathrin adaptors including AP1 and GGAs thereby promoting clathrin-coated vesicle formation (Figure 17) (Ghosh et al., 2003). After transport to lysosomes, the lysosomal hydrolases dissociate from MPRs due to the low-pH milieu in lysosomes (Storrie and Desjardins, 1996) allowing MPRs to recycle back to the TGN in a TIP47-dependent manner (Díaz and Pfeffer, 1998). These findings highlight the first identified *bona fide* cargo receptor in the TGN and is often described as a “text-book” mechanism for cargo sorting in the TGN. In addition, there are also M6P-independent sorting pathways including sortilin that is a type I integral transmembrane protein and member of VPS10 protein family (Guo et al., 2014). Similar to MPR, sortilin can recruit APs and GGAs for clathrin recruitment and regulates traffic of lysosomal enzymes including acid sphingomyelinase and cathepsin D and H that traffic to lysosomes in an M6P-independent manner (Guo et al., 2014). Furthermore, Saftig and colleagues identified another sorting receptor lysosomal integral membrane protein type 2 (LIMP-2) that was described to regulate transport of  $\beta$ -glucocerebrosidase ( $\beta$ GC) to lysosomes in an MPR-independent manner (Gonzalez et al., 2014; Reczek et al., 2007). However, recent controversial findings challenged the status of LIMP-2 as an additional class of TGN sorting receptors. By solving the crystal

structure of LIMP-2, Zhao et al. could identify M6P residue that could facilitate MPR binding (Pakdel and von Blume, 2018; Zhao et al., 2014), while studies in living cells suggest LIMP-2 and its cargo are trafficked independently of MPR to lysosomes (Blanz et al., 2015; Pakdel and von Blume, 2018). These findings highlight the complexity of receptor-mediated sorting of soluble proteins in the TGN and will require further studies to clarify these contradictory results.

### 4.6.4 Secretory storage granule formation

In specialized secretory cells such as neuroendocrine cells, prohormones and neuropeptides are stored in secretory granules (SGs) and are secreted upon extracellular stimuli (Figure 17) (Borgonovo et al., 2006). While newly formed SGs are still immature and progress to mature SGs by removal of non-specific cargo by immature SG-derived vesicles leading to characteristic electrodense cores (Glombik and Gerdes, 2000). Typical cargos specific for SGs include chromogranin A (CgA), B (CgB), secretograninII (SGCII) and prohormone VGF that plays an important role during glucose-stimulated insulin secretion (GSIS) and is required for  $\beta$  cell survival (Borgonovo et al., 2006; Possenti et al., 1999; Stephens et al., 2012). There are two main models described that might also cooperate to sort these cargo into SGs (Arvan and Halban, 2003). The first model hypothesizes a sorting by retention mechanism by which all secretory proteins that are non-specific for SGs are removed through the maturation process by clathrin-coated vesicles and delivered to the TGN (Arvan and Halban, 2003; Borgonovo et al., 2006). Evidence for this hypothesis came from a study showing that clathrin adaptors GGAs were required for proper SG maturation (Kakhlon et al., 2006). The second sorting by entry model postulates that high  $\text{Ca}^{2+}$  concentrations and  $\text{pH} < 6.5$  in local environments in the TGN promote aggregation of SG cargos. Subsequently, the initial aggregation forms precipitates of additional regulated cargos leading to immature SG formation (Figure 17) (Borgonovo et al., 2006). Indeed, SG cargos often share biochemical and structural features and are highly acidic proteins that tend to aggregate at low pH (Bartolomucci et al., 2011). Despite the efforts over the past decades, the mechanism how SG cargos are sorted remains not fully understood. In the next section, I will focus on a novel sorting mechanism that shares similar features.

### 4.6.5 Calcium based sorting of soluble cargo at the TGN

The last section described the sorting of SG cargos that are secreted upon appropriate stimuli. The question arises how are constitutive soluble cargo proteins sorted into secretory vesicles? To date no cargo receptor was identified to facilitate sorting of this class of secretory proteins (Figure 17). The next sections will describe the identification and characterization of a novel calcium-based sorting mechanisms that promotes constitutive secretion of soluble secretory cargo into secretory transport carriers.

#### 4.6.5.1 Identification of genes required for constitutive secretion

To identify genes required for constitutive secretion, Malhotra and colleagues performed a genome wide RNAi screen in *Drosophila* S2 cell lines stably expressing signal-sequence tagged horseradish peroxidase (ss-HRP) (Bard et al., 2006). By using ss-HRP and measuring peroxidase activity in the medium, secretion of the reporter was measured in a high-throughput format (Bard et al., 2006). Control experiments demonstrated the robustness of the screen system since gene knockdown of a t-SNARE syntaxin 5 and a component of COPI coat  $\beta$ -COP resulted in significant reduction in HRP secretion (Bard et al., 2006). With this study, many novel genes were identified to be involved in Golgi organization and traffic (Bard et al., 2006). Importantly, one particular gene *twinstar* was found among the hits during this screen. *Twinstar* is the *Drosophila* orthologue of actin severing protein Cofilin-1. But how affects remodeling of F-actin in the cytosol the secretion of secretory proteins?

#### 4.6.5.2 F-actin remodeling by Cofilin is required for cargo sorting

Cofilin-1 belongs to the ADF/Cofilin family and shares ~70% sequence homology with actin depolymerizing factor (ADF) and both proteins display functional redundancies (McGough et al., 1997), therefore for simplicity Cofilin-1 and ADF will referred to as Cofilin hereafter. Cofilin has actin severing activity thereby cuts F-actin filaments without changing rates of depolymerization from the pointed ends (Bravo-Cordero et al., 2013). After severing by cofilin, free actin ends are then accessible to G-actin leading to actin polymerization (Ichetovkin et al.,

2002). By remodeling actin, Cofilin plays an important role during cytoskeleton dynamics, cell-migration and invasion (Bravo-Cordero et al., 2013). Additionally, von Blume et al. confirmed the results from the genomic wide screen by showing that Cofilin knockdown reduced HRP secretion compared to control cells in both *Drosophila S2* as well as human HeLa cell lines (von Blume et al., 2009). These results were also confirmed in yeast highlighting the importance of cofilin within this evolutionary conserved sorting mechanism (Curwin et al., 2012). Moreover, Cofilin depletion in HeLa cells resulted in accumulation of HRP in the TGN. By contrast, cofilin depletion had no effect on transport of integral transmembrane proteins such as VSV-G, p75 or GPI-anchored proteins to the cell surface (von Blume et al., 2009). To further identify cargos that are affected by cofilin depletion, a quantitative stable isotope labeling by amino acids in cell culture (SILAC) mass spectrometry (MS) approach was performed. The results displayed unaffected proteins, inhibited cargos and hyper-secreted cargos including the lysosomal hydrolase cathepsin D and the calcium binding protein Cab45 that will be a central factor for subsequent studies (von Blume et al., 2009).

### 4.6.5.3 Cofilin regulates the $\text{Ca}^{2+}$ -ATPase SPCA1 in the TGN

To gain mechanistic insights into Cofilin-dependent cargo sorting, in the subsequent study, von Blume et al. identified novel Cofilin interactors by an immunoprecipitation and MS approach (von Blume et al., 2011). In addition to actin, the Cofilin interactor Secretory Pathway  $\text{Ca}^{2+}$ -ATPase 1 (SPCA1) was identified (von Blume et al., 2011). SPCA1 is a  $\text{Ca}^{2+}/\text{Mn}^{2+}$  pump with 10 transmembrane helices and both C- and N-terminal tails facing to the cytosol required for efficient  $\text{Ca}^{2+}$  import in the *trans*-Golgi network (TGN) (Figure 18A) (Lissandron et al., 2010; Micaroni et al., 2016; Vanoevelen et al., 2005). SPCA1 has been associated with the rare genetic skin disorder Hailey-Hailey disease (Hu et al., 2000; Sudbrak, 2000). SPCA1 contains a nucleotide-binding domain (N) for ATP binding, a phosphorylation domain (P) that allows auto-phosphorylation and an actuator domain (A) that promotes desphosphorylation after cation import (Figure 18A) (Micaroni et al., 2016). The SDKTGTLT sequence that is characteristic for phosphorylation-type (P-Type) ATPases in which the aspartic acid is phosphorylated during the reaction cycle (Missiaen et al., 2007). During this cycle, SPCA1

reversibly switches between a  $E_1$  and  $E_2$  conformation (Dode et al., 2006, 2005). Cytoplasmic  $Ca^{2+}$  binds to sites in the transmembrane domains of SPCA1 in the  $E_1$  state leading to auto-phosphorylation at the aspartic acid residue of the P-Type sequence followed by a conformational change due to the high-energy  $E_1 \sim P(Ca^{2+})$  state of the phosphoenzyme (Figure 18B) (Missiaen et al., 2007).

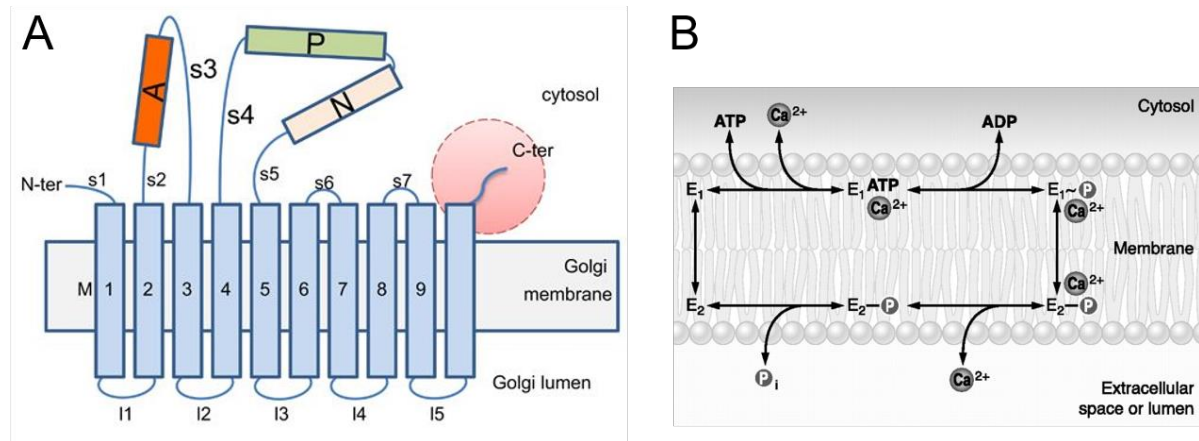


**Figure 18. The P-Type  $Ca^{2+}$ -ATPase SPCA1 regulates  $Ca^{2+}$  import at the TGN.** (A) Schematic domain structure of SPCA1. SPCA1 contains 10 transmembrane helices that are connected by 5 stalk- and luminal loops, respectively. N- and C-terminal tails of SPCA1 are facing to the cytosol. ATP-binding occurs at the nucleotide-binding domain (N), the phosphorylation domain (P) that allows auto-phosphorylation and the actuator domain (A) promotes desphosphorylation after cation import. (B) Reaction diagram of P-Type ATPase characteristic cation import cycle. The  $E_1$  conformation binds cytosolic  $Ca^{2+}$  with high affinity leading to phosphorylation of the P domain leading to the high-energy  $E_1 \sim P(Ca^{2+})$ . Subsequent conformational change leads to a low-energy  $E_2 \sim P$  state releasing the cation to the opposite compartment. Finally, dephosphorylation of  $E_2 \sim P$  enzyme leads to conformational change to  $E_1$  enzyme thereby resetting the cation import cycle. Figure A adapted from (Micaroni et al., 2016), Figure B adapted from Brini and Carafoli, 2009.

The conformational change leads to a low-energy  $E_2$ -P phosphoenzyme thereby releasing  $Ca^{2+}$  in the lumen of the TGN. Subsequently,  $E_2$ -P is hydrolyzed to close the cycle for another round of  $Ca^{2+}$ -import (Figure 18B) (Missiaen et al., 2007). Importantly, recent studies suggested that in addition to the ER with the sarcoplasmic-endoplasmic reticulum  $Ca^{2+}$  ATPase (SERCA) as *bona fide* cellular  $Ca^{2+}$  store, the Golgi complex also to function as a intracellular  $Ca^{2+}$  store

(Pizzo et al., 2010). Interestingly, the luminal  $\text{Ca}^{2+}$  concentrations in the ER ( $\sim 400 \mu\text{M}$ ) (Montero et al., 1995) are significantly smaller compared to the TGN ( $\sim 80 \mu\text{M}$ ) (Lissandron et al., 2010) indicating a  $\text{Ca}^{2+}$  concentration gradient across the secretory pathway (Pizzo et al., 2010). Release of luminal  $\text{Ca}^{2+}$  is mediated in the *cis*- and *medial* compartments through the inositol 1,4,5-trisphosphate (IP3) receptor activation, while the TGN remains insensitive to IP3 stimulation (Pizzo et al., 2010). Depletion of SPCA1 hence  $\text{Ca}^{2+}$ -import induces changes in Golgi morphologies (Pizzo et al., 2010). In addition, RNA knockdown of SPCA1 leads to reduced HRP secretion as well as Cab45 and cathepsin D hypersecretion resembling Cofilin depletion cargo sorting defects (von Blume et al., 2011). Immunoprecipitation experiments showed that Cofilin interacts with SPCA1 in an actin-dependent manner. In absence of Cofilin,  $\text{Ca}^{2+}$ -import by SPCA1 into the lumen of the SPCA1 was impaired (von Blume et al., 2011).

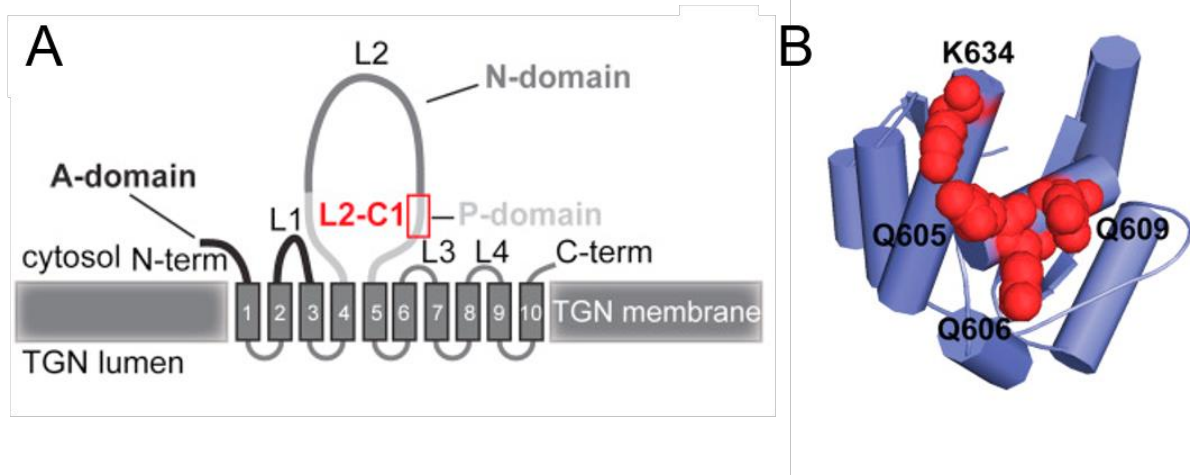


**Figure 19. Cofilin binds to a portion of the cytosolic P-domain of SPCA1.** (A) Schematic domain structure of SPCA1 with the nucleotide-binding domain (N), the phosphorylation domain (P) and the actuator domain (A). L2-C1 is a 132-amino acid stretch of the SPCA1 P-domain that is required for Cofilin binding. (B) Structural model of Cofilin binding site. The identified residues Q605/Q606/Q609/K634 forming charged surface patches are highlighted in red. Figure adapted from Blank and von Blume, 2017; Kienzle et al., 2014.

In addition, a follow-up study systematically dissected the critical Cofilin-to-SPCA1 binding sites showing that Cofilin interacts specifically with a 132-amino acid portion of the cytosolic

P-domain of SPCA1 that forms a loop (Kienzle et al., 2014). More specifically, by using structural modeling, the specific residues Q605/Q606/Q609/K634 were identified forming charged surface patches required for cofilin and F-actin recruitment (Kienzle et al., 2014). These results suggested a pivotal role of  $\text{Ca}^{2+}$ -import by SPCA1 that is regulated by Cofilin for sorting of a subset of secretory proteins. However, how does  $\text{Ca}^{2+}$ -influx promote secretory cargo sorting and vesicle formation?

#### 4.6.5.4 Cab45 – the soluble cargo sorter

As highlighted in the previous section,  $\text{Ca}^{2+}$ -import by SPCA1 to the TGN is crucial for the sorting mechanism. To follow the logical cascade, downstream factors should utilize  $\text{Ca}^{2+}$  ions in the lumen of the TGN to facilitate cargo sorting. Indeed, the subsequent study of Malhotra and colleagues shed light on this question and focused on the characterization of Cab45 that is a Golgi localizing  $\text{Ca}^{2+}$ -binding protein with thus far elusive function (Figure 20) (Honoré, 2009; Honoré and Vorum, 2000; Scherer et al., 1996).

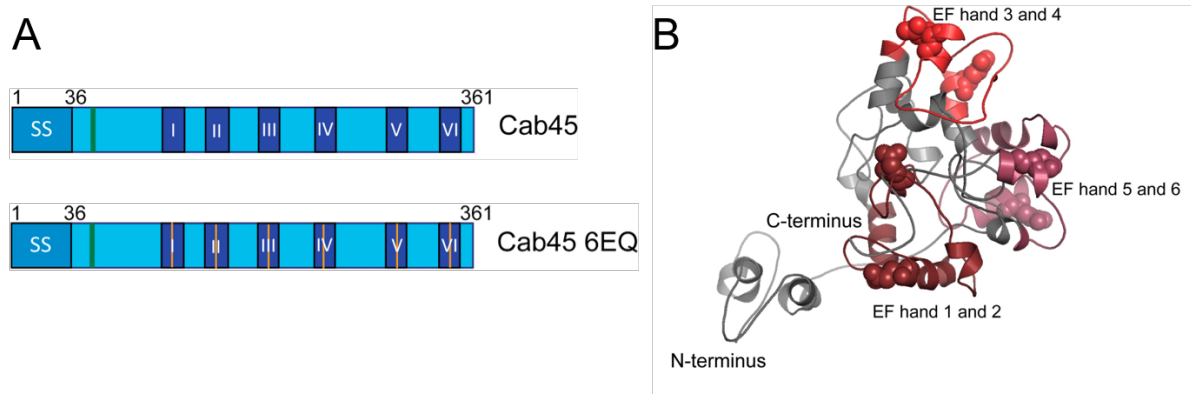


**Figure 20. Cab45 binds to  $\text{Ca}^{2+}$  ions with 6 EF-hand domains.** (A) Schematic cartoon and (B) molecular model of Cab45. EF-hand domains 1-6 are highlighted in blue (A) and in red (B). Site-directed mutagenesis of glutamic acid to glutamine residues within the EF-hand domains generates the  $\text{Ca}^{2+}$ -binding deficient mutant Cab45-6EQ. Figure adapted from Blank and von Blume, 2017.

Cab45 contains 6 EF-hand domains forming three functional pairs that enable  $\text{Ca}^{2+}$ -binding (Figure 20) (Blank and von Blume, 2017; Scherer et al., 1996). Analysis of Cab45 depletion

revealed a reduction in HRP and an elevated cathepsin D secretion as well as defects in TGN  $\text{Ca}^{2+}$  homeostasis (von Blume et al., 2012). Lysozyme C (LyzC) and cartilage oligomeric matrix protein (COMP) were identified as novel Cab45 interactors by immunoprecipitation and MS analysis (von Blume et al., 2012). Indeed, immunoprecipitation experiments confirmed interactions to LyzC and COMP of Cab45-WT but not a Cab45 variant with all EF-hand domains mutated suggesting  $\text{Ca}^{2+}$ -specific binding to secretory cargo (Figure 20) (von Blume et al., 2012).

### 4.6.5.5 Cofilin – SPCA1– Cab45: Model and open questions

These summarized results describe a unique mechanism that requires the cooperative action of F-actin and Cofilin to interact specifically with the P-domain of SPCA1 at the TGN. These interactions are required for SPCA1 pump activation that promotes  $\text{Ca}^{2+}$  influx by SPCA1 into the lumen of the TGN. Next, luminal increase in  $\text{Ca}^{2+}$  is required for Cab45 to selectively bind to secretory cargo proteins in a  $\text{Ca}^{2+}$ -dependent manner to promote cargo sorting and secretory vesicle formation in an yet unknown mechanism (Kienzle et al., 2014; von Blume et al., 2012, 2009; von Blume et al., 2011). However, there are still many open questions regarding the SPCA1-dependent cargo sorting mechanism. Therefore, the central task of this doctoral thesis was to better understand the molecular mechanisms underlying  $\text{Ca}^{2+}$ -based sorting of constitutively secreted cargo proteins.

## 5 Aims of this thesis

Protein secretion is crucial for cell-cell communication and autocrine signaling as well as tissue integrity, cellular homeostasis and cell survival. Defects in protein secretion or lipid transport are associated with a variety of severe diseases including diabetes (Harding et al., 2001), metabolic- and neurological disorders (Chen et al., 2001; Ong et al., 2015) and cancer (Welsh et al., 2003). In the TGN, newly synthesized lipids and proteins need to be sorted into distinct transport vesicles for their transport to their destined location to fulfill their functions. The sorting of transmembrane proteins as well soluble lysosomal hydrolases has been extensively studied in the past. However, the molecular mechanisms how lipid metabolism is coupled to cargo sorting of constitutively secreted proteins remained unclear. To better understand the underlying mechanisms how soluble secretory cargo is packaged into secretory vesicles, the main aims of this thesis are:

- 1) Assessing how  $\text{Ca}^{2+}$ -binding by Cab45 promotes cargo binding to better understand the role of  $\text{Ca}^{2+}$ -import during Cab45-mediated secretory cargo sorting
- 2) Developing a single-cell cargo sorting assay and corresponding data analysis workflow to monitor sorting kinetics of secretory and non-secretory cargo
- 3) Investigating how sphingomyelin metabolism and transport is coupled to SPCA1 and Cab45-dependent cargo sorting in the TGN

## 6 Results

### 6.1 Secretory cargo sorting by Ca<sup>2+</sup>-dependent Cab45 oligomerization at the *trans*-Golgi network

Sorting of transmembrane proteins as well as soluble lysosomal hydrolases at the TGN are well understood. However, the molecular mechanism underlying sorting of secretory cargos into transport carriers for their secretion remains elusive. We have previously described a sorting machinery that requires Ca<sup>2+</sup>-import into the TGN for sorting of secretory cargos at the TGN. The calcium ATPase SPCA1 promotes Ca<sup>2+</sup>-import into the TGN in an ADF/Cofilin-dependent manner. The TGN-luminal protein Cab45 together with active Ca<sup>2+</sup>-import are then required for efficient sorting of secretory cargos. Here, we show by using biochemical oligomerization assays of endogenous as well as recombinant proteins that Cab45 reversibly oligomerizes upon Ca<sup>2+</sup>-addition. Development of fluorescent microscopy-based oligomerization assays of fluorescently labeled recombinant Cab45 visualized Ca<sup>2+</sup>-dependent co-oligomerization of Cab45 with secretory cargos COMP and LyzC but not the lysosomal hydrolase cathepsin D. Direct stochastic optical reconstruction microscopy (dSTORM) showed that in the presence of Ca<sup>2+</sup>, Cab45 localized to dense clusters in the TGN while in the absence of Ca<sup>2+</sup>, Cab45 appeared in diffuse puncta suggesting Ca<sup>2+</sup>-dependent Cab45 oligomers in living cells. Visualization of the cellular localization of Cab45 and its Ca<sup>2+</sup>-binding deficient mutant Cab45-6EQ revealed mis-localization of Cab45-6EQ to cytoplasmic vesicles as well as increased Cab45-6EQ secretion. Finally, 3D structural illumination microscopy (SIM) revealed that Cab45 co-localizes with SPCA1 as well as secretory proteins in TGN microdomains. These findings provide novel mechanistic insights to the Ca<sup>2+</sup>-dependent and oligomerization-driven sorting mechanism of secretory cargos by Cab45 (Crevenna et al., 2016).

Attachment:

Crevenna, A.H.\*, Blank, B.\*, Maiser, A., Emin, D., Prescher, J., Beck, G., Kienzle, C., Bartnik, K., Habermann, B., **Pakdel, M.**, Leonhardt, H., Lamb, D.C., von Blume, J., 2016. Secretory cargo sorting by Ca<sup>2+</sup>-dependent Cab45 oligomerization at the *trans*-Golgi network. *J. Cell Biol.* 213, 305–314. \* These authors contributed equally to this work.

## 6.2 Activity of the SPCA1 Calcium Pump Couples Sphingomyelin Synthesis to Sorting of Secretory Proteins in the *trans*-Golgi Network

Newly synthesized lipids and secretory proteins are sorted at the TGN into transport vesicles for their passage to the plasma membrane or for secretion. However, how lipid synthesis and sorting of secretory proteins is coupled to establish trafficking routes that are specific for secretory cargos and lipids, is still unknown. By using a comparative proximity biotinylation proteomics approach of isolated secretory vesicles that are enriched in SM, a lipid associated in TGN-to-cell surface transport, we identified candidate proteins that are secreted in SM-rich carriers. Within SM-rich vesicles, we found Cab45, a TGN-resident protein that is required for a  $\text{Ca}^{2+}$ -dependent, oligomerization-driven sorting machinery. By using live-cell microscopy of the SM sensor EQ-SM together with Cab45-eGFP, we confirmed that Cab45 and SM exit the Golgi in the same type of vesicles. Furthermore, a secretory cargo LyzC also co-localized with EQ-SM in post-Golgi carriers. By using TIRF exocytosis assays, we revealed that both Cab45 and its cargo LyzC are co-secreted with EQ-SM in SM-rich secretory vesicles. Development of a retention using selective hooks (RUSH)-based cargo sorting assay allowed to monitor cargo sorting kinetics of LyzC and cathepsin D vesicles. Depletion of Cab45 lead to a significant kinetic delay of LyzC vesicle formation while cathepsin D sorting was not affected. Similarly, depletion of SM synthesis at the TGN resulted in a kinetic sorting delay of LyzC but not cathepsin D. To assess the effects of local sphingomyelin synthesis at the TGN on  $\text{Ca}^{2+}$ -import activity by SPCA1, a FRET-based  $\text{Ca}^{2+}$  import assay was applied. Disruption of SM synthesis in the TGN resulted in decreased  $\text{Ca}^{2+}$ -influx activity by SPCA1. Furthermore, by using a UV-crosslink competent metabolic precursor of SM, we showed in immunoprecipitation experiments that SPCA1 is closely associated with SM. These results demonstrate that local sphingomyelin synthesis controls SPCA1  $\text{Ca}^{2+}$  flux activity and thus is required for sorting of secretory proteins into SM-rich secretory vesicles in a Cab45-dependent oligomerization-driven sorting mechanism (Deng, Pakdel et al., 2018).

Attachment:

Deng, Y.\*, **Pakdel, M.\***, Blank, B., Sundberg, E.L., Burd, C.G., von Blume, J., 2018. Activity of the SPCA1 Calcium Pump Couples Sphingomyelin Synthesis to Sorting of Secretory Proteins in the Trans-Golgi Network. *Dev. Cell* 47, 464-478.e8. <https://doi.org/10.1016/j.devcel.2018.10.012>. \* **These authors contributed equally to this work.**

## 7 Discussion

The sorting, transport and secretion of secretory proteins is required for cellular homeostasis and cell survival. Secreted proteins are involved in a variety of important signaling pathways including the endocrine system, neurotransmission and immune responses (Haeusler et al., 2017; Lisman et al., 2007; Ritter and Hall, 2009). Furthermore, secreted extracellular matrix proteins provide structural support of cells and regulate cell adhesion and migration (Schiller and Fässler, 2013). To date, the best described sorting mechanisms for soluble proteins involve cargo receptors that capture soluble cargo by recognition of specific modifications and then promote the recruitment of coat proteins that drive vesicle budding. Given the structural diversity and absence of consensus motifs or protein modifications, the sorting of soluble secreted proteins is less well understood. Recent studies of the Cofilin, SPCA1 and Cab45-dependent sorting machinery have shed light into sorting of constitutively soluble secreted proteins at the TGN. However, the molecular action regarding  $\text{Ca}^{2+}$ -dependent Cab45 cargo binding as well as how lipid synthesis and sorting of secretory proteins are integrated to establish cargo-specific trafficking routes, were largely unknown (Deng et al., 2018). In this discussion, the key results of this thesis will be evaluated and contrasted to existing analogous molecular mechanisms found in the literature to underline the conceptual framework of this work.

### 7.1 SPCA1 regulation by Cofilin and F-actin dynamics

Previous work have shown that recruitment of F-actin by specific interactions of Cofilin to the cytosolic P-domain of SPCA1 promote  $\text{Ca}^{2+}$ -import activity and downstream cargo sorting (Kienzle et al., 2014). These results raise the question how F-actin polymerization versus depolymerization dynamics at the TGN regulate SPCA1 activity and whether SPCA1-dependent protein secretion is regulated by extracellular stimuli (Pakdel and von Blume, 2018). Cofilin actin binding and severing activity is regulated by a cell division control protein 42 (Cdc42) signaling cascade and indeed can be activated upon extracellular stimuli such as receptor tyrosine kinases, adhesion molecules, or G protein-coupled receptors (Farhan and

Hsu, 2016; Wang et al., 2007). Cdc42 then activates the p21-activated kinase (Pak1) that in turn activates LIM kinase (LIMK) that can mediate Cofilin regulation by phosphorylation of Cofilin at its Ser3 residue leading to its inactivation (Arber et al., 1998; Edwards et al., 1999; Rosso et al., 2004). Active non-phosphorylated Cofilin can sever F-actin filaments thereby controlling actin cytoskeleton dynamics. Notably, only active Cofilin can bind to the P-domain of SPCA1 and promote  $\text{Ca}^{2+}$  influx indicating a cooperative binding and recruitment of Cofilin and F-actin to SPCA1 (Kienzle et al., 2014). Similarly, the interaction of Cofilin to SPCA1 is dependent to an equilibrium of F-actin since Latrunculin A (LatA) or Jasplakinolide (Jasp) treatments to hyper-depolymerize or stabilize actin results in loss of interaction of Cofilin to SPCA1 indicating a tight control of actin polymerization and depolymerization required for SPCA1 activation (von Blume et al., 2011). Interestingly, Cdc42 is not only required for F-actin dynamics but also for anterograde and retrograde COPI transport indicating a direct role of Cdc42 during intra-Golgi transport (Farhan and Hsu, 2016; Park et al., 2015). Furthermore, Cdc42 binds to Wiskott–Aldrich syndrome protein (WASP) activating the Arp2/3 complex that is required for F-actin branching (Hänisch et al., 2009) and has been found to localize to the Golgi-complex (Luna et al., 2002; Matas et al., 2004). Given the tight control of F-actin dynamics that is required for SPCA1 activation, we hypothesize that not only Cofilin but also WASP and Arp2/3 could play a key role to establish functional branched F-actin networks for interactions to SPCA1. Another mode of Cofilin regulation is established by its membrane binding ability. It has been shown that Cofilin can bind to PI4P that is enriched in Golgi membranes as well as to PI4,5P at the PM (Yonezawa et al., 1990). Cofilin binding to PI4P and PI4,5P leads to the inhibition of actin binding (Bamburg, 1999). PI4P binding could facilitate the first steps of Cofilin recruitment to the Golgi followed by interactions to SPCA1. Phospholipase C (PLC) was shown to hydrolyze PI4,5P to inositol bisphosphate ( $\text{IP}_3$ ) and DAG promoting Cofilin activity after EGFR signaling (van Rheenen et al., 2007). Similarly, PLC could promote the PI4P hydrolysis (de Rubio et al., 2016) thereby regulating release of active Cofilin from the Golgi membrane to interact with SPCA1. These results clearly invoke a more complex view on the cytoskeletal dynamics than simply the recruitment of Cofilin and F-actin to SPCA1 during  $\text{Ca}^{2+}$ -dependent secretory protein sorting. Whether SPCA1 activation by Cofilin responds to upstream Cdc42 signaling and F-actin polymerization and depolymerization

dynamics or Cofilin constitutively activates SPCA1 remains unclear and will be topic for future investigation.

## 7.2 How does sphingomyelin promote SPCA1 activity?

Our work demonstrated that Cab45 and its cargo LyzC are sorted and transported to the PM for their secretion in SM-rich transport vesicles. Depletion of cellular SM synthesis leads to a kinetic delay of cargo sorting similar to Cab45 or SPCA1 depletion. SPCA1 is closely associated with SM hence resides in SM-rich membrane domains at the TGN. Furthermore, we showed that SPCA1  $\text{Ca}^{2+}$ -import activity is coupled to SM synthesis in the TGN (Deng et al., 2018). These findings immediately point towards the question how does SM promote SPCA1 activity on a molecular level? One hypothesis is that SPCA1 localization is favored to SM-rich membrane microdomains. Albeit the concept of lipid rafts remains controversial (Munro, 2003; Shaw, 2006), many recent studies now suggest the existence of SM- and cholesterol rich subdomains forming lipid-rafts that are more ordered and tightly packed thereby being separated from liquid-disordered membranes (Lingwood and Simons, 2010; Simons and Ehehalt, 2002). Lipid-rafts form dynamic nanometer-sized membrane domains that assemble through interactions of saturated hydrocarbon chains of SM to cholesterol. Furthermore, sphingolipid head groups can form hydrogen bonds with both cholesterol or other sphingolipids to stabilize these membrane assemblies by lipid-lipid and lipid-protein interactions to form functional domains (Lingwood and Simons, 2010). These interactions lead to a physical segregation to a thicker, liquid-ordered phase and on the contrary the thinner, liquid-disordered phase (Lingwood and Simons, 2010). Due to lacking structural information, the assembly state of SPCA1 in order to form a functional ion channel is so far not known. Assembly of SPCA1 into a thicker, liquid-ordered SM- and cholesterol-rich membrane domain could physically be favored and therefore promote its  $\text{Ca}^{2+}$ -import functionality. The association of GPI-anchored proteins with lipid rafts that act as sorting platforms at the TGN has been already described earlier in the introduction of this thesis (Muñiz and Zurzolo, 2014). In addition, recent studies described transmembrane proteins that are preferentially located in liquid-ordered raft phases such as LAT plasma membrane adaptor protein during T-cell antigen receptor (TCR)-activation (Zech et al., 2009). Another example for proteins associating in lipid-rafts are

palmitoylated transmembrane proteins. Palmitoylation is a reversible post-translational protein modification of a palmitate that is a 16-carbon saturated fatty acid (Linder and Deschenes, 2007). Palmitate can be added to Cys residues that are located in the cytoplasmic regions flanking transmembrane domains or within transmembrane domains (Salaun et al., 2010). Interestingly, some palmitoylated proteins showed enhanced association to lipid-rafts (Chakrabandhu et al., 2007; Lingwood and Simons, 2010). Similarly, palmitoylation of SPCA1 could contribute to its localization to SM-rich microdomains. Previous studies have shown that SPCA1 indeed resides in detergent-resistant membranes in the TGN that are often hallmarks for SM- and cholesterol-rich microdomains (Baron et al., 2010). Furthermore, purified microsomes containing SPCA1 that were depleted from cholesterol showed 47.5 % reduced SPCA1 ATPase activity (Baron et al., 2010). Similarly, our recent results suggested a significant reduction in  $\text{Ca}^{2+}$ -import activity by SPCA1 after SM depletion (Deng et al., 2018). These results indicate that the presence of both cholesterol and SM forming functional membrane microdomains could potentially be critical for SPCA1 assembly and localization. Along these lines our recent 3D-SIM findings from Crevenna et al. revealed that Cab45 preferentially co-localized in microdomain clusters with SPCA1 and LyzC and to a lesser extent to TGN-marker p230 and TGN46 (Crevenna et al., 2016). These results render further apparent assumptions that SPCA1-LyzC-Cab45 microdomains could also be specific for SM and cholesterol. Interestingly, one isoform of the plasma membrane  $\text{Ca}^{2+}$ -ATPases (PMCA4) that also belongs to the P-type ATPases was reported to be associated with lipid-rafts while the isoforms PMCA1-3 did not (Sepúlveda et al., 2006). Importantly, sequence alignment of PMCA1-PMCA4 revealed two regions in PMCA4 that differentially displayed Cys-compared to Ser residues in all other isoforms that could be palmitoylated (Sepúlveda et al., 2006). Treatment of hydroxylamine, that reversed protein palmitoylations disrupted PMCA4 association to lipid-rafts (Sepúlveda et al., 2006). On the contrary to SPCA1 and PMCA4, the ER-specific  $\text{Ca}^{2+}$ -pump SERCA was reported to reside in highly fluid membranes due the low cholesterol content of the ER (Baron et al., 2010; Ikonen, 2008). Interestingly, SERCA  $\text{Ca}^{2+}$ -import activity is decreased after elevated ER cholesterol content hence increased ER lipid order (Li et al., 2004). These findings suggest a functional adaptation of the different P-type ATPases to the local lipid environment to, if necessary, provide a functional platform for spatially regulated  $\text{Ca}^{2+}$ -influx. An alternative

hypothesis for the requirement of SM for SPCA1 activity could be that SPCA1 might directly bind to SM with a specific binding pocket. Importantly, this hypothesis is not mutually exclusive from the preferential assembly hypothesis of SPCA1 to lipid-rafts. Some evidence for this hypothesis is provided by our recent data utilizing a UV-crosslink competent metabolic precursor of SM called pac-sphingosine (pac-sph) that is pulsed to the medium of cells and metabolized within hours to SM at the TGN. Upon UV-crosslinking followed by immunoprecipitation of SPCA1 we could demonstrate that SPCA1 is closely associated with SM (Deng et al., 2018). Admittedly, these results lack proofs for specific SPCA1 binding sites for SM rather suggest their close proximity. Yet recent studies of voltage-activated potassium (Kv) channels in the PM suggested SM to be required for voltage sensing (Combs et al., 2013; Ramu et al., 2006; Xu et al., 2008). The studies conducted experiments using sphingomyelinases C and D (SMases C and D) that either removes the phosphocholine- or the choline headgroup, respectively (Xu et al., 2008). Addition of SMase D to *Xenopus* oocytes expressing the Kv2.1 channel showed a reduction of the conductance-voltage allowing channel activation at lower resting potentials (Ramu et al., 2006). Moreover, SMase C decreased Kv2.1 channel current by 90% independent of voltage. Notably, the channel inhibitory effect was independent of lipid-rafts in the PM since disruption of lipid-rafts by cholesterol depletion had no effect on channel currents (Xu et al., 2008). Finally, voltage-sensing domain mutagenesis combined with structural free energy mapping to X-ray structures of a Kv2.1-Kv1.2 chimera identified specific residues associated with SM hydrolysis by SMase D within a specific paddle motif within the voltage-sensing domains (Figure 21A) (Milescu et al., 2009). These results demonstrate that Kv channels directly and specifically interacts with structural motifs to SM to facilitate anchoring to the membrane surface as well as stabilizing the voltage sensor in an activated state (Figure 21A and B) (Milescu et al., 2009). Further studies involving SMase application revealed that the activity of the PM store-operated calcium release-activated calcium channel protein 1 (ORAI1) is also affected after SM depletion (Figure 21C) (Combs and Lu, 2015). ORAI1 is a Ca<sup>2+</sup>-channel that is activated during store-operated Ca<sup>2+</sup> entry (SOCE) and is crucial for T lymphocyte function. ORAI1 is activated in a STIM1-dependent manner by ER-to-PM contact sites after release of Ca<sup>2+</sup> from ER stores (Figure 21C) (Combs and Lu, 2015; Hogan, 2015).

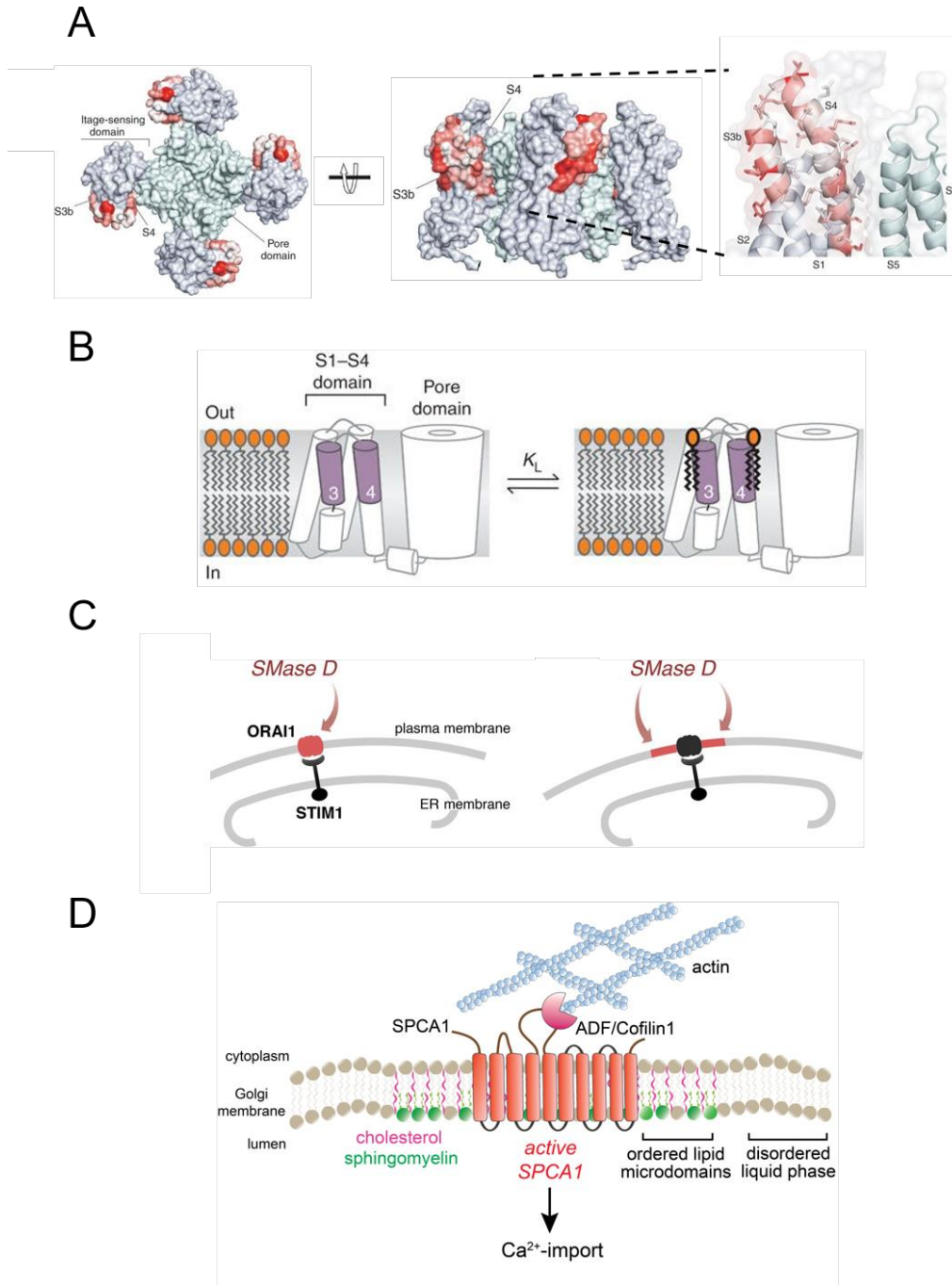


**Figure 21. Known ion pumps that require sphingomyelin for their proper activity. (A)** Surface representation of the voltage-activated potassium channel Kv2.1-Kv1.2 paddle chimeric protein in two different angles. The voltage-sensing domains S1-S4 are indicated in the model. Increasing free energy associated with the coupling between channel mutations and the lipid modification are shown by a color gradient from white to red displaying the S3b-S4 paddle motif with the suggested sphingomyelin binding sites in the zoom view. **(B)** Schematic model of voltage-activated potassium channels that require sphingomyelin (bold lipids) interactions to their paddle motifs for correct voltage sensing. Figures A

and B were adapted from Milesco et al., 2009. **(C)** ORAI1 is a store-operated  $\text{Ca}^{2+}$ -channel that is activated in a stromal interaction molecule 1 (STIM1)-dependent manner by ER-to-PM contact sites. Addition of SMases decrease  $\text{Ca}^{2+}$ -entry. Current models suggest either direct SM to ORAI1 interactions or SM microdomains for optimal ORAI1 activity. Figure C adapted from Hogan, 2015. **(D)** Active sphingomyelin metabolism at the TGN is required for optimal SPCA1  $\text{Ca}^{2+}$ -import activity. We hypothesize that sphingomyelin- and cholesterol form ordered lipid microdomains that favors correct SPCA1 assembly for its optimal activity. Alternatively, or additionally, direct interactions of SM to SPCA1 might be required to facilitate stabilization of critical domains required for  $\text{Ca}^{2+}$  pumping. Figure D adapted from Deng et al., 2018.

The mechanistic action how SM promotes ORAI1 activity is still unclear. Therefore, whether ORAI1 directly interacts with SM in a Kv-channel fashion remains to be elucidated. Similarly, SM could function as an agonist for SPCA1 to facilitate stabilization of critical domains required for  $\text{Ca}^{2+}$ -pumping. In fact, studies suggested the binding sequence VXXTLXXIY within transmembrane domains that is specific for SM molecules that contain C18 acyl-chain (SM 18) (Contreras et al., 2012). Global bioinformatic analysis of all related SM binding sequences found in mammalian transmembrane proteins revealed 672 novel candidate sphingolipid-binding proteins (Björkholm et al., 2014). However, SPCA1 was not found among these candidate proteins possibly due to the specificity to the C18 acyl-chain length of this binding motif (Björkholm et al., 2014). Since thus far there is no evidence for direct SM binding sites in SPCA1, this hypothesis is currently less likely. Conclusively, SPCA1 assembly and localization to heterogenic lipid-microdomains that contain both SM and cholesterol could provide a functional platform for spatially regulated  $\text{Ca}^{2+}$ -influx into the lumen of the TGN (Figure 21D). Spatially controlled  $\text{Ca}^{2+}$ -import could invoke local Cab45 oligomerization and cargo sorting hence couple  $\text{Ca}^{2+}$ -import and cargo sorting to SM-rich secretory vesicle formation (Figure 21D).

### 7.3 Coupling Cab45-cargo complexes to secretory vesicle formation

The last sections focused on Cofilin and F-actin recruitment that are required for SPCA1 activity. Furthermore, I have highlighted possible models how SM-rich microdomains may contribute to SPCA1 assembly and Ca<sup>2+</sup>-import activity. This section will now focus on coupling of Cab45-cargo complexes and secretory vesicle formation downstream of SPCA1 Ca<sup>2+</sup>-import. In Crevenna et al., we could demonstrate that Cab45 binds selectively to its cargo such as LyzC thereby differentiating cargo from non-cargo (Crevenna et al., 2016). Ca<sup>2+</sup>-binding to Cab45 induces a reversible oligomerization of Cab45 with its cargo (Crevenna et al., 2016). Our recent findings further suggests that Cab45 captures its cargo through Cab45-client condensation from the bulk milieu and is packaged in SM-rich secretory vesicles (Deng et al., 2018). These findings evidently point towards the question how Cab45 oligomerization and cargo binding are coupled to form *de novo* secretory vesicles that are a specific type of SM-rich carriers? A recent study of the Rothman laboratory suggested that palmitoylation of transmembrane cargo leads to their concentration at the cisternal rim of the *cis*-Golgi to promote COPI-dependent anterograde transport (Figure 22A) (Ernst et al., 2018). Cargo concentration then induces highly curved tubulo-vesicular membranes at the Golgi rims by an physical-chemical intrinsic property of palmitoylated cargo (Figure 22A) (Ernst et al., 2018). Since palmitoylated proteins showed enhanced association to SM- and cholesterol-rich microdomains (Chakrabandhu et al., 2007; Lingwood and Simons, 2010), a similar physical-chemical mechanism of palmitoylated cargo concentration could promote SM-rich secretory vesicle formation at the TGN. Swisspalm database (Blanc et al., 2015) analysis of all proteins that were identified in close proximity to EQ-SM in native purified SM-rich vesicles (Deng et al., 2018) revealed that out of 57 candidates, 24 proteins were associated with palmitoylation by either metabolic labeling of palmitate or chemical modification of S-palmitoylated Cys residues (unpublished data). Among these palmitoylated candidates, 3 of them were experimentally validated including epidermal growth factor receptor (EGFR), thioredoxin-related transmembrane protein 1 (TMX1), cytoskeleton-associated protein 4 (CKAP4) (Blanc et al., 2015). Interestingly, CKAP4 palmitoylation was shown to be required for its trafficking from ER to PM indicating initial evidence in favor of this hypothesis (Planey et al., 2009).

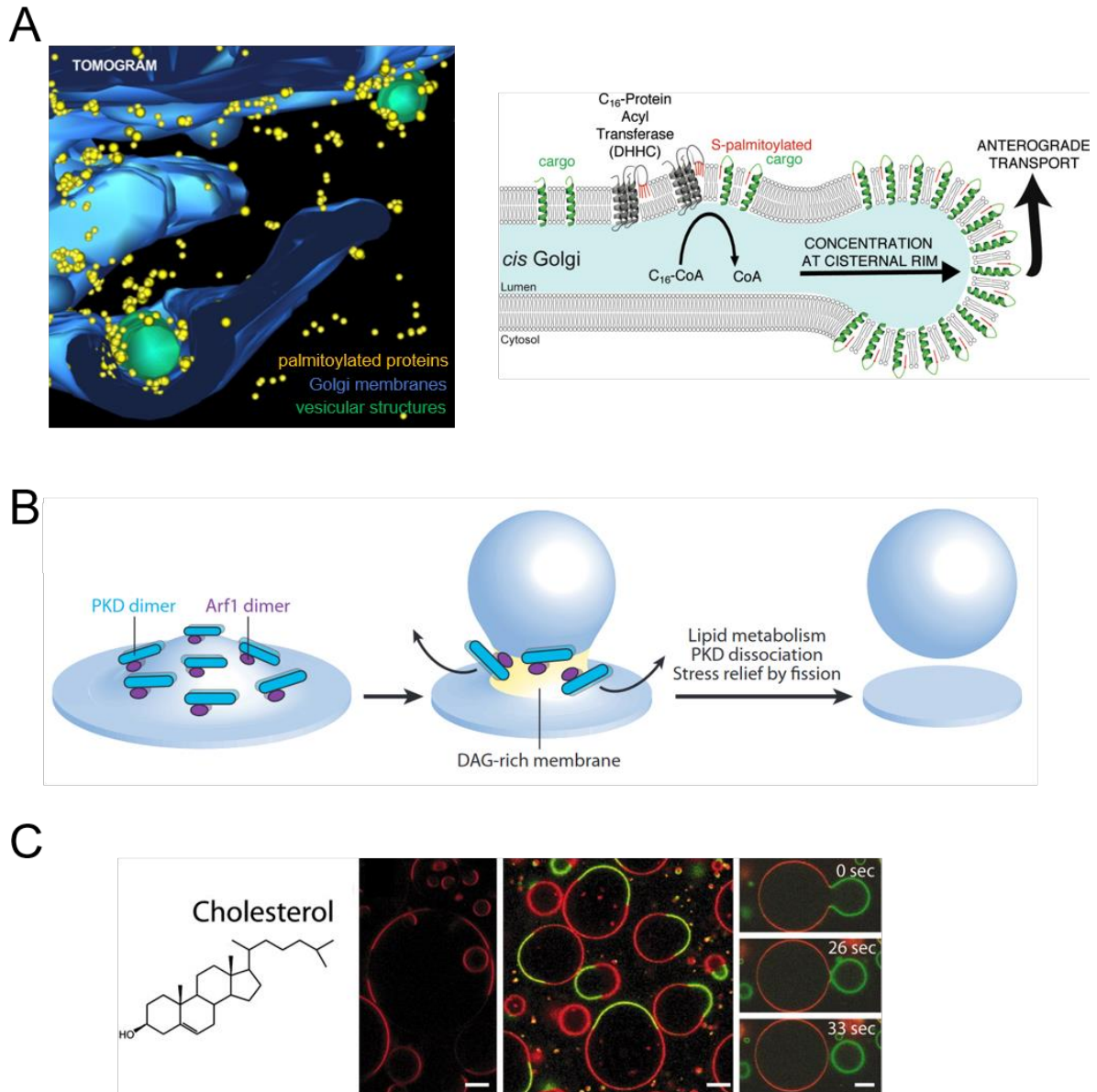


**Figure 22. Analogous mechanisms that might contribute secretory vesicle formation to couple sphingomyelin synthesis, SPCA1  $\text{Ca}^{2+}$ -import and Cab45 oligomerization-driven cargo sorting.** (A) Electron tomography shows concentration of palmitoylated proteins (yellow) to lateral rims of the Golgi membrane (blue) forming highly curved vesicular membranes (green). The model suggests clustering and curvature of the cargo as a physical-chemical intrinsic property of palmitoylated transmembrane proteins to promote COPI anterograde transport. Figure A adapted from Ernst et al., 2018. (B) Diacylglycerol (DAG) is synthesized during sphingomyelin synthesis from PC and ceramide. DAG is a conical lipid that can induce vesicle curvature and scission in TGN membranes in a protein kinase D (PKD)- and Arf1-dependent manner. Figure B adapted from Campelo and Malhotra, 2012. (C) *In vitro*

studies of giant unilamellar vesicles (GUV) consisting of DOPC/sphingomyelin/cholesterol visualized by DiI-C<sub>18</sub> labeling the l<sub>d</sub> phase (red) and cholera toxin that labels the l<sub>o</sub> phase (green) of cholesterol shows that cholesterol determines lipid phase separation. The right panel shows GUVs after injection of 26 mM sucrose solution inducing lipid phase separation, membrane curvature, outward budding and scission *in vitro*. Figure adapted from Bacia et al., 2005.

Moreover, we hypothesize that DAG that is also synthesized during SM-synthesis from PC and ceramide may contribute to membrane curvature of *de novo* forming SM-rich vesicles (Figure 22B) (Campelo and Malhotra, 2012). DAG is a conical lipid that concentrates to growing vesicular buds at the TGN stabilizing bud necks followed by a protein kinase D (PKD)- and Arf1-dependent membrane scission step (Figure 22B) (Campelo and Malhotra, 2012). We speculate that the spatiotemporal coupling of SM and DAG synthesis and Ca<sup>2+</sup>-import by SPCA1 could promote the decisive process of SM-rich secretory vesicle formation (Deng et al., 2018). In addition, another physical mechanism could be involved during secretory vesicle formation. Past studies suggested that lateral lipid phase separation can induce membrane curvature and scission (Figure 22C) (Bacia et al., 2005; Liu et al., 2006; Sackmann and Feder, 1995). Differences in membrane packing capability by formation of microdomains lead to lipid phase separation (Brown and London, 1998). Along this line, *in vitro* studies of giant unilamellar vesicles (GUVs) consisting of DOPC/SM/cholesterol suggested that cholesterol determines phase separation and is able to induce membrane curvature and fission (Figure 22C) (Bacia et al., 2005). Although these results were so far not confirmed *in vivo*, the physical process of lipid phase separation during SPCA1-dependent cargo sorting could contribute to SM-rich secretory vesicle formation. But how are Cab45-cargo complexes specifically targeted into budding secretory vesicles? One hypothesis is that Cab45 indeed is recruited by an integral transmembrane protein to SM-rich vesicles. Interestingly, preliminary data of the von Blume laboratory suggest that TGN46, an integral membrane protein that cycles between the TGN and PM, might be involved during membrane targeting. During proteomics analysis of SM-rich vesicles, TGN46 was also identified as a candidate protein (Deng et al., 2018). Preliminary results indicate that Cab45 interacts with TGN46 in immunoprecipitation experiments and is required for transport of LyzC into SM-rich vesicles (unpublished data). Alternatively, Cab45-

cargo complexes could follow a similar mechanism of zymogen granule formation in pancreatic acinar cells (Dartsch et al., 1998; Schmidt et al., 2000). These studies suggested that these enzymes form a “submembrane matrix” that is able to induce membrane budding to facilitate secretory granule formation at the TGN (Dartsch et al., 1998; Deng et al., 2018; Schmidt et al., 2000). These results underline the complexity of Cab45-cargo complex recruitment and secretory vesicle formation. How these important processes are mechanistically coupled will require further in-depth investigations.

## 8 Outlook and concluding remarks

Within the framework of this thesis, we have provided novel conceptual insights into how SM metabolism is coupled to sorting of secretory cargo at the TGN. Particularly, the results presented here, suggest a sorting mechanism that requires SM synthesis for the activity of SPCA1 to promote  $\text{Ca}^{2+}$ -import into the TGN for downstream Cab45-dependent oligomerization-driven sorting of cargo into SM-rich secretory vesicles. However, there are yet many open questions that need to be clarified. To assess whether SPCA1 activation by Cofilin is linked to the Cdc42 signaling pathway or Cofilin constitutively activates SPCA1, we need to dissect biochemically and by cell biological methods the Cdc42 signaling cascade. To better understand whether actin polymerization might also play a role during SPCA1 activation or SPCA1 positioning, further studies could focus on WASP and Arp2/3-dependent actin branching. Analyzing how SPCA1 functionality is promoted by the presence of SM in the TGN membrane, *in vitro* reconstitution systems of GUVs or liposomes could be developed to reconstitute the effects of different types of lipids on SPCA1 activity. Finally, to better study secretory vesicle formation at the TGN, quantitative super-resolution microscopy could improve the spatial resolution to better visualize SPCA1 distribution in microdomains to sites of newly forming secretory vesicles in dependence of active SM synthesis. Moreover, the role of SPCA1 or cargo palmitoylation for SPCA1 activity or secretory vesicle biogenesis should be examined using click-chemistry competent fatty acid analogs and combined with mutagenesis of predicted palmitoylation sites of either SPCA1 or cargos. These open questions certainly highlight the challenges for future studies. Taken together, these new insights presented in this work provide new prospects to realize in-depth investigations of the Golgi apparatus as the major trafficking hub and cargo sorting station within cells.

## 9 References

- Acar, M., Jafar-Nejad, H., Takeuchi, H., Rajan, A., Ibrani, D., Rana, N.A., Pan, H., Haltiwanger, R.S., Bellen, H.J., 2008. Rumi Is a CAP10 Domain Glycosyltransferase that Modifies Notch and Is Required for Notch Signaling. *Cell* 132, 247–258. <https://doi.org/10.1016/j.cell.2007.12.016>
- Almeida, C.G., Yamada, A., Tenza, D., Louvard, D., Raposo, G., Coudrier, E., 2011. Myosin 1b promotes the formation of post-Golgi carriers by regulating actin assembly and membrane remodelling at the trans-Golgi network. *Nat. Cell Biol.* 13, 779.
- Alonso Y Adell, M., Migliano, S.M., Teis, D., 2016. ESCRT-III and Vps4: a dynamic multipurpose tool for membrane budding and scission. *FEBS J.* 283, 3288–3302. <https://doi.org/10.1111/febs.13688>
- Anitei, M., Hoflack, B., 2011. Exit from the trans-Golgi network: from molecules to mechanisms. *Membr. Organelles* 23, 443–451. <https://doi.org/10.1016/j.ceb.2011.03.013>
- Antonny, B., Madden, D., Hamamoto, S., Orci, L., Schekman, R., 2001. Dynamics of the COPII coat with GTP and stable analogues. *Nat. Cell Biol.* 3, 531.
- Appenzeller-Herzog, C., Hauri, H.-P., 2006. The ER-Golgi intermediate compartment (ERGIC): in search of its identity and function. *J. Cell Sci.* 119, 2173. <https://doi.org/10.1242/jcs.03019>
- Arber, S., Barbayannis, F.A., Hanser, H., Schneider, C., Stanyon, C.A., Bernard, O., Caroni, P., 1998. Regulation of actin dynamics through phosphorylation of cofilin by LIM-kinase. *Nature* 393, 805.
- Archibald, J.M., 2015. Endosymbiosis and Eukaryotic Cell Evolution. *Curr. Biol.* 25, R911–R921. <https://doi.org/10.1016/j.cub.2015.07.055>
- Aridor, M., Fish, K.N., Bannykh, S., Weissman, J., Roberts, T.H., Lippincott-Schwartz, J., Balch, W.E., 2001. The Sar1 Gtpase Coordinates Biosynthetic Cargo Selection with Endoplasmic Reticulum Export Site Assembly. *J. Cell Biol.* 152, 213. <https://doi.org/10.1083/jcb.152.1.213>
- Arvan, P., Halban, P.A., 2003. Sorting Ourselves Out: Seeking Consensus on Trafficking in the Beta-Cell. *Traffic* 5, 53–61. <https://doi.org/10.1111/j.1600-0854.2004.00152.x>
- Athanasiadis, A., Anderluh, G., Maček, P., Turk, D., 2001. Crystal Structure of the Soluble Form of Equinatoxin II, a Pore-Forming Toxin from the Sea Anemone *Actinia equina*. *Structure* 9, 341–346. [https://doi.org/10.1016/S0969-2126\(01\)00592-5](https://doi.org/10.1016/S0969-2126(01)00592-5)
- Aviram, N., Ast, T., Costa, E.A., Arakel, E.C., Chuartzman, S.G., Jan, C.H., Haßdenteufel, S., Dudek, J., Jung, M., Schorr, S., Zimmermann, R., Schwappach, B., Weissman, J.S., Schuldiner, M., 2016. The SND proteins constitute an alternative targeting route to the endoplasmic reticulum. *Nature* 540, 134.
- Aviram, N., Schuldiner, M., 2017. Targeting and translocation of proteins to the endoplasmic reticulum at a glance. *J. Cell Sci.* 130, 4079. <https://doi.org/10.1242/jcs.204396>
- Bacia, K., Schwille, P., Kurzchalia, T., 2005. Sterol structure determines the separation of phases and the curvature of the liquid-ordered phase in model membranes. *Proc. Natl. Acad. Sci. U. S. A.* 102, 3272. <https://doi.org/10.1073/pnas.0408215102>
- Baker, R.W., Hughson, F.M., 2016. Chaperoning SNARE assembly and disassembly. *Nat. Rev. Mol. Cell Biol.* 17, 465.
- Bamburg, J.R., 1999. Proteins of the ADF/Cofilin Family: Essential Regulators of Actin Dynamics. *Annu. Rev. Cell Dev. Biol.* 15, 185–230. <https://doi.org/10.1146/annurev.cellbio.15.1.185>
- Bandhuvula, P., Saba, J.D., 2007. Sphingosine-1-phosphate lyase in immunity and cancer: silencing the siren. *Trends Mol. Med.* 13, 210–217. <https://doi.org/10.1016/j.molmed.2007.03.005>
- Bannykh, S.I., Rowe, T., Balch, W.E., 1996. The organization of endoplasmic reticulum export complexes. *J. Cell Biol.* 135, 19. <https://doi.org/10.1083/jcb.135.1.19>

- Bard, F., Casano, L., Mallabiabarrena, A., Wallace, E., Saito, K., Kitayama, H., Guizzunti, G., Hu, Y., Wendler, F., DasGupta, R., Perrimon, N., Malhotra, V., 2006. Functional genomics reveals genes involved in protein secretion and Golgi organization. *Nature* 439, 604.
- Barfield, R.M., Fromme, J.C., Schekman, R., 2009. The Exomer Coat Complex Transports Fus1p to the Plasma Membrane via a Novel Plasma Membrane Sorting Signal in Yeast. *Mol. Biol. Cell* 20, 4985–4996. <https://doi.org/10.1091/mbc.E09-04-0324>
- Barlowe, C.K., Miller, E.A., 2013. Secretory Protein Biogenesis and Traffic in the Early Secretory Pathway. *Genetics* 193, 383. <https://doi.org/10.1534/genetics.112.142810>
- Baron, S., Vangheluwe, P., Sepúlveda, M.R., Wuytack, F., Raeymaekers, L., Vanoevelen, J., 2010. The secretory pathway Ca<sup>2+</sup>-ATPase 1 is associated with cholesterol-rich microdomains of human colon adenocarcinoma cells. *Biochim. Biophys. Acta BBA - Biomembr.* 1798, 1512–1521. <https://doi.org/10.1016/j.bbamem.2010.03.023>
- Bartolomucci, A., Possenti, R., Mahata, S.K., Fischer-Colbrie, R., Loh, Y.P., Salton, S.R.J., 2011. The Extended Granin Family: Structure, Function, and Biomedical Implications. *Endocr. Rev.* 32, 755–797. <https://doi.org/10.1210/er.2010-0027>
- Beck, K., Boswell, B.A., Ridgway, C.C., Bächinger, H.P., 1996. Triple Helix Formation of Procollagen Type I Can Occur at the Rough Endoplasmic Reticulum Membrane. *J. Biol. Chem.* 271, 21566–21573. <https://doi.org/10.1074/jbc.271.35.21566>
- Behnia, R., Munro, S., 2005. Organelle identity and the signposts for membrane traffic. *Nature* 438, 597.
- Berg, B. van den, Clemons Jr, W.M., Collinson, I., Modis, Y., Hartmann, E., Harrison, S.C., Rapoport, T.A., 2003. X-ray structure of a protein-conducting channel. *Nature* 427, 36.
- Berninsone, P.M., Hirschberg, C.B., 2000. Nucleotide sugar transporters of the Golgi apparatus. *Curr. Opin. Struct. Biol.* 10, 542–547. [https://doi.org/10.1016/S0959-440X\(00\)00128-7](https://doi.org/10.1016/S0959-440X(00)00128-7)
- Berridge, M.J., Irvine, R.F., 1989. Inositol phosphates and cell signalling. *Nature* 341, 197.
- Bi, X., Corpina, R.A., Goldberg, J., 2002. Structure of the Sec23/24–Sar1 pre-budding complex of the COPII vesicle coat. *Nature* 419, 271.
- Bielli, A., Haney, C.J., Gabreski, G., Watkins, S.C., Bannykh, S.I., Aridor, M., 2005. Regulation of Sar1 NH<sub>2</sub> terminus by GTP binding and hydrolysis promotes membrane deformation to control COPII vesicle fission. *J. Cell Biol.* 171, 919. <https://doi.org/10.1083/jcb.200509095>
- Björkholm, P., Ernst, A.M., Hacke, M., Wieland, F., Brügger, B., von Heijne, G., 2014. Identification of novel sphingolipid-binding motifs in mammalian membrane proteins. *Biochim. Biophys. Acta BBA - Biomembr.* 1838, 2066–2070. <https://doi.org/10.1016/j.bbamem.2014.04.026>
- Blanc, M., David, F., Abrami, L., Migliozi, D., Armand, F., Bürgi, J., van der Goot, F.G., 2015. SwissPalm: Protein Palmitoylation database. *F1000Research* 4, 261. <https://doi.org/10.12688/f1000research.6464.1>
- Blank, B., von Blume, J., 2017. Cab45—Unraveling key features of a novel secretory cargo sorter at the trans-Golgi network. *SI Protein Traffick.* 96, 383–390. <https://doi.org/10.1016/j.ejcb.2017.03.001>
- Blanz, J., Zunke, F., Markmann, S., Damme, M., Braulke, T., Saftig, P., Schwake, M., 2015. Mannose 6-phosphate-independent Lysosomal Sorting of LIMP-2. *Traffic* 16, 1127–1136. <https://doi.org/10.1111/tra.12313>
- Block, M.R., Glick, B.S., Wilcox, C.A., Wieland, F.T., Rothman, J.E., 1988. Purification of an N-ethylmaleimide-sensitive protein catalyzing vesicular transport. *Proc. Natl. Acad. Sci.* 85, 7852. <https://doi.org/10.1073/pnas.85.21.7852>
- Bohnsack, M.T., Schleiff, E., 2010. The evolution of protein targeting and translocation systems. *Biochim. Biophys. Acta BBA - Mol. Cell Res.* 1803, 1115–1130. <https://doi.org/10.1016/j.bbamcr.2010.06.005>
- Bonfanti, L., Mironov, A.A., Martínez-Menárguez, J.A., Martella, O., Fusella, A., Baldassarre, M., Buccione, R., Geuze, H.J., Mironov, A.A., Luini, A., 1998. Procollagen Traverses the Golgi Stack

- without Leaving the Lumen of Cisternae: Evidence for Cisternal Maturation. *Cell* 95, 993–1003. [https://doi.org/10.1016/S0092-8674\(00\)81723-7](https://doi.org/10.1016/S0092-8674(00)81723-7)
- Bonifacino, J.S., 2004. The GGA proteins: adaptors on the move. *Nat. Rev. Mol. Cell Biol.* 5, 23.
- Bonifacino, J.S., Glick, B.S., 2004. The Mechanisms of Vesicle Budding and Fusion. *Cell* 116, 153–166. [https://doi.org/10.1016/S0092-8674\(03\)01079-1](https://doi.org/10.1016/S0092-8674(03)01079-1)
- Bonifacino, J.S., Traub, L.M., 2003. Signals for Sorting of Transmembrane Proteins to Endosomes and Lysosomes. *Annu. Rev. Biochem.* 72, 395–447. <https://doi.org/10.1146/annurev.biochem.72.121801.161800>
- Borgne, R.L., Hoflack, B., 1997. Mannose 6-Phosphate Receptors Regulate the Formation of Clathrin-coated Vesicles in the TGN. *J. Cell Biol.* 137, 335–345. <https://doi.org/10.1083/jcb.137.2.335>
- Borgonovo, B., Ouwendijk, J., Solimena, M., 2006. Biogenesis of secretory granules. *Curr. Opin. Cell Biol.* 18, 365–370. <https://doi.org/10.1016/j.ceb.2006.06.010>
- Bornemann, T., Jöckel, J., Rodnina, M.V., Wintermeyer, W., 2008. Signal sequence-independent membrane targeting of ribosomes containing short nascent peptides within the exit tunnel. *Nat. Struct. Amp Mol. Biol.* 15, 494.
- Bousset, L., Mary, C., Brooks, M.A., Scherrer, A., Strub, K., Cusack, S., 2014. Crystal structure of a signal recognition particle Alu domain in the elongation arrest conformation. *RNA* 20, 1955–1962. <https://doi.org/10.1261/rna.047209.114>
- Braakman, I., Hebert, D.N., 2013. Protein Folding in the Endoplasmic Reticulum. *Cold Spring Harb. Perspect. Biol.* 5. <https://doi.org/10.1101/cshperspect.a013201>
- Brandizzi, F., Barlowe, C., 2013. Organization of the ER–Golgi interface for membrane traffic control. *Nat. Rev. Mol. Cell Biol.* 14, 382–392. <https://doi.org/10.1038/nrm3588>
- Braulke, T., Bonifacino, J.S., 2009. Sorting of lysosomal proteins. *Biochim. Biophys. Acta* 1793, 605–614. <https://doi.org/10.1016/j.bbamcr.2008.10.016>
- Bravo-Cordero, J.J., Magalhaes, M.A.O., Eddy, R.J., Hodgson, L., Condeelis, J., 2013. Functions of cofilin in cell locomotion and invasion. *Nat. Rev. Mol. Cell Biol.* 14, 405.
- Brini, M., Carafoli, E., 2009. Calcium Pumps in Health and Disease. *Physiol. Rev.* 89, 1341–1378. <https://doi.org/10.1152/physrev.00032.2008>
- Brown, D.A., London, E., 1998. FUNCTIONS OF LIPID RAFTS IN BIOLOGICAL MEMBRANES. *Annu. Rev. Cell Dev. Biol.* 14, 111–136. <https://doi.org/10.1146/annurev.cellbio.14.1.111>
- Brown, D.A., Rose, J.K., 1992. Sorting of GPI-anchored proteins to glycolipid-enriched membrane subdomains during transport to the apical cell surface. *Cell* 68, 533–544. [https://doi.org/10.1016/0092-8674\(92\)90189-J](https://doi.org/10.1016/0092-8674(92)90189-J)
- Budnik, A., Stephens, D.J., 2009. ER exit sites – Localization and control of COPII vesicle formation. *FEBS Lett.* 583, 3796–3803. <https://doi.org/10.1016/j.febslet.2009.10.038>
- Campelo, F., Malhotra, V., 2012. Membrane Fission: The Biogenesis of Transport Carriers. *Annu. Rev. Biochem.* 81, 407–427. <https://doi.org/10.1146/annurev-biochem-051710-094912>
- Carvalho, P., Stanley, A.M., Rapoport, T.A., 2010. Retrotranslocation of a Misfolded Luminal ER Protein by the Ubiquitin-Ligase Hrd1p. *Cell* 143, 579–591. <https://doi.org/10.1016/j.cell.2010.10.028>
- Causeret, C., Geeraert, L., Van der Hoeven, G., Mannaerts, G.P., Van Veldhoven, P.P., 2000. Further characterization of rat dihydroceramide desaturase: Tissue distribution, subcellular localization, and substrate specificity. *Lipids* 35, 1117–1125. <https://doi.org/10.1007/s11745-000-0627-6>
- Chakrabandhu, K., Hérics, Z., Huault, S., Dost, B., Peng, L., Conchonaud, F., Marguet, D., He, H., Hueber, A., 2007. Palmitoylation is required for efficient Fas cell death signaling. *EMBO J.* 26, 209. <https://doi.org/10.1038/sj.emboj.7601456>
- Chen, C.-D., Huff, M.E., Matteson, J., Page, L., Phillips, R., Kelly, J.W., Balch, W.E., 2001. Furin initiates gelsolin familial amyloidosis in the Golgi through a defect in Ca(2+) stabilization. *EMBO J.* 20, 6277–6287. <https://doi.org/10.1093/emboj/20.22.6277>

- Combs, D.J., Lu, Z., 2015. Sphingomyelinase D inhibits store-operated  $\text{Ca}^{2+}$  entry in T lymphocytes by suppressing ORAI current. *J. Gen. Physiol.* 146, 161. <https://doi.org/10.1085/jgp.201511359>
- Combs, D.J., Shin, H.-G., Xu, Y., Ramu, Y., Lu, Z., 2013. Tuning voltage-gated channel activity and cellular excitability with a sphingomyelinase. *J. Gen. Physiol.* 142, 367. <https://doi.org/10.1085/jgp.201310986>
- Connolly, T., Gilmore, R., 1989. The signal recognition particle receptor mediates the GTP-dependent displacement of SRP from the signal sequence of the nascent polypeptide. *Cell* 57, 599–610. [https://doi.org/10.1016/0092-8674\(89\)90129-3](https://doi.org/10.1016/0092-8674(89)90129-3)
- Connolly, T., Gilmore, R., 1986. Formation of a functional ribosome-membrane junction during translocation requires the participation of a GTP-binding protein. *J. Cell Biol.* 103, 2253. <https://doi.org/10.1083/jcb.103.6.2253>
- Contreras, F.-X., Ernst, A.M., Haberkant, P., Björkholm, P., Lindahl, E., Gönen, B., Tischer, C., Elofsson, A., von Heijne, G., Thiele, C., Pepperkok, R., Wieland, F., Brügger, B., 2012. Molecular recognition of a single sphingolipid species by a protein's transmembrane domain. *Nature* 481, 525.
- Crevenna, A.H., Blank, B., Maiser, A., Emin, D., Prescher, J., Beck, G., Kienzle, C., Bartnik, K., Habermann, B., Pakdel, M., Leonhardt, H., Lamb, D.C., von Blume, J., 2016. Secretory cargo sorting by  $\text{Ca}^{2+}$ -dependent Cab45 oligomerization at the trans-Golgi network. *J. Cell Biol.* 213, 305–314. <https://doi.org/10.1083/jcb.201601089>
- Črnigoj Kristan, K., Viero, G., Dalla Serra, M., Maček, P., Anderluh, G., 2009. Molecular mechanism of pore formation by actinoporins. *Cnidarian Toxins Venoms* 54, 1125–1134. <https://doi.org/10.1016/j.toxicon.2009.02.026>
- Curwin, A.J., von Blume, J., Malhotra, V., 2012. Cofilin-mediated sorting and export of specific cargo from the Golgi apparatus in yeast. *Mol. Biol. Cell* 23, 2327–2338. <https://doi.org/10.1091/mbc.E11-09-0826>
- Dartsch, H., Kleene, R., Kern, H.F., 1998. In vitro condensation-sorting of enzyme proteins isolated from rat pancreatic acinar cells. *Eur. J. Cell Biol.* 75, 211–222. [https://doi.org/10.1016/S0171-9335\(98\)80115-5](https://doi.org/10.1016/S0171-9335(98)80115-5)
- Day, K.J., Staehelin, L.A., Glick, B.S., 2013. A three-stage model of Golgi structure and function. *Histochem. Cell Biol.* 140, 239–249. <https://doi.org/10.1007/s00418-013-1128-3>
- De Craene, J.-O., Bertazzi, D., Bär, S., Friant, S., 2017. Phosphoinositides, Major Actors in Membrane Trafficking and Lipid Signaling Pathways. *Int. J. Mol. Sci.* 18, 634. <https://doi.org/10.3390/ijms18030634>
- De Matteis, M.A., Luini, A., 2008. Exiting the Golgi complex. *Nat. Rev. Mol. Cell Biol.* 9, 273–284. <https://doi.org/10.1038/nrm2378>
- de Rubio, R.H.G., Malik, S., Smrcka, A., 2016. PI4P Hydrolysis is a Major Mechanism for GPCR-dependent DAG Generation and PKC/PKD Activation. *FASEB J.* 30, 1190.7-1190.7. [https://doi.org/10.1096/fasebj.30.1\\_supplement.1190.7](https://doi.org/10.1096/fasebj.30.1_supplement.1190.7)
- Deng, Y., Pakdel, M., Blank, B., Sundberg, E.L., Burd, C.G., von Blume, J., 2018. Activity of the SPCA1 Calcium Pump Couples Sphingomyelin Synthesis to Sorting of Secretory Proteins in the Trans-Golgi Network. *Dev. Cell* 47, 464-478.e8. <https://doi.org/10.1016/j.devcel.2018.10.012>
- Deng, Y., Rivera-Molina, F.E., Toomre, D.K., Burd, C.G., 2016. Sphingomyelin is sorted at the *trans* Golgi network into a distinct class of secretory vesicle. *Proc. Natl. Acad. Sci.* 113, 6677. <https://doi.org/10.1073/pnas.1602875113>
- Denic, V., Quan, E.M., Weissman, J.S., 2006. A Luminal Surveillance Complex that Selects Misfolded Glycoproteins for ER-Associated Degradation. *Cell* 126, 349–359. <https://doi.org/10.1016/j.cell.2006.05.045>

- Denks, K., Vogt, A., Sachelaru, I., Petriman, N.-A., Kudva, R., Koch, H.-G., 2014. The Sec translocon mediated protein transport in prokaryotes and eukaryotes. *Mol. Membr. Biol.* 31, 58–84. <https://doi.org/10.3109/09687688.2014.907455>
- Di Paolo, G., De Camilli, P., 2006. Phosphoinositides in cell regulation and membrane dynamics. *Nature* 443, 651.
- Diekmann, Y., Pereira-Leal, J.B., 2013. Evolution of intracellular compartmentalization. *Biochem. J.* 449, 319. <https://doi.org/10.1042/BJ20120957>
- Dilks, K., Hand, N.J., Wesley Rose, R., Pohlschröder, M., 2004. Translocation of proteins across archaeal cytoplasmic membranes. *FEMS Microbiol. Rev.* 28, 3–24. <https://doi.org/10.1016/j.femsre.2003.07.004>
- Díaz, E., Pfeffer, S.R., 1998. TIP47: A Cargo Selection Device for Mannose 6-Phosphate Receptor Trafficking. *Cell* 93, 433–443. [https://doi.org/10.1016/S0092-8674\(00\)81171-X](https://doi.org/10.1016/S0092-8674(00)81171-X)
- Dode, L., Andersen, J.P., Raeymaekers, L., Missiaen, L., Vilsen, B., Wuytack, F., 2005. Functional Comparison between Secretory Pathway Ca<sup>2+</sup>/Mn<sup>2+</sup>-ATPase (SPCA) 1 and Sarcoplasmic Reticulum Ca<sup>2+</sup>-ATPase (SERCA) 1 Isoforms by Steady-state and Transient Kinetic Analyses. *J. Biol. Chem.* 280, 39124–39134. <https://doi.org/10.1074/jbc.M506181200>
- Dode, L., Andersen, J.P., Vanoevelen, J., Raeymaekers, L., Missiaen, L., Vilsen, B., Wuytack, F., 2006. Dissection of the Functional Differences between Human Secretory Pathway Ca<sup>2+</sup>/Mn<sup>2+</sup>-ATPase (SPCA) 1 and 2 Isoenzymes by Steady-state and Transient Kinetic Analyses. *J. Biol. Chem.* 281, 3182–3189. <https://doi.org/10.1074/jbc.M511547200>
- Domínguez-Martín, E., Hernández-Elvira, M., Vincent, O., Coria, R., Escalante, R., 2018. Unfolding the Endoplasmic Reticulum of a Social Amoeba: Dictyostelium discoideum as a New Model for the Study of Endoplasmic Reticulum Stress. *Cells* 7, 56. <https://doi.org/10.3390/cells7060056>
- Duran, J.M., Campelo, F., van Galen, J., Sachsenheimer, T., Sot, J., Egorov, M.V., Rentero, C., Enrich, C., Polishchuk, R.S., Goñi, F.M., Brügger, B., Wieland, F., Malhotra, V., 2012. Sphingomyelin organization is required for vesicle biogenesis at the Golgi complex. *EMBO J.* 31, 4535. <https://doi.org/10.1038/emboj.2012.317>
- Echard, A., Jollivet, F., Martinez, O., Lacapère, J.-J., Rousselet, A., Janoueix-Lerosey, I., Goud, B., 1998. Interaction of a Golgi-Associated Kinesin-Like Protein with Rab6. *Science* 279, 580. <https://doi.org/10.1126/science.279.5350.580>
- Edwards, D.C., Sanders, L.C., Bokoch, G.M., Gill, G.N., 1999. Activation of LIM-kinase by Pak1 couples Rac/Cdc42 GTPase signalling to actin cytoskeletal dynamics. *Nat. Cell Biol.* 1, 253.
- Ellgaard, L., Helenius, A., 2003. Quality control in the endoplasmic reticulum. *Nat. Rev. Mol. Cell Biol.* 4, 181.
- Elsner, M., Hashimoto, H., Nilsson, T., 2003. Cisternal maturation and vesicle transport: join the band wagon! (Review). *Mol. Membr. Biol.* 20, 221–229. <https://doi.org/10.1080/0968768031000114024>
- Emr, S., Glick, B.S., Linstedt, A.D., Lippincott-Schwartz, J., Luini, A., Malhotra, V., Marsh, B.J., Nakano, A., Pfeffer, S.R., Rabouille, C., Rothman, J.E., Warren, G., Wieland, F.T., 2009. Journeys through the Golgi—taking stock in a new era. *J. Cell Biol.* 187, 449. <https://doi.org/10.1083/jcb.200909011>
- Ernst, A.M., Syed, S.A., Zaki, O., Bottanelli, F., Zheng, H., Hacke, M., Xi, Z., Rivera-Molina, F., Graham, M., Rebane, A.A., Björkholm, P., Baddeley, D., Toomre, D., Pincet, F., Rothman, J.E., 2018. S-Palmitoylation Sorts Membrane Cargo for Anterograde Transport in the Golgi. *Dev. Cell* 47, 479–493.e7. <https://doi.org/10.1016/j.devcel.2018.10.024>
- Fagerberg, L., Jonasson, K., von Heijne, G., Uhlén, M., Berglund, L., 2010. Prediction of the human membrane proteome. *PROTEOMICS* 10, 1141–1149. <https://doi.org/10.1002/pmic.200900258>
- Farhan, H., Hsu, V.W., 2016. Cdc42 and Cellular Polarity: Emerging Roles at the Golgi. *Trends Cell Biol.* 26, 241–248. <https://doi.org/10.1016/j.tcb.2015.11.003>

- Favaloro, V., Spasic, M., Schwappach, B., Dobberstein, B., 2008. Distinct targeting pathways for the membrane insertion of tail-anchored (TA) proteins. *J. Cell Sci.* 121, 1832. <https://doi.org/10.1242/jcs.020321>
- Funato, K., Riezman, H., 2001. Vesicular and nonvesicular transport of ceramide from ER to the Golgi apparatus in yeast. *J. Cell Biol.* 155, 949. <https://doi.org/10.1083/jcb.200105033>
- Gabaldón, T., Pittis, A.A., 2015. Origin and evolution of metabolic sub-cellular compartmentalization in eukaryotes. *Biochimie* 119, 262–268. <https://doi.org/10.1016/j.biochi.2015.03.021>
- Ghosh, P., Dahms, N.M., Kornfeld, S., 2003. Mannose 6-phosphate receptors: new twists in the tale. *Nat. Rev. Mol. Cell Biol.* 4, 202.
- Gillingham, A.K., Munro, S., 2016. Finding the Golgi: Golgin Coiled-Coil Proteins Show the Way. *Trends Cell Biol.* 26, 399–408. <https://doi.org/10.1016/j.tcb.2016.02.005>
- Glick, B.S., 2000. Organization of the Golgi apparatus. *Curr. Opin. Cell Biol.* 12, 450–456. [https://doi.org/10.1016/S0955-0674\(00\)00116-2](https://doi.org/10.1016/S0955-0674(00)00116-2)
- Glick, B.S., Luini, A., 2011. Models for Golgi Traffic: A Critical Assessment. *Cold Spring Harb. Perspect. Biol.* 3, a005215–a005215. <https://doi.org/10.1101/cshperspect.a005215>
- Glick, B.S., Malhotra, V., 1998. The Curious Status of the Golgi Apparatus. *Cell* 95, 883–889. [https://doi.org/10.1016/S0092-8674\(00\)81713-4](https://doi.org/10.1016/S0092-8674(00)81713-4)
- Glombik, M.M., Gerdes, H.-H., 2000. Signal-mediated sorting of neuropeptides and prohormones: Secretory granule biogenesis revisited. *Biochimie* 82, 315–326. [https://doi.org/10.1016/S0300-9084\(00\)00195-4](https://doi.org/10.1016/S0300-9084(00)00195-4)
- Golgi, C., 1989a. On the structure of nerve cells1. *J. Microsc.* 155, 3–7. <https://doi.org/10.1111/j.1365-2818.1989.tb04294.x>
- Golgi, C., 1989b. On the structure of the nerve cells of the spinal ganglia1. *J. Microsc.* 155, 9–14. <https://doi.org/10.1111/j.1365-2818.1989.tb04295.x>
- Gomez-Lorenzo, M.G., Spahn, C.M.T., Agrawal, R.K., Grassucci, R.A., Penczek, P., Chakraborty, K., Ballesta, J.P.G., Lavandera, J.L., Garcia-Bustos, J.F., Frank, J., 2000. Three-dimensional cryo-electron microscopy localization of EF2 in the *Saccharomyces cerevisiae* 80S ribosome at 17.5 Å resolution. *EMBO J.* 19, 2710. <https://doi.org/10.1093/emboj/19.11.2710>
- Gonzalez, A., Valeiras, M., Sidransky, E., Tayebi, N., 2014. Lysosomal integral membrane protein-2: A new player in lysosome-related pathology. *Mol. Genet. Metab.* 111, 84–91. <https://doi.org/10.1016/j.ymgme.2013.12.005>
- Goud, B., Gleeson, P.A., 2010. TGN golgins, Rabs and cytoskeleton: regulating the Golgi trafficking highways. *Trends Cell Biol.* 20, 329–336. <https://doi.org/10.1016/j.tcb.2010.02.006>
- Griffiths, G., Hoflack, B., Simons, K., Mellman, I., Kornfeld, S., 1988. The mannose 6-phosphate receptor and the biogenesis of lysosomes. *Cell* 52, 329–341. [https://doi.org/10.1016/S0092-8674\(88\)80026-6](https://doi.org/10.1016/S0092-8674(88)80026-6)
- Griffiths, G., Simons, K., 1986. The trans Golgi network: sorting at the exit site of the Golgi complex. *Science* 234, 438. <https://doi.org/10.1126/science.2945253>
- Gulbins, E., Petrache, I. (Eds.), 2013. Sphingolipids in Disease, Handbook of Experimental Pharmacology. Springer Vienna, Vienna. <https://doi.org/10.1007/978-3-7091-1511-4>
- Guo, Y., Sirkis, D.W., Schekman, R., 2014. Protein Sorting at the trans-Golgi Network. *Annu. Rev. Cell Dev. Biol.* 30, 169–206. <https://doi.org/10.1146/annurev-cellbio-100913-013012>
- Gürkan, C., Stagg, S.M., LaPointe, P., Balch, W.E., 2006. The COPII cage: unifying principles of vesicle coat assembly. *Nat. Rev. Mol. Cell Biol.* 7, 727.
- Gutiérrez-Aguirre, I., BARLIČ, A., PODLESEK, Z., MAČEK, P., ANDERLUH, G., GONZÁLEZ-MAÑAS, J.M., 2004. Membrane insertion of the N-terminal  $\alpha$ -helix of equinatoxin II, a sea anemone cytolytic toxin. *Biochem. J.* 384, 421. <https://doi.org/10.1042/BJ20040601>
- Haeusler, R.A., McGraw, T.E., Accili, D., 2017. Biochemical and cellular properties of insulin receptor signalling. *Nat. Rev. Mol. Cell Biol.* 19, 31.

- Halic, M., Becker, T., Pool, M.R., Spahn, C.M.T., Grassucci, R.A., Frank, J., Beckmann, R., 2004. Structure of the signal recognition particle interacting with the elongation-arrested ribosome. *Nature* 427, 808.
- Halic, M., Beckmann, R., 2005. The signal recognition particle and its interactions during protein targeting. *Fold. Bind. Protein-Nucleic Acid Interact.* 15, 116–125. <https://doi.org/10.1016/j.sbi.2005.01.013>
- Halic, M., Blau, M., Becker, T., Mielke, T., Pool, M.R., Wild, K., Sinning, I., Beckmann, R., 2006. Following the signal sequence from ribosomal tunnel exit to signal recognition particle. *Nature* 444, 507.
- Hammond, A.T., Glick, B.S., Pelham, H.R.B., 2000. Dynamics of Transitional Endoplasmic Reticulum Sites in Vertebrate Cells. *Mol. Biol. Cell* 11, 3013–3030. <https://doi.org/10.1091/mbc.11.9.3013>
- Hammond, C., Braakman, I., Helenius, A., 1994. Role of N-linked oligosaccharide recognition, glucose trimming, and calnexin in glycoprotein folding and quality control. *Proc. Natl. Acad. Sci.* 91, 913. <https://doi.org/10.1073/pnas.91.3.913>
- Hanada, K., 2017. Ceramide Transport from the Endoplasmic Reticulum to the Trans Golgi Region at Organelle Membrane Contact Sites, in: Tagaya, M., Simmen, T. (Eds.), *Organelle Contact Sites: From Molecular Mechanism to Disease*. Springer Singapore, Singapore, pp. 69–81. [https://doi.org/10.1007/978-981-10-4567-7\\_5](https://doi.org/10.1007/978-981-10-4567-7_5)
- Hanada, K., Kumagai, K., Yasuda, S., Miura, Y., Kawano, M., Fukasawa, M., Nishijima, M., 2003. Molecular machinery for non-vesicular trafficking of ceramide. *Nature* 426, 803.
- Hänisch, J., Ehinger, J., Ladwein, M., Rohde, M., Derivery, E., Bosse, T., Steffen, A., Bumann, D., Misselwitz, B., Hardt, W.-D., Gautreau, A., Stradal, T.E.B., Rottner, K., 2009. Molecular dissection of Salmonella-induced membrane ruffling versus invasion. *Cell. Microbiol.* 12, 84–98. <https://doi.org/10.1111/j.1462-5822.2009.01380.x>
- Hannun, Y.A., Obeid, L.M., 2017. Sphingolipids and their metabolism in physiology and disease. *Nat. Rev. Mol. Cell Biol.* 19, 175.
- Hannun, Y.A., Obeid, L.M., 2008. Principles of bioactive lipid signalling: lessons from sphingolipids. *Nat. Rev. Mol. Cell Biol.* 9, 139.
- Hanson, P.I., Whiteheart, S.W., 2005. AAA+ proteins: have engine, will work. *Nat. Rev. Mol. Cell Biol.* 6, 519.
- Harayama, T., Riezman, H., 2018. Understanding the diversity of membrane lipid composition. *Nat. Rev. Mol. Cell Biol.* 19, 281.
- Harding, H.P., Zeng, H., Zhang, Y., Jungries, R., Chung, P., Plesken, H., Sabatini, D.D., Ron, D., 2001. Diabetes Mellitus and Exocrine Pancreatic Dysfunction in Perk<sup>-/-</sup> Mice Reveals a Role for Translational Control in Secretory Cell Survival. *Mol. Cell* 7, 1153–1163. [https://doi.org/10.1016/S1097-2765\(01\)00264-7](https://doi.org/10.1016/S1097-2765(01)00264-7)
- Hetz, C., 2012. The unfolded protein response: controlling cell fate decisions under ER stress and beyond. *Nat. Rev. Mol. Cell Biol.* 13, 89.
- Hiller, M.M., Finger, A., Schweiger, M., Wolf, D.H., 1996. ER Degradation of a Misfolded Luminal Protein by the Cytosolic Ubiquitin-Proteasome Pathway. *Science* 273, 1725. <https://doi.org/10.1126/science.273.5282.1725>
- Hogan, P.G., 2015. Sphingomyelin, ORAI1 channels, and cellular Ca<sup>2+</sup> signaling. *J. Gen. Physiol.* 146, 195. <https://doi.org/10.1085/jgp.201511479>
- Honda, A., Nogami, M., Yokozeki, T., Yamazaki, M., Nakamura, H., Watanabe, H., Kawamoto, K., Nakayama, K., Morris, A.J., Frohman, M.A., Kanaho, Y., 1999. Phosphatidylinositol 4-Phosphate 5-Kinase  $\alpha$  Is a Downstream Effector of the Small G Protein ARF6 in Membrane Ruffle Formation. *Cell* 99, 521–532. [https://doi.org/10.1016/S0092-8674\(00\)81540-8](https://doi.org/10.1016/S0092-8674(00)81540-8)
- Hong, Q., Gutiérrez-Aguirre, I., Barlič, A., Malovrh, P., Kristan, K., Podlesek, Z., Maček, P., Turk, D., González-Mañas, J.M., Lakey, J.H., Anderluh, G., 2002. Two-step Membrane Binding by

- Equinatoxin II, a Pore-forming Toxin from the Sea Anemone, Involves an Exposed Aromatic Cluster and a Flexible Helix. *J. Biol. Chem.* 277, 41916–41924. <https://doi.org/10.1074/jbc.M204625200>
- Honoré, B., 2009. The rapidly expanding CREC protein family: members, localization, function, and role in disease. *BioEssays* 31, 262–277. <https://doi.org/10.1002/bies.200800186>
- Honoré, B., Vorum, H., 2000. The CREC family, a novel family of multiple EF-hand, low-affinity Ca<sup>2+</sup>-binding proteins localised to the secretory pathway of mammalian cells. *FEBS Lett.* 466, 11–18. [https://doi.org/10.1016/S0014-5793\(99\)01780-9](https://doi.org/10.1016/S0014-5793(99)01780-9)
- Hu, Z., Bonifas, J.M., Beech, J., Bench, G., Shigihara, T., Ogawa, H., Ikeda, S., Mauro, T., Epstein, E.H.J., 2000. Mutations in ATP2C1, encoding a calcium pump, cause Hailey-Hailey disease. *Nat. Genet.* 24, 61–65. <https://doi.org/10.1038/71701>
- Huber, D., Boyd, D., Xia, Y., Olma, M.H., Gerstein, M., Beckwith, J., 2005. Use of Thioredoxin as a Reporter To Identify a Subset of *Escherichia coli* Signal Sequences That Promote Signal Recognition Particle-Dependent Translocation. *J. Bacteriol.* 187, 2983. <https://doi.org/10.1128/JB.187.9.2983-2991.2005>
- Ichetovkin, I., Grant, W., Condeelis, J., 2002. Cofilin Produces Newly Polymerized Actin Filaments that Are Preferred for Dendritic Nucleation by the Arp2/3 Complex. *Curr. Biol.* 12, 79–84. [https://doi.org/10.1016/S0960-9822\(01\)00629-7](https://doi.org/10.1016/S0960-9822(01)00629-7)
- Ikonen, E., 2008. Cellular cholesterol trafficking and compartmentalization. *Nat. Rev. Mol. Cell Biol.* 9, 125.
- Jackson, L.P., 2014. Structure and mechanism of COPI vesicle biogenesis. *Cell Organelles* 29, 67–73. <https://doi.org/10.1016/j.ceb.2014.04.009>
- Jahn, R., Scheller, R.H., 2006. SNAREs — engines for membrane fusion. *Nat. Rev. Mol. Cell Biol.* 7, 631.
- Jamieson, J.D., Palade, G.E., 1967. INTRACELLULAR TRANSPORT OF SECRETORY PROTEINS IN THE PANCREATIC EXOCRINE CELL. *J. Cell Biol.* 34, 577. <https://doi.org/10.1083/jcb.34.2.577>
- Jan, C.H., Williams, C.C., Weissman, J.S., 2014. Principles of ER cotranslational translocation revealed by proximity-specific ribosome profiling. *Science* 346. <https://doi.org/10.1126/science.1257521>
- Johnson, N., Powis, K., High, S., 2013. Post-translational translocation into the endoplasmic reticulum. *Funct. Struct. Divers. Endoplasmic Reticulum* 1833, 2403–2409. <https://doi.org/10.1016/j.bbamcr.2012.12.008>
- Jonikas, M.C., Collins, S.R., Denic, V., Oh, E., Quan, E.M., Schmid, V., Weibezahn, J., Schwappach, B., Walter, P., Weissman, J.S., Schuldiner, M., 2009. Comprehensive Characterization of Genes Required for Protein Folding in the Endoplasmic Reticulum. *Science* 323, 1693. <https://doi.org/10.1126/science.1167983>
- Kakhlon, O., Sakya, P., Larijani, B., Watson, R., Tooze, S.A., 2006. GGA function is required for maturation of neuroendocrine secretory granules. *EMBO J.* 25, 1590. <https://doi.org/10.1038/sj.emboj.7601067>
- Kawano, M., Kumagai, K., Nishijima, M., Hanada, K., 2006. Efficient Trafficking of Ceramide from the Endoplasmic Reticulum to the Golgi Apparatus Requires a VAMP-associated Protein-interacting FFAT Motif of CERT. *J. Biol. Chem.* 281, 30279–30288. <https://doi.org/10.1074/jbc.M605032200>
- Keenan, R.J., Freymann, D.M., Stroud, R.M., Walter, P., 2001. The Signal Recognition Particle. *Annu. Rev. Biochem.* 70, 755–775. <https://doi.org/10.1146/annurev.biochem.70.1.755>
- Kienzle, C., Basnet, N., Crevenna, A.H., Beck, G., Habermann, B., Mizuno, N., von Blume, J., 2014. Cofilin recruits F-actin to SPCA1 and promotes Ca<sup>2+</sup>-mediated secretory cargo sorting. *J. Cell Biol.* 206, 635–654. <https://doi.org/10.1083/jcb.201311052>
- Kienzle, C., von Blume, J., 2014. Secretory cargo sorting at the trans-Golgi network. *Trends Cell Biol.* 24, 584–593. <https://doi.org/10.1016/j.tcb.2014.04.007>

- Klausner, R.D., Sitia, R., 1990. Protein degradation in the endoplasmic reticulum. *Cell* 62, 611–614. [https://doi.org/10.1016/0092-8674\(90\)90104-M](https://doi.org/10.1016/0092-8674(90)90104-M)
- Klumperman, J., 2011. Architecture of the Mammalian Golgi. *Cold Spring Harb. Perspect. Biol.* 3. <https://doi.org/10.1101/cshperspect.a005181>
- Koch, H.-G., Moser, M., Müller, M., 2003. Signal recognition particle-dependent protein targeting, universal to all kingdoms of life, in: *Reviews of Physiology, Biochemistry and Pharmacology*. Springer Berlin Heidelberg, Berlin, Heidelberg, pp. 55–94. <https://doi.org/10.1007/s10254-002-0002-9>
- Koval, M., Pagano, R.E., 1991. Intracellular transport and metabolism of sphingomyelin. *Biochim. Biophys. Acta BBA - Lipids Lipid Metab.* 1082, 113–125. [https://doi.org/10.1016/0005-2760\(91\)90184-J](https://doi.org/10.1016/0005-2760(91)90184-J)
- Kumagai, K., Kawano-Kawada, M., Hanada, K., 2014. Phosphoregulation of the Ceramide Transport Protein CERT at Serine 315 in the Interaction with VAMP-associated Protein (VAP) for Inter-organelle Trafficking of Ceramide in Mammalian Cells. *J. Biol. Chem.* 289, 10748–10760. <https://doi.org/10.1074/jbc.M113.528380>
- Kwik, J., Boyle, S., Fooksman, D., Margolis, L., Sheetz, M.P., Edidin, M., 2003. Membrane cholesterol, lateral mobility, and the phosphatidylinositol 4,5-bisphosphate-dependent organization of cell actin. *Proc. Natl. Acad. Sci.* 100, 13964. <https://doi.org/10.1073/pnas.2336102100>
- Ladinsky, M.S., Mastronarde, D.N., McIntosh, J.R., Howell, K.E., Staehelin, L.A., 1999. Golgi Structure in Three Dimensions: Functional Insights from the Normal Rat Kidney Cell. *J. Cell Biol.* 144, 1135. <https://doi.org/10.1083/jcb.144.6.1135>
- Lang, K., Schmid, F.X., Fischer, G., 1987. Catalysis of protein folding by prolyl isomerase. *Nature* 329, 268.
- Lee, M.C.S., Miller, E.A., Goldberg, J., Orci, L., Schekman, R., 2004. BI-DIRECTIONAL PROTEIN TRANSPORT BETWEEN THE ER AND GOLGI. *Annu. Rev. Cell Dev. Biol.* 20, 87–123. <https://doi.org/10.1146/annurev.cellbio.20.010403.105307>
- Lewis, M.J., Pelham, H.R.B., 1990. A human homologue of the yeast HDEL receptor. *Nature* 348, 162.
- Li, Y., Ge, M., Ciani, L., Kuriakose, G., Westover, E.J., Dura, M., Covey, D.F., Freed, J.H., Maxfield, F.R., Lytton, J., Tabas, I., 2004. Enrichment of Endoplasmic Reticulum with Cholesterol Inhibits Sarcoplasmic-Endoplasmic Reticulum Calcium ATPase-2b Activity in Parallel with Increased Order of Membrane Lipids: IMPLICATIONS FOR DEPLETION OF ENDOPLASMIC RETICULUM CALCIUM STORES AND APOPTOSIS IN CHOLESTEROL-LOADED MACROPHAGES. *J. Biol. Chem.* 279, 37030–37039. <https://doi.org/10.1074/jbc.M405195200>
- Lilley, B.N., Ploegh, H.L., 2004. A membrane protein required for dislocation of misfolded proteins from the ER. *Nature* 429, 834.
- Linder, M.E., Deschenes, R.J., 2007. Palmitoylation: policing protein stability and traffic. *Nat. Rev. Mol. Cell Biol.* 8, 74.
- Lingwood, D., Simons, K., 2010. Lipid Rafts As a Membrane-Organizing Principle. *Science* 327, 46. <https://doi.org/10.1126/science.1174621>
- Linn, S.C., Kim, H.S., Keane, E.M., Andras, L.M., Wang, E., Merrill, A.H., 2001. Regulation of *de novo* sphingolipid biosynthesis and the toxic consequences of its disruption. *Biochem. Soc. Trans.* 29, 831. <https://doi.org/10.1042/bst0290831>
- Linxweiler, M., Schick, B., Zimmermann, R., 2017. Let's talk about Secs: Sec61, Sec62 and Sec63 in signal transduction, oncology and personalized medicine. *Signal Transduct. Target. Ther.* 2, 17002.
- Lippincott-Schwartz, J., Bonifacino, J.S., Yuan, L.C., Klausner, R.D., 1988. Degradation from the endoplasmic reticulum: Disposing of newly synthesized proteins. *Cell* 54, 209–220. [https://doi.org/10.1016/0092-8674\(88\)90553-3](https://doi.org/10.1016/0092-8674(88)90553-3)

- Lippincott-Schwartz, J., Roberts, T.H., Hirschberg, K., 2000. Secretory Protein Trafficking and Organelle Dynamics in Living Cells. *Annu. Rev. Cell Dev. Biol.* 16, 557–589. <https://doi.org/10.1146/annurev.cellbio.16.1.557>
- Lisman, J.E., Raghavachari, S., Tsien, R.W., 2007. The sequence of events that underlie quantal transmission at central glutamatergic synapses. *Nat. Rev. Neurosci.* 8, 597.
- Lissandron, V., Podini, P., Pizzo, P., Pozzan, T., 2010. Unique characteristics of Ca<sup>2+</sup> homeostasis of the trans-Golgi compartment. *Proc. Natl. Acad. Sci.* 107, 9198–9203. <https://doi.org/10.1073/pnas.1004702107>
- Liu, J., Kaksonen, M., Drubin, D.G., Oster, G., 2006. Endocytic vesicle scission by lipid phase boundary forces. *Proc. Natl. Acad. Sci.* 103, 10277. <https://doi.org/10.1073/pnas.0601045103>
- Long, K.R., Yamamoto, Y., Baker, A.L., Watkins, S.C., Coyne, C.B., Conway, J.F., Aridor, M., 2010. Sar1 assembly regulates membrane constriction and ER export. *J. Cell Biol.* 190, 115. <https://doi.org/10.1083/jcb.201004132>
- Losev, E., Reinke, C.A., Jellen, J., Strongin, D.E., Bevis, B.J., Glick, B.S., 2006. Golgi maturation visualized in living yeast. *Nature* 441, 1002.
- Luna, A., Matas, O.B., Martínez-Menárguez, J.A., Mato, E., Durán, J.M., Ballesta, J., Way, M., Egea, G., Malhotra, V., 2002. Regulation of Protein Transport from the Golgi Complex to the Endoplasmic Reticulum by CDC42 and N-WASP. *Mol. Biol. Cell* 13, 866–879. <https://doi.org/10.1091/mbc.01-12-0579>
- Mao, Y., Nickitenko, A., Duan, X., Lloyd, T.E., Wu, M.N., Bellen, H., Quioco, F.A., 2000. Crystal Structure of the VHS and FYVE Tandem Domains of Hrs, a Protein Involved in Membrane Trafficking and Signal Transduction. *Cell* 100, 447–456. [https://doi.org/10.1016/S0092-8674\(00\)80680-7](https://doi.org/10.1016/S0092-8674(00)80680-7)
- Margittai, É., Enyedi, B., Csala, M., Geiszt, M., Bánhegyi, G., 2015. Composition of the redox environment of the endoplasmic reticulum and sources of hydrogen peroxide. *Free Radic. Biol. Med.* 83, 331–340. <https://doi.org/10.1016/j.freeradbiomed.2015.01.032>
- Marsh, B.J., Howell, K.E., 2002. The mammalian Golgi — complex debates. *Nat. Rev. Mol. Cell Biol.* 3, 789.
- Martin, T.F.J., 1998. PHOSPHOINOSITIDE LIPIDS AS SIGNALING MOLECULES: Common Themes for Signal Transduction, Cytoskeletal Regulation, and Membrane Trafficking. *Annu. Rev. Cell Dev. Biol.* 14, 231–264. <https://doi.org/10.1146/annurev.cellbio.14.1.231>
- Martoglio, B., Dobberstein, B., 1998. Signal sequences: more than just greasy peptides. *Trends Cell Biol.* 8, 410–415. [https://doi.org/10.1016/S0962-8924\(98\)01360-9](https://doi.org/10.1016/S0962-8924(98)01360-9)
- Matas, O.B., Martínez-Menárguez, J., Egea, G., 2004. Association of Cdc42/N-WASP/Arp2/3 Signaling Pathway with Golgi Membranes. *Traffic* 5, 838–846. <https://doi.org/10.1111/j.1600-0854.2004.00225.x>
- Mateja, A., Paduch, M., Chang, H.-Y., Szydłowska, A., Kossiakoff, A.A., Hegde, R.S., Keenan, R.J., 2015. Structure of the Get3 targeting factor in complex with its membrane protein cargo. *Science* 347, 1152. <https://doi.org/10.1126/science.1261671>
- Matlin, K.S., 2002. The strange case of the signal recognition particle. *Nat. Rev. Mol. Cell Biol.* 3, 538.
- Matsuura-Tokita, K., Takeuchi, M., Ichihara, A., Mikuriya, K., Nakano, A., 2006. Live imaging of yeast Golgi cisternal maturation. *Nature* 441, 1007.
- Mayor, S., Riezman, H., 2004. Sorting GPI-anchored proteins. *Nat. Rev. Mol. Cell Biol.* 5, 110.
- Mazzarello, P., Garbarino, C., Calligaro, A., 2009. How Camillo Golgi became “the Golgi.” *FEBS Lett.* 583, 3732–3737. <https://doi.org/10.1016/j.febslet.2009.10.018>
- McGough, A., Pope, B., Chiu, W., Weeds, A., 1997. Cofilin changes the twist of F-actin: implications for actin filament dynamics and cellular function. *J. Cell Biol.* 138, 771–781.
- Mehnert, M., Sommer, T., Jarosch, E., 2013. Der1 promotes movement of misfolded proteins through the endoplasmic reticulum membrane. *Nat. Cell Biol.* 16, 77.

- Mellman, I., Simons, K., 1992. The Golgi complex: In vitro veritas? *Cell* 68, 829–840. [https://doi.org/10.1016/0092-8674\(92\)90027-A](https://doi.org/10.1016/0092-8674(92)90027-A)
- Meyer, D.I., Dobberstein, B., 1980a. A membrane component essential for vectorial translocation of nascent proteins across the endoplasmic reticulum: requirements for its extraction and reassociation with the membrane. *J. Cell Biol.* 87, 498. <https://doi.org/10.1083/jcb.87.2.498>
- Meyer, D.I., Dobberstein, B., 1980b. Identification and characterization of a membrane component essential for the translocation of nascent proteins across the membrane of the endoplasmic reticulum. *J. Cell Biol.* 87, 503. <https://doi.org/10.1083/jcb.87.2.503>
- Micaroni, M., Giacchetti, G., Plebani, R., Xiao, G.G., Federici, L., 2016. ATP2C1 gene mutations in Hailey–Hailey disease and possible roles of SPCA1 isoforms in membrane trafficking. *Cell Death Amp Dis.* 7, e2259.
- Milescu, M., Bosmans, F., Lee, S., Alabi, A.A., Kim, J.I., Swartz, K.J., 2009. Interactions between lipids and voltage sensor paddles detected with tarantula toxins. *Nat. Struct. Amp Mol. Biol.* 16, 1080.
- Mironov, A.A., Sesorova, I.V., Beznoussenko, G.V., 2013. Golgi's way: a long path toward the new paradigm of the intra-Golgi transport. *Histochem. Cell Biol.* 140, 383–393. <https://doi.org/10.1007/s00418-013-1141-6>
- Misra, S., Puertollano, R., Kato, Y., Bonifacino, J.S., Hurley, J.H., 2002. Structural basis for acidic-cluster-dileucine sorting-signal recognition by VHS domains. *Nature* 415, 933.
- Missiaen, L., Dode, L., Vanoevelen, J., Raeymaekers, L., Wuytack, F., 2007. Calcium in the Golgi apparatus. *Cell Calcium* 41, 405–416. <https://doi.org/10.1016/j.ceca.2006.11.001>
- Mogelsvang, S., Marsh, B.J., Ladinsky, M.S., Howell, K.E., 2004. Predicting Function from Structure: 3D Structure Studies of the Mammalian Golgi Complex. *Traffic* 5, 338–345. <https://doi.org/10.1111/j.1398-9219.2004.00186.x>
- Montero, M., Brini, M., Marsault, R., Alvarez, J., Sitia, R., Pozzan, T., Rizzuto, R., 1995. Monitoring dynamic changes in free Ca<sup>2+</sup> concentration in the endoplasmic reticulum of intact cells. *EMBO J.* 14, 5467–5475.
- Müller, L., de Escauriaza, M.D., Lajoie, P., Theis, M., Jung, M., Müller, A., Burgard, C., Greiner, M., Snapp, E.L., Dudek, J., Zimmermann, R., 2010. Evolutionary Gain of Function for the ER Membrane Protein Sec62 from Yeast to Humans. *Mol. Biol. Cell* 21, 691–703. <https://doi.org/10.1091/mbc.e09-08-0730>
- Muñiz, M., Zurzolo, C., 2014. Sorting of GPI-anchored proteins from yeast to mammals – common pathways at different sites? *J. Cell Sci.* 127, 2793. <https://doi.org/10.1242/jcs.148056>
- Munro, S., 2003. Lipid Rafts: Elusive or Illusive? *Cell* 115, 377–388. [https://doi.org/10.1016/S0092-8674\(03\)00882-1](https://doi.org/10.1016/S0092-8674(03)00882-1)
- Munro, S., Pelham, H.R.B., 1987. A C-terminal signal prevents secretion of luminal ER proteins. *Cell* 48, 899–907. [https://doi.org/10.1016/0092-8674\(87\)90086-9](https://doi.org/10.1016/0092-8674(87)90086-9)
- Nagahashi, M., Takabe, K., Terracina, K.P., Soma, D., Hirose, Y., Kobayashi, T., Matsuda, Y., Wakai, T., 2014. Sphingosine-1-Phosphate Transporters as Targets for Cancer Therapy. *BioMed Res. Int.* 2014, 1–7. <https://doi.org/10.1155/2014/651727>
- Nakamura, M.T., Yudell, B.E., Loor, J.J., 2014. Regulation of energy metabolism by long-chain fatty acids. *Prog. Lipid Res.* 53, 124–144. <https://doi.org/10.1016/j.plipres.2013.12.001>
- Nixon-Abell, J., Obara, C.J., Weigel, A.V., Li, D., Legant, W.R., Xu, C.S., Pasolli, H.A., Harvey, K., Hess, H.F., Betzig, E., Blackstone, C., Lippincott-Schwartz, J., 2016. Increased spatiotemporal resolution reveals highly dynamic dense tubular matrices in the peripheral ER. *Science* 354. <https://doi.org/10.1126/science.aaf3928>
- NobelPrize.org, 2018. The Nobel Prize in Physiology or Medicine 1906 Nobel Media AB 2018.
- Nyathi, Y., Wilkinson, B.M., Pool, M.R., 2013. Co-translational targeting and translocation of proteins to the endoplasmic reticulum. *Biochim. Biophys. Acta BBA - Mol. Cell Res.* 1833, 2392–2402. <https://doi.org/10.1016/j.bbamcr.2013.02.021>

- Odorizzi, G., Babst, M., Emr, S.D., 2000. Phosphoinositide signaling and the regulation of membrane trafficking in yeast. *Trends Biochem. Sci.* 25, 229–235. [https://doi.org/10.1016/S0968-0004\(00\)01543-7](https://doi.org/10.1016/S0968-0004(00)01543-7)
- Oliver, J.D., van der Wal, F.J., Bulleid, N.J., High, S., 1997. Interaction of the Thiol-Dependent Reductase ERp57 with Nascent Glycoproteins. *Science* 275, 86. <https://doi.org/10.1126/science.275.5296.86>
- Ong, W.-Y., Herr, D.R., Farooqui, T., Ling, E.-A., Farooqui, A.A., 2015. Role of sphingomyelinases in neurological disorders. *Expert Opin. Ther. Targets* 19, 1725–1742. <https://doi.org/10.1517/14728222.2015.1071794>
- Owen, D.J., Collins, B.M., Evans, P.R., 2004. ADAPTORS FOR CLATHRIN COATS: Structure and Function. *Annu. Rev. Cell Dev. Biol.* 20, 153–191. <https://doi.org/10.1146/annurev.cellbio.20.010403.104543>
- Pakdel, M., von Blume, J., 2018. Exploring new routes for secretory protein export from the trans-Golgi network. *Mol. Biol. Cell* 29, 235–240. <https://doi.org/10.1091/mbc.E17-02-0117>
- Paladino, S., Sarnataro, D., Pillich, R., Tivodar, S., Nitsch, L., Zurzolo, C., 2004. Protein oligomerization modulates raft partitioning and apical sorting of GPI-anchored proteins. *J. Cell Biol.* 167, 699. <https://doi.org/10.1083/jcb.200407094>
- Park, E., Rapoport, T.A., 2012. Mechanisms of Sec61/SecY-Mediated Protein Translocation Across Membranes. *Annu. Rev. Biophys.* 41, 21–40. <https://doi.org/10.1146/annurev-biophys-050511-102312>
- Park, S.-Y., Yang, J.-S., Schmider, A.B., Soberman, R.J., Hsu, V.W., 2015. Coordinated regulation of bidirectional COPI transport at the Golgi by CDC42. *Nature* 521, 529.
- Payraastre, B., Missy, K., Giuriato, S., Bodin, S., Plantavid, M., Gratacap, M.-P., 2001. Phosphoinositides : key players in cell signalling, in time and space. *Cell. Signal.* 13, 377–387. [https://doi.org/10.1016/S0898-6568\(01\)00158-9](https://doi.org/10.1016/S0898-6568(01)00158-9)
- Pelham, H.R., Rothman, J.E., 2000. The Debate about Transport in the Golgi—Two Sides of the Same Coin? *Cell* 102, 713–719. [https://doi.org/10.1016/S0092-8674\(00\)00060-X](https://doi.org/10.1016/S0092-8674(00)00060-X)
- Peterson, J.R., Ora, A., Van, P.N., Helenius, A., 1995. Transient, lectin-like association of calreticulin with folding intermediates of cellular and viral glycoproteins. *Mol. Biol. Cell* 6, 1173–1184. <https://doi.org/10.1091/mbc.6.9.1173>
- Pfeffer, S., Aivazian, D., 2004. Targeting Rab GTPases to distinct membrane compartments. *Nat. Rev. Mol. Cell Biol.* 5, 886.
- Phillips, M.J., Voeltz, G.K., 2015. Structure and function of ER membrane contact sites with other organelles. *Nat. Rev. Mol. Cell Biol.* 17, 69.
- Pike, L.J., Miller, J.M., 1998. Cholesterol Depletion Delocalizes Phosphatidylinositol Bisphosphate and Inhibits Hormone-stimulated Phosphatidylinositol Turnover. *J. Biol. Chem.* 273, 22298–22304. <https://doi.org/10.1074/jbc.273.35.22298>
- Pizzo, P., Lissandron, V., Pozzan, T., 2010. The trans-Golgi compartment. *Commun. Integr. Biol.* 3, 462–464. <https://doi.org/10.4161/cib.3.5.12473>
- Planey, S.L., Keay, S.K., Zhang, C.-O., Zacharias, D.A., Margolis, B., 2009. Palmitoylation of Cytoskeleton Associated Protein 4 by DHHC2 Regulates Antiproliferative Factor-mediated Signaling. *Mol. Biol. Cell* 20, 1454–1463. <https://doi.org/10.1091/mbc.e08-08-0849>
- Pollard, T.D., Borisy, G.G., 2003. Cellular Motility Driven by Assembly and Disassembly of Actin Filaments. *Cell* 112, 453–465. [https://doi.org/10.1016/S0092-8674\(03\)00120-X](https://doi.org/10.1016/S0092-8674(03)00120-X)
- Possenti, R., Rinaldi, A.M., Ferri, G.-L., Borboni, P., Trani, E., Levi, A., 1999. Expression, Processing, and Secretion of the Neuroendocrine VGF Peptides by INS-1 Cells<sup>1</sup>. *Endocrinology* 140, 3727–3735. <https://doi.org/10.1210/endo.140.8.6920>
- Potelle, S., Klein, A., Foulquier, F., 2015. Golgi post-translational modifications and associated diseases. *J. Inher. Metab. Dis.* 38, 741–751. <https://doi.org/10.1007/s10545-015-9851-7>

- Presley, J.F., Cole, N.B., Schroer, T.A., Hirschberg, K., Zaal, K.J.M., Lippincott-Schwartz, J., 1997. ER-to-Golgi transport visualized in living cells. *Nature* 389, 81.
- Qi, L., Tsai, B., Arvan, P., 2017. New Insights into the Physiological Role of Endoplasmic Reticulum-Associated Degradation. *Trends Cell Biol.* 27, 430–440. <https://doi.org/10.1016/j.tcb.2016.12.002>
- Raas-Rothschild, A., Pankova-Kholmyansky, I., Kacher, Y., Futerman, A.H., 2004. Glycosphingolipidoses: Beyond the enzymatic defect. *Glycoconj. J.* 21, 295–304. <https://doi.org/10.1023/B:GLYC.0000046272.38480.ef>
- Rabouille, C., Klumperman, J., 2005. The maturing role of COPI vesicles in intra-Golgi transport. *Nat. Rev. Mol. Cell Biol.* 6, 812.
- Raiborg, C., Bremnes, B., Mehlum, A., Gillooly, D.J., D'Arrigo, A., Stang, E., Stenmark, H., 2001. FYVE and coiled-coil domains determine the specific localisation of Hrs to early endosomes. *J. Cell Sci.* 114, 2255–2263.
- Ramu, Y., Xu, Y., Lu, Z., 2006. Enzymatic activation of voltage-gated potassium channels. *Nature* 442, 696.
- Rapoport, T., 1992. Transport of proteins across the endoplasmic reticulum membrane. *Science* 258, 931. <https://doi.org/10.1126/science.1332192>
- Rapoport, T.A., 2007. Protein translocation across the eukaryotic endoplasmic reticulum and bacterial plasma membranes. *Nature* 450, 663.
- Reczek, D., Schwake, M., Schröder, J., Hughes, H., Blanz, J., Jin, X., Brondyk, W., Van Patten, S., Edmunds, T., Saftig, P., 2007. LIMP-2 Is a Receptor for Lysosomal Mannose-6-Phosphate-Independent Targeting of  $\beta$ -Glucocerebrosidase. *Cell* 131, 770–783. <https://doi.org/10.1016/j.cell.2007.10.018>
- Resh, M.D., 2016. Fatty acylation of proteins: The long and the short of it. *Prog. Lipid Res.* 63, 120–131. <https://doi.org/10.1016/j.plipres.2016.05.002>
- Ritter, S.L., Hall, R.A., 2009. Fine-tuning of GPCR activity by receptor-interacting proteins. *Nat. Rev. Mol. Cell Biol.* 10, 819.
- Roghi, C., Allan, V.J., 1999. Dynamic association of cytoplasmic dynein heavy chain 1a with the Golgi apparatus and intermediate compartment. *J. Cell Sci.* 112, 4673.
- Rohrer, J., Kornfeld, R., Pfeffer, S.R., 2001. Lysosomal Hydrolase Mannose 6-Phosphate Uncovering Enzyme Resides in the trans-Golgi Network. *Mol. Biol. Cell* 12, 1623–1631. <https://doi.org/10.1091/mbc.12.6.1623>
- Rosso, S., Bollati, F., Bisbal, M., Peretti, D., Sumi, T., Nakamura, T., Quiroga, S., Ferreira, A., Cáceres, A., 2004. LIMK1 Regulates Golgi Dynamics, Traffic of Golgi-derived Vesicles, and Process Extension in Primary Cultured Neurons. *Mol. Biol. Cell* 15, 3433–3449. <https://doi.org/10.1091/mbc.e03-05-0328>
- Ruggiano, A., Foresti, O., Carvalho, P., 2014. ER-associated degradation: Protein quality control and beyond. *J. Cell Biol.* 204, 869. <https://doi.org/10.1083/jcb.201312042>
- Sackmann, E., Feder, T., 1995. Budding, fission and domain formation in mixed lipid vesicles induced by lateral phase separation and macromolecular condensation. *Mol. Membr. Biol.* 12, 21–28. <https://doi.org/10.3109/09687689509038491>
- Saint-Pol, A., Yélamos, B., Amessou, M., Mills, I.G., Dugast, M., Tenza, D., Schu, P., Antony, C., McMahon, H.T., Lamaze, C., Johannes, L., 2004. Clathrin Adaptor epsinR Is Required for Retrograde Sorting on Early Endosomal Membranes. *Dev. Cell* 6, 525–538. [https://doi.org/10.1016/S1534-5807\(04\)00100-5](https://doi.org/10.1016/S1534-5807(04)00100-5)
- Salaun, C., Greaves, J., Chamberlain, L.H., 2010. The intracellular dynamic of protein palmitoylation. *J. Cell Biol.* 191, 1229. <https://doi.org/10.1083/jcb.201008160>
- Saliba, A.-E., Vonkova, I., Gavin, A.-C., 2015. The systematic analysis of protein–lipid interactions comes of age. *Nat. Rev. Mol. Cell Biol.* 16, 753.

- Sato, K., 2004. COPII Coat Assembly and Selective Export from the Endoplasmic Reticulum. *J. Biochem. (Tokyo)* 136, 755–760. <https://doi.org/10.1093/jb/mvh184>
- Scherer, P.E., Lederkremer, G.Z., Williams, S., Fogliano, M., Baldini, G., Lodish, H.F., 1996. Cab45, a novel (Ca<sup>2+</sup>)-binding protein localized to the Golgi lumen. *J. Cell Biol.* 133, 257–268. <https://doi.org/10.1083/jcb.133.2.257>
- Schiller, H.B., Fässler, R., 2013. Mechanosensitivity and compositional dynamics of cell–matrix adhesions. *EMBO Rep.* 14, 509. <https://doi.org/10.1038/embor.2013.49>
- Schmidt, K., Dartsch, H., Linder, D., Kern, H.F., Kleene, R., 2000. A submembranous matrix of proteoglycans on zymogen granule membranes is involved in granule formation in rat pancreatic acinar cells. *J. Cell Sci.* 113, 2233.
- Schrag, J.D., Bergeron, J.J.M., Li, Y., Borisova, S., Hahn, M., Thomas, D.Y., Cygler, M., 2001. The Structure of Calnexin, an ER Chaperone Involved in Quality Control of Protein Folding. *Mol. Cell* 8, 633–644. [https://doi.org/10.1016/S1097-2765\(01\)00318-5](https://doi.org/10.1016/S1097-2765(01)00318-5)
- Schuldiner, M., Metz, J., Schmid, V., Denic, V., Rakwalska, M., Schmitt, H.D., Schwappach, B., Weissman, J.S., 2008. The GET Complex Mediates Insertion of Tail-Anchored Proteins into the ER Membrane. *Cell* 134, 634–645. <https://doi.org/10.1016/j.cell.2008.06.025>
- Scott, D.C., Schekman, R., 2008. Role of Sec61p in the ER-associated degradation of short-lived transmembrane proteins. *J. Cell Biol.* 181, 1095. <https://doi.org/10.1083/jcb.200804053>
- Sepúlveda, M.R., Berrocal-Carrillo, M., Gasset, M., Mata, A.M., 2006. The Plasma Membrane Ca<sup>2+</sup>-ATPase Isoform 4 Is Localized in Lipid Rafts of Cerebellum Synaptic Plasma Membranes. *J. Biol. Chem.* 281, 447–453. <https://doi.org/10.1074/jbc.M506950200>
- Sethi, M.K., Buettner, F.F.R., Krylov, V.B., Takeuchi, H., Nifantiev, N.E., Haltiwanger, R.S., Gerardy-Schahn, R., Bakker, H., 2010. Identification of Glycosyltransferase 8 Family Members as Xylosyltransferases Acting on O-Glycosylated Notch Epidermal Growth Factor Repeats. *J. Biol. Chem.* 285, 1582–1586. <https://doi.org/10.1074/jbc.C109.065409>
- Shaw, A.S., 2006. Lipid rafts: now you see them, now you don't. *Nat. Immunol.* 7, 1139.
- Shibata, Y., Voeltz, G.K., Rapoport, T.A., 2006. Rough Sheets and Smooth Tubules. *Cell* 126, 435–439. <https://doi.org/10.1016/j.cell.2006.07.019>
- Shimizu, T., 2009. Lipid Mediators in Health and Disease: Enzymes and Receptors as Therapeutic Targets for the Regulation of Immunity and Inflammation. *Annu. Rev. Pharmacol. Toxicol.* 49, 123–150. <https://doi.org/10.1146/annurev.pharmtox.011008.145616>
- Shin, H.-W., Hayashi, M., Christoforidis, S., Lacas-Gervais, S., Hoepfner, S., Wenk, M.R., Modregger, J., Uttenweiler-Joseph, S., Wilm, M., Nystuen, A., Frankel, W.N., Solimena, M., De Camilli, P., Zerial, M., 2005. An enzymatic cascade of Rab5 effectors regulates phosphoinositide turnover in the endocytic pathway. *J. Cell Biol.* 170, 607. <https://doi.org/10.1083/jcb.200505128>
- Siegel, V., Walter, P., 1988. Each of the activities of signal recognition particle (SRP) is contained within a distinct domain: Analysis of biochemical mutants of SRP. *Cell* 52, 39–49. [https://doi.org/10.1016/0092-8674\(88\)90529-6](https://doi.org/10.1016/0092-8674(88)90529-6)
- Simanshu, D.K., Kamlekar, R.K., Wijesinghe, D.S., Zou, X., Zhai, X., Mishra, S.K., Molotkovsky, J.G., Malinina, L., Hinchcliffe, E.H., Chalfant, C.E., Brown, R.E., Patel, D.J., 2013. Non-vesicular trafficking by a ceramide-1-phosphate transfer protein regulates eicosanoids. *Nature* 500, 463.
- Simons, K., Ehehalt, R., 2002. Cholesterol, lipid rafts, and disease. *J. Clin. Invest.* 110, 597–603. <https://doi.org/10.1172/JCI16390>
- Simons, K., Ikonen, E., 1997. Functional rafts in cell membranes. *Nature* 387, 569.
- Simons, K., Van Meer, G., 1988. Lipid sorting in epithelial cells. *Biochemistry* 27, 6197–6202. <https://doi.org/10.1021/bi00417a001>
- Simonsen, A., Lippe, R., Christoforidis, S., Gaullier, J.-M., Brech, A., Callaghan, J., Toh, B.-H., Murphy, C., Zerial, M., Stenmark, H., 1998. EEA1 links PI(3)K function to Rab5 regulation of endosome fusion. *Nature* 394, 494.

- Sitia, R., Meldolesi, J., 1992. Endoplasmic reticulum: a dynamic patchwork of specialized subregions. *Mol. Biol. Cell* 3, 1067–1072. <https://doi.org/10.1091/mbc.3.10.1067>
- Smith, E.R., Merrill Jr., A.H., Obeid, L.M., Hannun, Y.A., 2000. [28] - Effects of Sphingosine and Other Sphingolipids on Protein Kinase C, in: Merrill, A.H., Hannun, Y.A. (Eds.), *Methods in Enzymology*. Academic Press, pp. 361–373. [https://doi.org/10.1016/S0076-6879\(00\)12921-0](https://doi.org/10.1016/S0076-6879(00)12921-0)
- Söllner, T., Bennett, M.K., Whiteheart, S.W., Scheller, R.H., Rothman, J.E., 1993. A protein assembly-disassembly pathway in vitro that may correspond to sequential steps of synaptic vesicle docking, activation, and fusion. *Cell* 75, 409–418. [https://doi.org/10.1016/0092-8674\(93\)90376-2](https://doi.org/10.1016/0092-8674(93)90376-2)
- Sommer, T., Jentsch, S., 1993. A protein translocation defect linked to ubiquitin conjugation at the endoplasmic reticulum. *Nature* 365, 176.
- Spahn, C.M., Gomez-Lorenzo, M.G., Grassucci, R.A., Jørgensen, R., Andersen, G.R., Beckmann, R., Penczek, P.A., Ballesta, J.P., Frank, J., 2004. Domain movements of elongation factor eEF2 and the eukaryotic 80S ribosome facilitate tRNA translocation. *EMBO J.* 23, 1008. <https://doi.org/10.1038/sj.emboj.7600102>
- Stanley, P., 2011. Golgi Glycosylation. *Cold Spring Harb. Perspect. Biol.* 3. <https://doi.org/10.1101/cshperspect.a005199>
- Stefanovic, S., Hegde, R.S., 2007. Identification of a Targeting Factor for Posttranslational Membrane Protein Insertion into the ER. *Cell* 128, 1147–1159. <https://doi.org/10.1016/j.cell.2007.01.036>
- Stenmark, H., 2009. Rab GTPases as coordinators of vesicle traffic. *Nat. Rev. Mol. Cell Biol.* 10, 513.
- Stephens, S.B., Schisler, J.C., Hohmeier, H.E., An, J., Sun, A.Y., Pitt, G.S., Newgard, C.B., 2012. A VGF-Derived Peptide Attenuates Development of Type 2 Diabetes via Enhancement of Islet  $\beta$ -Cell Survival and Function. *Cell Metab.* 16, 33–43. <https://doi.org/10.1016/j.cmet.2012.05.011>
- Storrie, B., Desjardins, M., 1996. The biogenesis of lysosomes: Is it a kiss and run, continuous fusion and fission process? *BioEssays* 18, 895–903. <https://doi.org/10.1002/bies.950181108>
- Sudbrak, R., 2000. Hailey-Hailey disease is caused by mutations in ATP2C1 encoding a novel Ca<sup>2+</sup> pump. *Hum. Mol. Genet.* 9, 1131–1140. <https://doi.org/10.1093/hmg/9.7.1131>
- Tafesse, F.G., Sanyal, S., Ashour, J., Guimaraes, C.P., Hermansson, M., Somerharju, P., Ploegh, H.L., 2013. Intact sphingomyelin biosynthetic pathway is essential for intracellular transport of influenza virus glycoproteins. *Proc. Natl. Acad. Sci.* 110, 6406. <https://doi.org/10.1073/pnas.1219909110>
- Tagaya, M., Simmen, T. (Eds.), 2017. *Organelle Contact Sites, Advances in Experimental Medicine and Biology*. Springer Singapore, Singapore. <https://doi.org/10.1007/978-981-10-4567-7>
- Tanaka, K., Caaveiro, J.M.M., Morante, K., González-Mañas, J.M., Tsumoto, K., 2015. Structural basis for self-assembly of a cytolytic pore lined by protein and lipid. *Nat. Commun.* 6, 6337.
- Tessier, D.C., Dignard, D., Zapun, A., Radomska-Pandya, A., Parodi, A.J., Bergeron, J.J.M., Thomas, D.Y., 2000. Cloning and characterization of mammalian UDP-glucose glycoprotein: glucosyltransferase and the development of a specific substrate for this enzyme. *Glycobiology* 10, 403–412. <https://doi.org/10.1093/glycob/10.4.403>
- Thyberg, J., Moskalewski, S., 1999. Role of Microtubules in the Organization of the Golgi Complex. *Exp. Cell Res.* 246, 263–279. <https://doi.org/10.1006/excr.1998.4326>
- Traub, L.M., 2005. Common principles in clathrin-mediated sorting at the Golgi and the plasma membrane. *Biochim. Biophys. Acta* 1744, 415–437. <https://doi.org/10.1016/j.bbamcr.2005.04.005>
- Trombetta, E.S., Helenius, A., 2000. Conformational Requirements for Glycoprotein Reglucosylation in the Endoplasmic Reticulum. *J. Cell Biol.* 148, 1123. <https://doi.org/10.1083/jcb.148.6.1123>
- van Galen, J., Campelo, F., Martínez-Alonso, E., Scarpa, M., Martínez-Menárguez, J.Á., Malhotra, V., 2014. Sphingomyelin homeostasis is required to form functional enzymatic domains at the trans-Golgi network. *J. Cell Biol.* 206, 609. <https://doi.org/10.1083/jcb.201405009>

- van Meer, G., Voelker, D.R., Feigenson, G.W., 2008. Membrane lipids: where they are and how they behave. *Nat. Rev. Mol. Cell Biol.* 9, 112.
- van Rheenen, J., Song, X., van Roosmalen, W., Cammer, M., Chen, X., DesMarais, V., Yip, S.-C., Backer, J.M., Eddy, R.J., Condeelis, J.S., 2007. EGF-induced PIP<sub>2</sub> hydrolysis releases and activates cofilin locally in carcinoma cells. *J. Cell Biol.* 179, 1247. <https://doi.org/10.1083/jcb.200706206>
- Vanoevelen, J., Dode, L., Van Baelen, K., Fairclough, R.J., Missiaen, L., Raeymaekers, L., Wuytack, F., 2005. The Secretory Pathway Ca<sup>2+</sup>/Mn<sup>2+</sup>-ATPase 2 Is a Golgi-localized Pump with High Affinity for Ca<sup>2+</sup> Ions. *J. Biol. Chem.* 280, 22800–22808. <https://doi.org/10.1074/jbc.M501026200>
- Varki, A., Gagneux, P., 2015. Biological Functions of Glycans, in: *Essentials of Glycobiology* [Internet]. Cold Spring Harbor (NY): Cold Spring Harbor Laboratory Press, p. Chapter 7.
- Varki, A., Lowe, J.B., 2009. Biological Roles of Glycans, in: Varki, A., Cummings, R.D., Esko, J.D., Freeze, H.H., Stanley, P., Bertozzi, C.R., Hart, G.W., Etzler, M.E. (Eds.), *Essentials of Glycobiology*. Cold Spring Harbor Laboratory Press, Cold Spring Harbor (NY).
- Vembar, S.S., Brodsky, J.L., 2008. One step at a time: endoplasmic reticulum-associated degradation. *Nat. Rev. Mol. Cell Biol.* 9, 944.
- Venditti, R., Wilson, C., De Matteis, M.A., 2014. Exiting the ER: what we know and what we don't. *Spec. Issue Membr. Traffick.* 24, 9–18. <https://doi.org/10.1016/j.tcb.2013.08.005>
- von Blume, J., Alleaume, A.-M., Kienzle, C., Carreras-Sureda, A., Valverde, M., Malhotra, V., 2012. Cab45 is required for Ca<sup>2+</sup>-dependent secretory cargo sorting at the trans-Golgi network. *J. Cell Biol.* 199, 1057–1066. <https://doi.org/10.1083/jcb.201207180>
- von Blume, J., Duran, J.M., Forlanelli, E., Alleaume, A.-M., Egorov, M., Polishchuk, R., Molina, H., Malhotra, V., 2009. Actin remodeling by ADF/cofilin is required for cargo sorting at the trans-Golgi network. *J. Cell Biol.* 187, 1055–1069. <https://doi.org/10.1083/jcb.200908040>
- von Heijne, G., 1990. The signal peptide. *J. Membr. Biol.* 115, 195–201. <https://doi.org/10.1007/BF01868635>
- von Heijne, G., 1986. Towards a comparative anatomy of N-terminal topogenic protein sequences. *J. Mol. Biol.* 189, 239–242. [https://doi.org/10.1016/0022-2836\(86\)90394-3](https://doi.org/10.1016/0022-2836(86)90394-3)
- von Heijne, G., 1985. Signal sequences: The limits of variation. *J. Mol. Biol.* 184, 99–105. [https://doi.org/10.1016/0022-2836\(85\)90046-4](https://doi.org/10.1016/0022-2836(85)90046-4)
- von Blume, J., Alleaume, A.-M., Cantero-Recasens, G., Curwin, A., Carreras-Sureda, A., Zimmermann, T., van Galen, J., Wakana, Y., Valverde, M.A., Malhotra, V., 2011. ADF/Cofilin Regulates Secretory Cargo Sorting at the TGN via the Ca<sup>2+</sup> ATPase SPCA1. *Dev. Cell* 20, 652–662. <https://doi.org/10.1016/j.devcel.2011.03.014>
- Voorhees, R.M., Hegde, R.S., 2016. Toward a structural understanding of co-translational protein translocation. *Cell Organelles* 41, 91–99. <https://doi.org/10.1016/j.ceb.2016.04.009>
- Voss, M., Schröder, B., Fluhrer, R., 2013. Mechanism, specificity, and physiology of signal peptide peptidase (SPP) and SPP-like proteases. *Intramembrane Proteases* 1828, 2828–2839. <https://doi.org/10.1016/j.bbamem.2013.03.033>
- Wahlman, J., DeMartino, G.N., Skach, W.R., Bulleid, N.J., Brodsky, J.L., Johnson, A.E., 2007. Real-Time Fluorescence Detection of ERAD Substrate Retrotranslocation in a Mammalian In Vitro System. *Cell* 129, 943–955. <https://doi.org/10.1016/j.cell.2007.03.046>
- Wakana, Y., Kotake, R., Oyama, N., Murate, M., Kobayashi, T., Arasaki, K., Inoue, H., Tagaya, M., Linstedt, A., 2015. CARTS biogenesis requires VAP–lipid transfer protein complexes functioning at the endoplasmic reticulum–Golgi interface. *Mol. Biol. Cell* 26, 4686–4699. <https://doi.org/10.1091/mbc.E15-08-0599>
- Wallin, E., Heijne, G.V., 2008. Genome-wide analysis of integral membrane proteins from eubacterial, archaean, and eukaryotic organisms. *Protein Sci.* 7, 1029–1038. <https://doi.org/10.1002/pro.5560070420>

- Walter, P., Blobel, G., 1981a. Translocation of proteins across the endoplasmic reticulum. II. Signal recognition protein (SRP) mediates the selective binding to microsomal membranes of in-vitro-assembled polysomes synthesizing secretory protein. *J. Cell Biol.* 91, 551. <https://doi.org/10.1083/jcb.91.2.551>
- Walter, P., Blobel, G., 1981b. Translocation of proteins across the endoplasmic reticulum III. Signal recognition protein (SRP) causes signal sequence-dependent and site-specific arrest of chain elongation that is released by microsomal membranes. *J. Cell Biol.* 91, 557. <https://doi.org/10.1083/jcb.91.2.557>
- Walter, P., Blobel, G., 1980. Purification of a membrane-associated protein complex required for protein translocation across the endoplasmic reticulum. *Proc. Natl. Acad. Sci. U. S. A.* 77, 7112–7116.
- Walter, P., Ibrahimi, I., Blobel, G., 1981. Translocation of proteins across the endoplasmic reticulum. I. Signal recognition protein (SRP) binds to in-vitro-assembled polysomes synthesizing secretory protein. *J. Cell Biol.* 91, 545–550. <https://doi.org/10.1083/jcb.91.2.545>
- Wang, W., Eddy, R., Condeelis, J., 2007. The cofilin pathway in breast cancer invasion and metastasis. *Nat. Rev. Cancer* 7, 429.
- Warren, G., Malhotra, V., 1998. The organisation of the Golgi apparatus. *Curr. Opin. Cell Biol.* 10, 493–498. [https://doi.org/10.1016/S0955-0674\(98\)80064-1](https://doi.org/10.1016/S0955-0674(98)80064-1)
- Wegner, M.-S., Schiffmann, S., Parnham, M.J., Geisslinger, G., Grösch, S., 2016. The enigma of ceramide synthase regulation in mammalian cells. *Prog. Lipid Res.* 63, 93–119. <https://doi.org/10.1016/j.plipres.2016.03.006>
- Weihofen, A., Binns, K., Lemberg, M.K., Ashman, K., Martoglio, B., 2002. Identification of Signal Peptide Peptidase, a Presenilin-Type Aspartic Protease. *Science* 296, 2215. <https://doi.org/10.1126/science.1070925>
- Welsh, J.B., Sapinoso, L.M., Kern, S.G., Brown, D.A., Liu, T., Bauskin, A.R., Ward, R.L., Hawkins, N.J., Quinn, D.I., Russell, P.J., Sutherland, R.L., Breit, S.N., Moskaluk, C.A., Frierson, H.F., Hampton, G.M., 2003. Large-scale delineation of secreted protein biomarkers overexpressed in cancer tissue and serum. *Proc. Natl. Acad. Sci.* 100, 3410. <https://doi.org/10.1073/pnas.0530278100>
- Westrate, L.M., Lee, J.E., Prinz, W.A., Voeltz, G.K., 2015. Form Follows Function: The Importance of Endoplasmic Reticulum Shape. *Annu. Rev. Biochem.* 84, 791–811. <https://doi.org/10.1146/annurev-biochem-072711-163501>
- Wiertz, E.J.H., Jones, T.R., Sun, L., Bogyo, M., Geuze, H.J., Ploegh, H.L., 1996. The Human Cytomegalovirus US11 Gene Product Dislocates MHC Class I Heavy Chains from the Endoplasmic Reticulum to the Cytosol. *Cell* 84, 769–779. [https://doi.org/10.1016/S0092-8674\(00\)81054-5](https://doi.org/10.1016/S0092-8674(00)81054-5)
- Wiertz, E.J.H., Tortorella, D., Bogyo, M., Yu, J., Mothes, W., Jones, T.R., Rapoport, T.A., Ploegh, H.L., 1996. Sec61-mediated transfer of a membrane protein from the endoplasmic reticulum to the proteasome for destruction. *Nature* 384, 432.
- Wijesinghe, D.S., Massiello, A., Subramanian, P., Szulc, Z., Bielawska, A., Chalfant, C.E., 2005. Substrate specificity of human ceramide kinase. *J. Lipid Res.* 46, 2706–2716. <https://doi.org/10.1194/jlr.M500313-JLR200>
- Williams, T.A., Foster, P.G., Cox, C.J., Embley, T.M., 2013. An archaeal origin of eukaryotes supports only two primary domains of life. *Nature* 504, 231.
- Wilson, D.N., Doudna, Cate, J.H., 2012. The Structure and Function of the Eukaryotic Ribosome. *Cold Spring Harb. Perspect. Biol.* 4, a011536. <https://doi.org/10.1101/cshperspect.a011536>
- Wong, M., Munro, S., 2014. The specificity of vesicle traffic to the Golgi is encoded in the golgin coiled-coil proteins. *Science* 346. <https://doi.org/10.1126/science.1256898>
- Xie, W., Kanehara, K., Sayeed, A., Ng, D.T.W., Brodsky, J.L., 2009. Intrinsic Conformational Determinants Signal Protein Misfolding to the Hrd1/Htm1 Endoplasmic Reticulum-associated Degradation System. *Mol. Biol. Cell* 20, 3317–3329. <https://doi.org/10.1091/mbc.e09-03-0231>

- Xu, C., Ng, D.T.W., 2015. Glycosylation-directed quality control of protein folding. *Nat. Rev. Mol. Cell Biol.* 16, 742.
- Xu, Y., Ramu, Y., Lu, Z., 2008. Removal of phospho-head groups of membrane lipids immobilizes voltage sensors of K<sup>+</sup> channels. *Nature* 451, 826.
- Ye, Y., Shibata, Y., Yun, C., Ron, D., Rapoport, T.A., 2004. A membrane protein complex mediates retrotranslocation from the ER lumen into the cytosol. *Nature* 429, 841.
- Yonezawa, N., Nishida, E., Iida, K., Yahara, I., Sakai, H., 1990. Inhibition of the interactions of cofilin, destrin, and deoxyribonuclease I with actin by phosphoinositides. *J. Biol. Chem.* 265, 8382–8386.
- Yoshihisa, T., Barlowe, C., Schekman, R., 1993. Requirement for a GTPase-activating protein in vesicle budding from the endoplasmic reticulum. *Science* 259, 1466. <https://doi.org/10.1126/science.8451644>
- Zech, T., Ejsing, C.S., Gaus, K., de Wet, B., Shevchenko, A., Simons, K., Harder, T., 2009. Accumulation of raft lipids in T-cell plasma membrane domains engaged in TCR signalling. *EMBO J.* 28, 466. <https://doi.org/10.1038/emboj.2009.6>
- Zerial, M., McBride, H., 2001. Rab proteins as membrane organizers. *Nat. Rev. Mol. Cell Biol.* 2, 107.
- Zhao, Y., Ren, J., Padilla-Parra, S., Fry, E.E., Stuart, D.I., 2014. Lysosome sorting of  $\beta$ -glucocerebrosidase by LIMP-2 is targeted by the mannose 6-phosphate receptor. *Nat. Commun.* 5, 4321.
- Zhou, Y.-F., Metcalf, M.C., Garman, S.C., Edmunds, T., Qiu, H., Wei, R.R., 2016. Human acid sphingomyelinase structures provide insight to molecular basis of Niemann–Pick disease. *Nat. Commun.* 7, 13082.

## Widmung

Diese Dissertation ist meinen Eltern gewidmet.

Euer Mut ebnete mir diesen Weg.

این پایان نامه تقدیم می شود به پدر و مادرم.

شجاعت شما این مسیر را برایم هموار کرد.

### Danksagungen

An dieser Stelle möchte ich mich bei all jenen bedanken, die mich im Rahmen dieser Dissertation begleitet haben.

Zuallererst möchte ich mich bei meiner Gruppenleiterin Dr. Julia von Blume für ihre fortlaufende Betreuung und Leitung bedanken. Mir wurde ermöglicht nach kurzer Zeit an wichtigen Projekten zu arbeiten und meine eigenen Ideen einzubringen. Dabei wurde ich stets im wissenschaftlichen Bereich aber auch bei meinen außerfachlichen Aktivitäten innerhalb des Instituts unterstützt.

Des Weiteren gilt mein Dank an meinen Doktorvater Prof. Dr. Reinhard Fässler, der meine Dissertation begleitet hat. Ich möchte mich insbesondere für die wertvollen Ratschläge und kritischen Fragen, die oft aus einer anderen Perspektive gestellt wurden, und dadurch maßgeblich zur Entwicklung dieser Arbeit beigetragen haben, bedanken.

Ein besonderer Dank gilt auch an Prof. Dr. Christopher Burd aus der Yale School of Medicine in den USA. Unsere erfolgreiche Kollaboration und die vielen Videokonferenzen und persönlichen Treffen brachten viel Abwechslung in den wissenschaftlichen Alltag.

Eine Dissertation wäre nicht möglich ohne die Unterstützung des von Blume Labors. Dabei möchte ich vor allem bei Dr. Birgit Blank bedanken, die mich mit großer Geduld vor allem in der ersten Phase meiner Dissertation in alle Techniken und Abläufe eingelernt hat und tatkräftig an unserem Manuskript mitgewirkt hat. Danke an Gisela Beck, die stets alle organisatorischen Abläufe übernommen hat und immer hilfreiche praktische Ratschläge hatte. Des Weiteren möchte ich mich bei Renate Gautsch bedanken, die gewissenhaft viele Aufgaben vor allem im Bereich der Zellkultur übernommen hat. Danke an Tobias Hecht für hitzige Debatten mit einem anderen Blickwinkel auf gesellschaftliche Themen und das ein oder andere Feierabendbier außerhalb des Instituts. Ich bedanke mich bei Natalia Pacheco-Fernandez und Michael Raum für viele Diskussionen sei es wissenschaftlicher, gesellschaftlicher oder politischer Natur. Ein Dankeschön gilt auch an Mai-Ly Tran, die immer humorvoll und

hilfsbereit war, besonders zu Fragen und Anregungen bei Darstellung von Abbildungen. Danke an Wolfgang Fink für die technische Unterstützung und den vielen politischen und historischen Gesprächen.

An dieser Stelle möchte ich mich auch bei meinen Kollaborationspartnern Yongqiang Deng und Emma Sundberg bedanken, die unermüdlich an unserem Manuskript gearbeitet haben und wir gemeinsam aus einem Hinweis eine wissenschaftliche Publikation realisieren konnten.

Mein großer Dank gilt auch an Prof. Dr. Carsten Grashoff und an des gesamten Grashoff Labors für wertvolle Rückmeldungen und Vorschläge vor allem innerhalb unserer gemeinsamen Montagsseminaren.

Ich möchte mich auch bei der gesamten Abteilung für molekulare Medizin für ihre Hilfe bei alltäglichen Fragen und Vorschlägen bedanken. Ein besonderer Dank gilt an Hildegard Reiter für die Hilfe bei der Herstellung von stabilen Zelllinien. Vielen Dank auch für die kompetente Unterstützung bei der Mikroskopie durch Dr. Martin Spitaler und Markus Oster von der Imaging Facility des Max-Planck-Instituts für Biochemie.

Hierbei möchte ich mich auch bei meinem Thesis Advisory Committee Prof. Dr. Ralf Jungmann und Dr. Alvaro Crevenna bedanken, die während dieser Treffen sehr wertvolle Ratschläge und Anregungen beitragen konnten.

Ich möchte mich auch herzlich bei meiner Familie und meinen Freunden bedanken, die mich während meiner Dissertation moralisch unterstützt haben und für die ein oder andere Ablenkung vom wissenschaftlichen Alltag gesorgt haben.

Natürlich möchte ich mich an dieser Stelle auch herzlich bei meiner liebevollen Frau Alina bedanken, die mir während meiner Dissertation ausdauernd emotionalen Rückhalt gab. Mit ihrer Lebenslust, Heiterkeit und den vielen gemeinsamen, unvergesslichen Erlebnissen schenkte sie mir einen unschätzbaren Ausgleich vom Alltag.

Abschließend möchte ich hervorheben, dass diese Arbeit ohne die anhaltende Entschlossenheit und den eindrucksvollen Verdiensten meiner Eltern nicht entstanden wäre. Ihre hohe Wertschätzung in Bildung und ihre uneingeschränkte aufrichtige Unterstützung ebneten mir diesen Weg. Aus diesem Grund ist es mir eine große Freude diese Dissertation ihnen zu widmen.

# Secretory cargo sorting by Ca<sup>2+</sup>-dependent Cab45 oligomerization at the trans-Golgi network

Alvaro H. Crevenna,<sup>1\*</sup> Birgit Blank,<sup>2\*</sup> Andreas Maiser,<sup>3,4</sup> Derya Emin,<sup>1</sup> Jens Prescher,<sup>1</sup> Gisela Beck,<sup>2</sup> Christine Kienzle,<sup>2</sup> Kira Bartnik,<sup>1</sup> Bianca Habermann,<sup>2</sup> Mehrshad Pakdel,<sup>2</sup> Heinrich Leonhardt,<sup>3,4</sup> Don C. Lamb,<sup>1</sup> and Julia von Blume<sup>2</sup>

<sup>1</sup>Physical Chemistry, Department of Chemistry Center for Nanoscience, Nanosystems Initiative Munich and Center for Integrated Protein Science Munich, Ludwig Maximilians University Munich, 81377 Munich, Germany

<sup>2</sup>Max Planck Institute of Biochemistry, 82152 Martinsried, Germany

<sup>3</sup>Department of Biology II and <sup>4</sup>Center for Integrated Protein Science, Ludwig Maximilians University Munich, 82152 Martinsried, Germany

Sorting and export of transmembrane cargoes and lysosomal hydrolases at the trans-Golgi network (TGN) are well understood. However, elucidation of the mechanism by which secretory cargoes are segregated for their release into the extracellular space remains a challenge. We have previously demonstrated that, in a reaction that requires Ca<sup>2+</sup>, the soluble TGN-resident protein Cab45 is necessary for the sorting of secretory cargoes at the TGN. Here, we report that Cab45 reversibly assembles into oligomers in the presence of Ca<sup>2+</sup>. These Cab45 oligomers specifically bind secretory proteins, such as COMP and LyzC, in a Ca<sup>2+</sup>-dependent manner *in vitro*. In intact cells, mutation of the Ca<sup>2+</sup>-binding sites in Cab45 impairs oligomerization, as well as COMP and LyzC sorting. Superresolution microscopy revealed that Cab45 colocalizes with secretory proteins and the TGN Ca<sup>2+</sup> pump (SPCA1) in specific TGN microdomains. These findings reveal that Ca<sup>2+</sup>-dependent changes in Cab45 mediate sorting of specific cargo molecules at the TGN.

## Introduction

All newly synthesized secretory proteins arrive at the Golgi apparatus from the ER (Palade, 1975). In the very last subcompartment of the Golgi stack, which is generally referred to as the TGN, the diverse cargoes are sorted from each other and from the Golgi-resident proteins, packed into specific transport carriers, and exported to their respective destinations (De Matteis and Luini, 2008; Guo et al., 2014; Kienzle and von Blume, 2014). The sorting of lysosomal hydrolases is well understood (Kornfeld and Mellman, 1989; Traub and Kornfeld, 1997; Doray et al., 2002), as are the signals in the cytoplasmic domains of transmembrane cargoes that mediate their incorporation into clathrin-coated vesicles for their export from the TGN (Fölsch et al., 1999, 2001; Mellman and Nelson, 2008; Bonifacino, 2014). However, no cargo receptors for the sorting and packing of secretory proteins have been identified at the TGN.

In recent years, we have studied a novel and conserved cargo receptor-independent mechanism implicated in the sorting of secretory cargo at the TGN (von Blume et al., 2011; Curwin et al., 2012). In this process, F-actin and cofilin bind to, and activate, the TGN-specific Ca<sup>2+</sup> pump SPCA1 (Lissandron et al., 2010; Kienzle et al., 2014), which results in an influx of Ca<sup>2+</sup> into a specific domain of the TGN (von Blume et al., 2011). We

suggested that this transient local increase in Ca<sup>2+</sup> concentration involves Cab45, a protein that is required for secretory protein sorting and is normally retained in the TGN (Kienzle and von Blume, 2014). Here, we investigate how Ca<sup>2+</sup> and Cab45 act together to sort secretory proteins at the TGN.

## Results and discussion

Previous work has shown that soluble Ca<sup>2+</sup>-binding ER- or sarcoplasmic reticulum-resident proteins form oligomers in the presence of Ca<sup>2+</sup> (Meissner, 1975). Thus, we hypothesized that soluble Cab45 might oligomerize upon Ca<sup>2+</sup> binding. To investigate the state of Cab45 in cells, we incubated purified Golgi membranes under control or Ca<sup>2+</sup> depletion conditions, and subjected them to Blue NativePAGE gel electrophoresis, denaturing SDS-PAGE, and Western blotting (WB) with a Cab45 antibody. Under control conditions, Cab45 appears as low-(45 kD) and high molecular mass (1,000 kD) fractions (Fig. 1 A), but upon treatment of the membranes with the Ca<sup>2+</sup> chelator BAPTA-AM, the latter fraction was not evident (Fig. 1 A). On the denaturing SDS-PAGE, Cab45 is detectable at a molecular mass of ~50 kD and the Golgi preparation consists of a trans-Golgi compartment as visualized by the TGN46 Western blot.

\*A.H. Crevenna and B. Blank contributed equally to this paper.

Correspondence to Julia von Blume: [vonblume@biochem.mpg.de](mailto:vonblume@biochem.mpg.de); or Alvaro H. Crevenna: [alvaro.crevenna@cup.uni-muenchen.de](mailto:alvaro.crevenna@cup.uni-muenchen.de)

Abbreviations used in this paper: BB, breaking buffer; Cab45, Ca<sup>2+</sup> binding protein 45 kD; CD, circular dichroism; dSTORM, direct stochastic optical reconstruction microscopy; EFh, EF hand; SIM, structural illumination microscopy; WB, Western blotting; WT, wild type.

© 2016 von Blume et al. This article is distributed under the terms of an Attribution-Noncommercial-Share Alike-No Mirror Sites license for the first six months after the publication date [see <http://www.rupress.org/terms>]. After six months it is available under a Creative Commons License [Attribution-Noncommercial-Share Alike 3.0 Unported license, as described at <http://creativecommons.org/licenses/by-nc-sa/3.0/>].



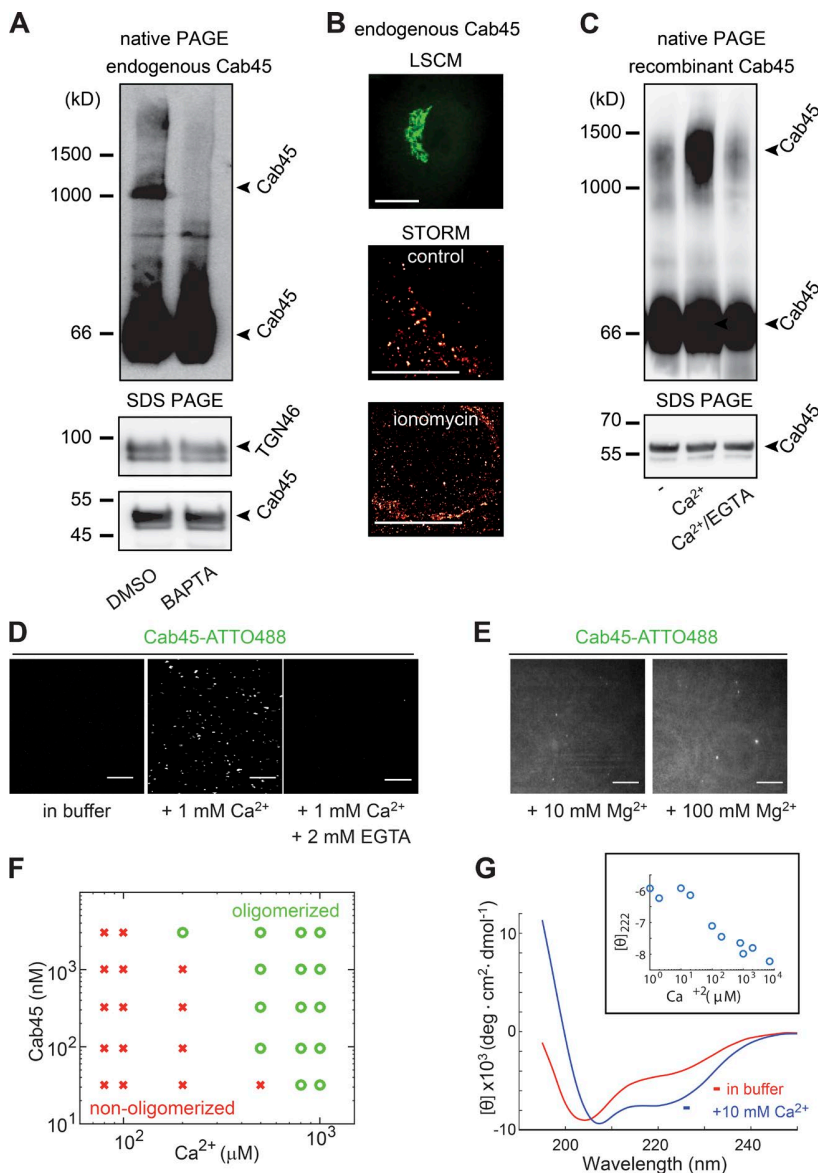


**Figure 1. Cab45 self-assembles in the presence of Ca<sup>2+</sup>.** (A) Purified Golgi membranes from HeLa cells were incubated with DMSO (control) or 25 μM BAPTA-AM for 15 min at 37°C. Subsequently, membranes were lysed in NativePAGE buffer containing 1% DDM, subjected to NativePAGE (3–12%, top) or denaturing SDS-PAGE and analyzed by WB with TGN46 (middle) or anti-Cab45 (bottom) antibodies. (B) Top: HeLa cells were fixed and stained with a Cab45 and an Alexa Fluor 488-labeled antibody and analyzed by laser scanning confocal microscopy (LSCM). Bottom two panels: HeLa cells were incubated with a Ca<sup>2+</sup>-containing buffer supplemented with DMSO (control) or a Ca<sup>2+</sup>-free Hanks' buffer containing 2 μM ionomycin and 5 mM EGTA (Palmer and Tsien, 2006) for 10 min. Then, cells were fixed and stained with the Cab45 antibody and a secondary, Cy5-labeled antibody. dSTORM imaging was performed using wide-field illumination and single fluorescent emitters were localized using a Gaussian least-squares fit. Bars, 10 μm. (C) Recombinant Cab45 was incubated in calcium-free buffer, with 1 mM Ca<sup>2+</sup> or with 1 mM Ca<sup>2+</sup> and 2 mM EGTA. Samples were subjected to NativePAGE (top) or SDS-PAGE (bottom) and analyzed by WB with an anti-Cab45 antibody. (D) Recombinant ATTO-488-labeled Cab45 was incubated as in (C) and analyzed by confocal microscopy. (E) Recombinant ATTO-488-labeled Cab45 was treated with 10 or 100 mM Mg<sup>2+</sup> and analyzed by confocal microscopy. Bars, 20 μm (F) Oligomerization of Cab45 was assessed by fluorescence microscopy as a function of Ca<sup>2+</sup> and protein concentration. (G) Far-UV CD analysis of recombinant Cab45 in the presence and absence of Ca<sup>2+</sup>. (Inset) Ellipticity of Cab45 at 222 nm plotted as a function of Ca<sup>2+</sup> concentration.

To visualize the effects of Ca<sup>2+</sup> on Cab45 in cells, untreated or ionomycin-treated HeLa cells were fixed and stained with a Cab45 antibody and imaged by direct stochastic optical reconstruction microscopy (dSTORM; Heilemann et al., 2008). In control cells, Cab45 was detected in dense clusters (Fig. 1 B). In contrast, in cells treated with ionomycin (a Ca<sup>2+</sup> ionophore) Cab45 appeared in much smaller and more diffuse punctae (Fig. 1 B) without an apparent effect on TGN morphology (Fig. S1 A). These findings suggest the existence of large, Ca<sup>2+</sup>-dependent Cab45 protein complexes in cells.

To gain further insights into the change in Cab45 organization by Ca<sup>2+</sup>, we switched to a reconstituted system. Recombinant Cab45 was incubated with Ca<sup>2+</sup> or Ca<sup>2+</sup>/EGTA or left untreated. Subsequent analysis by NativePAGE and WB of Cab45 incubated with Ca<sup>2+</sup> alone revealed the presence of both high and low molecular mass fractions, whereas the former was much less prominent in both untreated and Ca<sup>2+</sup>/EGTA-treated samples (Fig. 1 C). Next, we visualized ATTO488-labeled recombinant Cab45 with confocal microscopy. In the absence of Ca<sup>2+</sup>, we did not observe Cab45 oligomers. The addition of 1 mM Ca<sup>2+</sup> promoted

the formation of fluorescent Cab45 oligomers (Fig. 1 D), and excess EGTA reversed this change (Fig. 1 D). Oligomerization was Ca<sup>2+</sup> specific and was not affected by similar or higher concentration of Mg<sup>2+</sup> (Fig. 1 E). Furthermore, in a double titration experiment, we observed that oligomerization depends more strongly on the Ca<sup>2+</sup> concentration than on the Cab45 concentration (Fig. 1 F). In addition, measurements of the circular dichroism (CD) revealed a change in the secondary structure of Cab45 upon addition of Ca<sup>2+</sup> (Fig. 1 G), with the largest shift in secondary structure content occurring between 100 and 200 μM Ca<sup>2+</sup> (Fig. 1 G, inset). Analysis of the CD spectrum using CONTIN (Wiech et al., 1996) showed that the change reflected a decrease in β-sheet (from 0.31 to 0.23) with a concomitant increase in α-helicity (from 0.18 to 0.27) but no significant alteration in random coil content. Given that the concentration of Ca<sup>2+</sup> at the TGN is believed to be ~130 μM (Missiaen et al., 2004; Pizzo et al., 2011), the oligomer we observe likely represents the form of Cab45 physiologically found in the TGN of cells.

Cab45 is known to coprecipitate with secretory proteins from HeLa cell lysates such as COMP or LyzC (von Blume et

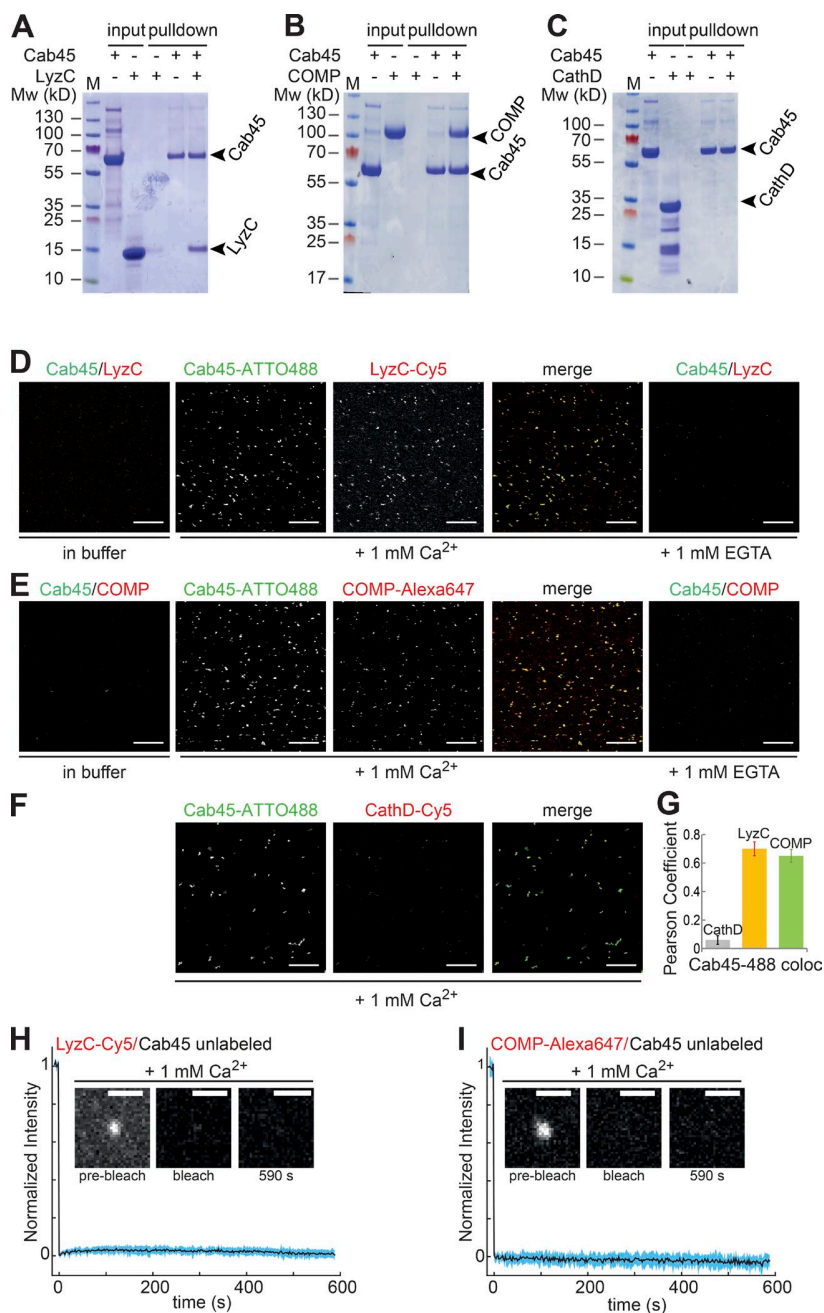


**Figure 2. Cargo recruitment by Cab45 oligomers.** (A–C) Pull-down experiments performed with His-tagged Cab45 and the potential cargo molecules LyzC (A), COMP (B), and CathepsinD (C), analyzed by SDS-PAGE and Coomassie staining. (D–F) In vitro oligomerization assay. Cab45 and LyzC (D), COMP (E) or CathepsinD (F), labeled as indicated, were incubated in Ca<sup>2+</sup>-free buffer, with Ca<sup>2+</sup> or Ca<sup>2+</sup>/EGTA. Bars, 20  $\mu$ m. (G) Pearson coefficient of colocalization between Cab45-ATTO488 and potential cargo molecules. Error bars represent SD from three independent experiments ( $n = 3$ ). Two images were quantified per experiment. (H and I) FRAP analysis of LyzC-Cy5 (H) and COMP-Alexa Fluor 647 (I) recruited to individual unlabeled Cab45 oligomers. The black line is the mean signal, whereas the light blue trace represents one SD on either side ( $n = 13$  for LyzC and 15 for COMP). The insets show examples of a Cab45 oligomer before bleaching (prebleach), immediately after bleaching (bleach), and  $\sim 10$  min after bleaching (590 s). Bar, 2  $\mu$ m.

al., 2012). To determine whether the interaction is direct, we incubated recombinant His-tagged Cab45 attached to nickel nitrilotriacetic acid beads with recombinant LyzC, COMP or CathepsinD (a lysosomal hydrolase) in the presence of Ca<sup>2+</sup> and performed pull-down experiments. SDS-PAGE analysis showed that both LyzC and COMP, but not CathepsinD, bound directly to Cab45 in the presence of Ca<sup>2+</sup> (Fig. 2, A–C). Next, we wanted to explore whether cargo molecules are recruited specifically by Cab45 oligomers. To this end, we incubated recombinant ATTO488-labeled Cab45 with LyzC-Cy5, COMP-Alexa Fluor 647, or CathepsinD-Cy5 in the presence of Ca<sup>2+</sup> or Ca<sup>2+</sup>/EGTA, or under Ca<sup>2+</sup>-free conditions, and analyzed the samples by confocal microscopy. Both LyzC and COMP were found to colocalize with Cab45 in the presence of Ca<sup>2+</sup>, which suggested cargo recruitment to the oligomeric form (Fig. 2, D, E, and G;

and Fig. S1, B and C). Colocalization was also reversible upon addition of EGTA (Fig. 2, D and E). Neither of the secretory proteins showed any detectable oligomerization in the absence of Cab45 (Fig. S1, B and C). CathepsinD did not interact with Cab45 at all (Fig. 2, F and G). Recruitment of cargo to Cab45 clusters appears to be stable, as there was no protein exchange within 10 min as assessed by FRAP (Fig. 2, H and I). Because Cab45 exists in at least two forms in the presence of Ca<sup>2+</sup>, we wanted to know which form binds cargo. Hence, we incubated Cab45-ATTO488 with fluorescently labeled LyzC or COMP and performed fluorescence cross-correlation spectroscopy in the absence and presence of Ca<sup>2+</sup>. We observed no cross-correlation between nonoligomerized Cab45 and either secretory protein in the absence or presence of 1 mM Ca<sup>2+</sup> (Fig. S1, D and E). Thus, only the oligomer seems capable of recruiting

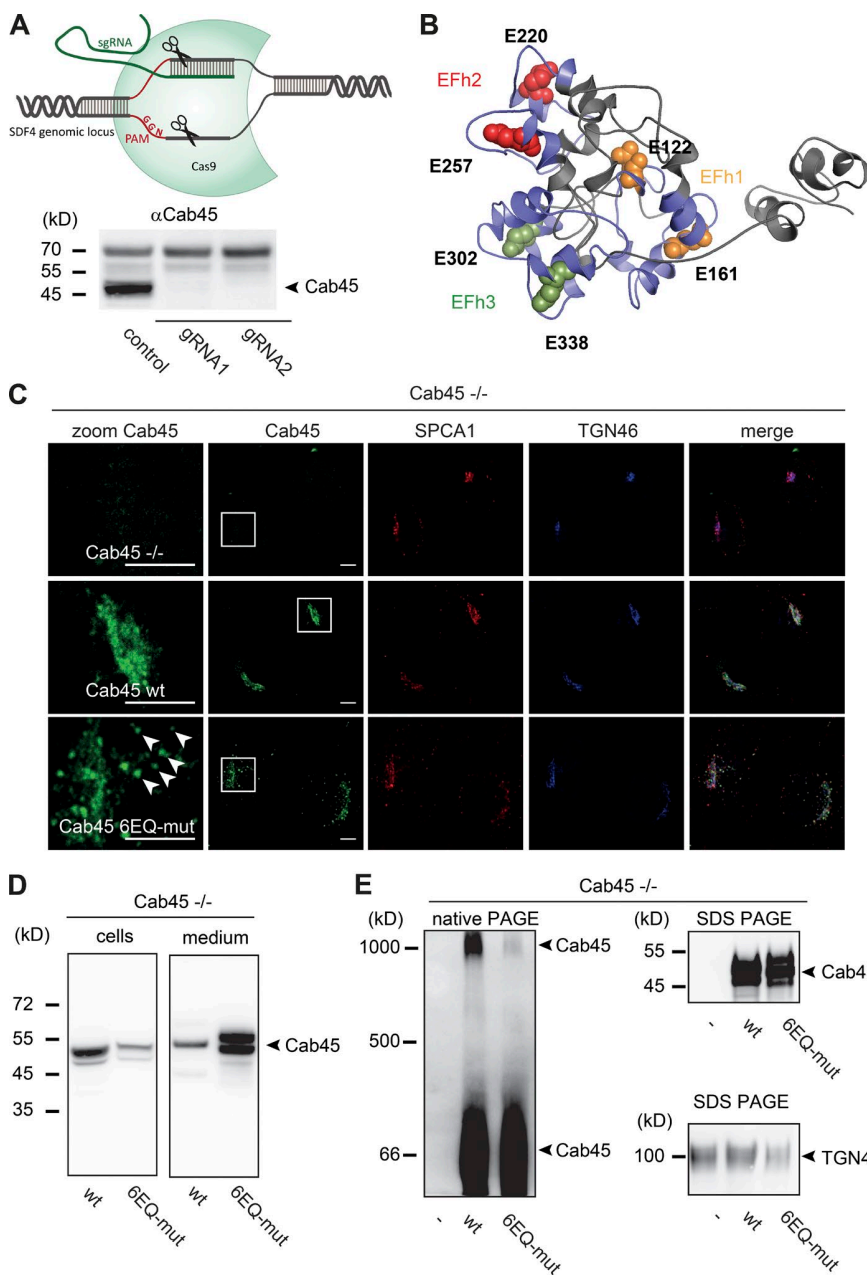


**Figure 3. Cab45 Ca<sup>2+</sup> binding is required for oligomerization in living cells.** (A) Cab45<sup>-/-</sup> cells were generated using CRISPR/Cas9 with 2 gRNAs targeting the SDF4 (Cab45) locus as described in Materials and methods. Single clones were picked and analyzed by WB with a Cab45 antibody. (B) Structural model of human Cab45. The three EFh pairs are highlighted in blue, and the glutamates (E) in contact with the ligand are shown in orange (EFh 1), red (EFh 2), and green (EFh 3). The Ca<sup>2+</sup>-binding-deficient mutant (Cab45-HA 6EQ-mut), in which all six Glu residues have been replaced by Gln, was described previously (von Blume et al., 2012). (C) Cells of the Cab45<sup>-/-</sup> knockout line, and its stable transfectants Cab45<sup>-/-</sup> Cab45-HA WT or Cab45<sup>-/-</sup> Cab45-HA 6EQ-mut, were fixed and stained with Cab45 (green), SPCA1 (red), and TGN46 (blue) antibodies and analyzed by fluorescence microscopy. Bars, 5 μm. (D) Cab45<sup>-/-</sup> cells expressing either Cab45-HA WT or Cab45-HA 6EQ-mut were incubated at 20°C in the presence of cycloheximide to allow proteins to accumulate in the TGN. After 2 h, cells were shifted to 37°C for an additional 2 h, and cells and media were collected and analyzed by Western blotting with the Cab45 antibody. (E) Golgi membranes extracted from Cab45<sup>-/-</sup>, Cab45<sup>-/-</sup> Cab45-HA WT, or Cab45<sup>-/-</sup> Cab45-HA 6EQ-mut lines were lysed in NativePAGE buffer containing 1% DDM, subjected to NativePAGE (3–12%) or SDS-PAGE, and analyzed by WB with a Cab45 or anti-TGN46 antibody.

secretory proteins (Fig. 2, D and E; and Fig. S1, D and E). Collectively, the data suggest that oligomeric Cab45 forms stable complexes with specific molecules, which can be released when reducing the Ca<sup>2+</sup> concentration.

To further investigate the role of Cab45 during cargo sorting in living cells, we generated a Cab45 knockout HeLa cell line (Cab45<sup>-/-</sup>) using CRISPR/Cas9 technology (Cong et al., 2013; Fig. 3 A and Fig. S2 A). To test for the effects on protein secretion, we transfected these cells with Flag-LyzC for 24 h or detected endogenous COMP directly. After 4-h incubation in serum-free medium, samples were collected, processed and analyzed by WB with specific antibodies and quantified (Fig. S2, B–E). Cab45<sup>-/-</sup> cells showed a significant reduction in secretion of COMP and LyzC (Fig. S2, B–E), similar to that seen in Cab45 siRNA lines (von Blume et al., 2012).

Cab45 has three consecutive EF hand (EFh) domains. A structural model of Cab45 was generated to visualize the arrangement of the three EFh domains in space (Fig. 3 B). Next, to investigate the role of its Ca<sup>2+</sup> binding sites on Cab45-mediated sorting and secretion, we transduced Cab45<sup>-/-</sup> cells with Cab45-HA wild-type (WT) or Cab45-HA 6EQ-mut in which all Ca<sup>2+</sup> binding sites have been mutated (Fig. 3 B). Although both proteins localized to the TGN as well as to SPCA1, Cab45 6EQ-mut was also observed in vesicles around the TGN, suggesting export of the normally TGN-resident protein (Fig. 3 C). To check this, Cab45 WT and Cab45 6EQ-mut cells were treated with cycloheximide and incubated at 20°C for 2 h to inhibit export from the TGN (von Blume et al., 2009). Cells were then shifted to 37°C to release the TGN-accumulated proteins, and cells and culture supernatant were analyzed by WB. Cab45 WT was predominantly found in the cell pellet (83%, *n* = 3), whereas a large proportion

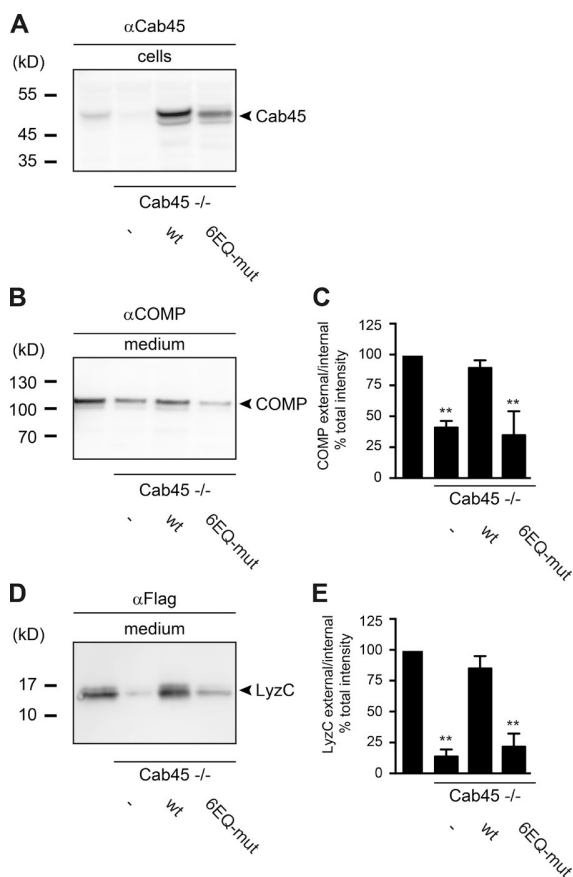


**Figure 4. Cab45 Ca<sup>2+</sup> binding is required for sorting in living cells.** (A) Cell lysates of Cab45<sup>-/-</sup>, Cab45<sup>-/-</sup> Cab45-HA WT or Cab45<sup>-/-</sup> Cab45-HA 6EQ-mut HeLa cells were analyzed by WB with a Cab45 antibody. (B and D) Cell culture supernatants of the same cells were incubated in serum-free medium for 4 h at 37°C. Media and cell extracts were blotted and probed with antibodies against COMP (B) or Flag (LyzC; D). Western blots from three independent experiments were quantified by densitometry using the ImageJ software. Bar graphs represent the densitometry values of external COMP (C) and LyzC (E) normalized to internal protein contents, respectively. Error bars represent SD calculated of three independent experiments of secreted COMP (C) or LyzC (E), respectively (n = 3). \*\*, P < 0.01 (compared datasets).

of the Cab45 6EQ-mut was detected in the culture supernatant (94%, n = 3; Fig. 3 D). To test whether Ca<sup>2+</sup>-dependent oligomerization was responsible for Cab45 secretion, Golgi membranes purified from Cab45<sup>-/-</sup>, Cab45<sup>-/-</sup> Cab45-HA WT, or Cab45<sup>-/-</sup> Cab45-HA 6EQ-mut cells were analyzed by NativePAGE and WB. Like the endogenous protein (Fig. 1 A), Cab45-HA WT was detectable in low and high molecular mass forms, but the latter was missing from cells expressing Cab45 6EQ-mut (Fig. 3 E).

Finally, we assessed the role of these mutations in TGN sorting (Fig. 4). The expression level of Cab45 in control, Cab45<sup>-/-</sup>, Cab45<sup>-/-</sup> WT, or 6EQ-mut HeLa cells was analyzed by WB (Fig. 4 A). In addition, supernatants from these cell cultures expressing Flag-LyzC were analyzed by WB (Fig. 4, B and D) and quantified (Fig. 4, C and E). Cab45 WT, but not the Cab45 6EQ-mut protein, rescued secretion of both LyzC and COMP (Fig. 4, B–E). These results thus demonstrate that Cab45 oligomerization in cells requires its Ca<sup>2+</sup>-binding sites and that Ca<sup>2+</sup>-dependent Cab45 oligomerization is necessary for sorting in living cells.

Given that Cab45 oligomerization is Ca<sup>2+</sup> dependent, these oligomers might form in the vicinity of SPCA1. To investigate the distribution of Cab45, SPCA1, and cargo (LyzC) in intact cells, we used 3D structural illumination microscopy (SIM; Schermelleh et al., 2010; Cardoso et al., 2012). HeLa cells stably expressing HA-SPCA1 were fixed and stained with antibodies specific for Cab45 and HA (SPCA1: Fig. 5 A and Fig. S3, A–C; Flag LyzC: Fig. 5 B and Fig. S3, D–F; p230 [a TGN resident]: Fig. 5 C and Fig. S3, G–I; or TGN46: Fig. 5 D and Fig. S3, J–L, antibodies, respectively). The analysis revealed that ~60% and 30% Cab45 colocalized, in small clusters with SPCA1 and LyzC, respectively (Fig. 5 E). In contrast, only 10% of p230 and 18% of TGN46 colocalized with Cab45 (Fig. 5 E). These results suggest that oligomerized Cab45 may preferentially accumulate near SPCA1 to segregate cargo. The close proximity between these components may suggest the formation of a functional sorting module regulated by Ca<sup>2+</sup>. The inhomogeneous distribution of Cab45 observed at the TGN may be related to two recently postulated TGN sub-compartments, trans-Golgi compartment1 (tGo1) and tGo2 (Aulestia et al., 2015). In particular, Cab45 may be present only at the tGo1, the compartment in which SPCA1 is active (Aulestia et al., 2015).

In summary, our results suggest the following mechanism for Cab45-mediated sorting at the TGN. Upon SPCA1-mediated Ca<sup>2+</sup> influx into the lumen, Cab45 binds Ca<sup>2+</sup>, triggering a conformational change and allowing oligomerization. Cab45 oligomers then bind specific proteins, thereby sorting cargo from noncargo (Fig. 5 F). We propose to refer to this Cab45 sorting oligomer as a *cernosome*, from the Latin *cernere*, which means to choose, sift, separate, decide, or distinguish. The required dissociation of the Cab45 cargo complex (because Cab45 is not packed into transport carriers) may then occur either by reduction of free calcium levels or via a signal such as phosphorylation by a Golgi kinase (e.g., Golgi casein kinase Fam20C; Tagliabracci et al., 2012). The cernosome represents an elegant means of segregating different cargoes by recognition of the Cab45 oligomer. This is therefore a unique way to export cargo independent of a bona fide cargo receptor.

## Materials and methods

### Antibodies, plasmids, and cell culture

The commercial antibodies used in this study, and their sources, are as follows: Anti-COMP (rabbit polyclonal, ab74524; Abcam), anti-FLAG (mouse monoclonal, F3165; Sigma-Aldrich), and anti-TGN46 (sheep polyclonal, AHP500G; AbD Serotec) were used for WB, together with the secondary antibodies sheep (sc-2770, sc-2303, rabbit sc-2301 and mouse sc-2314) obtained from Santa Cruz Biotechnology, Inc. Anti-HA (rat monoclonal, 11867423001; Roche), anti-FLAG (mouse monoclonal; F3165; Sigma-Aldrich), anti-GM130 (mouse monoclonal, 610822; BD Biosciences), and anti-ATP2C1 (mouse monoclonal, HPA035116; Sigma-Aldrich) were used for immunofluorescence microscopy. The secondary antibodies Alexa Fluor 488 rabbit (A21206), Alexa Fluor 594 mouse (A21203), and Alexa Fluor 488 rat (A21208) were purchased from Thermo Fisher Scientific. For STORM measurements Cy5-conjugated AffiniPure (rabbit, 711–175-152; Jackson ImmunoResearch Laboratories, Inc.) was used for Cab45 as a secondary antibody and Alexa Fluor 488 sheep (A11015) for TGN46 (Thermo Fisher Scientific). The recombinant proteins COMP-FLAG (COMP-3659H; Creative BioMart), COMP (ab104358; Abcam), LysozymeC (Sigma-Aldrich), and LysozymeC-Cy5 (LS1-S5-1; Nanocs) were used for in vitro analysis.

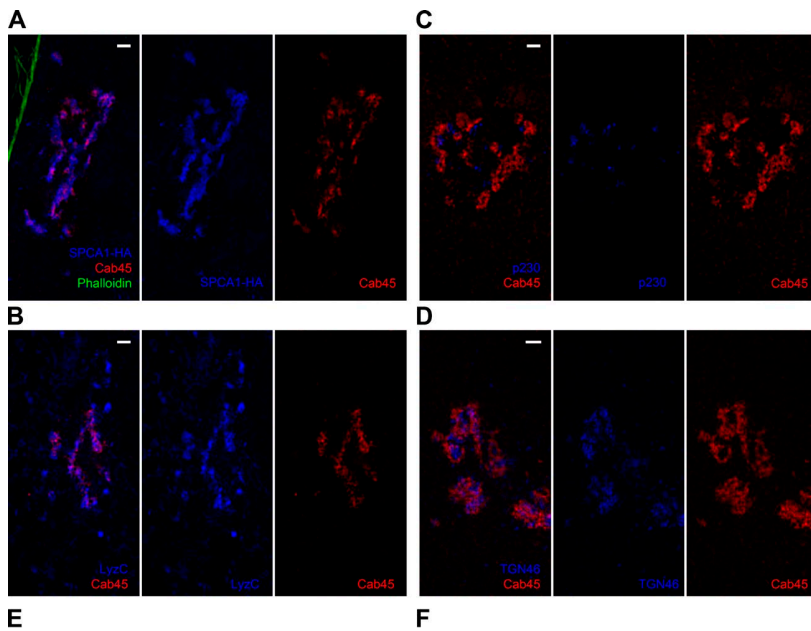
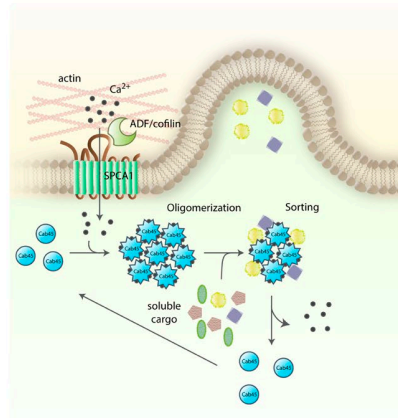
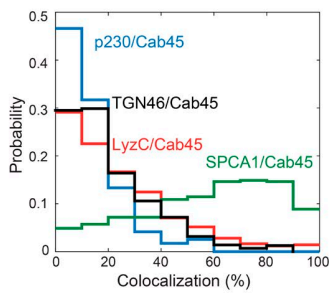


**Figure 5. SPCA1, Cab45 and cargo cluster in the TGN.** To obtain higher resolution, 3D SIM was applied. HeLa cells expressing HA-SPCA1 were fixed and stained with anti-HA and anti-Cab45 antibodies and phalloidin and analyzed by 3D SIM. (A) Representative cross section showing the locally overlapping distributions of SPCA1 and Cab45 in the TGN. Bar, 5  $\mu$ m. (B) HeLa cells expressing Flag-LyzC were fixed and stained with Flag (LyzC) and Cab45 antibodies. Bar, 5  $\mu$ m. (C) HeLa cells were fixed and stained with p230 and Cab45 antibodies. Bar, 5  $\mu$ m. (D) HeLa cells were fixed and stained with TGN46 and Cab45 antibodies. (E) Probability (i.e., normalized frequency) of Cab45 colocalization with SPCA1, LyzC, p230, and TGN46. Depiction of the image quantification is shown in Fig. S3 (C, F, I, and J). (F) Schematic depiction of the putative Cab45-based sorting mechanism. Cab45 undergoes a conformational change upon the SPCA1-mediated local increase in  $Ca^{2+}$  concentration in the TGN lumen. As a consequence, Cab45 binds cargo proteins and separates them from other soluble proteins in the TGN by sequestering them in putative subdomains. This sorting mechanism might enable cells to pack soluble cargos into vesicles and recycle Cab45 for a new cycle of sorting by extrusion of internal  $Ca^{2+}$ .



### Plasmids

The pLPCX-based plasmids used for production of full-length WT and mutant Cab45 were generated by RT-PCR from HeLa cells total RNA. The cDNA was then amplified using the primers HA-Cab45-F 5'-CGTGGATCCATGGTCTGGCCCTGGGTG-3' and HA-Cab45-R 5'-GCA GAATTCTTAAGCGTAGTCTGGGACGTCGTATGGGTAAAACCTCTCGTGCACGCTGCG-3' and ligated into the pLPCX backbone using BglII and EcoRI restriction sites. The Cab45 mutant was generated by inserting point mutations in EFh 1 (E122Q), EFh 2 (E161Q), EFh 3 (E220Q), EFh 4 (E257Q), EFh 5 (E302Q), and EFh 6 (E338Q).

The cDNA of SPCA1-HA was amplified with 5'-CTGGTTCGACATGAAGGTTGCACGTTTTCAAAAAATACCTAATG-3' and 5'-GCAGAATTCTTAAGCGTAGTCTGGGACGTCGTATGGGTATACTTCAAGAAAAGATGATGATGTGCGAACTAACATG-3' and ligated into the pLPCX backbone using SalI and EcoRI restriction sites.

For the expression of a HIS-SUMO-tagged version of Cab45 in SF9 cells, the cDNA was amplified from the pLPCX-Cab45 (WT) plasmid with the primers 5'-CAGCGTCTCAAGGTCGGCCTGCCA ACCACTCGTC-3' (forward) and 5'-CAGTCTAGATTAACCTCTCGTGCACGCTGCG-3' (reverse) and inserted into a pInsect Secretory SUMOstar Vector (3106; Life Sensors). The guide RNA oligos and their complementary sequences used for CRISPR/Cas9 targeting of Cab45 were phosphorylated and annealed by a temperature

gradient. Afterward, oligos were inserted into the PX459 mammalian expression vector (48139; Addgene) with BbsI restriction sites (Ran et al., 2013). Flag-LyzC in a pcDNA3.1 backbone was a gift from V. Malhotra (Centre for Genomic Regulation, Barcelona, Spain; von Blume et al., 2012).

### Cell culture and stable transfection

WT HeLa cells and HeLa cells stably expressing Cab45-HA WT and Cab45-HA-6EQ-mut or SPCA1-HA, and Cab45 CRISPR KO cells (see CRISPR/Cas9 knockout cell lines section for details) were grown in DMEM (PAA) medium containing 10% FCS at 37°C with 5% CO<sub>2</sub>. To generate cell lines stably expressing Cab45-HA WT or Cab45-HA-6EQ-mut, VSV-G pseudotyped retroviral vectors were produced by transient transfection of HEK293T cells. Viral particles were concentrated from cell culture supernatant and used for infection (Pfeifer et al., 2000).

### Transient transfections

For secretion experiments, 10<sup>7</sup> HeLa cells were transfected with 20  $\mu$ g Flag-LyzC using a TransIT-HeLaMONSTER transfection kit (Mirus) and incubated for 24 h before the secretion experiment. For Cab45 knockout, 7  $\times$  10<sup>5</sup> HeLa cells were transfected with 4  $\mu$ g of the PX459 vector encoding the sgRNA and Cas9 with the aid of the same reagent.

### CRISPR/Cas9 knockout cell lines

The guide sequence of 20 nt targeting human Cab45 (also known as SDF4) was designed using the CRISPR design tool at [www.genome-engineering.org/crispr](http://www.genome-engineering.org/crispr) (Hsu et al., 2013) and cloned into a mammalian expression vector (pX459) bearing the Cas9 coding sequence, the sequences encoding the RNA components and a puromycin selection cassette (plasmid 48139; Addgene; Ran et al., 2013). The guide sequences used to target exon 2 of human Cab45 were 5'-TTCTGATGGACGCGTCTGCA-3' (guide 1) and 5'-TTGATGAGGACGCGGAGCCG-3' (guide 2). A total of 4 µg of the pX459 vector containing the sequence of the sgRNA was transfected into HeLa cells. 24 h after transfection, cells were selected for 48 h in 2 µg/ml puromycin. Then, 100 cells were seeded in 15-cm culture dishes and cultured until single-cell colonies were large enough to be manually scraped off the dish and transferred to 96-well plates. Single clones were then expanded and screened for Cab45 by WB.

### Generation of an anti-Cab45 antibody

For antibody generation, full-length recombinant Cab45 protein (tagged with His-Sumo; see Purification of recombinant proteins section for details) was prepared with TiterMax Gold Adjuvant liquid (Sigma-Aldrich) according to the manufacturer's protocol. Rabbits were injected and boosted three times before serum collection. Sera were incubated (while stirring) at room temperature for 1 h and then at 4°C overnight. After centrifugation for 30 min at 5,000 g, supernatants were collected and stored at -20°C.

### Purification of recombinant proteins

His-Sumo-tagged Cab45 was expressed from the pI-secSUMOstar plasmid in SF9 cells and purified from cell supernatants by nickel-based affinity chromatography using an NaP, pH 8.0, buffer containing 500 mM NaCl and cOmplete His-tag Purification Resin (Roche). After elution with 250 mM imidazole, proteins were dialyzed against 20 mM Pipes, pH 6.8, containing 500 mM NaCl and 10% glycerol vol/vol for storage.

### Protein labeling

Recombinant Cab45 and the putative cargoes COMP and CathepsinD were labeled with NHS-ATTO488 (Sigma-Aldrich) or maleimide Alexa Fluor 647 (Thermo Fisher Scientific) according to the manufacturers' instructions.

### CD spectroscopy

CD measurements were performed in a 1-mm (path length) cuvette at 10°C on a JASCO J-715 spectrometer. Protein samples (0.2 mg/ml) were dissolved in 1.3 mM Pipes, pH 6.8, 33 mM NaCl, and 0.7% glycerol, and the indicated amounts of Ca<sup>2+</sup> were added before spectra were recorded. A mean of 10 (±Ca<sup>2+</sup> analysis) or 4 (titration assay) independent spectra (from 195 to 250 nm with 0.1 nm spacing) were recorded. CONTIN analysis was done using CDPro. CONTIN decomposes the CD signal into six secondary structure elements: regular α-helical, distorted α-helical, regular β sheet, distorted β sheet, turn, and unordered. Reported values in the main text for the α-helical and β sheet content were the sum of regular and distorted fractions for each secondary element.

### Purification of Golgi membranes

HeLa or HeLa S3 cells stably expressing Cab45-HA WT or Cab45-HA-6EQ-mut were harvested and pelleted. Pellets were then washed once in breaking buffer (BB; 10 mM Tris, pH 7.4, and 250 mM sucrose), diluted 1:5 in BB supplemented with complete Tablets Mini EDTA-free (Roche), and homogenized with a European Molecular Biology Laboratory cell cracker. After addition of 1 mM EDTA, the sucrose

concentration of the homogenate was adjusted to 37% (wt/vol) and overlaid with 35% and 29% sucrose in 10 mM Tris, pH 7.4. Cellular components were separated by ultracentrifugation for 3 h at 133,000 g. The Golgi membrane fraction was isolated, adjusted to BB conditions, and snap-frozen in liquid nitrogen for storage at -80°C.

### Analysis of the size distribution of native Cab45

Golgi membranes extracted from HeLa cells were diluted in BB and pelleted by centrifugation at 100,000 g for 1 h. The pellet was resuspended in 50 µl BB and incubated with DMSO or BAPTA-AM (25 µM) for 15 min at 37°C. Membranes were subsequently lysed in NativePAGE sample buffer (Thermo Fisher Scientific) supplemented with 1% DDM for 15 min and centrifuged at 20,000 g for 30 min at 4°C. The same protocol was followed for membranes extracted from the cell lines Cab45<sup>-/-</sup>, Cab45<sup>-/-</sup> Cab45-HA WT, and Cab45<sup>-/-</sup> Cab45-HA 6EQ-mut. Supernatants were aliquoted into microcentrifuge tubes and stored at -80°C. Recombinant His-Sumo-tagged Cab45 was either left untreated or incubated with 1 mM Ca<sup>2+</sup> or 1 mM Ca<sup>2+</sup>/1 mM EGTA for 15 min on ice before electrophoresis.

### NativePAGE

Golgi membranes or recombinant Cab45 were supplemented with 5% G-250 sample additive (Thermo Fisher Scientific) and loaded on a NativePAGE Novex Bis-Tris Gel (3–12%; Thermo Fisher Scientific). After transfer of the proteins onto a polyvinylidene fluoride membrane for 90 min, the membrane was immersed in 6% acetic acid for 15 min, then air-dried and washed with 100% methanol. Finally, membranes were blocked with 4% BSA in TBS for 30 min and incubated with the primary antibody overnight at 4°C.

### Immunofluorescence microscopy

For immunostaining, HeLa cells were cultured on glass slides, fixed for 10 min with 4% paraformaldehyde, washed with PBS, and subsequently permeabilized for 5 min in 0.2% Triton X-100 and 0.5% SDS in 4% BSA solution. After washing again in PBS and blocking of slides for 1 h in 4% BSA, cells were incubated with the primary antibody followed with the secondary antibody, each for 1 h at room temperature. Slides were then mounted with Prolong gold antifade reagent (Thermo Fisher Scientific) and viewed at 22°C on a ZEISS confocal laser-scanning LSM 780 microscope equipped with a 40× (NA 1.4 oil) Plan-Apochromat or 100× (NA 1.46 oil) objective. For detection of Alexa Fluor, the 488-nm laser line was used. Pictures were acquired using Leica software (ZEN 2010) and processed, merged, and gamma adjusted in ImageJ (version 1.37).

### Generation of a structural model of Cab45

The Cab45 structure was predicted using the Phyre2 server (Kelley and Sternberg, 2009) using the intensive mode. Six templates were chosen by the server to model human Cab45: 3q5i(A), 2f33(A), 3ek7(A), 4p5w(A), 3lij(A), and 4p60(B). The model was displayed using MacPyMOL (PyMOL Molecular Graphics System, version 1.7.4; Schrödinger, LLC). EFh (as defined in CDD entry cd00051) were assigned and predicted using SMART (Letunic et al., 2015) and CD search (Marchler-Bauer et al., 2015), and the more divergent EFh 2 was confirmed using HHPred (Söding, 2005). All EFhs were highlighted in the structure.

### LyzC and COMP sorting assays

HeLa control cells and Cab45 knockout cells or cells stably expressing pLPCX-Cab45-HA WT or pLPCX-Cab45-HA 6EQ-mut, respectively, were transfected with Flag-LyzC. Cells were washed five times with serum-free medium and then grown in serum-free medium for 4 h. Cells

were then counted and lysed in PBS supplemented with 1% CHAPS. Media from each cell line were collected, clarified by passage through a 0.45- $\mu\text{m}$  filter (EMD Millipore) and centrifuged at 5,000 g for 15 min. Samples were then concentrated using a 3 kD molecular mass cutoff spin column (EMD Millipore). Cell lysates and concentrated media were subsequently analyzed by WB using an anti-COMP or anti-Flag antibody (to detect LyzC).

### Fluorescence fluctuation spectroscopy and fluorescence correlation spectroscopy

Fluorescence fluctuation spectroscopy and fluorescence correlation spectroscopy with pulsed interleaved excitation (Müller et al., 2005) were performed on a home-built confocal multiparameter fluorescence detection setup (Müller et al., 2005), which uses spectral and polarization separation in addition to fluorescence-lifetime information. The system is built around a Nikon TE2000 microscope. As picosecond excitation sources, we used an amplified frequency-doubled diode laser (PicoTA; PicoQuant) at 480 nm and a diode laser at 636 nm (LDH-P-C-635b; PicoQuant) for fluorophore excitation. Each laser is coupled into a single-mode fiber (AMS Technologies), collimated (Schäfer & Kirchhoff) and focused on the sample by a 60 $\times$  1.27 NA water-immersion objective (Plan Apo VC 60 $\times$  WI; Nikon). A mean excitation power of 10  $\mu\text{W}$  was used, measured at the rear aperture of the objective. A dichroic mirror (DualLine z532/635; AHF Analysentechnik) separates excitation and emission beam paths. The collected fluorescence is focused on an 80- $\mu\text{m}$  pinhole (Thorlabs) via the microscope tube lens, and is passed through an emission filter (BrightLine HC 582/75; AHF Analysentechnik). Fluorescence is collected by one or more single-photon-counting avalanche photodiodes (SPQR-16; PerkinElmer) and registered by independent time-correlated single photon counting data collection cards (SPC-154; Becker & Hickl). The lasers and data collection cards are synchronized by the laser controller (Sepia; PicoQuant). For the fluorescence correlation spectroscopy measurements, labeled Cab45 was diluted to a concentration of  $\sim 10$  nM in 20 mM Pipes, pH 6.8, and 500 mM NaCl. The solutions were preincubated for 5 min before measurements were started to allow for equilibration of the sample. To calculate diffusion coefficients for Cab45 and Cab45 cargo complexes, the focus size was fixed by assuming a diffusion coefficient of 400  $\mu\text{m}^2/\text{s}$  for carboxylic acid-free ATTO488 (taken from <http://www.picoquant.com/appnotes.htm>). Cab45 and Cab45 cargo complexes were measured at least three times for 150 s. All experiments were performed at 22°C.

### FRAP and colocalization

FRAP experiments were conducted on a spinning-disk confocal microscope system (Revolution system; Andor Technology) consisting of a base (TE2000E; Nikon) and a spinning-disk unit (CSU10; Yokogawa Electric Corporation) with a 100 $\times$  oil immersion objective (NA 1.49; Nikon) at 20°C. The detection path was equipped with an Optosplit II (Cairn Research Ltd.) for dual-color detection, a filter set for EGFP and Cy5 (BS562, HC525/50, and ET605/70; AHF Analysentechnik AG), and a DU-897 Ixon EMCCD camera (Andor Technology). In addition, a triple-band dichroic beam splitter was used to separate laser excitation from fluorescence emission (Di01-T405/488/568/647; Semrock). The excitation was controlled with a tunable acousto-optic filter (Gooch & Housego). FRAP experiment were done by first acquiring five frames, then applying a bleaching pulse for 5 s and finally acquiring 300 frames. The chosen time interval between consecutive frames was between 2 s. ZEN 2010 software (ZEISS) was used for image acquisition, whereas image analysis was done with ImageM.

### 3D SIM

Superresolution imaging with 3D SIM was performed with a DeltaVision OMX v3 (GE Healthcare) equipped with a 100 $\times$ /1.40 NA PlanApo oil immersion objective (Olympus), Cascade II:512 EMC CD cameras (Photometrics), and 405-, 488-, and 593-nm diode lasers. Samples were mounted with VECTASHIELD Mounting Medium (Vector Laboratories) and illuminated with coherent scrambled laser light directed through a movable optical grating. Image stacks with 15 images per plane (five phases, three angles) and a z-distance of 125 nm were acquired at  $\sim 23^\circ\text{C}$  and subjected to a computational reconstruction (softWoRX; Applied Precision).

### 3D SIM image analysis

3D SIM raw data were first reconstructed with the software softWoRx 6.0 Beta 19 (unreleased) and corrected for color shifts. A custom-made macro in Fiji (Schindelin et al., 2012) was used to establish composite TIFF stacks that are subsequently loaded as RGB into the velocity calculation software (Velocity 6.1.2; PerkinElmer). Structures were obtained, segmented, and measured in all channels by using the threshold commands “threshold using intensity” and “exclude objects by size.” Reconstruction artifacts and background were also removed. Colocalizing structures were recognized by the “intersect and compartmentalize” command and quantified according to volume and number. Several small volumes belonging to one compartment were combined. Cab45 was set as 100%. Overlapping volumes were used to calculate the degree of overlap in percentage. Finally, a histogram was calculated using 10% bins.

### dSTORM microscopy

To visualize Cab45 in the TGN with dSTORM, HeLa cells were incubated with  $\text{Ca}^{2+}/\text{Mg}^{2+}$ -containing HBSS (Invitrogen) supplemented with 2 g/l glucose, 490  $\mu\text{M}$   $\text{MgCl}_2$ , and 450  $\mu\text{M}$   $\text{MgSO}_4$ ; 300 mOsmol/l, pH 7.4, and DMSO or the same buffer without  $\text{Ca}^{2+}$  containing 2  $\mu\text{M}$  ionomycin and 5 mM EGTA (Palmer and Tsien, 2006) and incubated for 10 min. Then, cells were fixed as described in the Immunofluorescence microscopy section and stained with an anti-Cab45 primary and a Cy5-labeled secondary antibody. Before performing dSTORM imaging, a glucose oxidase-based oxygen scavenging buffer was added according to a slightly modified version of the protocol described in (Dempsey et al., 2011). Imaging buffer contained 100 mM mercaptoethylamine (Fluka) as a reducing agent, 2.5% (wt/vol) glucose (Sigma-Aldrich), 0.5 mg/ml glucose oxidase (Sigma-Aldrich), and 3  $\mu\text{l}/\text{ml}$  catalase suspension (concentration  $\sim 20$ –50 mg/ml; Sigma-Aldrich). dSTORM imaging (Heilemann et al., 2008) was performed at room temperature (22°C) on a combined wide-field/total internal reflection fluorescence microscope described previously (Prescher et al., 2015) using a home-built microscope stage in combination with a SR Apo total internal reflection fluorescence 100 $\times$  oil objective (Nikon) with a numerical aperture of 1.49. Images were detected by an EMCCD camera (DU860D-CS0-BV; Andor Technology) using Solis software (version 4.19.3; Andor Technology).

For each dSTORM image, a movie stack comprising 10,000 frames at a frame rate of 20 Hz was acquired using wide-field illumination. Cy5 fluorophores were excited at a wavelength of  $\lambda_{\text{exc}} = 642$  nm and a laser power of 50 mW, which was measured at the output of the objective. In some cases, additional activation was required, which was realized by changing the imaging mode to activation cycles, where each cycle consisted of one activation frame ( $\lambda_{\text{exc}} = 488$  nm), followed by nine imaging frames ( $\lambda_{\text{exc}} = 642$  nm). Laser power for imaging was kept at 50 mW, whereas the power of the activating laser was gradually increased from 0 to  $\sim 2$  mW over the course of data acquisition.

## dSTORM image analysis

Rendering and analysis of the acquired dSTORM images was performed using a home-written software created with MATLAB R2014b (The MathWorks) as described elsewhere (Prescher et al., 2015). In brief, a 2D Gaussian function was fitted to the detected point-spread functions using Levenberg-Marquard's nonlinear least squares algorithm. Sample drift was corrected by pixel-wise cross-correlation of each frame of the image stack with the first frame of this stack. As demonstrated previously (Bates et al., 2007), image drift can then be obtained by tracking of the centroid position of the correlation function. A polynomial fit was applied to the obtained drift function to reduce fluctuations caused by fluorophore blinking. For rendering of the final high-resolution image, each localized molecule was displayed by a 2D Gaussian function with a fixed amplitude of 1,000 counts and a standard deviation corresponding to the respective image resolution, which was derived from the localization accuracy and was on average  $39 \pm 8$  nm. Events that appeared in two or more consecutive frames within a distance  $<1$  px (120 nm) were considered as originating from the same fluorescent molecule. Localized molecules with  $<300$  detected photons were discarded. Further, all molecules with an ellipticity  $E = |(\sigma_x - \sigma_y)/(\sigma_x + \sigma_y)| > 15\%$  were discarded for the control cells as well as all events with  $E > 50\%$  for the ionomycin-treated cells.

## Statistical analysis

Statistical significance was analyzed in an unpaired Student's *t* test using GraphPad Prism software. Compared datasets were statistically significant when *p*-values were  $<0.01$  (\*\*).

## Online supplemental material

Fig. S1 shows by STORM microscopy that the TGN remains intact in ionomycin treated cells. In addition, cargo clustering by Cab45 and  $\text{Ca}^{2+}$  and fluorescence cross-correlation spectroscopy experiments show that only the  $\text{Ca}^{2+}$  bound form of Cab45 binds cargo. In Fig. S2, we show control experiments for the Cab45 CRSIPR/Cas9 cell lines (immunofluorescence and secretion assays). Fig. S3 visualizes different quantification images from 3D SIM images depicted in Fig. 5. Online supplemental material is available at <http://www.jcb.org/cgi/content/full/jcb.201601089/DC1>.

## Acknowledgments

We thank H. Reiter for retroviral transfections. We thank W. Neupert and M. Harner for insightful discussions. We thank S. Suppmann from the Max Planck Institute biochemistry core facility for Cab45 expression and purification.

The group of J. von Blume is funded by an Emmy Noether Fellowship (project BL 1186/1-1), by Deutsche Forschungsgemeinschaft CRC914 (TP A09), and by an FP7 Marie Curie Career Reintegration Grant. J. von Blume is supported by the Max Planck Institute of Biochemistry and by the department of Molecular Medicine of Reinhard Fässler. The group of D.C. Lamb is grateful for financial support from the Deutsche Forschungsgemeinschaft through SFB1035 (project A11) and the Center for NanoScience Munich. D.C. Lamb and H. Leonhardt are supported by the Excellence Clusters Nanosystems Initiative Munich and Center for integrated Protein Science Munich.

The authors declare no competing financial interests.

Submitted: 25 January 2016

Accepted: 6 April 2016

## References

- Aulestia, F.J., M.T. Alonso, and J. García-Sancho. 2015. Differential calcium handling by the cis and trans regions of the Golgi apparatus. *Biochem. J.* 466:455–465. <http://dx.doi.org/10.1042/BJ20141358>
- Bates, M., B. Huang, G.T. Dempsey, and X. Zhuang. 2007. Multicolor super-resolution imaging with photo-switchable fluorescent probes. *Science*. 317:1749–1753. <http://dx.doi.org/10.1126/science.1146598>
- Bonifacino, J.S. 2014. Adaptor proteins involved in polarized sorting. *J. Cell Biol.* 204:7–17. <http://dx.doi.org/10.1083/jcb.201310021>
- Cardoso, M.C., K. Schneider, R.M. Martin, and H. Leonhardt. 2012. Structure, function and dynamics of nuclear subcompartments. *Curr. Opin. Cell Biol.* 24:79–85. <http://dx.doi.org/10.1016/j.cob.2011.12.009>
- Cong, L., F.A. Ran, D. Cox, S. Lin, R. Barretto, N. Habib, P.D. Hsu, X. Wu, W. Jiang, L.A. Marraffini, and F. Zhang. 2013. Multiplex genome engineering using CRISPR/Cas systems. *Science*. 339:819–823. <http://dx.doi.org/10.1126/science.1231143>
- Curwin, A.J., J. von Blume, and V. Malhotra. 2012. Cofilin-mediated sorting and export of specific cargo from the Golgi apparatus in yeast. *Mol. Biol. Cell*. 23:2327–2338. <http://dx.doi.org/10.1091/mbc.E11-09-0826>
- De Matteis, M.A., and A. Luini. 2008. Exiting the Golgi complex. *Nat. Rev. Mol. Cell Biol.* 9:273–284. <http://dx.doi.org/10.1038/nrm2378>
- Dempsey, G.T., J.C. Vaughan, K.H. Chen, M. Bates, and X. Zhuang. 2011. Evaluation of fluorophores for optimal performance in localization-based super-resolution imaging. *Nat. Methods*. 8:1027–1036. <http://dx.doi.org/10.1038/nmeth.1768>
- Doray, B., K. Bruns, P. Ghosh, and S. Kornfeld. 2002. Interaction of the cation-dependent mannose 6-phosphate receptor with GGA proteins. *J. Biol. Chem.* 277:18477–18482. <http://dx.doi.org/10.1074/jbc.M201879200>
- Fölsch, H., H. Ohno, J.S. Bonifacino, and I. Mellman. 1999. A novel clathrin adaptor complex mediates basolateral targeting in polarized epithelial cells. *Cell*. 99:189–198. [http://dx.doi.org/10.1016/S0092-8674\(00\)81650-5](http://dx.doi.org/10.1016/S0092-8674(00)81650-5)
- Fölsch, H., M. Pypaert, P. Schu, and I. Mellman. 2001. Distribution and function of AP-1 clathrin adaptor complexes in polarized epithelial cells. *J. Cell Biol.* 152:595–606. <http://dx.doi.org/10.1083/jcb.152.3.595>
- Guo, Y., D.W. Sirkis, and R. Schekman. 2014. Protein sorting at the trans-Golgi network. *Annu. Rev. Cell Dev. Biol.* 30:169–206. <http://dx.doi.org/10.1146/annurev-cellbio-100913-013012>
- Heilemann, M., S. van de Linde, M. Schüttelpe, R. Kasper, B. Seefeldt, A. Mukherjee, P. Tinnefeld, and M. Sauer. 2008. Subdiffraction-resolution fluorescence imaging with conventional fluorescent probes. *Angew. Chem. Int. Ed. Engl.* 47:6172–6176. <http://dx.doi.org/10.1002/anie.200802376>
- Hsu, P.D., D.A. Scott, J.A. Weinstein, F.A. Ran, S. Konermann, V. Agarwala, Y. Li, E.J. Fine, X. Wu, O. Shalem, et al. 2013. DNA targeting specificity of RNA-guided Cas9 nucleases. *Nat. Biotechnol.* 31:827–832. <http://dx.doi.org/10.1038/nbt.2647>
- Kelley, L.A., and M.J.E. Sternberg. 2009. Protein structure prediction on the Web: a case study using the Phyre server. *Nat. Protoc.* 4:363–371. <http://dx.doi.org/10.1038/nprot.2009.2>
- Kienzle, C., and J. von Blume. 2014. Secretory cargo sorting at the trans-Golgi network. *Trends Cell Biol.* 24:584–593. <http://dx.doi.org/10.1016/j.tcb.2014.04.007>
- Kienzle, C., N. Basnet, A.H. Crevenna, G. Beck, B. Habermann, N. Mizuno, and J. von Blume. 2014. Cofilin recruits F-actin to SPCA1 and promotes  $\text{Ca}^{2+}$ -mediated secretory cargo sorting. *J. Cell Biol.* 206:635–654. <http://dx.doi.org/10.1083/jcb.201311052>
- Kornfeld, S., and I. Mellman. 1989. The biogenesis of lysosomes. *Annu. Rev. Cell Biol.* 5:483–525. <http://dx.doi.org/10.1146/annurev.cb.05.110189.002411>
- Letunic, I., T. Doerks, and P. Bork. 2015. SMART: recent updates, new developments and status in 2015. *Nucleic Acids Res.* 43:D257–D260. <http://dx.doi.org/10.1093/nar/gku949>
- Lissandron, V., P. Podini, P. Pizzo, and T. Pozzan. 2010. Unique characteristics of  $\text{Ca}^{2+}$  homeostasis of the trans-Golgi compartment. *Proc. Natl. Acad. Sci. USA*. 107:9198–9203. <http://dx.doi.org/10.1073/pnas.1004702107>
- Marchler-Bauer, A., M.K. Derbyshire, N.R. Gonzales, S. Lu, F. Chitsaz, L.Y. Geer, R.C. Geer, J. He, M. Gwadz, D.I. Hurwitz, et al. 2015. CDD: NCBI's conserved domain database. *Nucleic Acids Res.* 43:D222–D226. <http://dx.doi.org/10.1093/nar/gku1221>
- Meissner, G. 1975. Isolation and characterization of two types of sarcoplasmic reticulum vesicles. *Biochim. Biophys. Acta*. 389:51–68. [http://dx.doi.org/10.1016/0005-2736\(75\)90385-5](http://dx.doi.org/10.1016/0005-2736(75)90385-5)
- Mellman, I., and W.J. Nelson. 2008. Coordinated protein sorting, targeting and distribution in polarized cells. *Nat. Rev. Mol. Cell Biol.* 9:833–845. <http://dx.doi.org/10.1038/nrm2525>

- Missiaen, L., K. Van Acker, K. Van Baelen, L. Raeymaekers, F. Wuytack, J.B. Parys, H. De Smedt, J. Vanoevelen, L. Dode, R. Rizzuto, and G. Callewaert. 2004. Calcium release from the Golgi apparatus and the endoplasmic reticulum in HeLa cells stably expressing targeted aequorin to these compartments. *Cell Calcium*. 36:479–487. <http://dx.doi.org/10.1016/j.ceca.2004.04.007>
- Müller, B.K., E. Zaychikov, C. Bräuchle, and D.C. Lamb. 2005. Pulsed interleaved excitation. *Biophys. J.* 89:3508–3522. <http://dx.doi.org/10.1529/biophysj.105.064766>
- Palade, G. 1975. Intracellular aspects of the process of protein synthesis. *Science*. 189:867. <http://dx.doi.org/10.1126/science.189.4206.867-b>
- Palmer, A.E., and R.Y. Tsien. 2006. Measuring calcium signaling using genetically targetable fluorescent indicators. *Nat. Protoc.* 1:1057–1065. <http://dx.doi.org/10.1038/nprot.2006.172>
- Pfeifer, A., T. Kessler, S. Silletti, D.A. Cheresh, and I.M. Verma. 2000. Suppression of angiogenesis by lentiviral delivery of PEX, a noncatalytic fragment of matrix metalloproteinase 2. *Proc. Natl. Acad. Sci. USA*. 97:12227–12232. <http://dx.doi.org/10.1073/pnas.220399597>
- Pizzo, P., V. Lissandron, P. Capitanio, and T. Pozzan. 2011. Ca<sup>2+</sup> signalling in the Golgi apparatus. *Cell Calcium*. 50:184–192. <http://dx.doi.org/10.1016/j.ceca.2011.01.006>
- Prescher, J., V. Baumgärtel, S. Ivanchenko, A.A. Torrano, C. Bräuchle, B. Müller, and D.C. Lamb. 2015. Super-resolution imaging of ESCRT-proteins at HIV-1 assembly sites. *PLoS Pathog.* 11:e1004677. <http://dx.doi.org/10.1371/journal.ppat.1004677>
- Ran, F.A., P.D. Hsu, J. Wright, V. Agarwala, D.A. Scott, and F. Zhang. 2013. Genome engineering using the CRISPR-Cas9 system. *Nat. Protoc.* 8:2281–2308. <http://dx.doi.org/10.1038/nprot.2013.143>
- Schermelleh, L., R. Heintzmann, and H. Leonhardt. 2010. A guide to super-resolution fluorescence microscopy. *J. Cell Biol.* 190:165–175. <http://dx.doi.org/10.1083/jcb.201002018>
- Schindelin, J., I. Arganda-Carreras, E. Frise, V. Kaynig, M. Longair, T. Pietzsch, S. Preibisch, C. Rueden, S. Saalfeld, B. Schmid, et al. 2012. Fiji: an open-source platform for biological-image analysis. *Nat. Methods*. 9:676–682. <http://dx.doi.org/10.1038/nmeth.2019>
- Söding, J. 2005. Protein homology detection by HMM-HMM comparison. *Bioinformatics*. 21:951–960. <http://dx.doi.org/10.1093/bioinformatics/bti125>
- Tagliabracci, V.S., J.L. Engel, J. Wen, S.E. Wiley, C.A. Worby, L.N. Kinch, J. Xiao, N.V. Grishin, and J.E. Dixon. 2012. Secreted kinase phosphorylates extracellular proteins that regulate biomineralization. *Science*. 336:1150–1153. <http://dx.doi.org/10.1126/science.1217817>
- Traub, L.M., and S. Kornfeld. 1997. The trans-Golgi network: a late secretory sorting station. *Curr. Opin. Cell Biol.* 9:527–533. [http://dx.doi.org/10.1016/S0955-0674\(97\)80029-4](http://dx.doi.org/10.1016/S0955-0674(97)80029-4)
- von Blume, J., J.M. Duran, E. Forlanelli, A.-M. Alleaume, M. Egorov, R. Polishchuk, H. Molina, and V. Malhotra. 2009. Actin remodeling by ADF/cofilin is required for cargo sorting at the trans-Golgi network. *J. Cell Biol.* 187:1055–1069. <http://dx.doi.org/10.1083/jcb.200908040>
- von Blume, J., A.-M. Alleaume, G. Cantero-Recasens, A. Curwin, A. Carreras-Sureda, T. Zimmermann, J. van Galen, Y. Wakana, M.A. Valverde, and V. Malhotra. 2011. ADF/cofilin regulates secretory cargo sorting at the TGN via the Ca<sup>2+</sup> ATPase SPCA1. *Dev. Cell*. 20:652–662. <http://dx.doi.org/10.1016/j.devcel.2011.03.014>
- von Blume, J., A.-M. Alleaume, C. Kienzle, A. Carreras-Sureda, M. Valverde, and V. Malhotra. 2012. Cab45 is required for Ca<sup>2+</sup>-dependent secretory cargo sorting at the trans-Golgi network. *J. Cell Biol.* 199:1057–1066. <http://dx.doi.org/10.1083/jcb.201207180>
- Wiech, H., B.M. Geier, T. Paschke, A. Spang, K. Grein, J. Steinkötter, M. Melkonian, and E. Schiebel. 1996. Characterization of green alga, yeast, and human centrins. Specific subdomain features determine functional diversity. *J. Biol. Chem.* 271:22453–22461. <http://dx.doi.org/10.1074/jbc.271.37.22453>

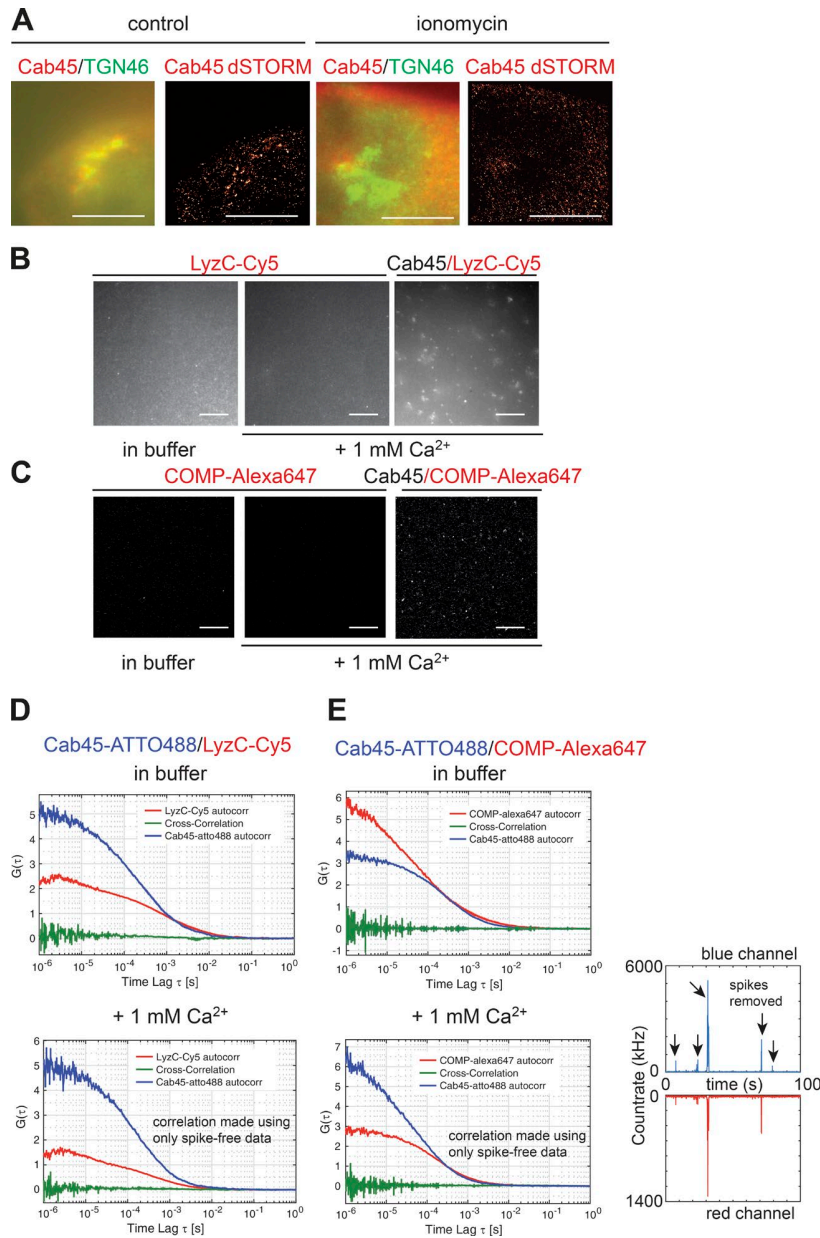


Figure S1. **Cargo recruitment by Cab45 oligomers.** (A) HeLa cells were fixed and incubated with media containing DMSO (control) or Ca<sup>2+</sup>-free Hanks buffer containing 2  $\mu$ M ionomycin and 5 mM EGTA for 10 min. Subsequently, cells were fixed and stained with a Cab45 and TGN46 antibodies and Cy5- (Cab45) or Alexa Fluor 488-labeled (TGN46) secondary antibodies. Wide-field illumination imaging was performed (red/green merge, first image, third image) and dSTORM single fluorescent emitters were localized using a Gaussian least-squares fit. Bars, 10  $\mu$ m. For the in vitro clustering assay, Cy5-labeled LyzC (B) or Alexa Fluor 647-labeled COMP (C) was left untreated (left), incubated with Ca<sup>2+</sup> (middle), or incubated with unlabeled Cab45 (right). Cluster formation was assessed by fluorescence microscopy. Bars, 20  $\mu$ m. (D) Fluorescence cross-correlation spectroscopy of ATTO488-labeled Cab45 and LyzC-Cy5 in the absence (top) or presence of 1 mM Ca<sup>2+</sup> (bottom). (E) Fluorescence cross-correlation spectroscopy of ATTO488-labeled Cab45 and Alexa Fluor 647-labeled COMP in the absence (top) or presence of 1 mM Ca<sup>2+</sup> (bottom). In the presence of 1 mM Ca<sup>2+</sup>, clusters of Cab45 form that can be observed as “spikes” or large fluorescence fluctuations in the raw data of both channels (E, right panel, bottom). To calculate the cross-correlation curve shown these spikes (marked with an arrow) were excluded for analysis.

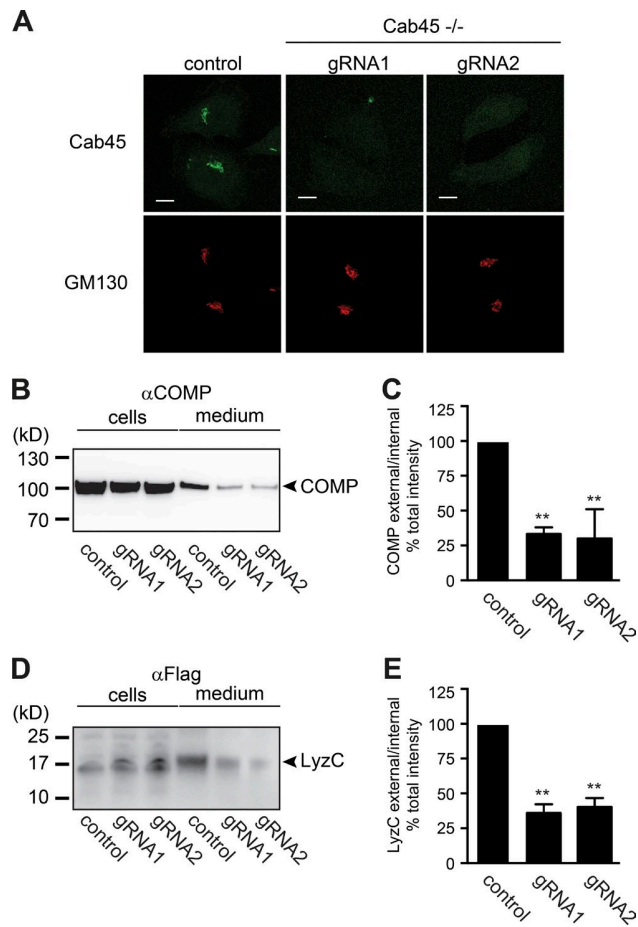


Figure S2. **Cab45 Ca<sup>2+</sup> binding is required for cargo sorting in living cells.** (A) Control, Cab45<sup>-/-</sup> (gRNA1) or Cab45<sup>-/-</sup> (gRNA2) HeLa cells were stained with a Cab45 and GM130 antibodies and analyzed by fluorescence microscopy. Bars, 5 μM. (B–E) Control, Cab45<sup>-/-</sup> (gRNA1), or Cab45<sup>-/-</sup> (gRNA2) HeLa cells were transfected with LyzC and incubated in serum-free medium for 4 h. Cells and media were collected and analyzed by SDS-PAGE and WB with anti-COMP (B) or anti-Flag (LyzC) antibodies (D), respectively. Three Western blots from independent experiments shown in B or D were quantified. Bars graphs represent the densitometry values of external COMP (C) or LyzC (E) normalized to internal COMP or LyzC values, respectively. Error bars show mean of three independent experiments ± SD (n = 3). \*\*, P < 0.01 (compared datasets).

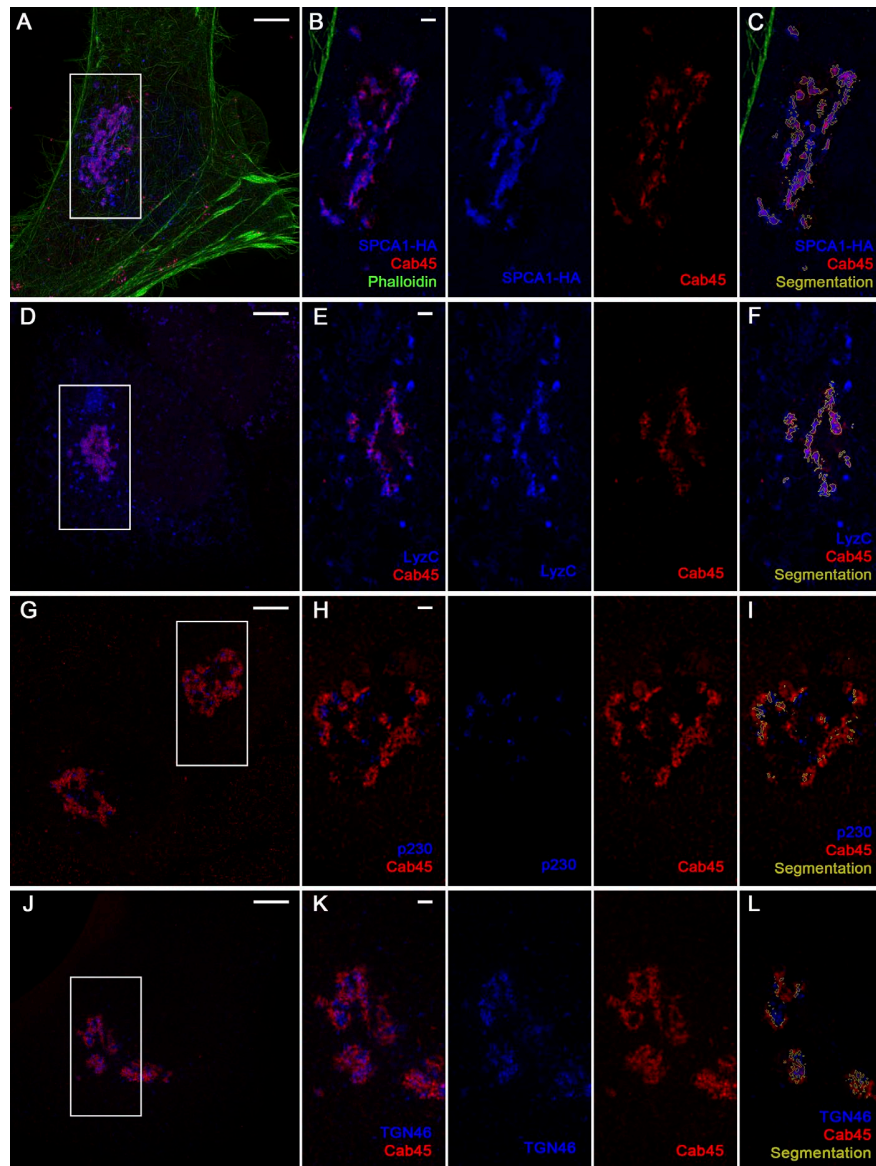
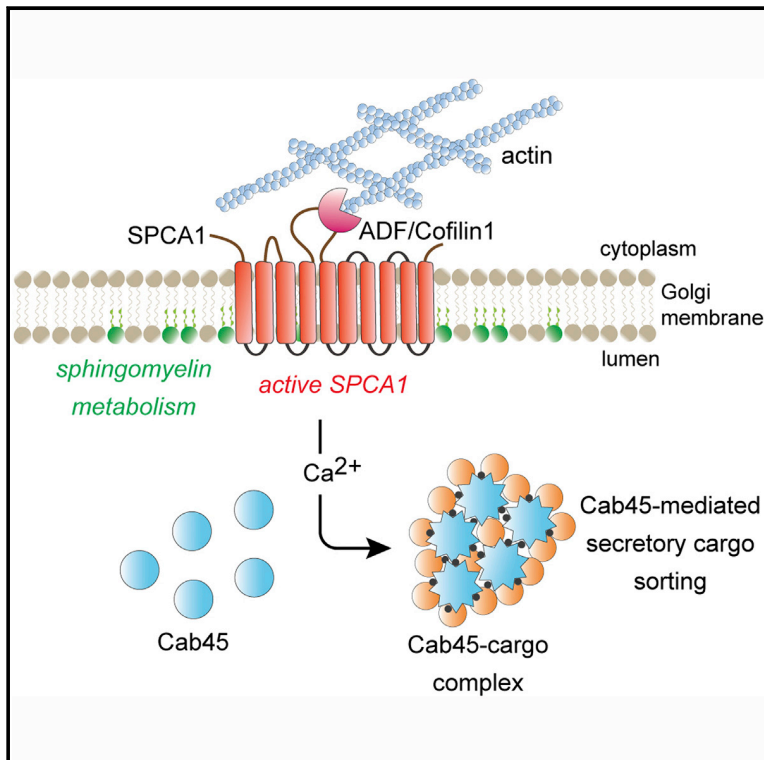


Figure S3. **SPCA1, Cab45, and cargo cluster in the TGN.** 3D SIM images shown in Fig. 5 depicted as maximum intensity projection (A, D, G, and J; bar, 5  $\mu\text{m}$ , top) or overlay and cross section of colocalized SPCA1/Cab45 (B) or LyzC/Cab45 (E), p230/Cab45 (H), or TGN46/Cab45 (K) structures (inset boxes are shown below at 2 $\times$  magnification; bar, 1  $\mu\text{m}$ ). Segmentation masks of colocalized SPCA/Cab45 (C), LyzC/Cab45 (F), p230/Cab45 (I), or TGN46/Cab45 (L) used for measurements shown in the graph in Fig. 4 D.

# Developmental Cell

## Activity of the SPCA1 Calcium Pump Couples Sphingomyelin Synthesis to Sorting of Secretory Proteins in the *Trans*-Golgi Network

### Graphical Abstract



### Authors

Yongqiang Deng, Mehrshad Pakdel, Birgit Blank, Emma L. Sundberg, Christopher G. Burd, Julia von Blume

### Correspondence

christopher.burd@yale.edu (C.G.B.), vonblume@biochem.mpg.de (J.v.B.)

### In Brief

In the *trans*-Golgi network, newly synthesized proteins and lipids are sorted into distinct vesicular carriers that mediate inter-organelle transport and secretion. Deng et al. delineate a  $\text{Ca}^{2+}$ -dependent, oligomerization-driven sorting mechanism whereby Golgi membrane sphingomyelin stimulates SPCA1 calcium pump activity to induce Cab45 oligomerization-dependent client protein packaging into vesicles.

### Highlights

- Golgi membrane sphingomyelin stimulates SPCA1  $\text{Ca}^{2+}$  ATPase
- $\text{Ca}^{2+}$  binding by Cab45 causes it to oligomerize in the lumen of the TGN
- Oligomeric Cab45 condenses secreted protein clients within the luminal milieu
- Cab45 clients are secreted via vesicles enriched in sphingomyelin



# Activity of the SPCA1 Calcium Pump Couples Sphingomyelin Synthesis to Sorting of Secretory Proteins in the *Trans*-Golgi Network

Yongqiang Deng,<sup>1,3</sup> Mehrshad Pakdel,<sup>2,3</sup> Birgit Blank,<sup>2</sup> Emma L. Sundberg,<sup>1</sup> Christopher G. Burd,<sup>1,\*</sup> and Julia von Blume<sup>2,4,\*</sup>

<sup>1</sup>Department of Cell Biology, Yale University School of Medicine, New Haven, CT, USA

<sup>2</sup>Max Planck Institute of Biochemistry, Am Klopferspitz 18, 82152 Martinsried, Germany

<sup>3</sup>These authors contributed equally

<sup>4</sup>Lead Contact

\*Correspondence: [christopher.burd@yale.edu](mailto:christopher.burd@yale.edu) (C.G.B.), [vonblume@biochem.mpg.de](mailto:vonblume@biochem.mpg.de) (J.v.B.)

<https://doi.org/10.1016/j.devcel.2018.10.012>

## SUMMARY

How the principal functions of the Golgi apparatus—protein processing, lipid synthesis, and sorting of macromolecules—are integrated to constitute cargo-specific trafficking pathways originating from the *trans*-Golgi network (TGN) is unknown. Here, we show that the activity of the Golgi localized SPCA1 calcium pump couples sorting and export of secreted proteins to synthesis of new lipid in the TGN membrane. A secreted Ca<sup>2+</sup>-binding protein, Cab45, constitutes the core component of a Ca<sup>2+</sup>-dependent, oligomerization-driven sorting mechanism whereby secreted proteins bound to Cab45 are packaged into a TGN-derived vesicular carrier whose membrane is enriched in sphingomyelin, a lipid implicated in TGN-to-cell surface transport. SPCA1 activity is controlled by the sphingomyelin content of the TGN membrane, such that local sphingomyelin synthesis promotes Ca<sup>2+</sup> flux into the lumen of the TGN, which drives secretory protein sorting and export, thereby establishing a protein- and lipid-specific secretion pathway.

## INTRODUCTION

After protein and lipid secretory cargo traverses the Golgi cisternae, it is sorted into distinct vesicular transport carriers that bud from the *trans*-Golgi network (TGN) and mediate inter-organelle transport and secretion. Elucidating the mechanisms by which proteins and lipids are selected to be incorporated into Golgi-derived carriers is fundamental for understanding organelle biogenesis pathways. At present, these sorting mechanisms are poorly understood (Anitei and Hoflack, 2011; De Matteis and Luini, 2008; Kienzle and von Blume, 2014).

Many integral membrane proteins, such as recycling sorting receptors, present sorting signals to the cytoplasm that are recognized by cytosolic coat proteins that concentrate cargo and elicit budding of a transport carrier (Ang and Fölsch,

2012; Bonifacino, 2014; Fölsch et al., 2003). However, most Golgi-derived transport vesicles, such as those that mediate secretion, lack cytoplasmic coats, and the mechanisms that coordinate cargo selection, carrier budding, and fission are poorly understood (Kienzle and von Blume, 2014; Pakdel and von Blume, 2018). An especially vexing question regards how soluble secreted proteins for which no integral membrane sorting receptors have been identified are packaged into Golgi-derived secretory carriers. Existing models posit that such proteins are captured non-selectively as components of the aqueous bulk (Pfeffer and Rothman, 1987), yet some proteins, such as insulin and other peptide hormones, are concentrated in an essentially pure form in secretory vesicles (Huttner and Tooze, 1989; Molinete et al., 2000; Tooze et al., 1991; Tooze and Huttner, 1990). A secreted Ca<sup>2+</sup> binding protein, Cab45, binds to soluble secreted proteins and is proposed to concentrate bound proteins from the bulk milieu prior to export from the TGN (von Blume et al., 2011; Crevenna et al., 2016; Scherer et al., 1996).

In addition to its role in protein sorting, the Golgi apparatus is also considered a “lipid-based sorting station” (van Meer et al., 2008). How the lipid content of Golgi-derived carriers is determined and if the membranes of different carriers contain the same or different proportions of lipids are unknown. Synthesis of complex sphingolipids, such as sphingomyelin (SM) and gangliosides, occurs in the Golgi apparatus, from where they are trafficked to other organelles, principally the plasma membrane (PM), which contains a high proportion of cellular sphingolipid (van Meer et al., 2008). Interfering with sphingolipid synthesis in the Golgi apparatus impairs glycosylation of secretory cargo and slows the rate of secretion from the cell (Duran et al., 2012; Subathra et al., 2011; Tafesse et al., 2013; van Galen et al., 2014; Wakana et al., 2015), suggesting that glycoprotein processing, sphingolipid synthesis, and anterograde trafficking are coupled (Campelo et al., 2017; Capasso et al., 2017). A potential mechanism to couple sphingolipid synthesis and vesicle formation is suggested by the finding that production of diacylglycerol (DAG), a lipid that is produced during SM synthesis and that promotes negative membrane curvature, is necessary for fission of at least one class of transport vesicle from the TGN membrane (Baron and Malhotra, 2002; Campelo and Malhotra, 2012; Litvak et al., 2005; Sarri et al., 2011).



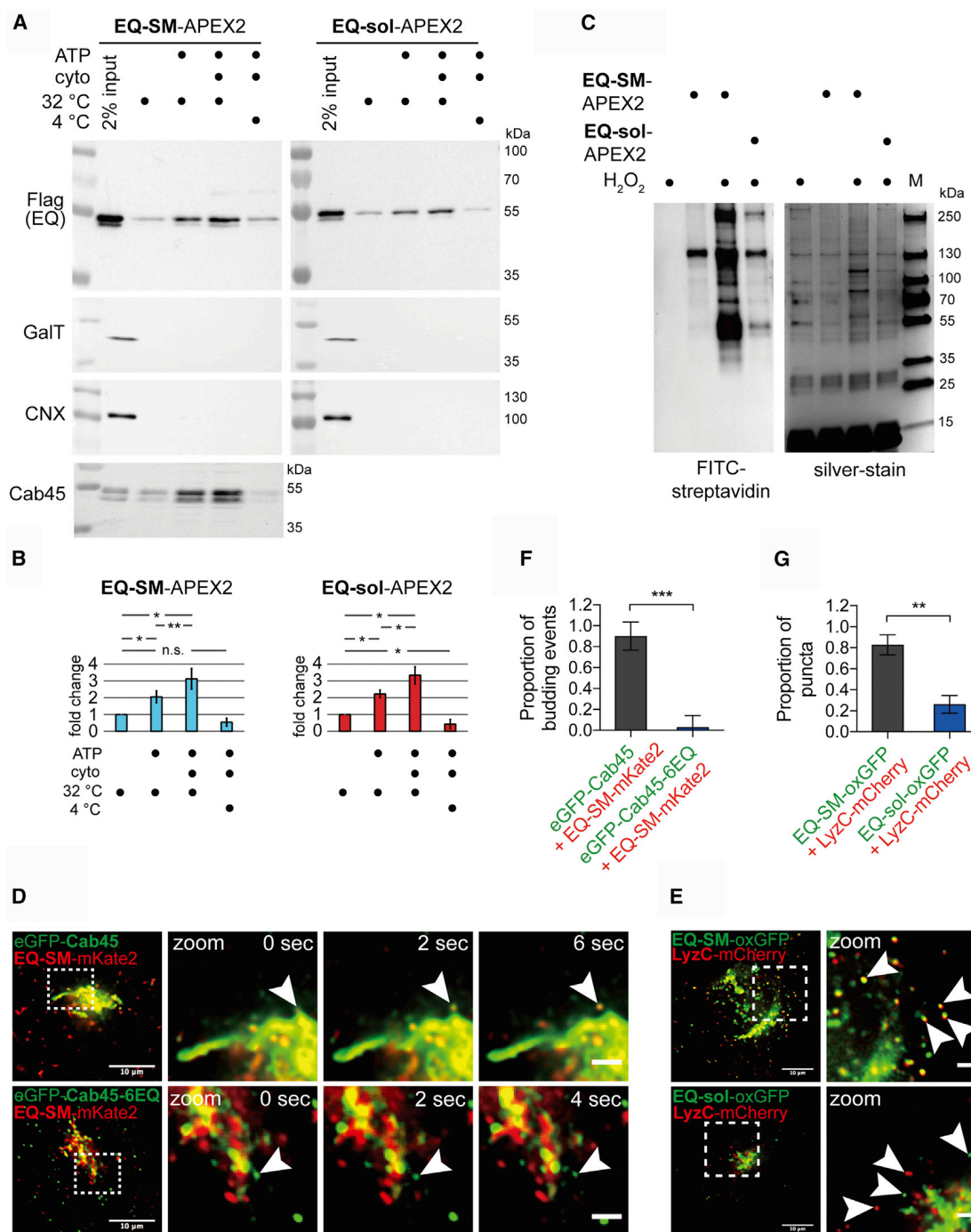


**Figure 1. Comparative Proteomics of Golgi-Derived Vesicles Identifies Cab45 as a Cargo of the Sphingomyelin Secretion Pathway**

(A) Preparation of Golgi-derived vesicles. Cell lines expressing EQ-SM-APEX2 or EQ-sol-APEX2 were permeabilized and then incubated with rat liver cytosol, ATP generating reaction components, at 32°C or on ice for 45 min, as indicated. Released vesicular material was collected by centrifugation, and the relative proportions of EQ-SM-APEX2 or EQ-sol-APEX2,  $\beta$ 1,4-galactosyltransferase (GalT; a resident of late Golgi compartments), calnexin (CNX; an ER resident), and Cab45, in each fraction were determined by immunoblotting. Note that EQ-SM-APEX2, EQ-sol-APEX2, and Cab45 are detected in the budded vesicle fractions, but GalT (a Golgi resident) and CNX (an ER resident) are not. An example experiment for EQ-SM-APEX2 and EQ-sol-APEX2 is shown. Proteomic analyses were performed for two independent vesicle preparations. See also [Table S1](#).

(B) Proportions of EQ-SM-APEX2 and EQ-sol-APEX2 in vesicle fractions. The fold increases in the amounts of EQ-SM-APEX2 and EQ-sol-APEX2 in the vesicle fractions (mean  $\pm$  SD; 3 independent experiments) are plotted.

(C) Purification of biotinylated proteins from vesicle fractions. Vesicle fractions from EQ-SM-APEX2- or EQ-sol-APEX2-expressing or control (no EQ probe) cells were incubated with APEX-mediated biotinylation reagents unless otherwise noted. Detergent (1% TritonX-100 and 0.1% SDS) was added to solubilize

(legend continued on next page)

The most abundant sphingolipid, SM, is synthesized in the luminal leaflets of Golgi membranes (Barenholz and Thompson, 1980) and then transported to the PM. To visualize SM trafficking in cells, we engineered a natural SM-binding protein, equinatoxin II, produced by the marine organism, *Actinia equina*, into a non-toxic SM reporter protein, termed “EQ-SM” (Deng et al., 2016). When addressed to the secretory pathway as a fusion to a fluorescent protein, EQ-SM is observed to be exported from the TGN in pleiomorphic carriers and to be released from the cell via exocytosis, where it remains bound to SM in the PM (Deng et al., 2016). The population of putative secretory carriers observed to bud from the TGN containing EQ-SM is also enriched with a secreted glycosylphosphatidylinositol (GPI)-anchored fluorescent reporter protein, to a similar extent as EQ-SM containing exocytic carriers observed to fuse with the PM (Deng et al., 2016). These observations suggest that SM and GPI-anchored proteins are sorted in the Golgi into a distinct arm of the secretory pathway that we refer to as the “sphingomyelin secretion (SMS) pathway” to suggest its role in trafficking SM from the TGN to the PM. To date, no native proteins have been identified that rely on the SMS pathway for secretion.

Here, we identify native protein cargo of the SMS pathway using unbiased proteomics analyses of Golgi-derived vesicles that contain EQ-SM. One identified protein, Cab45, was previously implicated in calcium-dependent sorting of a subset of secreted proteins, hereafter referred to as Cab45 “clients” (von Blume et al., 2012; Crevenna et al., 2016). We show that Cab45 and its clients are secreted via the SMS pathway and that sorting into the SMS pathway requires active SPCA1, a TGN-localized calcium pump. Cab45- and  $\text{Ca}^{2+}$ -dependent sorting of soluble secretory cargo in the TGN fails when SM synthesis in the TGN is disrupted due to deficient  $\text{Ca}^{2+}$  pumping activity by SPCA1, which resides in sphingolipid-rich membrane. Our findings reveal an unanticipated functional coupling between SM synthesis in the TGN membrane and  $\text{Ca}^{2+}$ -dependent sorting of soluble secretory cargo within the lumen of the TGN.

## RESULTS

### Identification of Native Protein Cargos of the SMS Pathway

We have previously shown that EQ-SM is exported from the Golgi in a distinct secretory transport carrier (Deng et al., 2016). A comparative proximity biotinylation proteomics approach was implemented to identify candidate native proteins that are secreted with EQ-SM via the SMS pathway. The general

strategy entailed collecting vesicle-enriched fractions produced by permeabilized HeLa cells that express EQ-SM, or a control protein that does not bind SM, termed “EQ-sol,” as fusions to engineered ascorbate peroxidase 2 (APEX2) (Hung et al., 2016), followed by APEX2-mediated biotinylation and comparative proteomic analyses of proteins purified on streptavidin matrix. HeLa cell lines stably expressing EQ-SM-APEX2 or EQ-sol-APEX2 were constructed and confirmed to elicit biotinylation of Golgi-localized proteins by in situ fluorescein isothiocyanate (FITC)-streptavidin detection (data not shown), confirming that they localize similarly to previously characterized GFP-tagged forms of EQ-SM and EQ-sol (Deng et al., 2016). As a source of Golgi-derived vesicles, we applied a previously published protocol to generate a crude vesicle fraction from permeabilized cells (Wakana et al., 2012). The PMs of cells expressing EQ-SM-APEX2 or control EQ-sol-APEX2 were permeabilized, the cytosol was washed out, and conditions were established to generate Golgi-derived vesicles containing EQ-SM-APEX2 or EQ-sol-APEX2, but not galactose transferase T1 (GalT), a resident of the *trans*-Golgi, or calnexin, a resident of the endoplasmic reticulum (ER) (Figures 1A and 1B). The appearance of EQ-SM-APEX2 or EQ-sol-APEX2 in vesicle fractions was promoted approximately 3-fold by incubation of permeabilized cells at a physiological temperature (32°C) with exogenous cytosol and an ATP regeneration system.

To identify native proteins that are specifically co-packaged with EQ-SM-APEX2 or EQ-sol-APEX2 into budded vesicles, vesicle fractions from permeabilized cells were incubated with APEX biotinylation reagents to elicit labeling of vicinal proteins. Lysis buffer containing detergent was then used to solubilize vesicle content, biotin-labeled proteins were purified on a solid streptavidin matrix (Figure 1C), and mass spectrometry was applied to identify proteins in each vesicle fraction. We defined candidate cargo proteins of the SMS pathway as those proteins containing a signal sequence, a transmembrane domain, or a GPI anchor, that were identified in EQ-SM-APEX2 vesicle fractions, but not in EQ-sol-APEX2 vesicle fractions, in each of two independent vesicle preparations.

One protein that met these criteria is Cab45 (Table S1), a soluble  $\text{Ca}^{2+}$ -binding protein that has been previously characterized as a Golgi-localized protein that facilitates sorting and secretion of certain proteins, including lysozyme C (LyzC) and cartilage oligomeric matrix protein (COMP) (von Blume et al., 2012; Crevenna et al., 2016). The presence of Cab45 in the EQ-SM-APEX2 budded vesicle fraction was also validated by immunoblotting of permeabilized cell vesicle fractions

---

vesicle-associated proteins, and biotinylated proteins were purified using immobilized streptavidin. An aliquot of each purified fraction was separated by SDS-PAGE, and proteins were visualized by silver stain. Biotinylated proteins in each fraction were identified by blotting with fluorescent streptavidin. The migration of protein molecular mass standards is indicated to the right of each gel.

(D) Example micrographs of cells expressing eGFP-Cab45 and EQ-SM-mKate2. Each micrograph shows the Golgi and surrounding cytoplasm of cells expressing the indicated fluorescent proteins. Cab45-6EQ is an engineered variant of Cab45 that does not bind  $\text{Ca}^{2+}$ . To quantify the proportion of Golgi-derived vesicles containing both proteins, time-lapse movies were acquired and examined to identify vesicular and tubular profiles that underwent budding and fission from the Golgi apparatus. The arrowheads indicate a budding vesicle. Data were collected from 3 independent experiments. Merge bars, 10  $\mu\text{m}$ . Zoom bars, 2  $\mu\text{m}$ .

(E) LyzC is exported from the Golgi in vesicles marked by EQ-SM, but not EQ-sol. Images of the Golgi region of cells expressing mCherry-tagged LyzC and EQ-SM-oxGFP or EQ-sol-oxGFP are shown. Arrowheads point to post-Golgi cytoplasmic vesicles. Merge bars, 10  $\mu\text{m}$ . Zoom bars, 2  $\mu\text{m}$ .

(F) The mean ( $\pm$  SD) proportion of 26 budding events from 4 cells expressing eGFP-Cab45 and EQ-SM as well as 32 budding events from 9 cells expressing eGFP-Cab45-6EQ and EQ-SM are plotted. Data were collected from 2 independent experiments. (G) The mean ( $\pm$  SD) proportion of detected post-Golgi LyzC vesicles that were either EQ-SM ( $n = 185$  vesicles from 6 cells) or EQ-sol ( $n = 146$  vesicles from 5 cells) positive was quantified. Data were collected from 2 independent experiments.

(Figure 1A). These data suggest that Cab45 exits the Golgi in vesicles enriched in SM.

Next, we investigated if Cab45 and EQ-SM exit the Golgi in the same or distinct carriers using time-lapse imaging of fluorescently tagged Cab45 (eGFP-Cab45) and EQ-SM (EQ-SM-mKate2) in live cells (Figure 1D). Tubular and vesicular structures containing Cab45 were observed to bud and fission from the TGN, and the proportion of these putative secretory carriers that also contained EQ-SM was determined. This analysis showed that nearly all Cab45 containing vesicles (23/26 budding events) also contained EQ-SM (Figure 1F). Importantly, a  $\text{Ca}^{2+}$  binding-defective mutant form of Cab45 (“Cab45-6EQ”) and EQ-SM are exported from the TGN via a different carrier(s) (2/32 budding events), indicating a physiologic requirement for  $\text{Ca}^{2+}$  binding for co-sorting of Cab45 and EQ-SM upon exit from the Golgi.

### **$\text{Ca}^{2+}$ -Dependent Sorting of a Cab45 Client into the SMS Pathway**

$\text{Ca}^{2+}$  binding by Cab45 drives its oligomerization, recognition of secretory clients, and efficient client secretion (von Blume et al., 2012; Crevenna et al., 2016). Therefore, we tested whether EQ-SM is also enriched in cytoplasmic vesicles that contain a Cab45-dependent cargo, LyzC, using live-cell fluorescence microscopy of cells expressing LyzC-mCherry and either EQ-SM or EQ-sol expressed with a C-terminal fusion to oxGFP, a form of GFP optimized for use within the secretory pathway (Costantini et al., 2015) (Figure 1E). We observed that  $83\% \pm 10\%$  LyzC-mCherry puncta are also labeled by EQ-SM-oxGFP, but EQ-sol, which does not recognize SM, was detected in only  $26\% \pm 9\%$  of the LyzC-mCherry puncta (Figure 1G). These data indicate that a Cab45 client, LyzC, is sorted into TGN-derived vesicles that contain EQ-SM.

We next addressed Cab45 structural requirements for LyzC sorting. Structural modeling of Cab45 (Blank and von Blume, 2017; Crevenna et al., 2016) suggests that pairs of contiguous EF hand domains form three structurally independent modules that we term EFh1 (consisting of EF hands 1 and 2), EFh2 (EF hands 3 and 4), and EFh3 (EF hands 5 and 6) (Figure 2A). To determine which EF hand modules are required for Cab45 oligomerization, we first visualized  $\text{Ca}^{2+}$ -dependent oligomerization by using confocal microscopy of ATTO488-labeled recombinant Cab45 compared to Cab45-EFh mutants in which the  $\text{Ca}^{2+}$  binding sites of each functional EFh pair was mutated (Figure 2B). The addition of 1 mM  $\text{Ca}^{2+}$  promoted the formation of fluorescent Cab45 oligomers of wild-type (WT) and EFh2-mut, but not EFh1-mut, EFh3-mut, and EFh1+3-mut (Figures 2B and 2C). In line with this observation, circular dichroism (CD) measurements showed a change in the secondary structure upon addition of  $\text{Ca}^{2+}$  of Cab45-WT and EFh2-mut, but not EFh1-mut, EFh3-mut, and EFh1+3-mut (Figure S1A). Confocal microscopy of HeLa cells expressing Cab45-EFh mutants showed that EFh1-mut, EFh3-mut, and EFh1+3-mut co-localize with p230, a TGN marker, and also to cytoplasmic vesicles, similar to Cab45-6EQ, while EFh2-mut showed reduced cytoplasmic vesicular localization (Figures S1B and S1C). These results indicate that EFh1 and EFh3 are critical for  $\text{Ca}^{2+}$ -induced change in secondary structure, oligomerization of Cab45, and correct localization in the TGN.

To correlate these results to the sorting of a Cab45 client into the SMS pathway, we first monitored transit of GFP-tagged LyzC through the secretory pathway in cells expressing mutant forms of Cab45. A gene replacement strategy was employed where native Cab45 was depleted by Cab45 small interfering RNAs (siRNAs) and then siRNA-resistant WT or mutant forms of Cab45 were expressed. To monitor trafficking of a single cohort of LyzC, the “retention using selective hooks” (RUSH) system (Boncompain et al., 2012) was used to synchronously release LyzC-eGFP from the ER by addition of biotin to the culture medium. Accordingly, the streptavidin binding peptide (SBP) sequence was appended to the C terminus of LyzC, followed by enhanced GFP (LyzC-SBP-eGFP). Whereas in the absence of added biotin, LyzC-SBP-eGFP is restricted to the ER (Figure 3A), 20 min after biotin addition to the culture medium, nearly all LyzC-SBP-eGFP localized to the Golgi apparatus. At 40 and 60 min after biotin addition, vesicles containing LyzC-SBP-eGFP are observed in the cytoplasm (mean number of vesicles/cell:  $26 \pm 11$  and  $36 \pm 15$ , respectively) (Figures 3A and 3B). In contrast, in cells depleted of Cab45, LyzC-SBP-eGFP is largely retained within the Golgi apparatus, with just  $6 \pm 5$  and  $14 \pm 10$  vesicles per cell observed 40 and 60 min after ER release, respectively (Figures 3A, 3B, S2A, and S2B). Expression of siRNA-resistant, hemagglutinin (HA) epitope-tagged Cab45-WT restored export of LyzC-SBP-eGFP from the Golgi ( $27 \pm 12$  vesicles per cell and  $33 \pm 14$  vesicles per cell, respectively), however, a  $\text{Ca}^{2+}$  binding defective mutant protein form of Cab45 (Cab45-6EQ-HA) did not ( $5 \pm 5$  vesicles per cell and  $10 \pm 8$  vesicles per cell, respectively) (Figures 3A and 3B), even though both proteins were expressed at similar levels (data not shown). Importantly, Cathepsin D, which is not a Cab45 client (Crevenna et al., 2016), does not co-localize within the same post-Golgi vesicles and showed no export defect in Cab45-depleted cells, indicating that it is exported from the Golgi by a distinct carrier (Figures 3C and 3D). Next, we examined requirements for the EFh  $\text{Ca}^{2+}$  binding modules of Cab45 in promoting export of LyzC-SBP-eGFP from the Golgi apparatus. Expression of siRNA-resistant Cab45-EFh2-mut rescued LyzC-SBP-eGFP to WT levels ( $26 \pm 14$  and  $37 \pm 18$  at 40 and 60 min post release, respectively) (Figure 3E). Importantly, expression of Cab45-EFh1+3-mut ( $11 \pm 6$  and  $17 \pm 11$ , respectively) failed to rescue export of LyzC-SBP-eGFP from the Golgi (Figure 3E). These results demonstrate that  $\text{Ca}^{2+}$  binding by Cab45 EFh1 and EFh3 is required for efficient export of LyzC from the Golgi apparatus.

### **EQ-SM, Cab45, and LyzC Are Exocytosed via the Same Carrier**

The results establish that EQ-SM, Cab45, and LyzC exit the Golgi in the same carrier, and we next sought to determine if these proteins are also secreted from the cell via the same carrier. Secretion of endogenous Cab45 and the requirement for Cab45 for efficient secretion of LyzC were confirmed by probing the cell medium of cycloheximide (CHX)-treated HeLa cells with anti-Cab45 antiserum (Figures 4A, S2A, and S2B). To determine if Cab45 and LyzC are exocytosed in vesicles of the SMS pathway, we used time-lapse total internal reflection fluorescence microscopy (TIRFM) of live cells co-expressing EQ-SM-mKate2 or EQ-sol-mKate2 and pHluorin-Cab45 or LyzC-pHluorin (Figure 4). Exocytic events were identified in movies

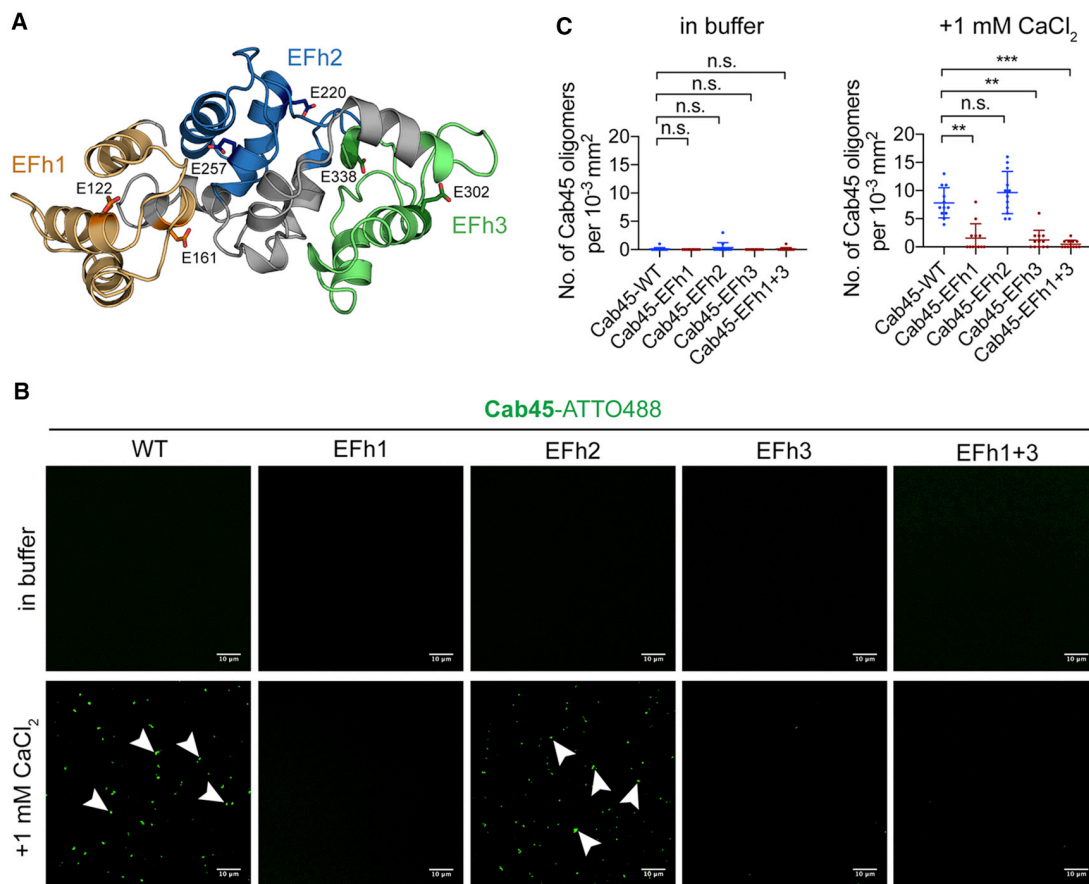


**Figure 2. Cab45 Oligomerization and Client Binding Requires EF Hand Modules 1 and 3**

(A) Model of Cab45 EF hand modules. Structural modeling predicts that contiguous pairs of EF hands function as independent Ca<sup>2+</sup>-binding modules (Crevenna et al., 2016); EF hand module 1 (consisting of EF hands 1 and 2) is orange, EF hand module 2 (consisting of EF hands 3 and 4) is blue, and EF hand module 3 (consisting of EF hands 5 and 6) is green. The positions and amino acid side chains of calcium binding glutamic acid residues from each module are indicated. These residues were replaced by glutamine in Cab45 EFh mutants to disable Ca<sup>2+</sup> binding.

(B) *In vitro* oligomerization assay analyzed by confocal microscopy. Recombinant Cab45-WT and the Cab45-EFh1, Cab45-EFh2, Cab45-EFh3, and Cab45-EFh1+3 mutants labeled with ATTO488, were incubated in Ca<sup>2+</sup>-free buffer or with 1 mM CaCl<sub>2</sub>. Bars, 10 μm. Arrowheads indicate fluorescent puncta of Cab45 oligomers.

(C) Quantification of *in vitro* oligomerization assay. Data are presented as mean number of Cab45 puncta per 10<sup>-3</sup> mm<sup>2</sup> area from 12 regions of interest (± SD) from 2 independent experiments.

See also Figure S1.

by the flash of fluorescence emitted by pHLuorin upon encountering the neutral pH of the culture medium, and then the presence of EQ-SM-mKate2 or EQ-sol-mKate2 was scored (Figure 4B). We observed that 98% ± 5% (40/42 exocytic events in 8 cells) of the pHLuorin-Cab45 containing vesicles also contained EQ-SM-mKate2, but just 46% ± 37% of pHLuorin-Cab45 containing vesicles contained EQ-sol-mKate2 (14/30 exocytic events in 8 cells). We next examined exocytosis of EQ reporters with LyzC and observed that 81% ± 15% (n = 15 cells) of LyzC-pHLuorin exocytosed vesicles also contained EQ-SM-mKate2, but just 43 ± 22 (n = 12 cells) of LyzC-pHLuorin vesicles contained EQ-sol-mKate2 (Figure 4C). These data, considered together with the results of the Golgi export assays, confirm that Cab45 and the Cab45 client, LyzC, are sorted into the SMS pathway. We note that substantially fewer Cab45 exocytic events were observed compared to LyzC events, possibly

indicating that Cab45 is retrieved from a post-Golgi compartment while the Cab45 client continues on the anterograde pathway.

To address Cab45 structural requirements for the co-sorting of LyzC and EQ-SM, we conducted TIRFM-based exocytosis assays in genome-edited Cab45 null cells (Crevenna et al., 2016) that re-express Cab45 or the Cab45-EFh1+3 mutant by transfection (Figure 4D). In control cells that re-express Cab45-WT, 76% ± 14% (n = 14 cells) of exocytic vesicles contained both LyzC-pHLuorin and EQ-SM-mKate2, a value that is similar to that of LyzC-pHLuorin and EQ-SM-mKate2 in unmodified cells (Figure 4D). In contrast, in cells expressing EFh1+3-mut, only 53% ± 14% (n = 20 cells) of LyzC-pHLuorin containing exocytic vesicles also contained EQ-SM-mKate2 (Figure 4D). Importantly, disruption of TGN Ca<sup>2+</sup> homeostasis by deletion of SPCA1 reduced the number of exocytic vesicles containing both

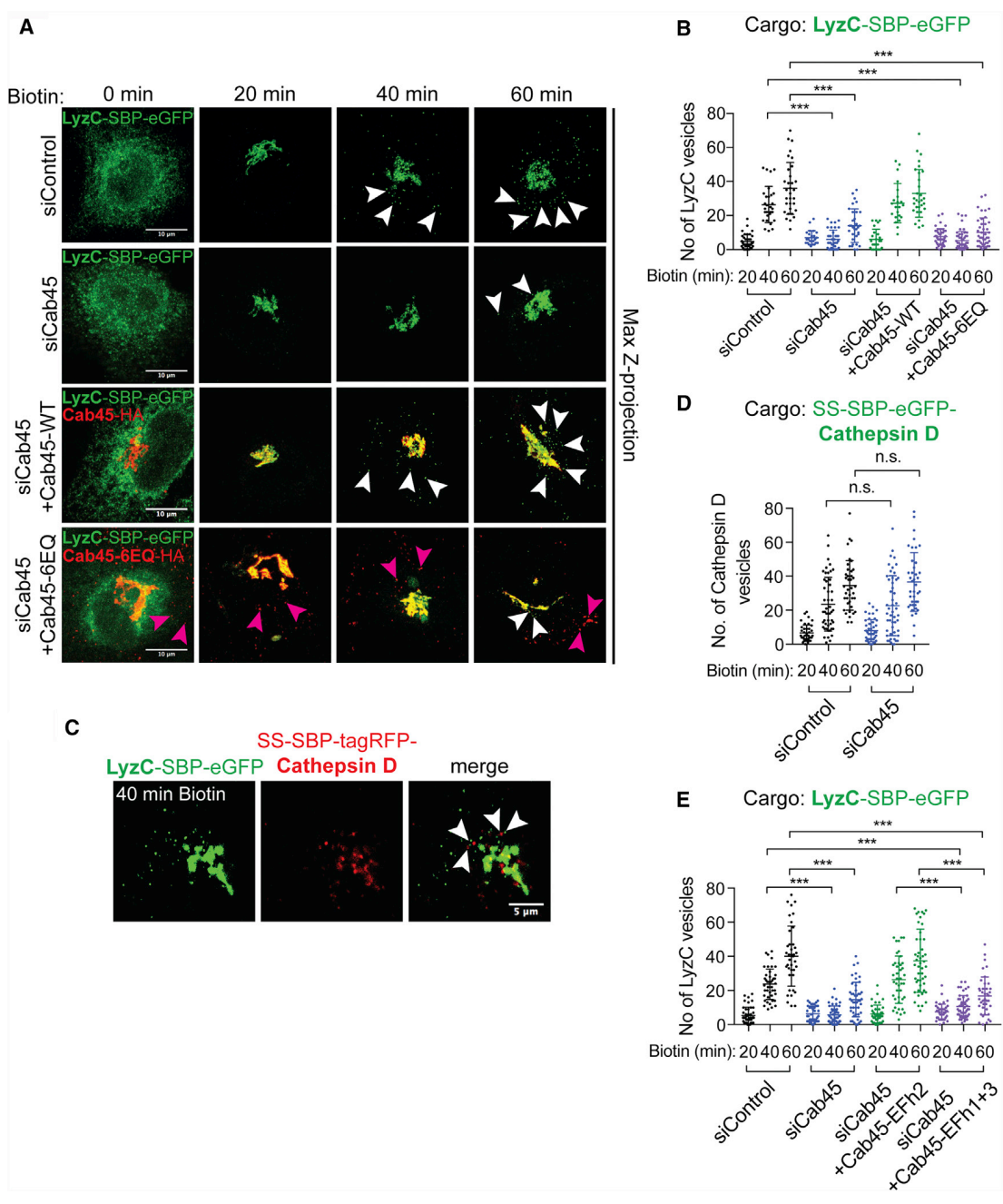


**Figure 3.  $Ca^{2+}$  Binding by Cab45 Is Required for the Sorting of a Cab45 Client, Lysozyme C (LyzC), into Golgi-Derived Vesicles**  
 (A and B) (A) HeLa cells were transfected with Cab45 siRNA and a plasmid that directs expression of siRNA-insensitive HA-epitope tagged Cab45-WT or the  $Ca^{2+}$  binding defective Cab45-6EQ mutant variant. All cells were co-transfected with plasmids that direct expression of a LyzC—streptavidin binding peptide (SBP)—eGFP fusion protein (LyzC-SBP-eGFP) and streptavidin-KDEL “anchor” that confers ER retention of SBP-containing proteins. Biotin was added to the culture medium to elicit release of LyzC-SBP-eGFP from the ER (0 min). Micrographs were captured after fixing cells 20, 40, and 60 min after biotin addition, and the number of cytoplasmic vesicles was determined at each time point. Arrowheads point to cytoplasmic vesicles. Note that Golgi-derived vesicles containing LyzC-SBP-eGFP are abundant in the cytoplasm of cells that express native, but not  $Ca^{2+}$  binding defective, Cab45. Magenta arrowheads point to Cab45-6EQ cytoplasmic vesicles that localize to distinct vesicles from LyzC-SBP-eGFP. See also Figure S1. Vesicle counts from at least 22 cells per condition are plotted in (B). The means of 3 independent experiments ( $\pm$  SD) are plotted.  
 (C) Cathepsin D and LyzC fusion proteins are exported from the Golgi in different vesicles. HeLa cells were transfected with plasmids that direct expression of LyzC-SBP-eGFP or SS-SBP-tagRFP-Cathepsin D fusion proteins. Proteins were released from the ER by the addition of biotin, and the cargo loads of Golgi derived cytoplasmic vesicles were determined as described in the legend for (A). Micrographs show representative cells 40 min after release of cargo from the ER. Bars, 5  $\mu$ m.

(legend continued on next page)

LyzC-pHluorin and EQ-SM-mKate2 to only  $51\% \pm 24\%$  ( $n = 10$  cells) (Figure 4D), and this effect was rescued to  $82\% \pm 12\%$  ( $n = 10$  cells) by re-expression of SPCA1-WT (Figure 4D). Furthermore, by using RUSH assays, we observed that cytoplasmic LyzC vesicle counts were significantly reduced after 40 and 60 min of biotin addition in SPCA1 null cells, while this effect was rescued by re-expression of SPCA1-WT (Figure S2C). In addition, SPCA1 depletion slowed the rate of LyzC secretion into the culture medium (Figures S2A and S2B) (von Blume et al., 2012). These data demonstrate that  $\text{Ca}^{2+}$  binding by Cab45 promotes the sorting of LyzC into secretory vesicles of the SMS pathway in an SPCA1-dependent manner.

### Depletion of SM Synthases Causes Mis-sorting of LyzC

Having established roles for Cab45 and SPCA1 in  $\text{Ca}^{2+}$ -dependent sorting of LyzC into Golgi-derived exocytic vesicles of the SMS pathway, we next sought to determine if SM synthesis is required for Cab45-dependent sorting. Using RUSH-based sorting assays, we examined export of LyzC and Cathepsin D from the Golgi of cells depleted of SM synthases by siRNA (Figure S3A). Both SMS1, which localizes to the Golgi apparatus, and SMS2, which localizes to the PM, were depleted because published work shows that toxicity of exogenously added short chain ceramide is ameliorated only when both enzymes are depleted (Duran et al., 2012; van Galen et al., 2014). Whereas 40 min after release of LyzC-SBP-eGFP from the ER, control siRNA cells contained  $29 \pm 10$  vesicles per cell, SMS1/2-depleted cells contained  $9 \pm 7$  vesicles per cell (Figure 4E). Notably, SMS1 and SMS2 depletion did not affect the number of post-Golgi vesicles containing SS-SBP-eGFP-Cathepsin D ( $25 \pm 16$  versus  $21 \pm 13$  vesicles per cell cytoplasm) (Figure 4F). These data indicate that depletion of SMS1/2 selectively decreases the rate of export of LyzC, but not Cathepsin D, from the Golgi.

TIRFM-based exocytosis assays revealed that SM synthesis is required for the co-sorting of LyzC-pHluorin and EQ-SM into exocytic vesicles (Figure 4G). For these experiments, we used a fortuitously obtained genome-edited HeLa cell line that expresses reduced amounts of SMS1 and SMS2 (“SMS1/2-edited”). Quantitative mass spectrometry analysis of sphingolipids in this cell line shows that the sum total of all SM species is reduced by  $31\% \pm 6.4\%$  (SEM) (Figure S3B), a level that is below the detection limit for EQ-SM (Figures S3B–S3E). Upon fusion of EQ-SM containing vesicles with the PM of SMS1/2-edited cells, EQ-SM rapidly diffuses from the site of exocytosis, in contrast to parental cells where EQ-SM remains at the site of fusion (Figures S3C and S3D), indicating that these secretory vesicles are depleted of SM. Whereas in unmodified parental cells  $81\% \pm 15\%$  ( $n = 15$  cells) of LyzC-pHluorin containing exocytic vesicles contained EQ-SM-mKate2, in SMS1/2-depleted cells only  $55\% \pm 10\%$  ( $n = 15$  cells) contained both of these proteins (Fig-

ure 4G). Depletion of SMS1/2 was also observed to slow the secretion of LyzC into the medium (Figures S2A and S2B). Importantly, re-expression solely of SMS1 in SMS1/2-edited cells restored co-sorting of LyzC-pHluorin and EQ-SM-mKate2 to control levels (Figure 4G). We note that the magnitude of the effect of SMS1/2 depletion on co-sorting of LyzC and EQ-SM is similar to that observed for the co-sorting of these proteins in Cab45-EFh1+3 mutant cells (53%; Figure 4D) and that of LyzC and EQ-sol in unmodified parental cells (43%; Figure 4C). The results establish that Cab45 mediates  $\text{Ca}^{2+}$ -dependent sorting of LyzC into the SMS pathway and that SM synthesis is necessary for sorting.

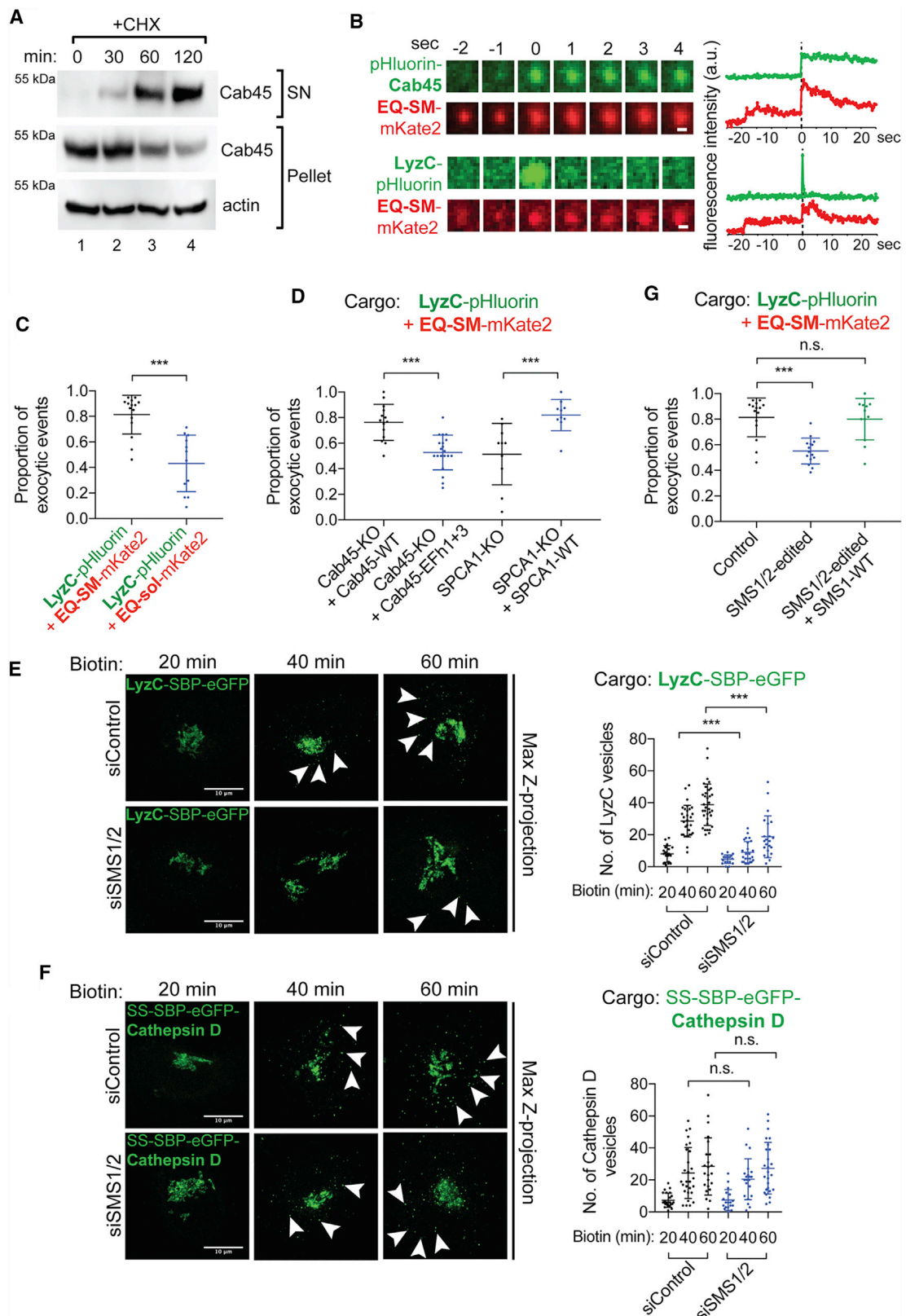
### SPCA1 Associates with Sphingolipid in TGN Membrane

The  $\text{Ca}^{2+}$  pump activity of SPCA1 maintains  $\text{Ca}^{2+}$  in the lumen of the TGN (Lissandron et al., 2010). Curiously, SPCA1 is reported to purify with detergent-resistant membrane (Baron et al., 2010) and its optimal activity in reconstituted liposomes requires the presence of SM (Chen et al., 2017), leading us to hypothesize that SPCA1 may provide a mechanistic link between the SM biosynthetic pathway and Cab45-mediated sorting and secretion. Accordingly, we asked if SPCA1 resides in a Golgi compartment where SM is produced. Two observations indicate that this is the case. First, endogenous SMS1 and SPCA1 partially co-localize in the TGN (Figure 5A). This was determined by comparing the localization of an endogenously expressed SNAP-tagged SMS1 fusion protein generated by genome editing to that of endogenous SPCA1, which was detected by indirect immunofluorescence. Quantitation of co-localization with an endogenous TGN protein, p230, indicates that both SMS1 localizes predominantly to the TGN, while SPCA1 localizes to multiple Golgi compartments (Figure 5A; Table S2).

Co-localization of SMS1 and SPCA1 implies that SPCA1 resides in SM-rich membrane. We tested this first by directly visualizing SPCA1 and sphingolipids (Figure 5A). To visualize sphingolipids in situ, we utilized a modified sphingolipid metabolic precursor, pac-sphingosine (pacSph), that contains a “clickable” chemical bond that can be derivatized with a fluorescent moiety (Haberkant et al., 2016). A gene-edited HeLa cell line lacking sphingosine 1-phosphate lyase (encoded by *SGPL1*) was used for these experiments to restrict metabolism of pacSph to the sphingolipid pathway (Gerl et al., 2016; Haberkant et al., 2016). In pilot experiments, a pulse-chase protocol was established, which resulted in prominent localization of pacSph to the Golgi apparatus (Figure S4A). In the time frame of these experiments (30 min pulse, 60 min chase), pacSph is incorporated into ceramide and SM, but not other sphingolipids (Gerl et al., 2016; Haberkant et al., 2016). Importantly, Golgi localization is prevented by inhibition of ceramide synthase with fumonisins B1, indicating that incorporation of pacSph into Golgi membrane requires its conversion to ceramide (Figure S4B). These results

(D) Export of Cathepsin D from the Golgi is unaffected by Cab45 gene silencing. The SS-SBP-eGFP-Cathepsin D fusion protein was released from the ER of Cab45 siRNA-silenced or control cells by addition of biotin. The mean number of post-Golgi vesicles per cell (>39 cells per condition,  $\pm$  SD) are plotted from 3 independent experiments as a function of time. Vesicle counts for Cab45 siRNA and control siRNA cell populations are not statistically significant.

(E)  $\text{Ca}^{2+}$  binding by EFh modules 1 and 3 is required for efficient export of LyzC from the Golgi apparatus. Cells were depleted of endogenous Cab45 by siRNA, and siRNA-insensitive Cab45 cDNAs with mutations in each of the EF hand modules were expressed. The number of cytoplasmic vesicles containing LyzC-SBP-eGFP per cell was determined after release of LyzC-SBP-eGFP from the ER. Only the data for EFh2 and EFh1+3 are shown in this figure; additional data are shown in Figure S1. The mean vesicle counts from at least 38 cells per condition ( $\pm$  SD) are plotted.



(legend on next page)

demonstrate that SPCA1 and pacSph-labeled sphingolipids co-localize at the TGN (Figure 5A).

To directly examine if SPCA1 and sphingolipids are associated in the Golgi, we took advantage of a diazirine ring incorporated into the fatty acyl chain of pacSph that can mediate lipid-protein crosslinking upon exposure to ultraviolet (UV) light (Gerl et al., 2016; Haberkant et al., 2016). After pulse labeling the Golgi of oxGFP-SPCA1-expressing cells with pacSph, the cells were exposed to UV light and solubilized with detergent, and oxGFP-SPCA1 was immunopurified (Figures 5B and 5C). To determine if pacSph crosslinked to SPCA1, the purified material was subjected to click-mediated biotinylation of pacSph and crosslinked lipid was detected using streptavidin. The results show that UV exposure elicits crosslinking of pacSph to SPCA1. Importantly, inhibition of ceramide synthase with fumonisins B1 substantially eliminates crosslinking (Figure 5D), indicating that SPCA1 is intimately associated with a complex sphingolipid, likely SM.

### Golgi Ca<sup>2+</sup> Homeostasis Is Perturbed by SM Depletion

Published results indicate that optimal activity of recombinant SPCA1 requires SM in its resident membrane (Chen et al., 2017). To determine if *in vivo* SPCA1 activity is influenced by a reduction in SM in the TGN membrane, we monitored Ca<sup>2+</sup> influx into Golgi compartments of control and SM-depleted (i.e., SMS1/2 siRNA) cells using an established TGN-localized fluorescence resonance energy transfer (FRET)-based Ca<sup>2+</sup> sensor (Go-D1cpv) (von Blume et al., 2011; Kienzle et al., 2014; Lissandron et al., 2010). Cells were depleted of Ca<sup>2+</sup> using ionomycin, and then Ca<sup>2+</sup> was added and Go-D1cpv FRET signals were recorded. Fluorescence signals reflecting TGN [Ca<sup>2+</sup>] were normalized to  $\Delta R/R_0$ , where  $\Delta R$  is the change in the ratio of YFP/CFP emission intensity at any time, and  $R_0$  is the value obtained before the addition of 2.2 mM Ca<sup>2+</sup> at the first frame (Figures 6A and 6B). Upon addition of Ca<sup>2+</sup> (2.2 mM CaCl<sub>2</sub>) to the culture medium, control cells showed a 47.19% ± 7.34% increase in FRET signal. Depletion of SPCA1 by siRNA resulted in a reduced rate of calcium influx and a reduction of the maximal FRET value

to 31.93% ± 5.38% (Figures 6B and 6C). In SMS1/2 siRNA-depleted cells, the rate of Ca<sup>2+</sup> influx and maximal FRET value was reduced to 36.99% ± 5.44%. Re-expression of Golgi localized SM synthase 1 in SMS1/2-depleted cells not only restored the rate of Ca<sup>2+</sup> influx but also resulted in a modest (7.74% FRET signal), reproducible increase in maximal FRET value to 54.93% ± 10.62%. In addition, ectopic overexpression of SPCA1 in SMS1/2-depleted cells restored Ca<sup>2+</sup> influx to control levels (Figures 6B and 6C), though it did not alter Ca<sup>2+</sup> influx in control cells (Figures S5A and S5B). The results show that depletion of SM impairs the TGN Ca<sup>2+</sup> uptake mediated by SPCA1.

Rescue of Ca<sup>2+</sup> influx in the Golgi of SMS1/2-depleted cells by overexpression of SPCA1 led us to determine if overexpression of SPCA1 impacts the deficiencies in cargo sorting and secretion of SM-depleted cells. We first monitored the number of Golgi-derived LyzC-containing vesicles in SMS1/2-depleted cells expressing either SPCA1 or as control, SMS1, using RUSH assays (Figure 6D). Whereas 40 and 60 min after release of LyzC-SBP-eGFP from the ER, cytoplasmic vesicle counts were significantly decreased in SMS1/2-depleted compared to control siRNA cells, they were rescued to the control level by overexpression of SPCA1 (Figure 6D). Importantly, expression of siRNA-resistant SMS1 also rescues Golgi export of LyzC in these cells, demonstrating that synthesis of SM in the TGN sustains secretory cargo export from the TGN. TIRFM-based exocytosis assays (Figure 6E) to evaluate co-sorting of LyzC-pHluorin and EQ-SM-mKate2 into exocytic vesicles in SMS1/2-edited cells showed that overexpression of SPCA1, but not SPCA1-D350A, a mutant defective in Ca<sup>2+</sup> transport (Dode et al., 2005; Sorin et al., 1997), rescued cargo sorting into secretory vesicles. These results demonstrate that depletion of SM selectively impairs LyzC cargo sorting through reduced activity of SPCA1, impacting TGN Ca<sup>2+</sup> homeostasis.

## DISCUSSION

Mechanisms for sorting and packaging soluble cargo proteins into transport vesicles within the secretory pathway typically

### Figure 4. Cab45, LyzC, and EQ-SM Are Exocytosed via the Same Vesicles in a Sphingomyelin Synthesis-Dependent Manner

(A) Cell culture supernatants and whole cell lysates of HeLa cells were collected after 0, 30, 60, and 120 min incubation with cycloheximide (CHX) and probed for Cab45 by immunoblotting.

(B) Time-lapse gallery of Cab45, LyzC, and EQ-SM exocytosis. Galleries show example exocytic events of pHluorin-Cab45 or LyzC, and EQ-SM-mKate2 captured by TIRFM. The corresponding graphs show the summed fluorescence intensities for each frame in each channel over time.

(C) LyzC is co-sorted with EQ-SM, but not EQ-sol, into exocytic vesicles. The mean proportions of exocytic events observed in 3 independent experiments (± SD) where LyzC-pHluorin containing vesicles also released mKate2-tagged EQ-SM or EQ-sol are indicated (362 events/15 cells for LyzC+EQ-SM and 268 events/12 cells for LyzC+EQ-sol).

(D) Cab45 EFh1 and EFh3 and SPCA1 are required for the co-sorting of LyzC and EQ-SM. Genome-edited Cab45 null cells expressed Cab45-WT or Cab45-EFh1+3-mut by transfection or genome-edited SPCA1 null cells that expressed or did not express SPCA1-WT by transfection. The cargo loads of exocytic vesicles were determined as described for (B). The means (± SD) are shown for n = 239 events/14 cells for Cab45-WT, n = 128 events/10 cells for Cab45-EFh1+3, n = 163 events/10 cells for SPCA1-KO, and n = 157 events/10 cells for SPCA1-WT.

(E) Depletion of sphingomyelin synthases (SMS1 and SMS2) delays export of LyzC-SBP-eGFP from the Golgi apparatus. HeLa cells were transfected with siRNAs targeting SMS1 and SMS2 or non-targeted control for 2 days prior to transfection with a plasmid that directs expression of LyzC-SBP-eGFP and the streptavidin-KDEL "anchor." The number of cytoplasmic vesicles per cell was determined at the indicated time points after release of LyzC-SBP-eGFP from the ER by addition of biotin. Arrowheads point to cytoplasmic vesicles. Bars, 10 μm. Vesicle counts (mean ± SD) from at least 18 cells per condition in 3 independent experiments are plotted in the graph on the right.

(F) Depletion of SMS1 and SMS2 does not delay export of SS-SBP-eGFP-Cathepsin D vesicles from the Golgi apparatus. Arrowheads point to cytoplasmic vesicles. Assays were conducted as in (A). Bars, 10 μm. Vesicle counts from at least 18 cells per condition in 3 independent experiments are plotted (mean ± SD).

(G) TIRF microscopy-based sorting assays were used to determine the proportion of LyzC-pHluorin exocytic vesicles that also contained EQ-SM-mKate2 (mean ± SD) in genome-edited HeLa cells (SMS1/2-edited) that express SMS1 and SMS2 at reduced levels.

See also Figure S3.

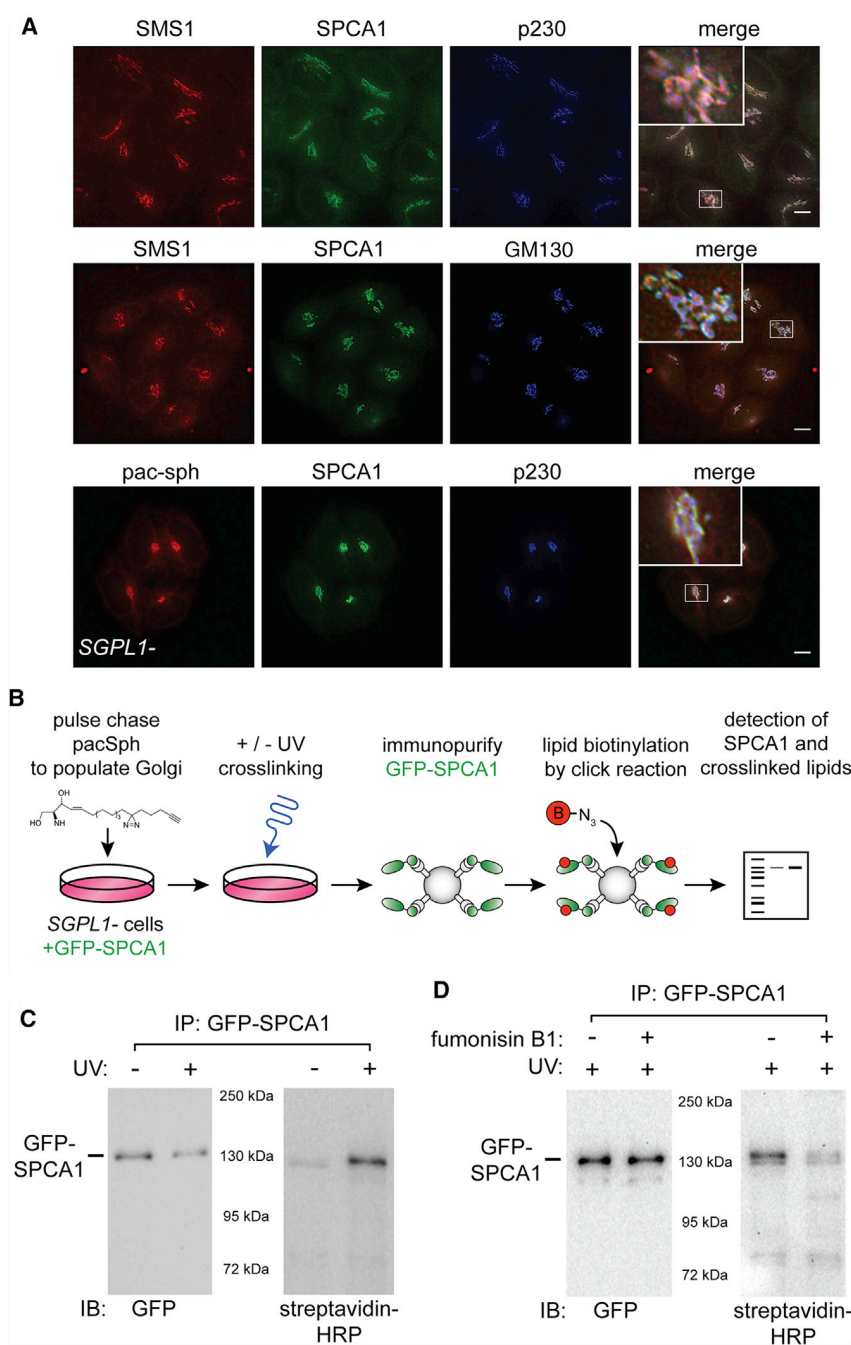


**Figure 5. SPCA1 Associates with Sphingolipid in Golgi Membrane**

(A) SMS1, SPCA1, and pacSph localize to the TGN. Antisera to SPCA1, p230 (TGN), or GM130 (*cis* Golgi) were used to detect each protein by immunofluorescence microscopy in gene-edited HeLa cells. To detect endogenous SMS1, an SMS1-SNAP tag fusion protein (constructed by genome editing) was labeled with SNAP-Cell 647-SiR. To visualize sphingolipids in situ, sphingosine-1-phosphate lyase deficient (*SGPL1*<sup>-</sup>) HeLa cells were pulse labeled with 0.6 μM pacSph for 30 min, followed by a chase period of 1 hr. Fixed, permeabilized cells were incubated with click chemistry reagents to covalently attach an Alexa647 fluorophore to pacSph. Cells were visualized by deconvolution fluorescence microscopy. Quantitative evaluation of co-localization was accomplished by determining Pearson's correlation coefficients (Table S2). Scale bars, 10 μm. Insets in the merged images show a higher magnification view of the Golgi region.

(B) Schematic diagram of protocol used to test for UV-induced crosslinking of SPCA1 and pacSph.

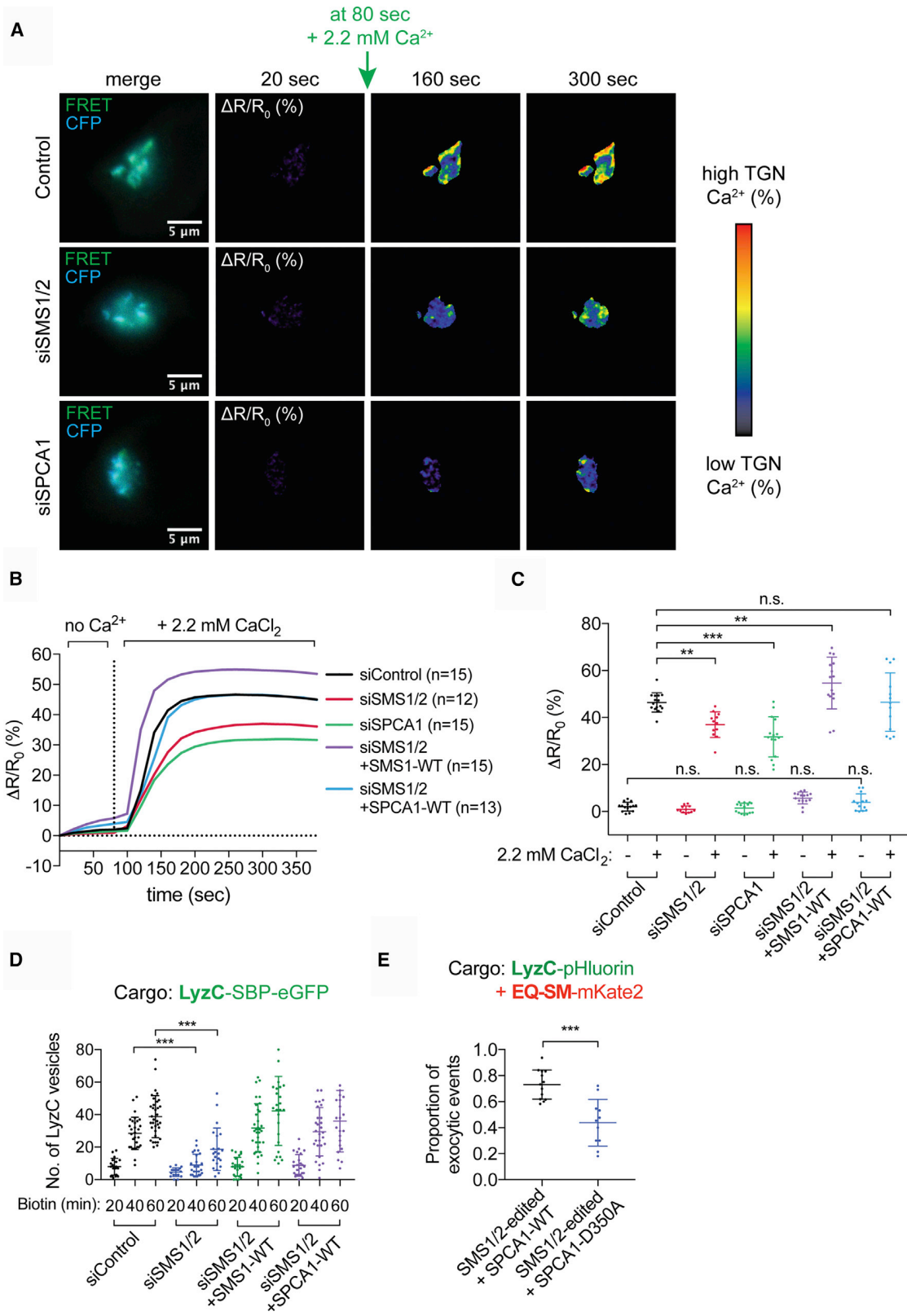
(C) SPCA1 and pacSph can be crosslinked. The left panel is an anti-GFP immunoblot showing GFP-SPCA1 that was immunopurified from the UV treated and untreated samples. In the right-hand blot, the same samples were probed with streptavidin-HRP to detect pacSph crosslinked to SPCA1.

(D) An inhibitor of ceramide synthase, fumonisins B1, prevents crosslinking of SPCA1 and pacSph. Cells were incubated with fumonisins B1 (50 μM) for 24 hr prior to initiating the pulse labeling with pacSph. The left- and right-hand blots were processed as in (C).

See also Figure S4 and Table S2.

involve transmembrane sorting receptors that contain a luminal domain that recognizes the cargo protein and a cytoplasmic domain capable of eliciting the recruitment of coat proteins that effect vesicle budding. At the TGN, this is best exemplified by the cation-independent mannose phosphate receptor that recognizes soluble lysosomal pro-enzymes decorated with mannose 6-phosphate and elicits their packaging into clathrin-coated vesicles that mediate TGN-to-endosome trafficking (Kornfeld and Mellman, 1989). Sorting of soluble secreted proteins, however, is far less well understood, especially in recognition of their structural diversity and lack of iden-

tified sorting motifs that might be recognized by an integral membrane sorting receptor. One class of soluble secreted proteins relies on Cab45 for efficient secretion (von Blume et al., 2012; Kienzle et al., 2014), and data presented here indicate that secretion of Cab45 and Cab45 clients is mediated by a Golgi-derived carrier whose membrane is enriched in SM. In support of this conclusion, a subset of vesicles that emerge from the TGN contain Cab45 and the SM-binding protein, EQ-SM. Importantly, a similar proportion of vesicles contain LyzC and EQ-SM, confirming that these proteins are co-sorted in the Golgi into a common secretory carrier of the SMS pathway. Depletion or deletion of Cab45, SPCA1, or SMS1/2 all result in an accumulation of LyzC in the Golgi, though it is eventually exported from the TGN and secreted via vesicles that are not enriched with EQ-SM. Under these conditions, LyzC is secreted via vesicles that also contain a bulk secretion marker, EQ-sol, leading us to speculate that secretion by this alternative pathway is via non-specific, bulk flow secretion. Under control of SPCA1, Cab45 mediates a



(legend on next page)

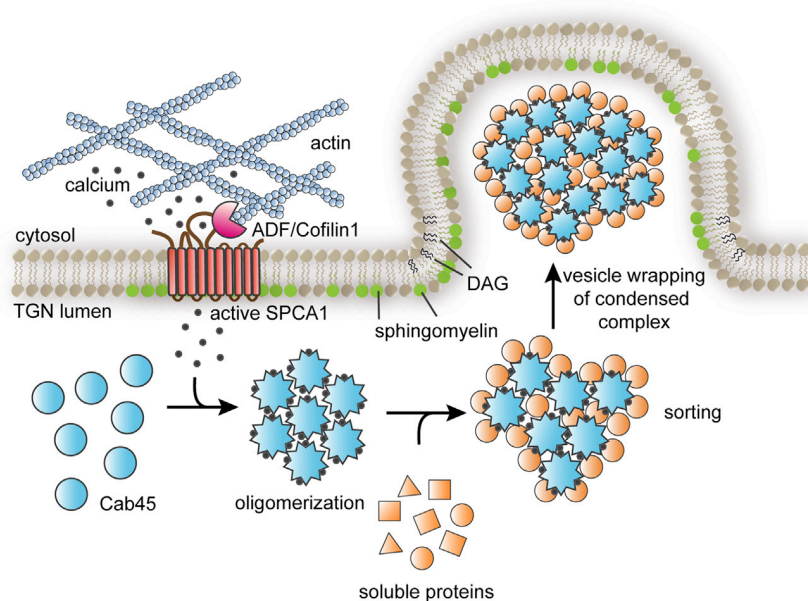


**Figure 7. SPCA1 Links Sphingomyelin Synthesis to  $\text{Ca}^{2+}$ -Dependent Secretory Protein and Lipid Sorting in the TGN**

The model depicts the events leading to the sorting and export of secretory cargo from the TGN, where the convergence of sphingomyelin synthesis and  $\text{Ca}^{2+}$  import into the lumen of the TGN drives the formation of a secretory carrier enriched in Cab45-client complexes. Secretory cargo sorting is initiated by SPCA1-mediated  $\text{Ca}^{2+}$  influx, which is triggered by binding of ADF/cofilin1 to SPCA1 in the cytoplasm, where F-actin is associated with the TGN membrane. Synthesis of sphingomyelin in the TGN membrane potentiates SPCA1-mediated  $\text{Ca}^{2+}$  pumping in a region of the TGN membrane enriched in sphingomyelin. The local elevation of luminal  $\text{Ca}^{2+}$  drives oligomerization of Cab45, which binds to soluble secretory protein clients, condensing them from the bulk milieu. The second product of SM synthesis, diacylglycerol (DAG), promotes engulfment of Cab45-client complexes by generating negative membrane curvature, leading to the formation of a secretory carrier enriched in oligomeric Cab45-client complexes.

concentrative sorting step that increases the rate of secretion of its clients above that of bulk flow.

Prior work has shown that SPCA1-mediated influx of  $\text{Ca}^{2+}$  into the TGN is stimulated by recruitment of F-actin via cofilin1 to the P-domain of SPCA1 (Kienzle et al., 2014), and this study demonstrates that SM potentiates SPCA1-mediated  $\text{Ca}^{2+}$  influx (Figure 6). Binding of calcium causes Cab45 to undergo  $\text{Ca}^{2+}$ -dependent oligomerization and secretory client recognition (Crevenna et al., 2016). We find that SPCA1, SMS1, and sphingolipids populate the TGN and that SPCA1  $\text{Ca}^{2+}$  pumping activity is promoted by maintenance of a physiologic level of SM in the TGN. At present, the mechanism by which SM-rich membrane facilitates SPCA1-mediated calcium pumping is unknown. Specific interactions between SM and the paddle domain of PM voltage-gated  $\text{K}^+$  channels are critical for voltage sensing (Combs et al., 2013; Milescu et al., 2009; Ramu et al., 2006; Xu et al., 2008), and it may be that SM acts as an agonist by binding to a site(s) on SPCA1 to activate  $\text{Ca}^{2+}$  pumping. Consistent with this, a systematic survey of SPCA1 activity in reconstituted proteoliposomes of differing lipid composition showed that SPCA1

activity is highest in vesicles containing SM (Chen et al., 2017). Local hotspots of SPCA1 activity, linked to synthesis and local enrichment of SM within the TGN membrane, will define TGN sorting domains and cargo exit sites.

How is Cab45-mediated client sorting linked to the formation of a secretory carrier? Our findings suggest that a local increase in  $\text{Ca}^{2+}$  concentration within the lumen of the TGN drives Cab45 oligomerization and client capture through Cab45-client condensation from the bulk milieu (Figure 7). Within the lumen of the TGN, Cab45 is concentrated within discrete regions that we speculate are sites of Cab45-mediated sorting and carrier formation (Crevenna et al., 2016). Surprisingly, we observed that sorting of LyzC into the SMS pathway is largely ablated by a modest (31%) decrease in cellular SM. This leads us to suggest that carrier formation is coupled to local SM synthesis by SMS1, which maintains a supply of membrane to sustain carrier formation at and budding from the TGN. Synthesis of SM produces an equivalent amount of DAG, a lipid that promotes negative membrane curvature of a bilayer, shown to be necessary for the formation and fission of a subset of secretory carriers from the

**Figure 6. SM Depletion Inhibits  $\text{Ca}^{2+}$  Influx into the TGN**

(A) Example time-lapse images of Golgi  $\text{Ca}^{2+}$  influx assays in control, siRNA SMS1/2, or SPCA1-depleted HeLa cells expressing the Go-D1-cpv Golgi  $\text{Ca}^{2+}$  sensor. Fluorescence micrographs of the FRET sensor in the TGN are shown in the left column. Cells were incubated with ionomycin to deplete  $\text{Ca}^{2+}$  from the lumen of the TGN, and then live-cell ratiometric FRET microscopy was used to monitor  $\text{Ca}^{2+}$  influx by measuring the  $\Delta\text{R}/\text{R}_0$  FRET ratio of YFP/CFP channels over time after addition of 2.2 mM  $\text{CaCl}_2$  to the cell medium, where  $\text{R}_0$  is the FRET ratio value obtained before addition of 2.2 mM  $\text{CaCl}_2$  (20 s time point). The color-coded  $\Delta\text{R}/\text{R}_0$  heatmap scale is shown on the right. Images are shown for representative cells 160 and 300 s after addition of  $\text{CaCl}_2$  at 80 s. Scale bars, 5  $\mu\text{m}$ . (B) Quantification of FRET images shown in (A), as well as that of siRNA-treated cells expressing siRNA-insensitive SMS1 or SPCA1 cDNAs. Fluorescence signals reflecting TGN  $[\text{Ca}^{2+}]$  are presented as  $\Delta\text{R}/\text{R}_0$ . Data are plotted as the mean  $\text{Ca}^{2+}$  influx over time. Data were acquired for at least 12 cells per condition in 2 independent experiments. (C) Data shown in (B) are plotted as the mean  $\pm$  SD  $\text{Ca}^{2+}$  influx before  $\text{Ca}^{2+}$  addition (at 80 s) or after  $\text{Ca}^{2+}$  addition (at 300 s). Data were acquired for at least 12 cells per condition in 2 independent experiments. (D) The number of LyzC vesicles was quantified in HeLa control or SMS1/2 siRNA-depleted cells expressing either LyzC-SBP-eGFP alone or co-transfected with SMS1-WT or SPCA1-WT. Mean vesicle counts  $\pm$  SD from at least 18 cells per condition in 3 independent experiments are plotted. (E) TIRF microscopy-based sorting assays were used to determine the proportion of LyzC-pHluorin exocytic vesicles that also contained EQ-SM-mKate2 in SMS1/2-edited cells that express either SPCA1-WT or SPCA1-D350A, a mutant that has no  $\text{Ca}^{2+}$  influx activity (means  $\pm$  SD in 3 independent experiments; total of 201 events/13 cells for SPCA1-WT; total of 144 events/11 cells for SPCA1-D350A). See also Figure S5.

TGN (Baron and Malhotra, 2002; Campelo and Malhotra, 2012; Litvak et al., 2005; Sarri et al., 2011). We speculate that chemical and physical coupling of SM synthesis, DAG production, Ca<sup>2+</sup> influx, and capture of secretory cargo by Cab45 promotes engulfment of oligomeric Cab45-client complexes by TGN membrane, leading to vesicle budding (Figure 7). As no integral membrane receptor(s) for Cab45 clients has been identified, we suggest the formation of secretory carriers of the SMS pathway carrying Cab45-client complexes resembles that of zymogen granule formation in pancreatic acinar cells, where the enzymes are proposed to form a “submembrane matrix” that deforms the membrane to induce budding of a secretory granule from the TGN (Dartsch et al., 1998; Schmidt et al., 2000). Thus, a common mechanism may be employed for the formation of secretory carriers containing different pools of proteins destined for secretion.

New questions regarding spatiotemporal coupling of the events that lead to cargo capture and sorting in the SMS pathway are raised by the findings presented here. A critical issue regards how secretory load is sensed and coupled to SPCA1-mediated Ca<sup>2+</sup> influx, which is stimulated by ADF/Cofilin and F-actin in the cytoplasm. Related to this is the synthesis of SM in the Golgi, which is promoted by non-vesicular transport of ceramide and cholesterol (Ngo and Ridgway, 2009; Parmar and Duncan, 2016; Wakana et al., 2015) at ER-TGN contact sites, so it is of interest to determine if the formation of carriers of the SMS pathway are chemically and physically coupled to the non-vesicular ceramide transport machinery. Intriguingly, siRNA-mediated depletion of components of the non-vesicular ER-to-TGN transport machinery perturbs glycosylation of secretory cargo in the Golgi and slows the rate of secretion (Wakana et al., 2015). Finally, the mechanism by which, and location where, Cab45-client complexes are dissociated, and if Cab45 is then retrieved to the TGN for re-use will be essential to elucidate. The conceptual framework that emerges from our findings, along with new methods developed, present new opportunities for understanding the core function of the Golgi apparatus as a macromolecular trafficking hub within the cell.

## STAR★METHODS

Detailed methods are provided in the online version of this paper and include the following:

- [KEY RESOURCES TABLE](#)
- [CONTACT FOR REAGENT AND RESOURCE SHARING](#)
- [EXPERIMENTAL MODEL AND SUBJECT DETAILS](#)
- [METHOD DETAILS](#)
  - DNA Manipulations
  - Antisera
  - Cell Culture and Engineering
  - siRNA Silencing
  - Vesicle Budding and APEX2-Mediated Biotinylation
  - Protein Detection by Immunoblotting, Silver Staining, or Immunofluorescence
  - Lipidomics
  - Fluorescence Microscopy and Image Analysis
  - RUSH Cargo Sorting Assay Using Confocal Microscopy

- RUSH Cargo Sorting Assay Using Western Blot Analysis
- *In Vivo* Golgi Vesicle Budding Assays
- Pac-Sphingosine Labeling
- Pac-Sphingosine Crosslinking
- Ca<sup>2+</sup> Influx Assay
- Quantitative Real-Time PCR
- Purification of Recombinant Proteins and Labeling
- Cab45 Oligomerization Assay
- Circular Dichroism Spectroscopy

## ● [QUANTIFICATION AND STATISTICAL ANALYSIS](#)

## SUPPLEMENTAL INFORMATION

Supplemental Information includes five figures and three tables and can be found with this article online at <https://doi.org/10.1016/j.devcel.2018.10.012>.

## ACKNOWLEDGMENTS

We are grateful to Andreas Ernst for advice with pacSph labeling, Michael Caplan and Zhe Lu for assistance interpreting the Ca<sup>2+</sup> influx assays, Peter Vangheluwe for SPCA1 antiserum, and Franck Perez for RUSH plasmids. Research reported in this publication was supported by the following sources: the National Institute of General Medical Sciences of the United States National Institutes of Health under award numbers GM095766 and GM060221 to C.G.B., award number T32GM007223 to E.L.S.; the “Plus3” Perspective Program (Boehringer Ingelheim Foundation), CRC914 (TP A09); a project grant (BL 1186/4-1) from the Deutsche Forschungsgemeinschaft (DFG) to J.v.B.; and the Max Planck Institute of Biochemistry and by the department led by Reinhard Fässler. Proteomic analyses were provided by the W.M. Keck Foundation Biotechnology Resource Laboratory at Yale University. Lipidomic analyses were provided by the Virginia Commonwealth University (VCU) Lipidomics/Metabolomics Core, which is supported by the NIH-NCI Cancer Center Support Grant P30 CA016059 to the VCU Massey Cancer Center, as well as a shared resource grant (S10RR031535) from the US National Institutes of Health.

## AUTHOR CONTRIBUTIONS

Conceptualization, C.G.B. and J.v.B.; Methodology, Y.D., M.P., C.G.B., and J.v.B.; Investigation, Y.D., M.P., B.B., E.L.S., and J.v.B.; Writing – Original Draft, C.G.B. and M.P.; Writing – Review & Editing, Y.D., M.P., B.B., E.L.S., C.G.B., and J.v.B.; Funding Acquisition, C.G.B. and J.v.B.; Resources, C.G.B. and J.v.B.; Supervision, C.G.B. and J.v.B.

## DECLARATION OF INTERESTS

The authors declare no competing interests.

Received: May 16, 2018

Revised: August 29, 2018

Accepted: October 5, 2018

Published: November 1, 2018

## REFERENCES

- Ang, S.F., and Fölsch, H. (2012). The role of secretory and endocytic pathways in the maintenance of cell polarity. *Essays Biochem.* 53, 29–39.
- Anitei, M., and Hoflack, B. (2011). Exit from the trans-Golgi network: from molecules to mechanisms. *Curr. Opin. Cell Biol.* 23, 443–451.
- Barenholz, Y., and Thompson, T.E. (1980). Sphingomyelins in bilayers and biological membranes. *Biochim. Biophys. Acta* 604, 129–158.
- Baron, C.L., and Malhotra, V. (2002). Role of diacylglycerol in PKD recruitment to the TGN and protein transport to the plasma membrane. *Science* 295, 325–328.

- Baron, S., Vangheluwe, P., Sepúlveda, M.R., Wuytack, F., Raeymaekers, L., and Vanoevelen, J. (2010). The secretory pathway Ca<sup>2+</sup>-ATPase 1 is associated with cholesterol-rich microdomains of human colon adenocarcinoma cells. *Biochim. Biophys. Acta* 1798, 1512–1521.
- Blank, B., and von Blume, J. (2017). Cab45-Unraveling key features of a novel secretory cargo sorter at the trans-Golgi network. *Eur. J. Cell Biol.* 96, 383–390.
- von Blume, J., Alleaume, A.M., Cantero-Recasens, G., Curwin, A., Carreras-Sureda, A., Zimmermann, T., van Galen, J., Wakana, Y., Valverde, M.A., and Malhotra, V. (2011). ADF/cofilin regulates secretory cargo sorting at the TGN via the Ca<sup>2+</sup> ATPase SPCA1. *Dev. Cell* 20, 652–662.
- von Blume, J., Alleaume, A.M., Kienzle, C., Carreras-Sureda, A., Valverde, M., and Malhotra, V. (2012). Cab45 is required for Ca<sup>2+</sup>-dependent secretory cargo sorting at the trans-Golgi network. *J. Cell Biol.* 199, 1057–1066.
- Boncompain, G., Divoux, S., Gareil, N., de Forges, H., Lescure, A., Latreche, L., Mercanti, V., Jollivet, F., Raposo, G., and Perez, F. (2012). Synchronization of secretory protein traffic in populations of cells. *Nat. Methods* 9, 493–498.
- Bonifacino, J.S. (2014). Adaptor proteins involved in polarized sorting. *J. Cell Biol.* 204, 7–17.
- Campelo, F., and Malhotra, V. (2012). Membrane fission: the biogenesis of transport carriers. *Annu. Rev. Biochem.* 81, 407–427.
- Campelo, F., van Galen, J., Turacchio, G., Parashuraman, S., Kozlov, M.M., García-Parajo, M.F., and Malhotra, V. (2017). Sphingomyelin metabolism controls the shape and function of the Golgi cisternae. *ELife* 6.
- Capasso, S., Sticco, L., Rizzo, R., Pirozzi, M., Russo, D., Dathan, N.A., Campelo, F., van Galen, J., Hölttä-Vuori, M., Turacchio, G., et al. (2017). Sphingolipid metabolic flow controls phosphoinositide turnover at the trans-Golgi network. *EMBO J.* 36, 1736–1754.
- Chen, J., De Raeymaecker, J., Hovgaard, J.B., Smaardijk, S., Vandecaetsbeek, I., Wuytack, F., Møller, J.V., Eggermont, J., De Maeyer, M., Christensen, S.B., et al. (2017). Structure/activity relationship of thapsigargin inhibition on the purified Golgi/secretory pathway Ca<sup>2+</sup>/Mn<sup>2+</sup>-transport ATPase (SPCA1a). *J. Biol. Chem.* 292, 6938–6951.
- Combs, D.J., Shin, H.G., Xu, Y., Ramu, Y., and Lu, Z. (2013). Tuning voltage-gated channel activity and cellular excitability with a sphingomyelinase. *J. Gen. Physiol.* 142, 367–380.
- Costantini, L.M., Balaban, M., Markwardt, M.L., Rizzo, M., Guo, F., Verkhusha, V.V., and Snapp, E.L. (2015). A palette of fluorescent proteins optimized for diverse cellular environments. *Nat. Commun.* 6, 7670.
- Crevenna, A.H., Blank, B., Maiser, A., Emin, D., Prescher, J., Beck, G., Kienzle, C., Bartnik, K., Habermann, B., Pakdel, M., et al. (2016). Secretory cargo sorting by Ca<sup>2+</sup>-dependent Cab45 oligomerization at the trans-Golgi network. *J. Cell Biol.* 213, 305–314.
- Dartsch, H., Kleene, R., and Kern, H.F. (1998). In vitro condensation-sorting of enzyme proteins isolated from rat pancreatic acinar cells. *Eur. J. Cell Biol.* 75, 211–222.
- De Matteis, M.A., and Luini, A. (2008). Exiting the Golgi complex. *Nat. Rev. Mol. Cell Biol.* 9, 273–284.
- Deng, Y., Rivera-Molina, F.E., Toomre, D.K., and Burd, C.G. (2016). Sphingomyelin is sorted at the trans Golgi network into a distinct class of secretory vesicle. *Proc. Natl. Acad. Sci. USA* 113, 6677–6682.
- Dode, L., Andersen, J.P., Raeymaekers, L., Missiaen, L., Vilsen, B., and Wuytack, F. (2005). Functional comparison between secretory pathway Ca<sup>2+</sup>/Mn<sup>2+</sup>-ATPase (SPCA) 1 and sarcoplasmic reticulum Ca<sup>2+</sup>-ATPase (SERCA) 1 isoforms by steady-state and transient kinetic analyses. *J. Biol. Chem.* 280, 39124–39134.
- Duran, J.M., Campelo, F., van Galen, J., Sachsenheimer, T., Sot, J., Egorov, M.V., Rentero, C., Enrich, C., Polishchuk, R.S., Goñi, F.M., et al. (2012). Sphingomyelin organization is required for vesicle biogenesis at the Golgi complex. *EMBO J.* 31, 4535–4546.
- Fölsch, H., Pypaert, M., Maday, S., Pelletier, L., and Mellman, I. (2003). The AP-1A and AP-1B clathrin adaptor complexes define biochemically and functionally distinct membrane domains. *J. Cell Biol.* 163, 351–362.
- Gerl, M.J., Bittl, V., Kirchner, S., Sachsenheimer, T., Brunner, H.L., Luchtenborg, C., Özbalci, C., Wiedemann, H., Wegehangel, S., Nickel, W., et al. (2016). Sphingosine-1-phosphate lyase deficient cells as a tool to study protein lipid interactions. *PLoS One* 11, e0153009.
- Gibson, D.G. (2009). Synthesis of DNA fragments in yeast by one-step assembly of overlapping oligonucleotides. *Nucleic Acids Res.* 37, 6984–6990.
- Haberkant, P., Stein, F., Höglinger, D., Gerl, M.J., Brügger, B., Van Veldhoven, P.P., Krijgsvelde, J., Gavin, A.C., and Schultz, C. (2016). Bifunctional sphingosine for cell-based analysis of protein-sphingolipid interactions. *ACS Chem. Biol.* 11, 222–230.
- Hung, V., Udeshi, N.D., Lam, S.S., Loh, K.H., Cox, K.J., Pedram, K., Carr, S.A., and Ting, A.Y. (2016). Spatially resolved proteomic mapping in living cells with the engineered peroxidase APEX2. *Nat. Protoc.* 11, 456–475.
- Huttner, W.B., and Tooze, S.A. (1989). Biosynthetic protein transport in the secretory pathway. *Curr. Opin. Cell Biol.* 1, 648–654.
- Kardash, E., Bandemer, J., and Raz, E. (2011). Imaging protein activity in live embryos using fluorescence resonance energy transfer biosensors. *Nat. Protoc.* 6, 1835–1846.
- Kienzle, C., Basnet, N., Crevenna, A.H., Beck, G., Habermann, B., Mizuno, N., and von Blume, J. (2014). Cofilin recruits F-actin to SPCA1 and promotes Ca<sup>2+</sup>-mediated secretory cargo sorting. *J. Cell Biol.* 206, 635–654.
- Kienzle, C., and von Blume, J. (2014). Secretory cargo sorting at the trans-Golgi network. *Trends Cell Biol.* 24, 584–593.
- Kornfeld, S., and Mellman, I. (1989). The biogenesis of lysosomes. *Annu. Rev. Cell Biol.* 5, 483–525.
- Lam, S.S., Martell, J.D., Kamer, K.J., Deerinck, T.J., Ellisman, M.H., Mootha, V.K., and Ting, A.Y. (2014). Directed evolution of APEX2 for electron microscopy and proximity labeling. *Nat. Methods* 12, 51.
- Lissandron, V., Podini, P., Pizzo, P., and Pozzan, T. (2010). Unique characteristics of Ca<sup>2+</sup> homeostasis of the trans-Golgi compartment. *Proc. Natl. Acad. Sci. USA* 107, 9198–9203.
- Litvak, V., Dahan, N., Ramachandran, S., Sabanay, H., and Lev, S. (2005). Maintenance of the diacylglycerol level in the Golgi apparatus by the Nir2 protein is critical for Golgi secretory function. *Nat. Cell Biol.* 7, 225–234.
- Milescu, M., Bosmans, F., Lee, S., Alabi, A.A., Kim, J.I., and Swartz, K.J. (2009). Interactions between lipids and voltage sensor paddles detected with tarantula toxins. *Nat. Struct. Mol. Biol.* 16, 1080–1085.
- Molinete, M., Irminger, J.C., Tooze, S.A., and Halban, P.A. (2000). Trafficking/sorting and granule biogenesis in the beta-cell. *Semin. Cell Dev. Biol.* 11, 243–251.
- Ngo, M., and Ridgway, N.D. (2009). Oxysterol binding protein-related Protein 9 (ORP9) is a cholesterol transfer protein that regulates Golgi structure and function. *Mol. Biol. Cell* 20, 1388–1399.
- Pakdel, M., and von Blume, J. (2018). Exploring new routes for secretory protein export from the trans-Golgi network. *Mol. Biol. Cell* 29, 235–240.
- Parmar, H.B., and Duncan, R. (2016). A novel tribasic Golgi export signal directs cargo protein interaction with activated Rab11 and AP-1-dependent Golgi-plasma membrane trafficking. *Mol. Biol. Cell* 27, 1320–1331.
- Pfeffer, S.R., and Rothman, J.E. (1987). Biosynthetic protein transport and sorting by the endoplasmic reticulum and Golgi. *Annu. Rev. Biochem.* 56, 829–852.
- Pfeifer, A., Kessler, T., Silletti, S., Cheresh, D.A., and Verma, I.M. (2000). Suppression of angiogenesis by lentiviral delivery of PEX, a noncatalytic fragment of matrix metalloproteinase 2. *Proc. Natl. Acad. Sci. USA* 97, 12227–12232.
- Ramu, Y., Xu, Y., and Lu, Z. (2006). Enzymatic activation of voltage-gated potassium channels. *Nature* 442, 696–699.
- Ran, F.A., Hsu, P.D., Wright, J., Agarwala, V., Scott, D.A., and Zhang, F. (2013). Genome engineering using the CRISPR-Cas9 system. *Nat. Protoc.* 8, 2281–2308.
- Sarri, E., Sicart, A., Lázaro-Díéguez, F., and Egea, G. (2011). Phospholipid synthesis participates in the regulation of diacylglycerol required for membrane trafficking at the Golgi complex. *J. Biol. Chem.* 286, 28632–28643.

- Scherer, P.E., Lederkremer, G.Z., Williams, S., Fogliano, M., Baldini, G., and Lodish, H.F. (1996). Cab45, a novel (Ca<sup>2+</sup>)-binding protein localized to the Golgi lumen. *J. Cell Biol.* *133*, 257–268.
- Schmidt, K., Dartsch, H., Linder, D., Kern, H.F., and Kleene, R. (2000). A sub-membranous matrix of proteoglycans on zymogen granule membranes is involved in granule formation in rat pancreatic acinar cells. *J. Cell Sci.* *113*, 2233–2242.
- Sorin, A., Rosas, G., and Rao, R. (1997). PMR1, a Ca<sup>2+</sup>-ATPase in yeast Golgi, has properties distinct from sarco/endoplasmic reticulum and plasma membrane calcium pumps. *J. Biol. Chem.* *272*, 9895–9901.
- Subathra, M., Qureshi, A., and Luberto, C. (2011). Sphingomyelin synthases regulate protein trafficking and secretion. *PLoS One* *6*, e23644.
- Tafesse, F.G., Sanyal, S., Ashour, J., Guimaraes, C.P., Hermansson, M., Somerharju, P., and Ploegh, H.L. (2013). Intact sphingomyelin biosynthetic pathway is essential for intracellular transport of influenza virus glycoproteins. *Proc. Natl. Acad. Sci. USA* *110*, 6406–6411.
- Tooze, S.A., Flatmark, T., Tooze, J., and Huttner, W.B. (1991). Characterization of the immature secretory granule, an intermediate in granule biogenesis. *J. Cell Biol.* *115*, 1491–1503.
- Tooze, S.A., and Huttner, W.B. (1990). Cell-free protein sorting to the regulated and constitutive secretory pathways. *Cell* *60*, 837–847.
- van Galen, J., Campelo, F., Martínez-Alonso, E., Scarpa, M., Martínez-Menárguez, J.Á., and Malhotra, V. (2014). Sphingomyelin homeostasis is required to form functional enzymatic domains at the trans-Golgi network. *J. Cell Biol.* *206*, 609–618.
- van Meer, G., Voelker, D.R., and Feigenson, G.W. (2008). Membrane lipids: where they are and how they behave. *Nat. Rev. Mol. Cell Biol.* *9*, 112–124.
- Wakana, Y., Kotake, R., Oyama, N., Murate, M., Kobayashi, T., Arasaki, K., Inoue, H., and Tagaya, M. (2015). CARTS biogenesis requires VAP-lipid transfer protein complexes functioning at the endoplasmic reticulum-Golgi interface. *Mol. Biol. Cell* *26*, 4686–4699.
- Wakana, Y., van Galen, J., Meissner, F., Scarpa, M., Polishchuk, R.S., Mann, M., and Malhotra, V. (2012). A new class of carriers that transport selective cargo from the trans Golgi network to the cell surface. *EMBO J.* *31*, 3976–3990.
- Xu, Y., Ramu, Y., and Lu, Z. (2008). Removal of phospho-head groups of membrane lipids immobilizes voltage sensors of K<sup>+</sup> channels. *Nature* *451*, 826–829.

## STAR★METHODS

## KEY RESOURCES TABLE

REAGENT or RESOURCE	SOURCE	IDENTIFIER
<b>Antibodies</b>		
Streptavidin-HRP	Thermo Fisher Scientific	Cat# PI-21130
Mouse monoclonal anti-FLAG	Sigma-Aldrich	Cat# F1804; RRID: AB_262044
Rat monoclonal anti-HA	Roche	Cat# 11867423001; RRID: AB_390918
Rabbit monoclonal anti-GaT	Abcam	Cat# ab178406
Mouse monoclonal anti-Calnexin	Millipore	Cat# MAB3126; RRID: AB_2069152
Mouse monoclonal anti-SPCA1	Abnova	Cat# H00027032-M01; RRID: AB_464127
Mouse monoclonal anti-p230	BD Biosciences	Cat# 611281; RRID: AB_398809
Sheep polyclonal anti-TGN46	AbD Serotec	Cat# AHP500G; RRID: AB_323104
Mouse monoclonal anti- $\beta$ -actin	Sigma-Aldrich	Cat# A5441; RRID: AB_476744
Rabbit polyclonal anti-SPCA1	Gift from Peter Vangheluwe, Department of Cellular and Molecular Medicine, University of Leuven, Belgium	N/A
Rabbit polyclonal anti-TGN46	AbD Serotec	Cat# AHP1586; RRID: AB_2303333
Mouse monoclonal anti-GM130	BD Biosciences	Cat# 610823; RRID: AB_398142
Mouse Monoclonal ANTI-FLAG® M2-Peroxidase (HRP)	Sigma-Aldrich	Cat# A8592; RRID: AB_439702
Goat anti-Rabbit IgG (H+L) Highly Cross-Adsorbed Secondary Antibody, Alexa Fluor 488	Thermo Fisher Scientific	Cat# A-11034; RRID: AB_2576217
Goat anti-Rabbit IgG (H+L) Highly Cross-Adsorbed Secondary Antibody, Alexa Fluor 546	Thermo Fisher Scientific	Cat# A-11035; RRID: AB_2534093
Goat anti-Mouse IgG (H+L) Highly Cross-Adsorbed Secondary Antibody, Alexa Fluor 488	Thermo Fisher Scientific	Cat# A-11029; RRID: AB_2534088
Goat anti-Mouse IgG (H+L) Highly Cross-Adsorbed Secondary Antibody, Alexa Fluor 546	Thermo Fisher Scientific	Cat# A-11030; RRID: AB_2534089
Donkey anti-Rat IgG (H+L) Highly Cross-Adsorbed Secondary Antibody, Alexa Fluor 594	Thermo Fisher Scientific	Cat# A-21209; RRID: AB_2535795
Donkey anti-Rat IgG (H+L) Highly Cross-Adsorbed Secondary Antibody, Alexa Fluor 488	Thermo Fisher Scientific	Cat# A-21208; RRID: AB_141709
Donkey anti-Mouse IgG (H+L) Highly Cross-Adsorbed Secondary Antibody, Alexa Fluor 594	Thermo Fisher Scientific	Cat# A-21203; RRID: AB_141633
Goat anti-Rabbit IgG (H+L) Poly-HRP Secondary Antibody, HRP	Thermo Fisher Scientific	Cat# 32260; RRID: AB_1965959
m-IgG $\kappa$ BP-HRP Antibody	Santa Cruz Biotechnology	Cat# sc-516102; RRID: AB_2687626
<b>Bacterial and Virus Strains</b>		
OmniMAX™ 2 T1 <sup>R</sup> <i>E. coli</i>	Thermo Fisher Scientific	Cat# C854003
<b>Chemicals, Peptides, and Recombinant Proteins</b>		
PhotoClick Sphingosine	Avanti	Cat# 900600P
Alexa Fluor™ 647 Azide	Thermo Fisher Scientific	Cat# A10277
Fetal Bovine Serum, charcoal stripped	Thermo Fisher Scientific	Cat# A3382101

(Continued on next page)

**Continued**

REAGENT or RESOURCE	SOURCE	IDENTIFIER
Fetal Bovine Serum, qualified, E.U.-approved, South America origin	Gibco™, Thermo Fisher Scientific	Cat# 10270106
FUMONISIN B1	Sigma-Aldrich	Cat# F1147
d-Biotin	SUPELCO	Cat# 47868
FuGENE® HD Transfection Reagent	Promega	Cat# E2311
Lipofectamine LTX Reagent with PLUS Reagent	ThermoFisher Scientific	Cat# 15338100
Lipofectamine™ 2000 Transfection Reagent	ThermoFisher Scientific	Cat# 11668027
Polyethyleneimine, linear, M.W. 25,000	Alfa Aesar	Cat# 43896.01
HiPerFect Transfection Reagent	Qiagen	Cat# 301705
ProLong™ Gold Antifade Mountant	ThermoFisher Scientific	Cat# P36934
Live Cell Imaging Solution	Molecular Probes	Cat# A14291DJ
HBSS, no calcium, no magnesium	Gibco	Cat# 14170088
Opti-MEM™ Reduced Serum Medium	Thermo Fisher Scientific	Cat# 31985070
<b>Critical Commercial Assays</b>		
Click-iT™ Cell Reaction Buffer Kit	Thermo Fisher Scientific	Cat# C10269
Pierce™ Silver Stain Kit	Thermo Fisher Scientific	Cat# 24612
RNeasy Mini Kit	Qiagen	Cat# 74106
iScript cDNA Synthesis kit	Bio-Rad	Cat# 1708890
iQ SYBR green Supermix	Bio-Rad	Cat# 1708880
4–20% Mini-PROTEAN® TGX™ Precast Protein Gels	Bio-Rad	Cat# 4561096
Atto 488 NHS ester	Sigma-Aldrich	Cat# 41698
<b>Experimental Models: Cell Lines</b>		
Human: T-REX™-HeLa Cell Line	Invitrogen	Cat# R71407; RRID: CVCL_D587
Human: HeLa Cell Line	CSL cell line service	Cat# 300194/p772_HeLa; RRID: CVCL_0030
<b>Oligonucleotides</b>		
siRNA targeting sequences, see <a href="#">Table S3</a>	This paper	N/A
Primers for cloning, see <a href="#">Table S3</a>	This paper	N/A
Primers for genomic validation, see <a href="#">Table S3</a>	This paper	N/A
<b>Recombinant DNA</b>		
pcDNA3 APEX2-NES	<a href="#">Lam et al. (2014)</a>	Addgene Plasmid #49386
N1-EQ-SM-mKate2	<a href="#">Deng et al. (2016)</a>	N/A
N1-EQ-sol-mKate2	<a href="#">Deng et al. (2016)</a>	N/A
pcDNA™5/FRT/TO	Invitrogen	V652020
pcDNA5-EQ-SM-APEX2	This paper	N/A
pcDNA5-EQ-sol-APEX2	This paper	N/A
N1-LyzC-phluorin	This paper	N/A
Phluorin-Cab45	This paper	N/A
pBluescript-SMS1-SNAP-tag	This paper	N/A
pLPCX-Cab45-WT/mut	<a href="#">von Blume et al. (2012)</a>	N/A
pLPCX-SPCA1-HA/mut	<a href="#">von Blume et al. (2012)</a>	N/A
pl-SUMOstar Insect	<a href="#">Crevenna et al. (2016)</a>	Life Sensors 3106
pl-SUMOstar-Cab45	<a href="#">Crevenna et al. (2016)</a>	N/A
pIRESneo3 Str-KDEL_ST-SBP-eGFP	<a href="#">Boncompain et al. (2012)</a>	Addgene Plasmid #65264
pIRESneo3 Str-KDEL_LyzC-SBP-eGFP	This paper	N/A
pIRESneo3 Str-KDEL_SS-SBP-eGFP-CathepsinD	This paper	N/A

(Continued on next page)

**Continued**

REAGENT or RESOURCE	SOURCE	IDENTIFIER
pIRESneo3 Str-KDEL_SS-SBP-tagRFP-CathepsinD	This paper	N/A
pCDNA3.1-Go-D1cpv	<a href="#">Lissandron et al. (2010)</a>	N/A
pLPCX-Go-D1cpv	This paper	N/A
pLPCX-SS-EGFP-Cab45	This paper	N/A
pLPCX-SS-EGFP-Cab45-6EQ	This paper	N/A
pLPCX-LyzC-mCherry	This paper	N/A
pLPCX-SMS1-HA	This paper	N/A
pLPCX-SMS1-HA-siResistant	This paper	N/A
pSpCas9(BB)-2A-Puro (PX459) V2.0	<a href="#">Ran et al. (2013)</a>	Addgene Plasmid #62988
oxGFP-SPCA1	This paper	N/A
Software and Algorithms		
ImageJ 1.52c	NIH	<a href="https://imagej.nih.gov/ij/">https://imagej.nih.gov/ij/</a>
Prism 7.0b for Mac OS X	Graphpad	<a href="https://www.graphpad.com/scientific-software/prism/">https://www.graphpad.com/scientific-software/prism/</a>
Image Lab Software Version 5.2.1 build 11	Bio-Rad	<a href="http://www.bio-rad.com/en-de/product/image-lab-software">http://www.bio-rad.com/en-de/product/image-lab-software</a>
Other		
μ-Dish 35 mm, high Glass Bottom	ibidi	Cat# 81158
Nunc Lab-Tek Chambered Coverglass, 1.0 borosilicate glass	Thermo Fisher Scientific	Cat# 15 5 411
Amicon Ultra-0.5 Centrifugal Filter Unit	Merck	Cat# UFC501096
GFP-Trap® beads	ChromoTek GmbH	Cat# gtma-20

**CONTACT FOR REAGENT AND RESOURCE SHARING**

Further information and requests for resources and reagents should be directed to and will be fulfilled by the Lead Contact, Julia von Blume ([vonblume@biochem.mpg.de](mailto:vonblume@biochem.mpg.de)).

**EXPERIMENTAL MODEL AND SUBJECT DETAILS**

HeLa cells were maintained in 5% CO<sub>2</sub> at 37°C in DMEM supplemented with 10% fetal bovine serum (Gibco, Grand Island, NY, United States). T-REX™-HeLa Cells (Thermo Fisher Scientific) were grown in 15 ug/ml blasticidin and 200 ug/ml zeocin. After transfecting with pcDNA5-EQ-SM/sol-APEX2, zeocin was replaced with 200 ug/ml hygromycin.

**METHOD DETAILS****DNA Manipulations**

APEX2 plasmid was acquired from Addgene (pcDNA3 APEX2-NES). APEX2 was PCR amplified and linked with EQ-SM/sol-Flag and inserted into pcDNA™5/FRT Vector (Invitrogen™).

LyzC-pHluorin was cloned by inserting LyzC into N1-pHluorin. SMS1-SNAP-tag repair template was generated by PCR amplified SMS1 left arm and right arm (around stop codon) from HeLa genomic DNA, linked with Flag-SNAP-tag and inserted into vector pBluescript II SK (+). LyzC-mCherry was cloned by amplifying LyzC-3xFlag and inserted N-terminally by EcoRI and BamHI sites into a pLPCX-mCherry vector.

Generation of plasmids that direct expression of WT and mutant Cab45 proteins and SPCA1-HA in pLPCX is described in ([von Blume et al., 2012](#)).

For expression of His-SUMO-tagged Cab45 in SF9 cells, Cab45 cDNA was amplified from pLPCX-Cab45-WT or EFh mutant plasmid and inserted into pI-Insect Secretory SUMOstar Vector (3106; Life Sensors) as described previously ([Crevenna et al., 2016](#)).

The RUSH vector pIRESneo3 Str-KDEL\_ST-SBP-eGFP was a gift from Franck Perez (Addgene plasmid # 65264). The ST region was replaced by amplifying LyzC-Flag ([von Blume et al., 2011](#)) and insertion into the pIRESneo3 backbone by Ascl and EcoRI cutting sites. To generate the SS-SBP-eGFP-Cathepsin D construct, first the Str-KDEL\_SS-SBP-eGFP construct was generated by amplifying human Growth Hormone (hGH) signal peptide to insert it into the pIRESneo3 backbone by Ascl and EcoRI cutting sites. In the second step, HA-Cathepsin D was C-terminally fused to SS-SBP-eGFP by overlap and extension PCR and inserted by Ascl and XhoI

into the pIRESneo3 vector. The SS-SBP-tagRFP-Cathepsin D construct was cloned by amplifying SS-SBP, tagRFP, Cathepsin D and the fragments were inserted by Gibson Assembly (Gibson, 2009) into the pIRESneo3 RUSH vector that was linearized with *Ascl* and *XhoI*. The Go-D1cpv (Lissandron et al., 2010) construct was cloned into pLPCX by restriction digestion with *HindIII* and *EcoRI*. eGFP-Cab45 and eGFP-Cab45-6EQ were cloned by amplifying eGFP and inserted after the signal sequence by using *HindIII* and *EcoRI* sites into either pLPCX-SS-Cab45 or pLPCX-SS-Cab45-6EQ mutant vector.

A siRNA resistant SMS1-HA variant was generated by mutating the siRNA binding site 5' – gacggcagcttcagcatcaagatta - 3' to 5' –gaTggAagTttTagTatAaaAatCa - 3'. For CRISPR/Cas9 targeting guide RNA oligos and their complementary sequences were cloned with suitable overhangs into a pX459 2.0 mammalian expression vector (Addgene plasmid # 62988) as described in (Ran et al., 2013). DNA oligonucleotides encoding CRISPR/Cas9 gRNA sequences were synthesized by Yale Keck Oligonucleotide Synthesis facility or by metabion international AG (Planegg, Germany). Oligonucleotides were annealed and cloned into pX459 2.0. The sequences of plasmids were confirmed by DNA sequencing.

Cab45-gRNA1: TTCTGATGGACGCGTCTGCA  
 Cab45-gRNA2: TTGATGAGGACGCGGAGCCG  
 SMS1-gRNA1: GAGGAGACTCGGCACAAGGG  
 SMS1-gRNA2: GGACTTGATCAACCTAACCC  
 SMS2-gRNA1: CGTCTTGACAACCGTCATGA  
 SMS2-gRNA2: AAAAGTACCCGGACTATATC  
 SMS1-tagging-gRNA: CATAACAGCTGTACAAAGTG  
 SGPL1-gRNA1: TGTGAAAGCTTTACCCCTCCC  
 SGPL1-gRNA2: CTTAAGGAGTACAGCTCTAT

### Antisera

Anti-FLAG (Sigma, F1804), anti-HA (rat monoclonal, 11867423001, Roche), anti-GaT (Abcam, ab178406), anti-Calnexin (Millipore, clone C8.B6), anti-SPCA1 (mouse monoclonal, H00027032-M01, Abnova), anti-p230 (mouse monoclonal, 611281, BD Biosciences), anti-TGN46 (sheep polyclonal, AHP500G, AbD Serotec), anti- $\beta$ -actin (mouse monoclonal, A5441, Sigma-Aldrich), anti-FLAG M2-Peroxidase (mouse monoclonal, A8592, Sigma-Aldrich). The anti-SPCA1 (rabbit polyclonal) antibody was a gift from Peter Vangheluwe, Department of Cellular and Molecular Medicine, University of Leuven, Belgium. Alexa Fluor Cross-Adsorbed secondary antibodies for immunofluorescence were purchased from Thermo Fisher Scientific (A-11034, A-11035, A-11029, A-11030, A-21209, A-21208, A-21203). Secondary anti-rabbit HRP conjugated antibodies were purchased from Thermo Fisher Scientific (32260), m-IgG $\kappa$  BP-HRP Antibody was from Santa Cruz Biotechnology (sc-516102).

For Cab45 antibody generation was performed by the immunization service by the animal facility of the Max Planck Institute of Biochemistry. Recombinant Cab45 full length protein (His Sumo tagged) was prepared in TiterMax Gold Adjuvant liquid (Sigma-Aldrich) according to the manufacturer's protocol. Rabbits were injected and boosted three times before collecting sera. Sera were stirred while incubated at room temperature for one hour and then at 4°C overnight. After centrifugation for 30 min at 5000 x g, collected supernatants were stored at – 20°C.

### Cell Culture and Engineering

HeLa cells were maintained in 5% CO<sub>2</sub> at 37°C in DMEM supplemented with 10% fetal bovine serum (Gibco, Grand Island, NY, United States). Cells were transfected with FuGENE HD (Promega), Lipofectamine 2000 (Thermo Fisher Scientific), 1.25 mg/ml Polyethylenimine (PEI) linear (Alfa Aesar) or Lipofectamine LTX PLUS (Thermo Fisher Scientific). To generate cell lines stably expressing Cab45-WT and Cab45-6EQ mutant VSV-G pseudotyped retroviral vectors were produced by transient transfection of HEK293T (human embryonic kidney) cells. To harvest virus particles, cell culture supernatants were filtered through 0.45- $\mu$ m filters. The virus particles were then concentrated from cell culture supernatants by spinning at 68.000 x g for 2h, followed by a second spin at 59.000 x g for 2.5h at RT. The pellet was resuspended in 200  $\mu$ l of HBSS (Pfeifer et al., 2000) and used for infection.

Stable cell lines expressing EQ-SM-APEX2 or EQ-sol-APEX2 were engineered as follows: HeLa T-Rex (Thermo Fisher Scientific) cells were transfected with pcDNA5/FRT-EQ-SM/sol-Flag-APEX2 and the recombinase pOG44. After two days, 200  $\mu$ g/ml hygromycin and 15  $\mu$ g/ml blasticidin was added to the medium and the cells were cultured for an additional 10 days and then expanded.

For gene editing cell lines using CRISPR/Cas9, HeLa cells were transfected with two gRNA against the same gene. For SMS1-SNAP-tag CRISPR cells, HeLa cells were transfected with one gRNA and a repair template that has Flag and SNAP-tag. For selection, 24 h post-transfection cells were selected for 48 h in 2  $\mu$ g/ml puromycin. 100 cells were then seeded in 15 cm culture dishes and cultured until single cell colonies were big enough to manually scrap them off the dish and transfer them to 96-well plates. Single clones were expanded and screened by PCR and Western Blotting. PCR amplification from the genomic DNA and gel electrophoresis were used to assess proper cleavage or tagging of the target sequences. The PCR products were confirmed by sequencing. For Cab45 KO and SMS1-SNAP-tag, protein levels were confirmed by Western Blotting.

### siRNA Silencing

For siRNA gene silencing following oligos were used: Cab45: 5' – GAGCCAGGACCUCACUCCUCCUCU - 3'; SMS1: 5' – GACGG CAGCUUCAGCAUCAAGAUUA - 3'; SMS2: 5'- UCAUAGUGGGACGCAGAUUCUGUU - 3'; SPCA1: 5'- CAUCGAGAAGUAAC AUUGCCUUUAU - 3' and a scrambled negative control from Invitrogen. The siRNA transfection mix was prepared by adding

20 nM siRNA and 12  $\mu$ l HiPerFect Transfection Reagent (Qiagen) to 100  $\mu$ l Opti-MEM reduced serum medium (Gibco by Life Technologies) and incubated 15 min at RT. The transfection mix was added to HeLa cells seeded on glass slides in either 6-wells or live cell  $\mu$ -dishes ( $\mu$ -Dish 35 mm, high Glass Bottom from ibidi). Cells were processed for further analysis after 48h for Cab45 and 72h for SMS1/2 silencing.

### Vesicle Budding and APEX2-Mediated Biotinylation

To monitor budding of vesicles containing EQ-SM-APEX2 or EQ-sol-APEX2 in permeabilized cells, cell lines that stably express two 10-cm dishes of cell lines that stably express EQ-SM-APEX2 or EQ-sol-APEX2 were treated with 2  $\mu$ g/ml tetracycline overnight to induce expression of EQ-SM/sol-APEX2 proteins. The next day, cells were trypsinized and harvested by centrifugation at 1000 g for 3 min. The cell pellet was washed with buffer A (20 mM Hepes, pH 7.4, 250 mM D-sorbitol, and 150 mM potassium acetate) and digitonin (40  $\mu$ g/ml) was added and incubated for 5 minutes on ice. Cells were washed one time with buffer A, resuspended in buffer A, and the mixture was then aliquoted into four tubes. The cells were incubated either with or without ATP regenerating system (1 mM ATP, 40 mM creatine phosphate, 0.2 mg/ml creatine phosphokinase and 0.1 mM GTP), with or without rat liver cytosol (1 mg/ml; Thermo Fisher Scientific), or incubated at 4°C or 32°C for 45 min. The reactions were centrifuged at 10,000 g for 10 minutes and the supernatant was collected and centrifuged at 100,000 g for 1 hour to collect vesicular material. The pelleted material was dissolved in SDS-PAGE loading dye and analyzed by SDS-PAGE. Streptavidin-HRP (Thermo Scientific Pierce, PI-21130) was used to detect biotinylated proteins.

For proteomic analyses of vesicle fractions, EQ-SM/sol-APEX2 stable cells from ten 15 cm dishes were processed as described above, except that biotinylation reactions were carried on S10 fractions. To do so, biotin-phenol (500  $\mu$ M) was added to the reactions and incubated for 20 min at 32°C. Next, H<sub>2</sub>O<sub>2</sub> (1 mM) was added and the reactions were tumbled for 1 minute at room temperature. The reaction was stopped by adding Trolox (1 mM) and sodium ascorbate (10 mM). The reactions were centrifuged at 10,000 g for 5 min and the supernatant was removed and then centrifuged at 100,000 g for 1 hour to collect vesicular material. The vesicle pellets were washed once with buffer A containing Trolox (1 mM) and sodium ascorbate (10 mM) to remove the biotin and recentrifuged at 100,000 g for 30 min.

Purification of biotinylated proteins was accomplished by affinity selection using NeutrAvidin beads. Pelleted vesicular material was solubilized in 1 ml RIPA buffer (50 mM Tris, 150 mM NaCl, 0.1% SDS, 1% Triton X-100 PH 7.5, 0.5% sodium deoxycholate, 10 mM sodium ascorbate, 1 mM Trolox, 2Xprotease inhibitor) and sonicated at 40W for 2 min. The solution was centrifuged at 13,000 g for 15 min and the supernatant was recovered and then incubated with 100  $\mu$ l NeutrAvidin beads for 6 hours at 4°C. The beads were washed with RIPA lysis buffer twice, once with 0.5 mL of 1 M KCl, once with 0.5 mL of 0.1 M Na<sub>2</sub>CO<sub>3</sub>, once with 0.5 mL of 2 M urea in 10 mM Tris-HCl pH 8.0, and three times with RIPA buffer. Purified proteins were eluted by boiling the beads in 100  $\mu$ l 2 $\times$  protein loading buffer for 5 min. Purified material was separated by SDS-PAGE on a 4–20% Mini-PROTEAN® TGX™ Precast Protein Gel (Bio-Rad). After staining with silver (Pierce™ Silver Stain Kit (24612), each lane was cut into five equal sized pieces and mass spectrometry was used to identify proteins in each gel piece. Mass spectrometry was done by the Yale Keck Biotechnology Resources Laboratory.

### Protein Detection by Immunoblotting, Silver Staining, or Immunofluorescence

For immunoblotting, proteins were transferred to nitrocellulose membrane and then blocked in PBS-T with 5% milk or in TBS-T with 5% BSA. After immunoblotting, proteins were detected by chemiluminescence. Images of immunoblots were acquired by ChemiDoc Imaging System (Bio-Rad).

For immunostaining, cells were cultured on glass slides, fixed for 10 min with 4% paraformaldehyde, washed with PBS and subsequently permeabilized for 5 min in 0.2% Triton-X 100 and 0.5% SDS in 4% BSA solution. After washing with PBS and blocking of slides for 1 h in 4% BSA, cells were incubated with primary and secondary antibody for 1 h at room temperature in blocking buffer in the dark. Glass slides were mounted with ProLong Gold (Thermo Scientific). For immunofluorescence after pac-sphingosine labeled cells, saponin was used to permeabilize cells.

### Lipidomics

One day after plating, cells from one 10 cm dish were collected by scraping, and washed twice with PBS. An aliquot was removed for protein quantification and the remainder was sent to the Virginia Commonwealth University Lipidomics/Metabolomics Core for mass spectrometry based sphingolipid analysis. Lipid levels were normalized to protein content.

### Fluorescence Microscopy and Image Analysis

For live cell deconvolution fluorescence microscopy, cells were washed twice with PBS, and the medium was replaced with live cell imaging solution (Molecular Probes) supplemented with 10 mM glucose. 3D image stacks were collected at 0.3  $\mu$ m z increments on a DeltaVision Elite workstation (Applied Precision) based on an inverted microscope (IX-70; Olympus) using a 60 $\times$ , 1.4 NA oil immersion lens. Images were captured with a sCMOS camera (CoolSnap HQ; Photometrics) and deconvolved with softWoRx (v.6.0) software using the iterative-constrained algorithm and the measured point spread function. Golgi budding experiments of living cells were performed at the widefield of the Imaging Facility of the Max Planck Institute of Biochemistry (MPIB-IF) on a GE Healthcare

DeltaVision Elite system based on an OLYMPUS IX-71 inverted microscope, an OLYMPUS 60x/1.42 PLAPON oil objective and a PCO sCMOS 5.5 camera. Budding events were scored manually from time lapse series. Quantitative co-localization analyses were done using softWoRx (v.6.0) software.

Analysis of vesicle numbers was carried out by a custom-made ImageJ macro. The macro uses ImageJ's rolling ball background subtraction algorithm, the enhance contrast function and a maximum z-projection of the RUSH reporter channel to cover all vesicles of the cell volume in a 2D image. After using a median filter, suitable cells were selected by drawing a polygon selection. A binary image was generated by the Threshold function. The threshold algorithm "Yen" was used by default while for low intensity images the threshold required manual correction. The vesicle objects in the binary images were compared and controlled by visual inspection with the original image. In the binary image, vesicle objects with sizes ranging from 4-20 pixels were then quantified by Analyze Particles function.

Confocal fluorescence microscopy of fixed cells was performed using a confocal laser-scanning microscope (LSM 780; Carl Zeiss) with a 40x/1.4 Plan-Apochromat oil or 100x/1.46 oil  $\alpha$ -Plan-Apochromat oil objective lens. For detection of Alexa Fluor, the 488 nm laser line was used. Pictures were acquired using Leica software (ZEN, 2010) and adjusted in ImageJ (version 1.51u).

Total internal reflection microscopy was done using a microscope (IX-70; Olympus) equipped with argon (488 nm) and argon/krypton (568 nm) laser lines, a TIRFM condenser (Olympus or custom condenser), a 60x 1.45 NA oil immersion objective lens (Olympus), and an EMCCD camera (iXon887; 0.18  $\mu$ m per pixel, 16 bits; Andor Technology). The TIRFM system was controlled by iQ software (Andor Technology). HeLa cells were grown in MatTek dishes and imaged 16–20 h after transfection. All experiments were done at 37°C in live cell imaging solution (Molecular Probes) containing 10 mM glucose, pH 7.4. Cells were imaged in one channel at 5 Hz or two channels by sequential excitation at 2 Hz.

Analysis of TIRF images was done as described in Deng et al (Deng et al., 2016). Briefly, each image stack was manually reviewed to identify putative vesicle fusion events that released pHluorin. The coordinates of the fusion events were labeled and a small region of interest around each exocytic event in each channel was used for further analysis. Circular regions with diameters of 4 pixels were used to calculate the intensity of a single vesicle. Colocalization of proteins in the same vesicle was determined manually based on the coincident appearance and release of fluorescence signals by each fusion protein. No nonlinear adjustments were made to alter fluorescent signals.

### **RUSH Cargo Sorting Assay Using Confocal Microscopy**

HeLa cells were cultured on sterile glass slides in 6-wells and gene silenced as described above. Cells were transfected using either pIRESneo3-LyzC-SBP-eGFP or pIRESneo3-SS-SBP-eGFP-Cathepsin D for 16h. Cells were incubated with 40  $\mu$ M d-Biotin (SUPELCO) in DMEM for 20, 40 and 60 min and as a control without d-Biotin to confirm the retention of the reporter. Cells were then washed once in 1x PBS and fixed in 4% PFA in PBS for 10 min and further processed for immunofluorescence microscopy as described above. Samples were acquired using a confocal laser-scanning microscope (LSM 780; Carl Zeiss). Only cells were processed that showed proper transport of the reporter to the Golgi after Biotin addition while cells showing ER signal after Biotin addition were discarded from the analysis. To cover the whole volume of the cells, typically 8-16 z-stacks with a step-size of 0.35  $\mu$ m were acquired of each field of view.

### **RUSH Cargo Sorting Assay Using Western Blot Analysis**

HeLa cells were cultured in 6-wells and gene silenced as described above. Cells were transfected with pIRESneo3-LyzC-SBP-eGFP for 16h. Cells were washed 3x in PBS followed by 3x with DMEM w/o FCS. Cells were incubated with or without 1 mL 40  $\mu$ M d-Biotin for 60 min in DMEM w/o FCS. Cell culture supernatants were collected and centrifuged for 5 min at 1,000 x g to pellet residual cells. Supernatants were concentrated by centrifugation at 16,000 x g for 8 min using Centrifugal Filters (Amicon Ultra, Ultracel 10K). Cell pellets were washed 3 times with PBS, trypsinized and transferred to tubes. Cells were then washed PBS and lysed with 1% TritonX-100 in 1 time with PBS. Concentrated supernatants and lysed cell pellets were further processed for SDS-PAGE and Western Blot analysis. Western Blot quantification from three independent experiments was performed by using Image Lab Version 5.2.1 build 11 (Bio-Rad) software. Supernatant signals were normalized to each corresponding actin signal of the cell pellet to correct for protein levels. Rates of secretion for each condition were determined by calculating the ratio of 60 min to 0 min LyzC-SBP-eGFP supernatant signals and were normalized to 100% of control cells and plotted as a bar graph.

### **In Vivo Golgi Vesicle Budding Assays**

HeLa cells seeded in live cell  $\mu$ -dishes were transfected with EQ-SM-mKate2 together with either eGFP-Cab45 or eGFP-Cab45-6EQ for 16h. Cells were acquired by live-cell widefield microscopy and focused at the Golgi region. Dual-channel acquisition for eGFP and mCherry was performed at 1 sec intervals for 100 frames. The time-lapse movies were analyzed by identifying each eGFP-Cab45 or GFP-Cab45-6EQ budding event from the Golgi. Cab45 budding events were then scored whether or not EQ-SM-mKate2 was also present. At least 26 budding events from 4 cells for eGFP-Cab45 and 32 budding events from 13 cells for eGFP-Cab45-6EQ were analyzed. The ratios of Cab45 budding with or without EQ-SM were calculated to total budding events. The average and SD of the ratios were plotted as a bar graph.

### Pac-Sphingosine Labeling

SGPL1 null HeLa cells were incubated with 0.5  $\mu$ M pacSph (Avanti, 900600) in DMEM/delipidated FBS (pre-warmed to 37°C) for 30 minutes at 37°C. The medium was then removed and the cells were washed three times with DMEM/delipidated FBS. Cells were then incubated in DMEM/FBS for 1 hour at 37°C. Cells were washed with PBS three times and the medium was replaced with 4% paraformaldehyde in PBS and incubated for 20 minutes. Cells were washed with PBS three times and then incubated with permeabilization and blocking Buffer (0.1% saponin with 5% serum in PBS) for 1 hour. For immunofluorescence detection of proteins in these cells, primary and secondary antibodies were added. Cells were then washed with PBS three times. A Click-iT™ Cell Reaction Buffer kit was used to click label pacSph according to the manufacturer's instructions (Thermo Fisher Scientific, C10269). After the reaction, cells were washed 5 times with PBS and then visualized by fluorescence microscopy.

### Pac-Sphingosine Crosslinking

SGPL1 null HeLa cells were transfected with 25  $\mu$ g oxGFP-SPCA1 and lipofectamine for 18 hours prior to labeling with pacSph (0.5  $\mu$ M) for 30 min and then chased in DMEM/FBS for 1 hour. Two 10-cm dishes cells were subjected to 365 nm UV (8W) (or kept in the dark, as control) for 10 min. The cells were collected and washed with PBS. The cell pellets were resuspended in lysis buffer (20 mM Tris, pH 7.5, 150 mM NaCl, 1% Triton, protein inhibitor) for 1 hour and then sonicated (with tip sonicator) for 30 seconds. The lysate was centrifuged for 30 min at 13,000  $\times$  g. The supernatant was collected and incubated with 15  $\mu$ l GFP-Trap beads (gtma-20, ChromoTek GmbH) for 1 hour. The beads were washed once with wash buffer (20 mM Tris, pH 7.5, 150 mM NaCl) and then incubated with Click reagents and azide-biotin (Thermo Fisher Scientific) for 1 hour. The beads were washed twice with wash buffer (20 mM Tris, pH 7.5, 150 mM NaCl, 0.1% Triton). 30  $\mu$ l SDS loading buffer was used to elute from the beads. 25  $\mu$ M Fumonisin B1 (Sigma) was added to the cells when transfected and in the pulse-chase experiments.

### Ca<sup>2+</sup> Influx Assay

Ca<sup>2+</sup> entry into the TGN was measured as described previously (Lissandron et al., 2010). Measurements of [Ca<sup>2+</sup>] in the TGN were performed using a fluorescent Ca<sup>2+</sup> sensor (Go-D1-cpv) expressed as a fusion to sialyltransferase which targets to the TGN. Changes in Ca<sup>2+</sup> concentration are observed as changes in the efficiency of FRET between CFP and YFP fluorescent proteins linked by a modified calmodulin and calmodulin-binding domain. HeLa cells were transfected with control, SPCA1, or SMS1/2 siRNAs for 72 h. Then Go-D1-cpv was transfected alone, or with siRNA resistant SMS1-HA, or SPCA1-HA. Ca<sup>2+</sup> entry into the TGN was measured in Ca<sup>2+</sup>-depleted cells after 1 h of incubation at 4°C in HBSS (20 mM Hepes, Ca<sup>2+</sup>/Mg<sup>2+</sup>-free HBSS [Gibco by Life Technologies], 2 g/l—1 glucose, 490  $\mu$ M MgCl<sub>2</sub>, and 450  $\mu$ M MgSO<sub>4</sub>; 300 mOsm/liter, pH 7.4) with 1  $\mu$ M ionomycin (Abcam) and 0.5 mM EGTA (von Blume et al., 2011). Then cells were washed twice in HBSS + 0.5 mM EGTA followed by three washes in HBSS only. Image acquisition was performed on a GE DeltaVision Elite as described above. To generate the images, the excitation filter (430/24), dual-band Sedat CFP/YFP beam splitter (Chroma Technology Corp.), and the emission filters (535/25 for FRET and 470/24 for CFP) were rapidly changed using an external filter wheel controlled by a motorized unit. Fluorescent signals reflecting TGN [Ca<sup>2+</sup>] were presented as  $\Delta R/R_0$ , where R<sub>0</sub> is the value obtained before addition of 2.2 mM CaCl<sub>2</sub> to the cell's bathing solution. Images were acquired using softWoRx 5.5 software (GE Healthcare). Image analysis was carried out by a custom-made ImageJ macro and is based on ratiometric FRET analysis described previously (Kardash et al., 2011; Kienzle et al., 2014). The macro uses ImageJ's rolling ball background subtraction algorithm followed by a mean filter to smooth the edges of the objects. A binary image was generated by the Auto Threshold function using the "Moments" algorithm. The images of the FRET and CFP channel were multiplied by the "ImageCalculator" plug-in with their respective binary images resulting in images that show 0 intensities outside of the threshold Golgi region while retaining intensities within the Golgi. Next, a ratio image of FRET/CFP was generated by using the "Ratio Plus" plug-in. The Golgi objects were detected by using the "Find Maxima" function and added to the ROI manager. The mean intensities of each ROI were then measured in the ratio image for each frame. The ratio values of each frame were subtracted to the first frame. These values were normalized to the first frame and presented as percentage  $\Delta R/R_0$  to obtain normalized ratio values before the addition of CaCl<sub>2</sub>. A pool of ~35% of SMS1/2 knock down cells that did not show a Ca<sup>2+</sup> influx defect due to knock down variability of two independent genes, were discarded. Samples that showed over 15% signal reduction of the maximum amplitude value compared to the last frame were discarded due to high photo bleaching.

### Quantitative Real-Time PCR

HeLa cells seeded in 6-wells were transfected with control or with SMS1/2 siRNA as described above. RNA was isolated from cells using the RNeasy Mini Kit (Qiagen). 1  $\mu$ g RNA was used for the reverse transcription reaction using the iScript cDNA Synthesis kit (Bio-Rad). Quantitative PCR reaction were performed with the LightCycler 480 II (Roche) using iQ SYBR green Supermix (Bio-Rad) with following primers that were described previously (van Galen et al., 2014): SMS1: 5' – ACTGTGAGCCTCTGGAGCAT – 3' and 5' – TGCTCCATTTTCAGGGTTTC – 3'; SMS2: 5' – CAATTCCTTGCTGCTTCTCC – 3' and 5' – CCTTTGTTTTGCTCCTCAG – 3'; GAPDH: 5' – TGCACCACCAACTGCTTAGC – 3' and 5' – GGCATGGACTGTGGTCATGAG – 3'. The Ct values of control and siRNA transfected samples of the experimental genes SMS1 and SMS2 were subtracted from the housekeeping gene GAPDH to obtain the  $\Delta$ Ct values. The  $\Delta$ Ct value of the siRNA transfected sample was then subtracted from the control value to obtain the  $\Delta\Delta$ Ct values. Next, by calculating  $2^{-\Delta\Delta Ct}$ , the relative expression fold change was determined for each replicate and plotted as a bar graph.

### **Purification of Recombinant Proteins and Labeling**

His-SUMO tagged Cab45 was expressed in SF9 cells with pI-secSUMOstar plasmid and purified from cell supernatants with nickel-based affinity chromatography using a NaP pH 8.0, 500 mM NaCl buffer and cComplete His-tag Purification Resin (Roche). Following elution by 250 mM imidazole, proteins were dialyzed to 20 mM PIPES, pH 6.8, 500 mM NaCl, 10% Glycerol for storage.

Recombinant Cab45 labeling with NHS-Atto488 (Sigma Aldrich) was performed according to manufacturer's instructions.

### **Cab45 Oligomerization Assay**

For oligomerization assays recombinant Cab45 proteins and EFh mutants were thawed on ice and centrifuged 15 min at 13,200 rpm at 4 °C to remove aggregates. Protein concentrations were adjusted to 2.5  $\mu$ M in PBS pH 7.4. For measurements proteins were diluted 1:100 in a total volume of 100  $\mu$ l in PBS pH 7.4 and analyzed in Lab-Tek 8 Chamber #1.0 borosilicate coverglass system (Nunc, Rochester, USA) with a LSM780 confocal microscope as described above under the indicated conditions.

### **Circular Dichroism Spectroscopy**

Circular dichroism spectroscopy (CD) measurements were performed in a 1-mm (path length) cuvette at 10 °C on a JASCO J-715 spectrometer. Protein samples (0.2 mg/ml) were dissolved in CD buffer (20 mM PIPES pH 6.8, 50 mM NaCl) and the indicated amounts of Ca<sup>2+</sup> were added before spectra were recorded. An average of 10 ( $\pm$  Ca<sup>2+</sup> analysis) independent spectra (from 195 to 250 nm with 0.1 nm spacing) were documented. Data was normalized to molecular ellipticity of protein and FFT filter was applied.

### **QUANTIFICATION AND STATISTICAL ANALYSIS**

For statistical evaluation GraphPad Prism version 7.0b for Mac OS X (GraphPad Software, La Jolla California USA) was used. RUSH cargo sorting assays were analyzed by using a non-parametric Kruskal-Wallis test followed by Dunn's multiple comparisons test. TIRF exocytosis assays were analyzed using Student's unpaired t-test. In vitro vesicle budding data were analyzed using a ratio paired t-test. The following P-value style was used:  $\leq 0.05$  (\*),  $\leq 0.01$  (\*\*),  $\leq 0.001$  (\*\*\*)

**Developmental Cell, Volume 47**

**Supplemental Information**

**Activity of the SPCA1 Calcium Pump Couples**

**Sphingomyelin Synthesis to Sorting of Secretory**

**Proteins in the *Trans*-Golgi Network**

**Yongqiang Deng, Mehrshad Pakdel, Birgit Blank, Emma L. Sundberg, Christopher G. Burd, and Julia von Blume**

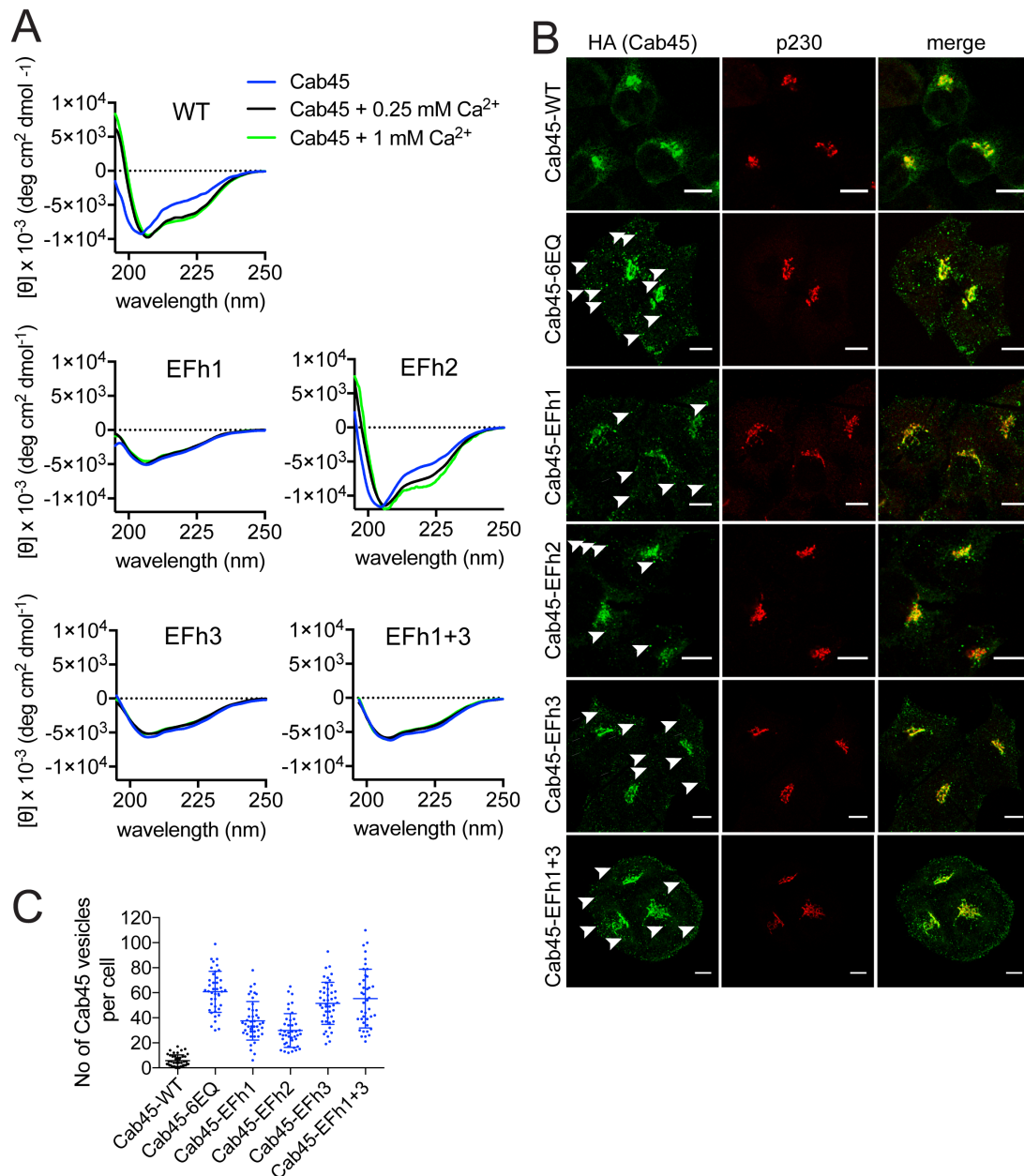


**Figure S1. Cab45 EFh mutant expression shows vesicular localization, Related to Figure 2. (A)** Far-UV CD analysis of recombinant Cab45 and the Cab45-EFh1, Cab45-EFh2, Cab45-EFh3 and Cab45-EFh1+3 mutants in the presence and absence of 0.25 mM or 1 mM  $\text{Ca}^{2+}$ . **(B)** HeLa Cab45-KO cells were stably transfected with either Cab45-WT or the mutants Cab45-6EQ, Cab45-EFh1, Cab45-EFh2, Cab45-EFh3 and Cab45-EFh1+3. Cells were visualized by anti-HA for Cab45 (green) and anti-p230 as a TGN marker (red)

and analyzed by confocal microscopy. Arrowheads point to cytoplasmic vesicles. Bars, 10  $\mu\text{m}$ . **(C)** The number of Cab45 vesicles per cell was quantified for Cab45-KO cells stably expressing Cab45-WT, and the mutants Cab45-6EQ, Cab45-EFh1, Cab45-EFh2, Cab45-EFh3 and Cab45-EFh1+3.

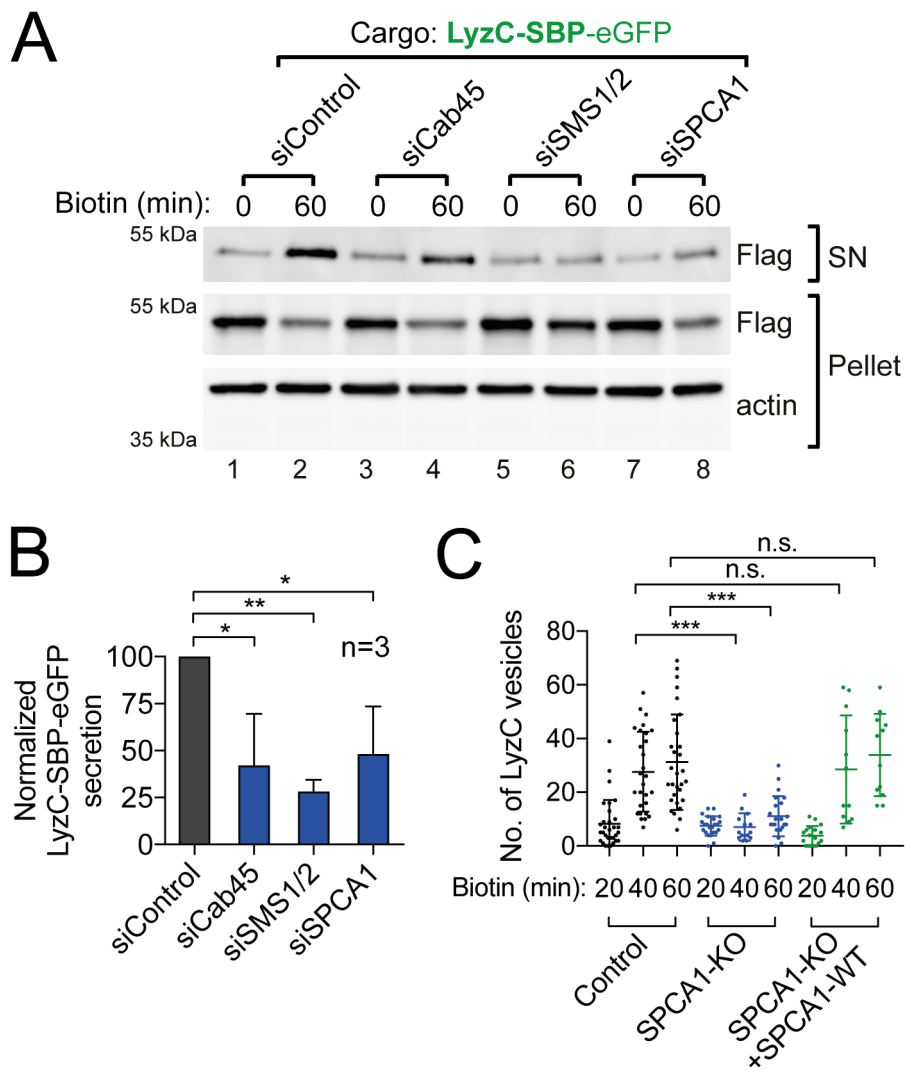


**Figure S2. Depletion of SPCA1 impairs LyzC secretion and cargo sorting, Related to Figure 3 and Figure 4. (A)** Depletion of SMS1/2, and SPCA1, cause retention of LyzC-SBP-eGFP within cells. HeLa cells transfected with control, Cab45, SMS1/2 and SPCA1 siRNA were transfected with LyzC-SBP-eGFP. Cell culture supernatants and whole cell lysates of cells were collected after 60 min incubation with Biotin and probed for FLAG epitope tagged LyzC-SBP-eGFP by immunoblotting. Actin was detected in the lysates as a loading control. **(B)** Semi-quantitative analysis of LyzC secretion by normalizing LyzC supernatant signals to their respective actin loading control. LyzC secretion was then determined by the ratio of 60 min to 0 min

samples after Biotin addition and normalized to control siRNA treated cells. The means ( $\pm$  s.d.) from 3 independent experiments are plotted. **(C)** The number of LyzC vesicles was quantified in HeLa control or SPCA1 null cells expressing either LyzC-SBP-eGFP alone, or co-transfected with SPCA1-WT. Vesicle counts (mean  $\pm$  s.d.) from at least 12 cells per condition in 3 independent experiments are plotted.

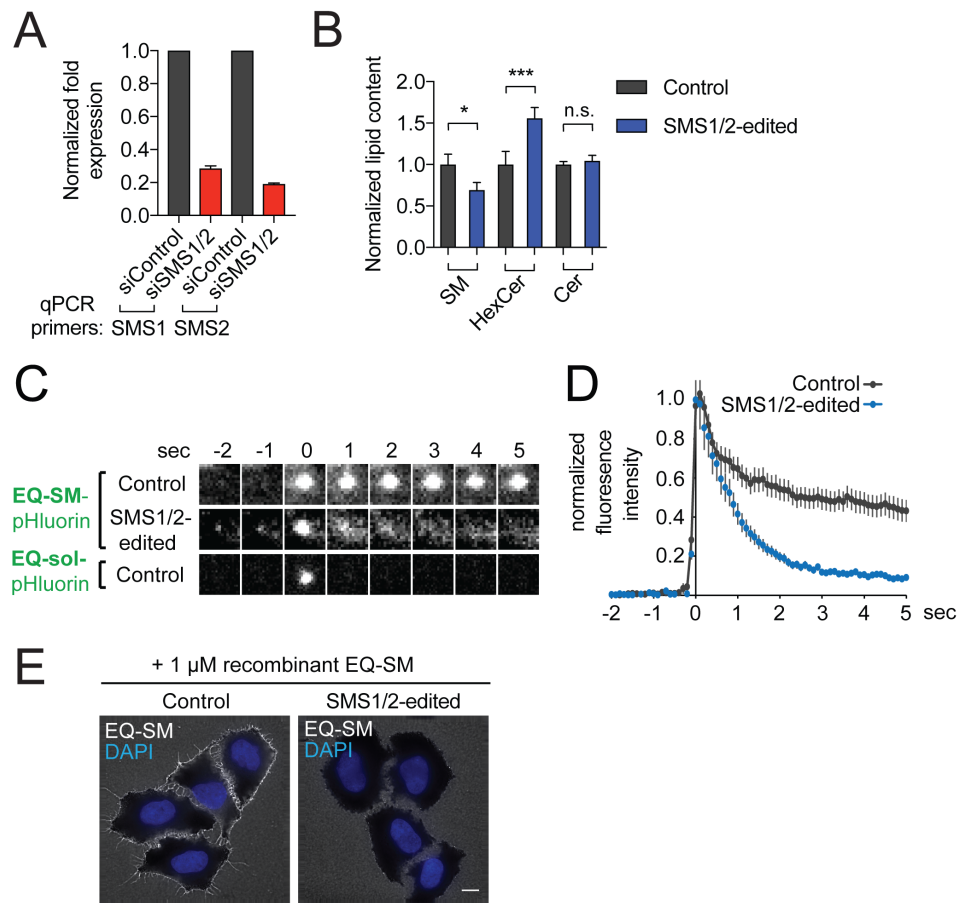


**Figure S3. Characterization of SM depleted cells lines, Related to Figure 4.** **(A)** Quantitative real-time PCR of cells treated with SMS1/2 siRNA confirmed a reduction of mRNA expression of SMS1 and SMS2 to 26.8% and 19% compared to cells treated with control siRNA. Samples were normalized to the housekeeping gene GAPDH and the data was presented as relative expression fold change normalized to control cells. A representative experiment with the means (s.e.m.) of technical triplicates is shown. **(B)** Sphingolipid analysis of SMS1 and SMS2 depleted cells. The relative amounts of the indicated sphingolipid species are shown. The values are the means (s.e.m.) of three replicate measurements.  $P < 0.05$  for SM,  $P < 0.01$  for HexCer. **(C)** Time-lapse TIRF micrographs of HeLa control or SMS1/2-edited cells expressing either EQ-SM-pHluorin or EQ-sol-pHluorin. Note that EQ-SM-

pHluorin remains bound to the plasma membrane at the site of exocytosis in unmodified control cells, but it dissipates from the site of exocytosis in SMS1/2-edited HeLa cells. A time-lapse gallery of micrographs showing dissipation of EQ-sol-pHluorin after exocytosis is shown for comparison. **(D)** Fluorescence intensity profiles of EQ-SM-pHluorin exocytosis. The normalized mean fluorescence intensities (s.e.m.) of 34 and 57 exocytic events (control and SMS1/2-edited, respectively) in TIRF micrographs are plotted. Fluorescence values were normalized to the peak intensity observed for each series. **(E)** HeLa control and SMS1/2-edited cells were incubated with 1  $\mu$ M recombinant EQ-SM to probe SM at the plasma membrane. EQ-SM containing a FLAG epitope was visualized by immunofluorescence of anti-FLAG (white) and DAPI to label the nucleus. Bars, 10  $\mu$ m.

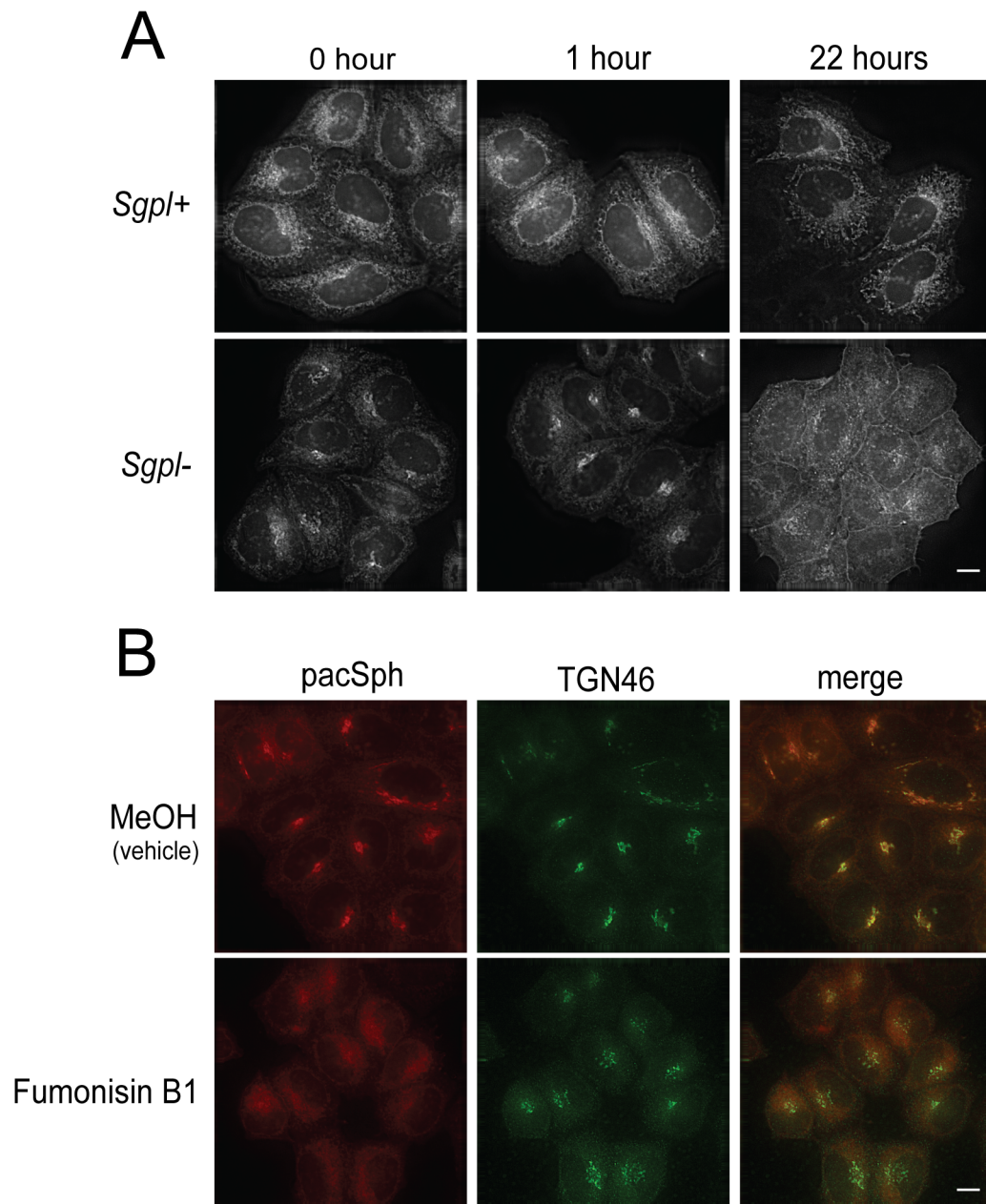


**Figure S4. Pac-sphingosine-labeled sphingolipids are trafficked to the Golgi apparatus and then the plasma membrane, Related to Figure 5. (A)** Time course of pacSph labeling of control (*SGPL1+*) and *SGPL1* null (*SGPL1-*) cells. *SGPL1-* HeLa cells and control parental cells (*SGPL1+*) were incubated with 0.6  $\mu$ M pacSph for 30 minutes, followed by a chase period of 1 or 22 hours in medium lacking pacSph. Fixed, permeabilized cells were incubated with click chemistry reagents to covalently attached Alexa647

fluorophore to pacSph. Cells were visualized by deconvolution fluorescence microscopy. Bars, 10  $\mu\text{m}$ . Note that pacSph-labeled sphingolipids are trafficked to the Golgi apparatus and then the plasma membrane. **(B)** An inhibitor of ceramide synthase, fumonisin B1 (FB1), prevents targeting of pacSph to the Golgi apparatus. *SGPL1*- HeLa cells were pre-incubated with FB1 (50  $\mu\text{M}$ ) for 24 hours, followed by labeling of cells with 0.6  $\mu\text{M}$  pacSph. Cells were processed to label pacSph with Alexa647 and for immunofluorescence detection of TGN46 to identify the Golgi apparatus. Scale bars, 10  $\mu\text{m}$ .

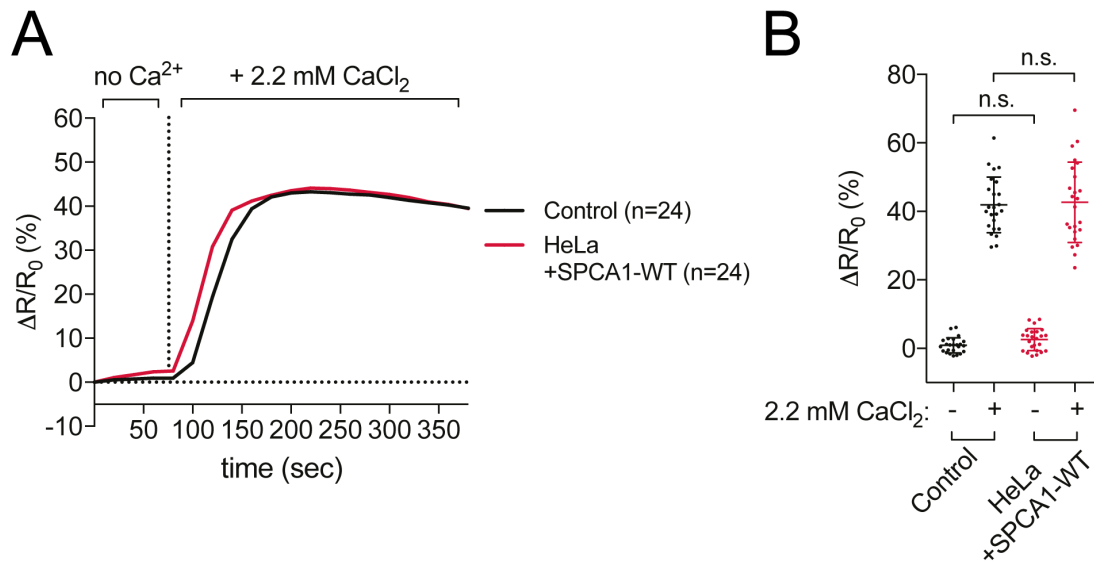


**Figure S5. Overexpression of SPCA1 does not alter Ca<sup>2+</sup> influx, Related to Figure 6. (A)** Quantification of FRET images of HeLa control cells and cells that overexpress SPCA1-WT. Fluorescence signals reflecting TGN [Ca<sup>2+</sup>] are presented as  $\Delta R/R_0$ . Data are plotted as the mean Ca<sup>2+</sup> influx over time. **(B)** Data are plotted as the mean  $\pm$  s.d. Ca<sup>2+</sup> influx at before Ca<sup>2+</sup> addition (at 80 sec) or after Ca<sup>2+</sup> addition (at 300 sec). Data was acquired for at least 24 cells per condition in two independent experiments.

object 1	object 2	R =	n
SPCA1	GM130	0.58 ± 0.07	37
	p230	0.54 ± 0.08	38
	SMS1	0.76 ± 0.06	75
SMS1	GM130	0.33 ± 0.06	37
	p230	0.62 ± 0.09	38
pacSph	GM130	0.49 ± 0.08	32
	p230	0.76 ± 0.06	22

**Table S2. Pearson's correlation analysis for Golgi residents, Related to**

**Figure 5.** The mean Pearson's correlation coefficients (R) ( $\pm$  s.d) were determined for the indicated pairs of proteins or pacSph-labeled lipids. The number of cells analyzed for each condition is indicated (n).